UCRL-51846

NUCLEAR DECAY SCHEME STUDIES OF 30-h $^{131}Te^{m}$, 25-min $^{131}Te^{g}$, AND 55.5-min ^{105}Cd

Sydney Vern Jackson
(Ph. D. Thesis)

Prepared for U.S. Energy Research & Development Administration under contract No. W-7405-Eng-48

Printed in the United States of America
Available from
National Technical Information Service
U. S. Department of Commerce
5285 Port Royal Road
Springfield, Virginia 22151
Price: Printed Copy $___*; Microfiche $2.25

*Pages	NTIS Selling Price
1-50	$4.00
51-150	$5.45
151-325	$7.60
326-500	$10.60
501-1000	$13.60

LAWRENCE LIVERMORE LABORATORY
University of California / Livermore, California / 94550

UCRL-51846

NUCLEAR DECAY SCHEME STUDIES OF 30-h $^{131}Te^{m}$, 25-min $^{131}Te^{g}$ AND 55.5-min ^{105}Cd

Sydney Vern Jackson

(Ph. D. Thesis)

VITA

Name: Sydney Vern Jackson.

Permanent address: 2226 Sugarloaf Avenue
Kalamazoo, Michigan 49002.

Degree and date to be conferred: Ph.D., 1975.

Date of birth: August 12, 1948.

Place of birth: Kalamazoo, Michigan.

Secondary education: Portage Central High School
Portage, Michigan
Graduated - June, 1966.

Colleges attended: Massachusetts Institute of Technology
Cambridge, Massachusetts
Sept. 1966 to June 1970
S.B. Chemistry, June, 1970.

University of Maryland
College Park, Maryland
Sept. 1970 to Aug. 1975
Ph.D., Aug., 1970.

Major: Nuclear Chemistry.

Publications: S.V. Jackson, W.B. Walters, and R.A. Meyer, "Radioactive Decay of 30-h $^{131}Te^{m}$ and 25-min $^{131}Te^{g}$ to Levels of ^{131}I," Phys. Rev. C11, 1323 (1975).

S.V. Jackson, E.A. Henry, and R.A. Meyer, "Decay of ^{49}Cr," Phys. Rev. (to be published 1975).

Positions held: National Science Foundation Fellow (2 yrs.)
Research Assistant (1 yr.)
Gillette-Harris Research Fellow (1 yr.)
Department of Chemistry
University of Maryland,
College Park, Maryland 20742

Associated Western Universities Fellow (1 yr.)
Lawrence Livermore Laboratory
Livermore, California 94550

Post-Doctoral Research Associate
Cyclotron Institute
Texas A&M University
College Station, Texas 77843

ABSTRACT

Title of Thesis: NUCLEAR DECAY SCHEME STUDIES OF 30-h $^{131}Te^{m}$, 25-min $^{131}Te^{g}$, AND 55.5-min ^{105}Cd

Sydney Vern Jackson, Doctor of Philosophy, 1975

Thesis directed by: Dr. William B. Walters
Assoc. Professor, Dept. of Chemistry
University of Maryland

Dr. Richard A. Meyer
Radiochemistry Division
Lawrence Livermore Laboratory

High-resolution Ge(Li) detectors have been used to observe γ-ray singles and coincidence spectra of 30-h $11/2^{-}$ $^{131}Te^{m}$, 25-min $3/2^{+}$ $^{131}Te^{g}$, and 55.5-min $5/2^{+}$ ^{105}Cd.

Sources of $^{131}Te^{m}$ and $^{131}Te^{g}$ were produced by neutron irradiation of enriched ^{130}Te metal, and, in the case of $^{131}Te^{m}$, were chemically purified to remove the ^{131}I daughter. A total of 190 and 80 γ-rays are attributed to the decays of $^{131}Te^{m}$ and $^{131}Te^{g}$, respectively; and 174 and 77 of these transitions have been placed in a ^{131}I level scheme involving 52 excited states. Absolute β group intensities were determined for the transitions to ^{131}I levels. Spin and parity assignments were made for all observed levels. The β feeding from the $11/2^{-}$ $^{131}Te^{m}$ to the $7/2^{+}$ ^{131}I ground state was determined to be (5.2 ± 3.0)% ($\log f_1 t = 10.5$). The isomeric transition of $11/2^{-}$ $^{131}Te^{m}$ to $3/2^{+}$ $^{131}Te^{g}$ was determined to be (22.2 ± 1.6)%. The 6-nsec isomer in ^{131}I at 1797 keV has been assigned as $15/2^{-}$ and interpreted as a $\pi\nu_1\nu_2$ three quasi-particle state.

Sources of ^{105}Cd were produced via the $^{106}Cd(n,2n)$

reaction on enriched ^{106}CdO using 14 MeV neutrons. A total of 274 γ-rays are attributed to the decay of ^{105}Cd, and 248 of these have been placed in a ^{105}Ag level scheme involving 50 excited states. Absolute values for the β^+/EC transition intensities to ^{105}Ag levels were determined. The β^+/EC feeding from the $5/2^+$ ^{105}Cd to the $7/2^+$ 25.5-keV isomeric state in ^{105}Ag was determined to be (51.4 ± 4.0)% (log*ft* = 5.4). Spin and parity assignments were made for all observed levels.

The experimentally determined level structures of ^{131}I and ^{105}Cd are interpreted in terms of the shell model and core excitation considerations with emphasis placed on the core coupling model and the three-particle models.

I DEDICATE THIS ENDEAVOR TO THE LATE

DR. CHARLES D. CORYELL

WHO FIRST INSPIRED ME TO STUDY NUCLEAR CHEMISTRY

AND TO

DR. WILLIAM B. WALTERS

WHO HAS BEEN VERY MUCH MORE TO ME THAN JUST MY

ACADEMIC ADVISOR FOR THE PAST NINE YEARS

ACKNOWLEDGEMENTS

Of all the people who inspired, influenced, supported or helped with this work, I would like to particularly thank Dr. William B. Walters who did all four, plus a great deal more. His constant availability for discussions, both scientific and personal, was invaluable. His guidance and encouragement, while not always preventing my own mistakes, could always be counted on and are something for which I shall always be grateful.

I wish to express my deep appreciation to Dr. Richard A. Meyer, who supervised my work at LLL. Without his help and hospitality, it would have been impossible to make the transition from Maryland to Livermore and complete this thesis in six months. His day-to-day availability for discussions, his help with experiments, and the free meals he and his wife, Ruth, supplied are all greatly appreciated.

I wish to thank Drs. Jon T. Larsen, Eugene A. Henry, and Robert G. Lanier for helping me become acclimated to LLL and in particular for guiding me through many of the mysteries of the LLL computer system. I also wish to express my appreciation to Dr. Lloyd G. Multauf for helping me to become familiar with, and allowing me to use, his 2-parameter coincidence system at LLL.

Dr. John D. Immele deserves special thanks for all the time he spent patiently guiding this experimentalist

through some of the mysteries of nuclear theory.

The help of Mr. J. Landrum and Mr. N. Smith with some chemical separations and of Ms. P. Schuster with the U. of Md. $\gamma\gamma$-coincidence system is gratefully acknowledged.

I would like to express my appreciation to the operating crews of the LLL pool-type reactor, the LLL ICT 14-MeV neutron generator, and the National Bureau of Standards reactor for their assistance in performing irradiations.

I wish to thank Mrs. Irene Baker for typing this manuscript.

I take great pleasure in thanking Dr. William H. Zoller, Ms. Julia Carroll, Dr. Phil Ray, Ms. Kathy Hickok, Ms. Linda Mitchell, Dr. Peter Molton, Mr. Richard Cahill, Mr. Pat Gallagher, and Ms. Lisa Coburn for their moral support and most of all for their friendship.

I give warm thanks to my parents and brothers who have given me so much support - both moral and tangible - for so long.

My financial support while in graduate school from the National Science Foundation, the Gillette Research Corporation, and Associated Western Universities, Inc. is gratefully acknowledged.

Much of this work was supported by the U.S. Atomic Energy Commission under Contract No. AT(40-1)-4028. The early work at LLL was performed under the auspices of the U.S. Atomic Energy Commission and supported by the Defense Advance Research Projects Agency. The later work at LLL

was performed under the auspices of the U.S. Energy Research and Development Agency. The computer analysis at the U. of Md. was supported by a grant of computer time from the U. of Md. Computer Science Center.

TABLE OF CONTENTS

TABLE OF CONTENTS (continued)

LIST OF TABLES

LIST OF TABLES (continued)

LIST OF TABLES (continued)

LIST OF FIGURES

LIST OF FIGURES (continued)

LIST OF FIGURES (continued)

LIST OF FIGURES (continued)

LIST OF FIGURES (continued)

LIST OF FIGURES (continued)

I. GENERAL INTRODUCTION

The exact nature of the nuclear force in the nuclear environment is presently unknown, thus the principal approach to understanding nuclei and nuclear properties is the development of nuclear models based on various simplifying assumptions. Experimental data on nuclear structure provide the impetus for the development of various models, with the success or failure of a model depending on its ability to explain the experimental observations. In turn, the theoretical model predictions provide much of the impetus for experimental investigations in order to test the theories. In the past decade, technological developments have allowed the detailed investigation of increasingly complex nuclear decay schemes, thereby greatly increasing the base of nuclear structure data which must be addressed by any nuclear model. This study of the levels of ^{131}I and ^{105}Ag, as observed in radioactive decay, was initiated in order to extend this data base. The resulting data provide a check on several recently developed theoretical models and some suggestions for future theoretical development.

No single nuclear model at present is able to successfully describe the properties of all nuclei, but many models are reasonably successful in predicting the structure and properties of a restricted set of nuclei. The basic model used to describe the ^{131}I and ^{105}Ag nuclides of this study is the "shell" or "independent-particle" model, originally formulated by Haxel, Jensen, and Suess (49Ha) and by Mayer (49Ma). This model has been discussed in detail in many

excellent reviews (e.g., 61Sh, 62Pr, 63Sh, 64La, 67Go). In this model, one describes each independent nucleon as moving in some average spherically symmetric potential resulting from all the other nucleons. In addition, each nucleon is subject to a strong spin-orbit interaction. In a manner analogous to the atomic electron case, the nucleons fill a prescribed orbital level scheme. Like nucleons are assumed to experience a strong pairing force which results in nucleons filling in pairs with anti-parallel angular momenta, thus, the ground state of an even-even nucleus is a highly correlated 0^+ state, and the total angular momentum of an odd-mass-number nucleus is just that of the odd nucleon remaining unpaired. Nuclear excitations in this model result from the promotion of the odd nucleon to a higher energy orbital or the breaking of a pair of nucleons and then recoupling them to a non-zero angular momentum.

The shell model is reasonably successful at predicting much systematic behavior of nuclei (e.g., the occurrence of "closed shells") and many of the ground state properties of nuclei (e.g., the ground state spin, parity, and magnetic dipole moment). However, this model cannot explain the low-lying level structure of many nuclei. In order to do this the model has been extended to include a residual two-body interaction between nucleons to account for those forces not included in the assumption of an average spherically symmetric central potential. Considerable success has been attained by approximating the residual interaction by a

residual force consisting of two separable parts, one having a short range and the other having a long range relative to the average internucleon distance.

The short range part of the residual force is a strong pairing (J=0) interaction between like nucleons. The pairing residual interaction was first treated by Bohr, Mottelson, and Pines (58Bo), Balyaev (59Ba2), and Kisslinger and Sorenson (60Ki, 63Ki) using the mathematical techniques developed by Bardeen, Cooper, and Schrieffer (57Ba) to describe superconductivity. The pairing force couples like nucleons to zero total angular momentum (J=0) and favors spherically symmetric nuclear distributions. The pairing correlations result in each nucleon, on the average, being surrounded by a cloud of like nucleons which causes a shift in the single particle energies. This situation is analogous to that of an ion in a classical liquid. The "nucleon-plus-cloud" is called a quasi-particle. The basis states of a model including the strong pairing force are the shell model states, and the quasi-particle energies, E_J, are given in terms of the original particle energies, ε_J (shell model state energies), by the equation:

$$E_J = \sqrt{(\varepsilon_J - \lambda)^2 + \Delta^2}. \qquad (1)$$

In this equation, λ is the chemical potential ($\simeq$ the fermi energy) which is adjusted to reflect the number of nucleons present in the nucleus, and Δ is approximately the nucleon pairing energy. As in the shell model case, nuclear excitations may result from the promotion of the odd nucleon, in

this case the odd quasi-particle, to a higher energy quasi-particle level.

The long range part of the residual force is usually approximated by a quadrupole (P_2, Q-Q, or J=2) force which acts between pairs of both like and unlike nucleons (quasi-particles or particles) coupling them to a total angular momentum of two (J=2). The effect of the quadrupole force in an even-even nucleus is usually determined by the quasi-particle random phase approximation (QRPA). States with J=2 are generated from a linear combination of all two-quasi-particle configurations of nucleons which can couple to J=2. As a large number of two-nucleon configurations are involved in each excitation, these excited states are referred to as being collective states. These microscopically described states are analogous to macroscopic shape vibrations of the entire nucleus, the energy spacing between groups of excited states being $\hbar\omega$ as calculated for a quantum harmonic oscillator. By analogy with vibrational waves in acoustics, each quantum of vibrational energy is termed a "phonon". Two phonons may be superimposed to obtain (in a spherical even-even nucleus) states with J= 0,2,4; three superimposed phonons will result in states with J= 0,2,3,4,6; etc. Experimentally, the members of the one-phonon and two-phonon (and possibly some of the three-phonon) excitation multiplets in even-even spherical nuclei have been observed and identified. In odd-mass spherical nuclei (e.g., ^{131}I and ^{105}Ag), nuclear excitations may result from the coupling of the

odd quasi-particle (or particle) in its ground state or in an excited state to a vibrational excitation of the even-even "core". In a pairing-plus-quadrupole model the core excitations are calculated microscopically using the QRPA, considering all possible pairs coupling to J=2 from the core, and then the odd quasi-particle is coupled microscopically to the vibrational configuration.

The quadrupole residual force may also be treated in a macroscopic fashion by considering excited states in an odd-mass spherical nucleus as resulting from a coupling between the unpaired nucleon (particle or quasi-particle) and a quadrupole vibration of the even-even core made up of the remaining nucleons. The quadrupole vibration is considered to be harmonic, and the phonon energy is determined experimentally in the even-even "core" nucleus. This model is called the "particle-phonon coupling" or the "intermediate coupling" model, and was originally suggested by Bohr (52Bo). It has been discussed in detail by many authors (e.g., 53Bo, 54Ch, 55Fo, 57La, 61Sh). The interaction between the odd nucleon and the quadrupole vibration is treated phenomenologically as being a function of a spherical harmonic of second order, $Y_{2\mu}(\theta, \phi)$. In this model, multiplets of levels are predicted to lie at $\sim\hbar\omega$ and $\sim 2\hbar\omega$ above the single quasi-particle energies in an odd-mass nucleus. In the limit of no interaction each multiplet is degenerate; however, residual interactions and configuration mixing cause splitting of the multiplets. This model considers

only the quadrupole vibration excitations of the even-even core. A more general particle-core coupling model has been suggested by de-Shalit (61Sh) which couples the unpaired nucleon to the experimentally determined states of the even-even core. Such a model, then, is not restricted to collective vibrational core excitations, but may include other core excitations such as two-proton and two-neutron states. In this model, however, it is necessary to treat the particle-core interaction in a more general way than considering it to be a function of $Y_{2\mu}(\theta, \phi)$.

To explain the level structures of the odd-mass iodine and silver nuclei, four distinct models have been developed as extensions of the shell model. These are: (1.) the pairing-plus-quadrupole model of Kisslinger and Sorenson (60Ki, 63Ki), (2.) the intermediate coupling (single particle plus phonon) model (68Ru), (3.) the dressed three quasi-particle (3QP) model of Kuriyama, Marumori, and Matsuyanagi (71Ku, 72Ku, 74Ku1, 74Ku2, 74Ku3, 74Ku4, 74Ma3), and (4.) the three-particle plus quadrupole vibration model (Alaga model) (67Al, 73Al, 73Pa, 74Ci, 74Va). These models are all based on the shell model but differ principally in five major areas, those being: (1.) whether the model considers nucleons as particles or quasi-particles, (2.) how many (quasi-) particles are treated(1 and/or 3), (3.) how many phonons are explicitly considered (0 to 3), (4.) whether the interaction between particles and phonons is treated microscopically or macroscopically, and (5.) exactly what shell model config-

urations are included in the model. I shall compare and contrast these four theories according to which Feynman diagrams each model considers and how each treats the interactions and configurations depicted in the diagrams. Feynman diagrams are becoming more and more a part of the language of the nuclear theoretician, and their use in nuclear theory has been described in detail by Baranger (67Ba) and by Mattuck (67Ma). Diagrams have the advantage of being essentially pictures of what is happening inside a quantal system in perturbation theory, and, hence, they give some feeling for what physical configurations and processes are being considered by a nuclear model.

In presenting Feynman diagrams I shall adopt the formalism that a line segment will represent a particle or quasi-particle in a specific shell model single particle state, and that a vertex (dot) will represent an interaction (or scattering) in the nucleus. Thus, each vertex represents a matrix element in the perturbation calculation. Figure 1 depicts a particle (a) and a hole (b) propagating in some configuration. As holes and particles are mathematically similar I will generally employ simply an undirected line segment (Figure 1c) to represent either a particle or a hole. (Nota bene: the calculations on iodine (silver) nuclei treat one and/or three particles (holes).) Since the only forces being considered are two body forces, each vertex must have four line segments attached to it as shown in Figure 2. A diagram may be scanned from bottom to top,

Figures

1. Feynman diagram of a particle or hole in some particular shell-model orbital. An undirected line segment (c) will generally represent either case.

2. Feynman diagram depicting a two-body interaction (scattering). Two particles propagating in the shell-model states, 1 and 2, scatter into the states, 3 and 4.

3. Feynman diagram of a one-phonon configuration (a) with several of the microscopic configurations indicated. The wiggly line (b) will generally be employed to indicate a phonon.

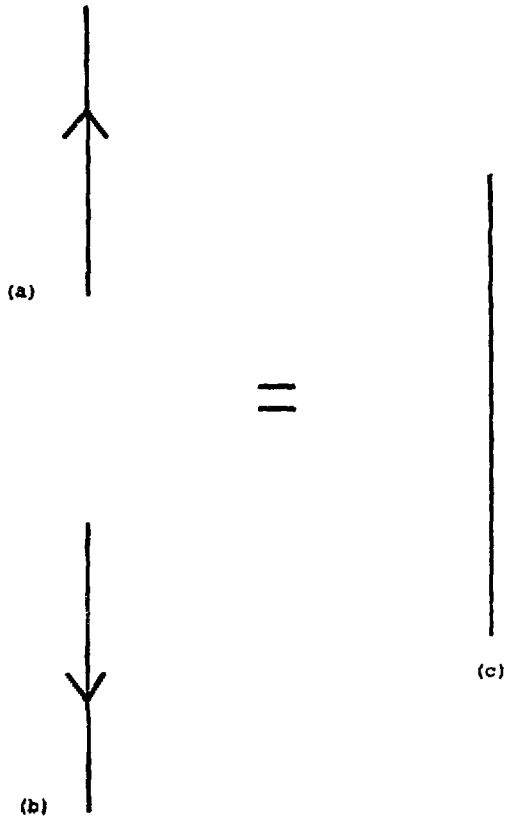
(a)
(b)
(c)

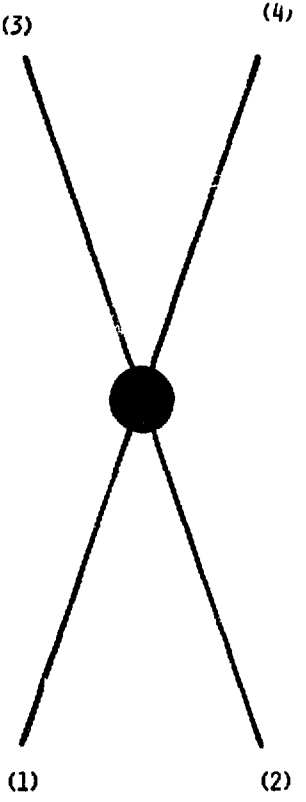
(3)
(4)
(1)
(2)

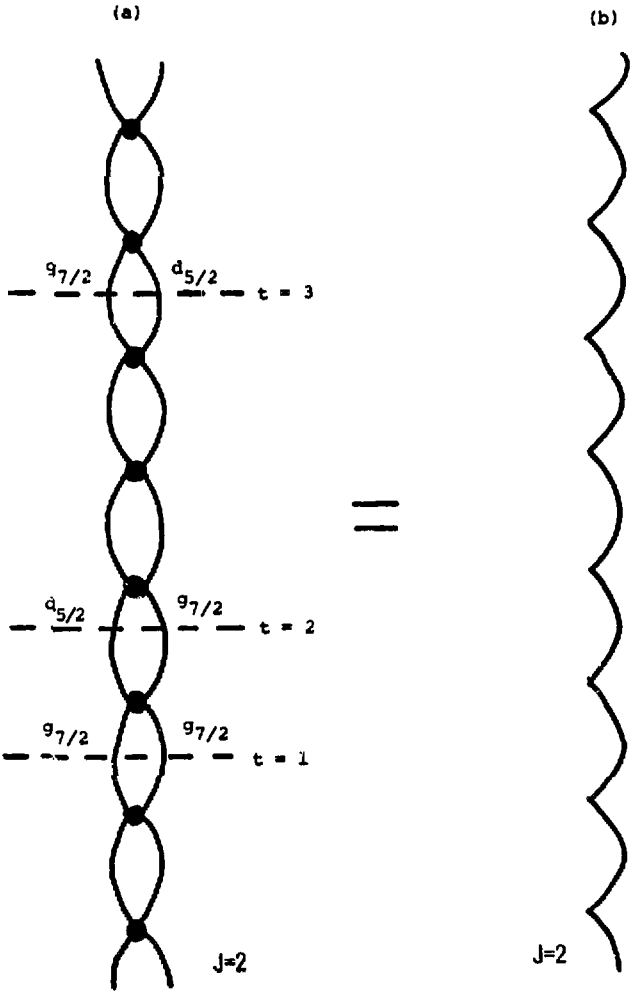
(a)
(b)
$g_{7/2}$
$d_{5/2}$
t = 3
$d_{5/2}$
$g_{7/2}$
t = 2
$g_{7/2}$
$g_{7/2}$
t = 1
J=2
J=2

considering the system as propagating forward in time. Thus, the diagram shown in Figure 2 represents particles in the shell model orbitals "1" and "2"undergoing an interaction and emerging in the single particle states "3" and "4", which may or may not be the same as the original ones.

The configurations depicted in a diagram may be determined by drawing a horizontal line, which may be thought of as giving an instantaneous picture of the nuclear configuration. Figure 3a depicts the Feynman diagram of a single phonon and illustrates some of the possible configurations involved when using as basis states the single particle shell model levels between the "magic numbers", 50 and 82. Note that the total angular momentum is always J=2 and that only two particles at a time participate in the total configuration. At time t=1 the configuration is $(g_{7/2}\ g_{7/2})_2$, and at time t=3, several interactions later, the configuration is $(g_{7/2}\ d_{5/2})_2$. As phonons are often treated in theoretical models as explicit entities, I shall generally depict phonons as wiggly lines as in Figure 3b, noting that microscopically they are two-particle configurations coupled to J=2 by the residual quadrupole interaction.

Before discussing the four theoretical models in detail, it is important to note exactly which shell model levels are of interest for the odd-mass iodine and silver nuclei, all of which are odd-proton nuclei. These are just the shell model levels in the unfilled major shells: $50 < N < 82$

(for Ag and I), $28 < Z < 50$ (for Ag), and $50 < Z < 82$ (for I). The shell model states between 50 and 82 are (in approximate order of increasing energy) $1g_{7/2}$, $2d_{5/2}$, $2d_{3/2}$, $3s_{1/2}$, and $1h_{11/2}$. The shell model states between 28 and 50 are $2p_{3/2}$, $1f_{7/2}$, $2p_{1/2}$, and $1g_{7/2}$. These then or at least some of these, are the basis states for all four theoretical models as applied to silver and iodine nuclei.

The pairing-plus-quadrupole model has already been discussed in some detail above. This model considers only single quasi-particles and up to two phonon excitations. Diagram segments showing the zero, one, and two phonon configurations and interactions included in the model are presented in Figures 1c, 4, and 5. Figure 4, for example, depicts a quasi-particle propagating in time, an interaction (1) which creates a phonon and may or may not change the particle configuration, then an interaction (2) which destroys the phonon leaving only the original single particle configuration, etc. The diagrams in Figure 5 may be interpreted similarly. All legal diagrams consist of sequences of these segments. Note that the requirement of having only two-body forces eliminates any diagram where two phonons are created or destroyed at a vertex. For Ag and I nuclei, the odd quasi-particle is always a quasi-proton in the last unfilled major shell. The phonons are calculated microscopically for the even-even core using the QRPA, and the interaction between quasi-particles and phonons is treated microscopically.

Figures

4. Feynman diagram depicting the configurations and interactions involved in treating one-particle plus one-phonon states.

5. Feynman diagrams showing the possible configurations and interactions when treating two-phonon states.

6. Feynman diagrams showing the possible configurations and interactions when treating three-phonon states. The numbers indicate the number of phonons present at a particular instant in time.

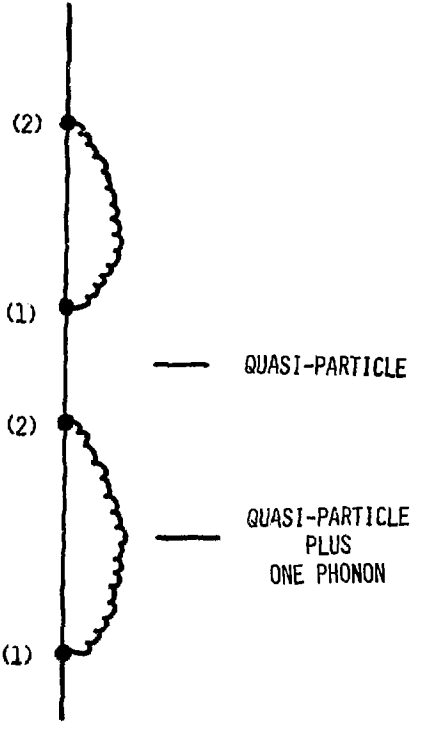
(2)
(1)
QUASI-PARTICLE
(2)
QUASI-PARTICLE
PLUS
ONE PHONON
(1)

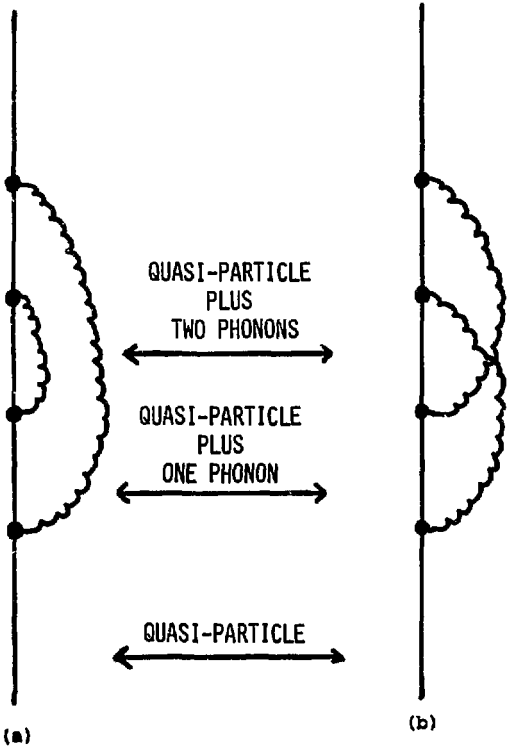
QUASI-PARTICLE
PLUS
TWO PHONONS
QUASI-PARTICLE
PLUS
ONE PHONON
QUASI-PARTICLE
(a)
(b)

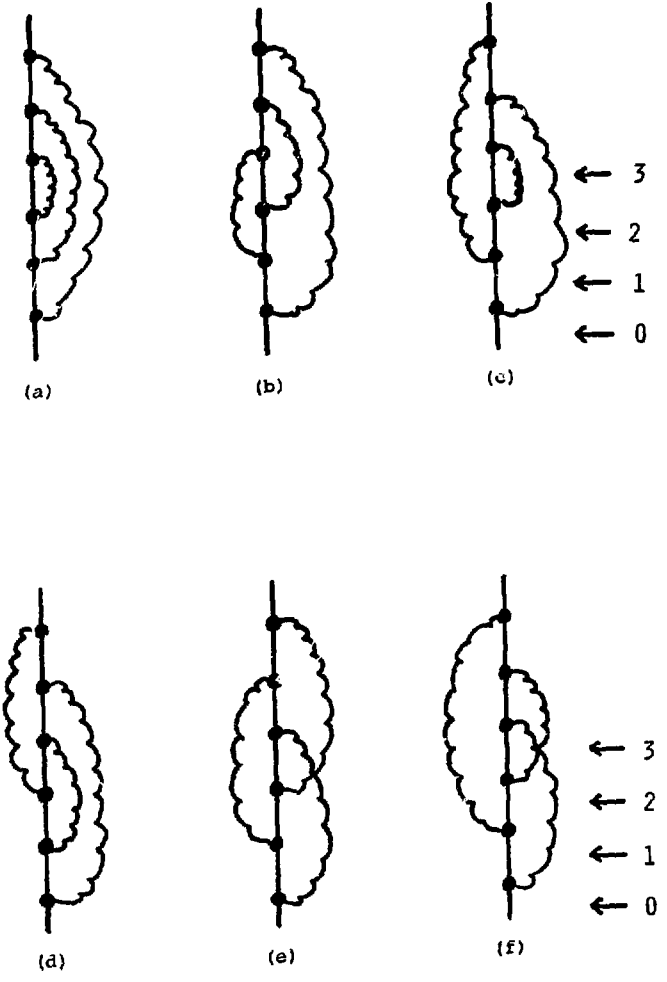
(a)
(b)
(c)
3
2
1
0
(d)
(e)
(f)
3
2
1
0

The intermediate coupling model as applied by Rustgi et al. (68Ru) considers single particles and up to three phonon excitations. The diagrams included in this model, then, are those shown in Figures 1, 4, and 5 as well as the set of three-phonon diagrams presented in Figure 6. The line segments in this model represent particles (instead of quasi-particles) in the proton valence orbitals. The phonons are macroscopic phonons as determined from the experimental states of the even-even core, and the interaction between a phonon and a particle is treated macroscopically as a function of $Y_{2\mu}(\theta,\phi)$.

These two models, treating one particle or quasi-particle plus several phonons, have some degree of success in predicting the level structures of the odd-mass iodine and silver nuclei (e.g., see Figure 36). One of their major failings, however, is their inability to explain the low-lying second $5/2^+$ state observed in odd-mass iodine nuclei and the very low-lying first $7/2^+$ state observed in odd-mass silver nuclei. It has been observed that in odd-mass spherical nuclei in which a large spin (J) shell model level of opposite parity is being filled, there occurs a low-lying state of spin J-1. These states have been termed "anomalous coupling states", and their position and properties have not been explained by pairing-plus-quadrupole or intermediate coupling calculations. Models have been developed which explicitly consider three particles (or quasi-particles) distributed among the shell model valence orbitals. These

models, the 3QP model and the Alaga model, explain the anomolous coupling states as having the dominant configuration, $(J)^3_{J-1}$.

The dressed three quasi-particle model of Kuriyama et al. treats both one- and three-quasi-particle configurations and includes both a pairing and a quadrupole force. The three quasi-particles may be either three quasi-protons or one quasi-proton plus two quasi-neutrons. Thus, both the proton and the neutron shell model valence orbitals are included in the configuration space. A great many different diagrams are included in this model, all the segments of which are presented in Figure 7. In essence, all diagrams are allowed which have one or three quasi-particles present and which have vertices representing J=0 (pairing) and J=2 (quadrupole) interactions. The model also includes backwards amplitudes to introduce ground state correlations, however, these are not of crucial importance in treating odd-mass nuclei. No phonon excitations are explicitly included in the model, however, configurations and interactions which are essentially quasi-particle plus phonon in character are treated by the inclusion of a large number of shell model orbitals in the configuration space. By chaining together the proper segments from Figure 7, a diagram may be constructed which is essentially equivalent to the diagram in Figure 4. This is illustrated in Figure 8, in which 8a is essentially equal to 8b as long as 8a includes sufficient quasi-particle configuration combinations in the pair correlated by the J=2 residual interaction.

Figures

7. The Feynman diagram segments (showing configurations and interactions) which are included in the dressed three quasi-particle model of Kuriyama et al. (71Ku). (Backwards amplitude diagrams have not been included here).

8. Feynman diagram of a series of microscopic J=2 two-particle interactions with one spectator particle (a) as treated by the dressed three quasi-particle model. If enough two-particle configurations are included, then the microscopic picture (a) is approximately equivalent to a phonon, shown macroscopically in (b).

9. The microscopic exchange diagram included in the dressed three quasi-particle model.

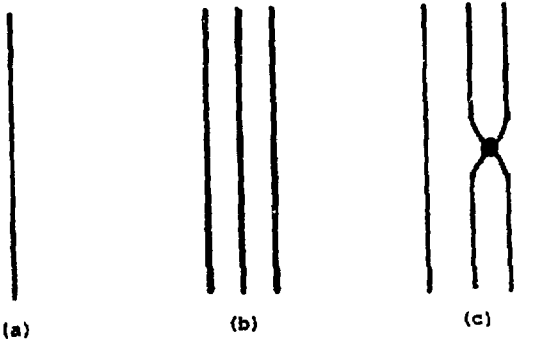
(a)
(b)
(c)
(d)
(e)

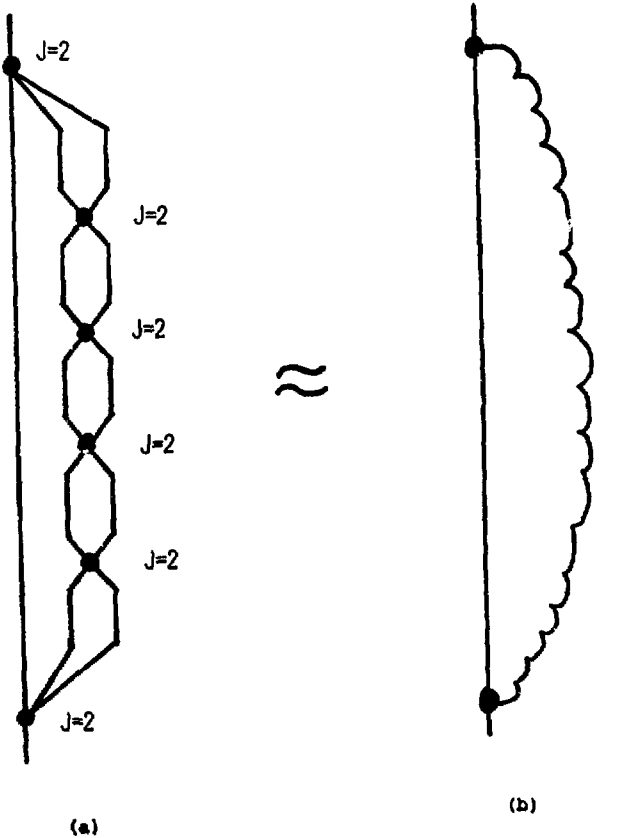

(a) (b)

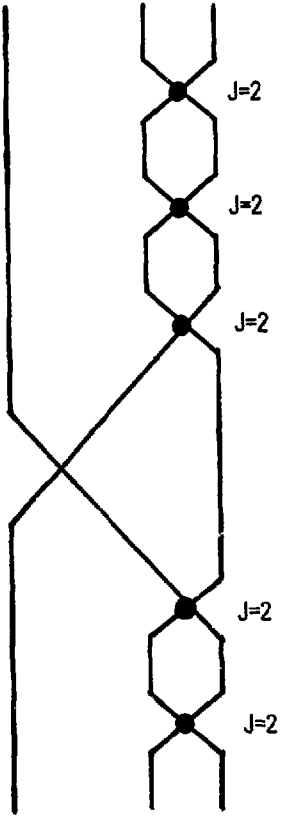
J=2
J=2
J=2
J=2
J=2

The treatment of the T=2 interaction in a three quasi-particle configuration in a detailed microscopic fashion and the inclusion of backwards amplitudes results in the 3QP model considering a quasi-particle plus phonon diagram (Figure 4) as well as a large number of additional diagrams. Of particular importance among the new diagrams is the so called exchange diagram depicted in Figure 9. This diagram, in essence, mixes the odd quasi-particle with the phonon, thereby explicitly including the interference of the odd quasi-particle and the phonon excitation. The pairing-plus-quadrupole model and the intermediate coupling model do not consider this diagram, as they determine the phonon from either calculating or observing the even-even core and thus, have no way of including the odd quasi-particle in their phonon excitation. This, therefore, results in a violation of the Pauli principle, because, microscopically, there are configurations in their diagrams in which the odd quasi-particle is also a part of the phonon.

The inclusion of the exchange diagram (Figure 9) in the 3QP model precludes any violation of the Pauli principle, and the calculation of this diagram has a marked effect, particularly when the three quasi-particles are in the same shell model orbital. In this case the Racah coefficient which arises in the coupling calculation results in the energy of the J-1 state being greatly reduced relative to the other four possible total couplings (J-2, J, J+1, J+2). This effect is particularly large for nuclei in which

pairs of nucleons in one particular orbital make a large contribution to the J=2 phonon state. This is precisely the case for nuclei which are filling the large spin opposite parity levels between shell closures. In the silver nuclei, for example, the $1g_{9/2}$ shell model orbital, which is being filled, provides the principal proton configuration contribution to the 2^+ phonon, and hence, a low-lying J-1 = 7/2 level is predicted. Thus, the explicit treatment of the exchange diagram arising from three quasi-particles interacting via a quadrupole force leads to an understanding of the anomolous coupling state. In the odd-mass silver nuclei the low-lying $7/2^+$ state is seen as predominantly $(1g_{9/2})^3_{7/2}$ in character. In the iodine nuclei, the second $5/2^+$ state is interpreted as being principally $(1g_{7/2})^3_{5/2}$ in character. The effect in iodine nuclei is not as marked as in silver, however, because in the iodine nuclei, proton orbitals other than $1g_{7/2}$ make major contributions to the quadrupole vibration.

Like the 3QP model, the Alaga model explicitly considers three-proton configurations, and this results in the same interpretation of the anomolous coupling states. However, the details of the model are very different. The Alaga model treats nucleons as particles, and considers only three-proton configurations using the $2p_{1/2}$, $2p_{3/2}$, and $1g_{5/2}$, basis states in the case of silver or the $3s_{1/2}$, $2d_{3/2}$, $2d_{5/2}$, and $1g_{7/2}$ basis states in the case of iodine. Up

to three phonons are explicitly considered, and the interaction between a particle and a phonon is treated macroscopically. Only the pairing interaction is treated microscopically by the model, whereas the quadrupole residual interaction is effectively included by renormalizing the coupling strength between a particle and a phonon. It should be noted that in this three particle plus quadrupole vibrator model the phonon excitation ($\hbar\omega$) is that of the tin core, three proton particles (holes) removed from iodine (silver).

The diagrams included in the framework of the Alaga model depict three particles and up to three phonons. Some examples of diagrams considered by the model are shown in Figure 10. The allowed three particle segments, Figures 10a and 10b, are the same as the two in Figures 7b and 7c, with the dot representing only a J=0 interaction. The phonon segments of the diagrams, Figures 10c and 10d, include all those shown in Figures 4,5,and 6 (with the addition of two spectator particles) as well as all possible combinations in which a phonon is created in an interaction with one of the three particles and destroyed in an interaction with another, Figures 10e through 10i.

While no quadrupole residual interaction is explicitly included in the model, an effective quadrupole interaction between pairs of nucleons is treated by the inclusion of interactions such as that shown by the diagram in Figure 11. The circled region may be regarded as a "macroscopic vertex",

Figures

10. Example diagrams included in the Alaga mode. All diagrams depict three particles (holes) and up to three phonons.

11. Feynman diagram depicting a J=2 interaction in the framework of the Alaga model. The circled region may be thought of as a "macroscopic" vertex.

12. The exchange diagram included in the Alaga model. This "macroscopic" diagram is topologically equivalent to the exchange diagram in Figure 9.

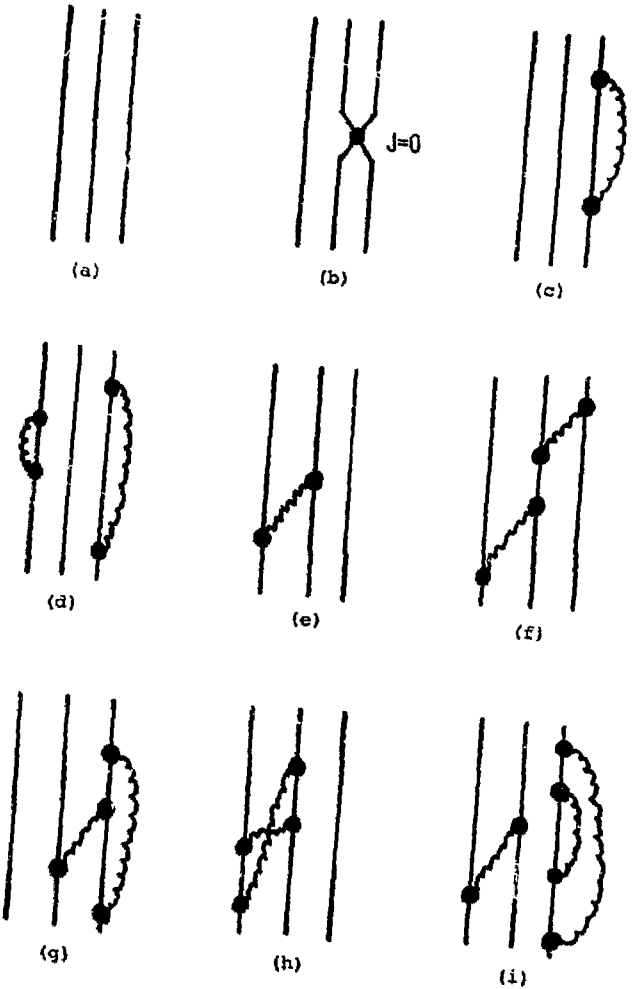
J=0
(a)
(b)
(c)
(d)
(e)
(f)
(g)
(h)
(i)

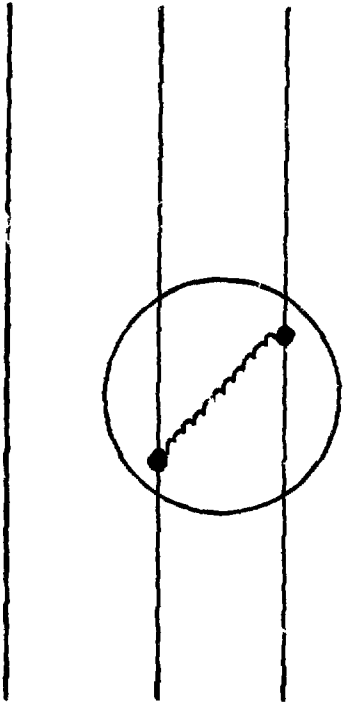

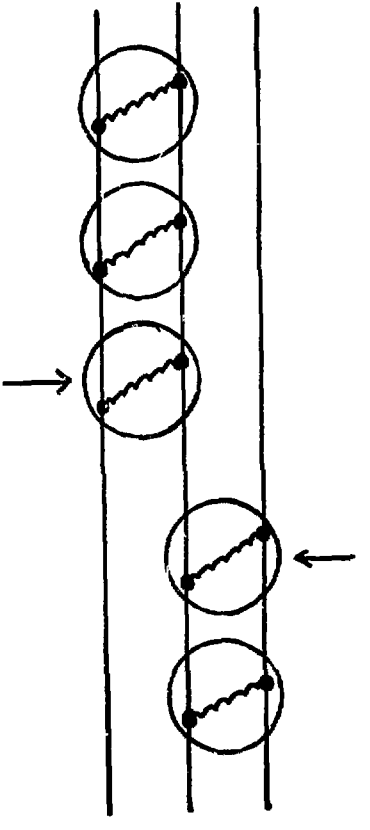

with the two particles correlated by a macroscopic J=2 interaction. The phonon "exchange" between particles may be thought of as analogous with the pion exchange between nucleons in the bare nucleon-nucleon interaction. (In the diagrams I have been presenting, the details of the pion exchange are "hidden" in the black vertices.) In the detailed calculation, the particle-phonon coupling strength is renormalized to effectively reproduce the quadrupole contribution to the residual interaction. The configuration in Figure 11, then, is effectively a particle-plus-phonon configuration. This fact leads directly to the important exchange diagram included in this model, the calculation of which leads to the anomolous coupling states. This diagram is pictured in Figure 12. It is the macroscopic equivalent of the exchange diagram in Figure 9, which may be seen if one were to take the diagram in Figure 12, blacken the circles, and then twist the diagram by 180° at each of the "macroscopic vertices" indicated by arrows. (Nota bene: The size or shape of a Feynman diagram has no significance; rather, the important property of a Feynman diagram is its topology, i.e., the way in which the various lines are connected together. If one can form a new diagram by twisting it 180° out of the page at a vertex, then the new diagram is identical to the old diagram.)

In summary, the four principal theoretical models all explain many features of the odd-mass iodine and silver level schemes. The three-particle theories represent a step

taken to correct for the Pauli principle violation inherent in the single-particle theories. As a result of this correction, they are able to explain the experimentally observed anomolous coupling states. The dressed three quasi-particle model of Kuriyama et al. is perhaps to be preferred over the Alaga model as it considers quasi-particles, performs a consistently microscopic calculation, and has a large single particle configuration space and can thus, in principle, calculate levels having configurations which cannot be considered by the Alaga model (e.g., $\pi\nu^2$ states and single quasi-particle states in the odd-mass silver and iodine nuclei). It should be noted, however, that the 3QP model cannot treat two-phonon or three-phonon excitations, as these would require the explicit treatment of five quasi-particles and seven quasi-particles, respectively. At present these models have calculated only states having configurations involving proton(s) and proton(s) plus phonon(s) and these calculations have been limited to states having relatively low excitation energies and spin values.

This study of the levels of ^{131}I and ^{105}Ag as observed in radioactive decay was initiated in order to provide nuclear structure data with which to test the theoretical models being applied to the odd-mass iodine and silver nuclei. The large β-decay Q-values involved allow the population of excited states which thus far have not been calculated by the models. Thus, this investigation was also undertaken in order that the results might provide a guide for future development of the theoretical models.

II. APPARATUS AND TECHNIQUES

A. Detectors.

During the course of this investigation, lithium-drifted germanium, Ge(Li), semiconductor detectors were employed in γ-ray spectroscopic studies which included direct γ-ray singles spectroscopy, Compton anti-coincidence γ-ray spectroscopy, and two-parameter γ-γ coincidence spectroscopy. A large number of different detectors were used, all of which were available from commercial suppliers. The Ge(Li) crystals were mounted in vacuum-sealed cryostats and cooled to liquid nitrogen temperature with a copper dipstick. Required high voltage bias for the crystals ranged from 1000 to 4000 volts of a specific polarity. X-rays and low energy γ-rays (typically $\lesssim$200 keV) were observed with small volume planar Ge(Li) x-ray detectors. These detectors typically had an active volume of ~0.5 cm^3, a thin beryllium window, and a full width at half maximum (FWHM) resolution of ~0.5 keV for the 59.5-keV γ-ray of ^{241}Am. Higher energy γ-rays ($\gtrsim$100 keV) were observed with a wide variety of larger volume Ge(Li) detectors of both the true coaxial crystal and the closed-end crystal types. These detectors ranged in size from 7 cm^3 to 80 cm^3 and in FWHM from 1.8 keV to 2.8 keV for the 1332-keV γ-ray of ^{60}Co . They had

rated efficiencies relative to a 3" by 3" NaI(Tl) detector ranging from ~1% to ~16% for the 1332-keV ^{60}Co γ-ray counted at a source-detector distance of 25 cm.

B. Gamma-Ray Singles Spectroscopy.

In direct γ-ray singles spectroscopy, pulses from the Ge(Li) crystals were initially amplified by integrally mounted low-noise field-effect transistor (FET) preamplifiers. Preamplifier output pulses were shaped and amplified by commercially available linear pulse amplifiers including the CANBERRA 1413 (Canberra Industries) and the ORTEC 450 and 452 (Ortec, Inc.) amplifiers. The analog pulses from these amplifiers were analyzed by either a 4096- or 8192-channel analog-to-digital converter (ADC), which converted the analog signal (0-10 volts) linearly to a digital address (0-4095 or 0-8191) and then added one to that address in a 4096- or 8192-word computer memory. At the end of a count, then, the direct γ-ray singles spectrum was stored in the computer memory and displayed on an oscilliscope. The output modes available to any one memory were digital printer, teletype, x-y analog plotter, and computer-compatible magnetic tape deck.

Gamma-ray singles spectra were also observed in a Compton anti-coincidence mode using a Compton-suppres-

sion spectrometer. This system has been described in detail elsewhere (69Ca) . A 7 cm^3 planar Ge(Li) detector (FWHM of 2.0 keV at 1332 keV) was mounted in a NaI(Tl) anti-Compton annulus consisting of two 9" by 13" NaI(Tl) crystals. Most Compton-scattered γ-rays escaping from the Ge(Li) crystal were observed in the NaI(Tl) crystals. Amplified pulses from the associated photomultiplier tubes were appropriately timed and delayed to provide an anti-coincidence gate pulse for the ADC. In this manner, then, the observation of Compton events in the central Ge(Li) detector was greatly reduced. The peak-to-minimum continuum value for this system was measured to be 640 to 1 for the 662-keV γ-ray of ^{137}Cs. This corresponds to a Compton-suppression factor of ~12 or a removal of 92% of the Compton events. The resulting increase in the signal-to-background ratio allowed the observation of numerous weak γ-ray transitions which could not be observed in direct singles spectra.

C. Two-Parameter γ-γ Coincidence Spectroscopy.

Two different two-parameter analysis systems were used in this study. At the Lawrence Livermore Laboratory (LLL) γ-γ coincidence data were accumulated using two large volume (~50-60 cm^3) Ge(Li) detectors in close proximity. Both detectors were of the true

coaxial type as this detector design results in the shortest and least varying pulse rise time and hence is best for fast-timing applications. Radiation sources were placed ~5 cm away from the detector faces such that an angle of 90° was formed by the positions of the source and the Ge(Li) crystals. A Pb absorber was placed between the detectors to reduce "detector cross-talk" which results from the observation of photons which were Compton scattered from one detector to the other. The electronic apparatus for this system is shown in Figures 13, 14, and 15.

As shown in Figure 13, the pulses from the Ge(Li) crystals were first amplified by FET preamplifiers, the outputs of which were split for simultaneous energy and timing resolution. The energy pulses were amplified by ORTEC 450 amplifiers and shaped so as to optimize energy resolution. The amplifier output signal from one detector was sent to a TENNELEC TC 592P Digital Rate Meter (Tennelec, Inc.) to allow continuous monitoring of the singles count rate in the detector. The output signals from both amplifiers were then routed through CANBERRA 1464 Base Line Restorer/Pile-up Rejectors to optimize the energy resolution at high count rate. The Restorer/Rejectors and the CANBERRA 1457 Delay Amplifiers delayed the

energy signals relative to the timing signals in order to meet the timing criteria of the TENNELEC TC 621 Stretcher Multiplexers as these units required the logical gate pulses to precede the linear energy pulses. With a logical gate pulse present, the Stretcher Multiplexers held the energy signals for analysis by the two-parameter analysis system (shown in Figure 14).

The timing pulses from the preamplifiers were sent to the ORTEC 454 Timing Filter Amplifiers which appropriately shaped and amplified them for analysis by the ORTEC 463 Constant Fraction Timing Discriminators. The ORTEC 463 timing modules operate on the "amplitude rise-time-compensation" timing technique (ARC timing) which, as its name implies, compensates for the timing "walk" which is the result of variations in preamplifier pulse height and rise time. This technique is more precise than leading-edge or zero-crossover timing. The fast timing logic signals from the ORTEC 463 units were sent to a LeCROY 108H Time-to-Amplitude Converter (TAC) (LeCroy Research Systems, Inc.) with one signal being a "start" pulse and the other being a "stop" pulse. The "stop" pulse was delayed for ~30-60 nsec by one or more CANBERRA 1458 Delay Units in order to insure that it arrived at the TAC after the "start"

pulse. The TAC produced output pulses proportional to the time difference between the "start" and "stop" pulses. The TAC output pulses were then analyzed by a CANBERRA 1431 Single Channel Analyzer (SCA) which was set to give an output pulse only for an input pulse which was a prompt γ-γ coincidence (~ '15 nsec from the prompt coincidence in ^{60}Co decay). Each logic pulse output from the SCA, then, represented a γ-γ coincidence and was sent to the TENNELEC TC 520 Multiplex Control to provide a logical gate pulse for the stretcher multiplexers and the two-parameter analysis system. The SCA pulses were also sent to a CANBERRA 1774 Dual Scaler which kept track of total coincidence events and to a CANNBERRA 1776 Dual Counter/Timer which continuously monitored the coincidence rate.

With gate pulses present the coincident events held in the stretcher multiplexers were subjected to a two-parameter analysis by the system shown in Figure 14. The TENNELEC TC 501 ADC processed first the "start" side energy signal and then the "stop" side signal, converting the 0-10 volt analog signals linearly to digital addresses, 0 to 8191. These pairs of numbers were stored in the PDP 11/05 Computer (Digital Equipment Corp., Inc.), and when 186 pairs had been accumulated they were recorded on computer compatible mag-

Figures

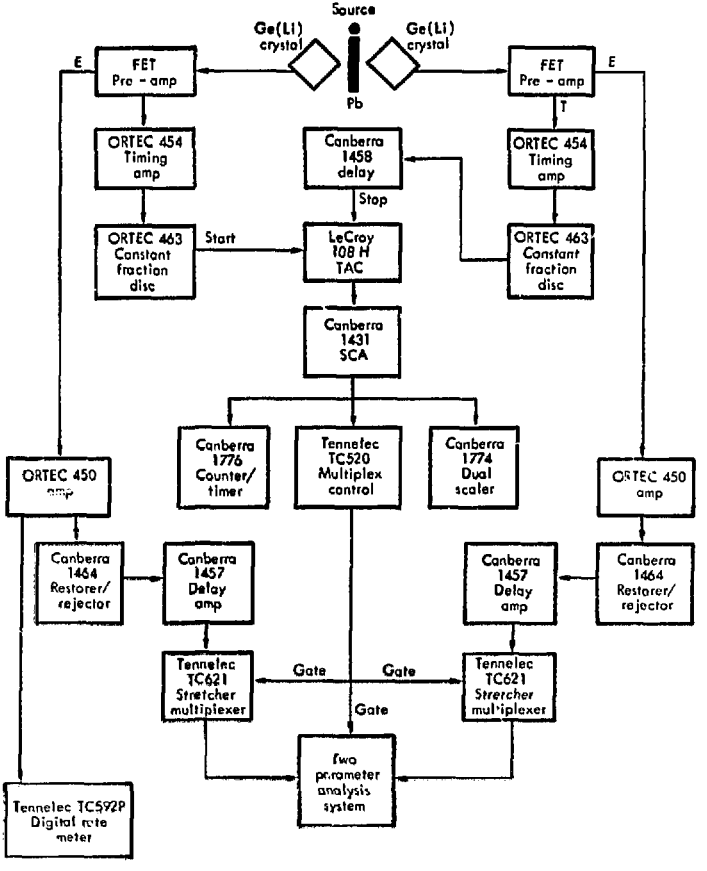
Source
Ge(Li) crystal
Ge(Li) crystal
Pb
E
FET Pre - amp
FET Pre - amp
E
T
ORTEC 454 Timing amp
Canberra 1458 delay
ORTEC 454 Timing amp
Stop
ORTEC 463 Constant fraction disc
Start
LeCroy 108 H TAC
ORTEC 463 Constant fraction disc
Canberra 1431 SCA
Canberra 1776 Counter/ timer
Tennelec TC520 Multiplex control
Canberra 1774 Dual scaler
ORTEC 450 amp
ORTEC 450 amp
Canberra 1464 Restorer/ rejector
Canberra 1457 Delay amp
Canberra 1457 Delay amp
Canberra 1464 Restorer/ rejector
Tennelec TC621 Stretcher multiplexer
Gate
Gate
Tennelec TC621 Stretcher multiplexer
Gate
Two parameter analysis system
Tennelec TC592P Digital rate meter

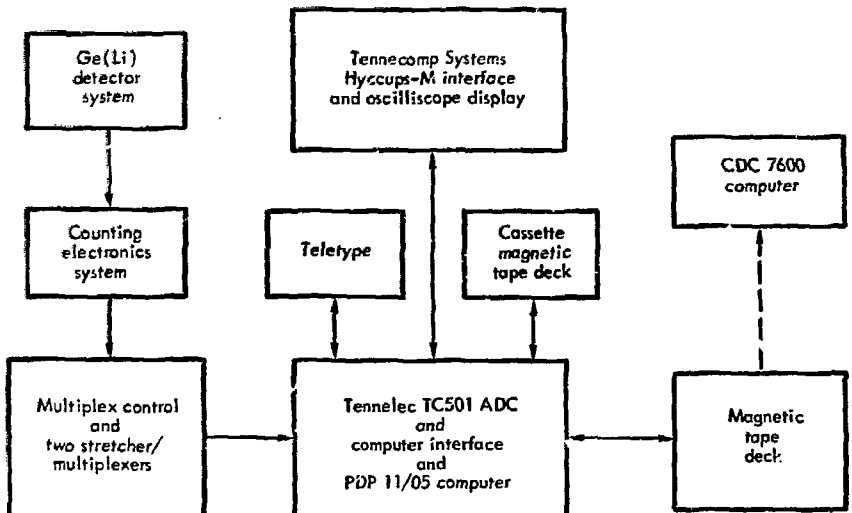
Ge(Li) detector system
Tennecomp Systems Hyccups-M interface and oscilliscope display
CDC 7600 computer
Counting electronics system
Teletype
Cassette magnetic tape deck
Multiplex control and two stretcher/ multiplexers
Tennelec TC501 ADC and computer interface and PDP 11/05 computer
Magnetic tape deck

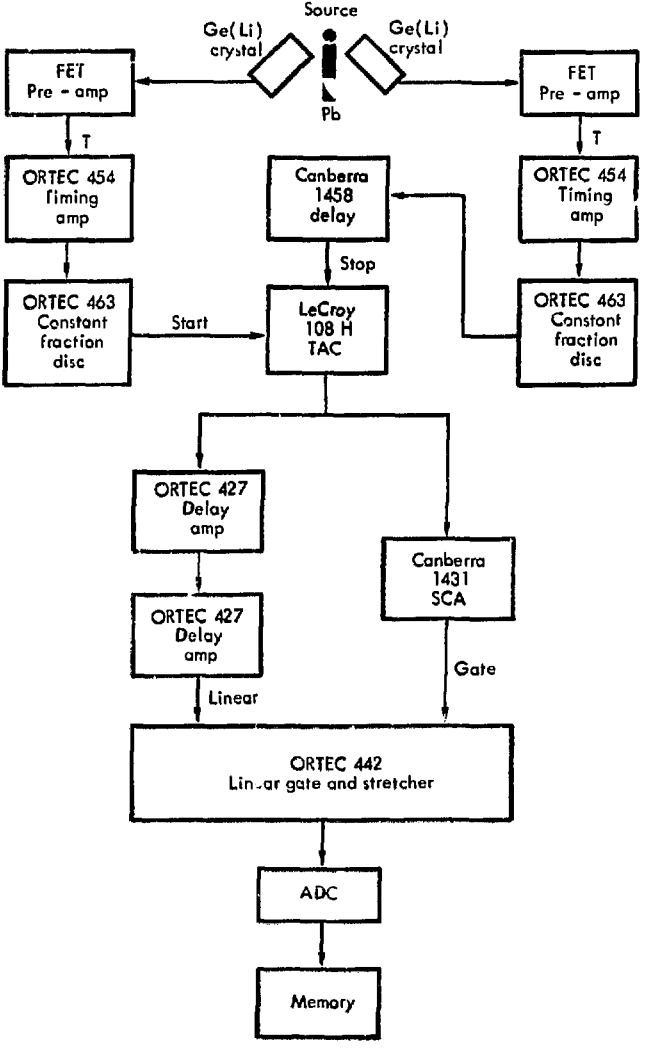
Source
Ge(Li) crystal
Ge(Li) crystal
Pb
FET Pre - amp
FET Pre - amp
T
T
ORTEC 454 Timing amp
Canberra 1458 delay
ORTEC 454 Timing amp
Stop
ORTEC 463 Constant fraction disc
Start
LeCroy 108 H TAC
ORTEC 463 Constant fraction disc
ORTEC 427 Delay amp
Canberra 1431 SCA
ORTEC 427 Delay amp
Gate
Linear
ORTEC 442 Linear gate and stretcher
ADC
Memory

netic tape. One 2400-ft magnetic tape recorded approximately 3.8×10^6 coincidence events. This tape could be "played back" into the PDP 11/05 Computer or taken to the LLL CDC 7600 Computer System for analysis. During operation, communication between the operator and the computer was performed via a teletype terminal. Computer programs were read in from either punched paper tape or magnetic tape cassettes. As well as recording all coincidence pairs on magnetic tape, the computer also stored the any-coincidence spectra from each of the detectors and displayed them on an oscilloscope display in various formats as determined by the TENNECOMP HYCCUPS-M Interface (Tennecomp Systems, Inc.) under the control of the operator.

The timing "window" used to determine γ-γ coincidences was set on the SCA by using the electronics system shown in Figure 15. From the detectors to the TAC this system was the same as the timing portion of the system shown in Figure 13. The TAC output was then split with one signal going to the SCA as before and the other being routed through two ORTEC 437 Delay Amplifiers with the delay set so that the SCA logic output signal and the delayed TAC signal occurred simultaneously. The delayed TAC output was then sent to the linear input of an ORTEC 442 Linear Gate and Stretcher and the SCA logic output was used as a gating

signal. In an ungated mode the linear gate output, when analyzed by an ADC, resulted in a time spectrum showing a sharp prompt coincidence peak on a plateau background of random coincidences. By operating the linear gate in a gated mode, the SCA was set to accept only TAC pulses in the prompt coincidence peak.

The Ge(Li) detectors used with this γ-γ coincidence system had optimum FWHM energy resolutions of 2.3 and 2.5 keV at 1332 keV. However, because of a wide variety of factors, including high count rate, poor gain stabilization due to poorly stabilized room temperature, and the required use of the CANBERRA 1417 Delay Amplifier in the energy analysis portion of the system, the effective energy resolutions over a long experiment (>12 hours) were 3.0 and 3.3 keV. The singles count rate was held between 9000 and 14,000 counts/sec at which rate the coincidence rate (for ^{105}Cd) was ~2200-2700 coincidences/min. Under these conditions the prompt γ-γ coincidence peak in the time spectrum had a FWHM time resolution of ~15 nsec and a full width at tenth maximum (FW.1M) of ~35 nsec. The SCA timing gate was set at the FW.1M limits resulting in a real-to-random coincidence ratio of ~15 to one. The energy range which could be observed under these conditions was approximately 150 to 3000 keV.

The second two-parameter γ-γ coincidence system

used in this investigation was located at the University of Maryland (UM) and was quite similar in principle to the one just described. A detailed description of the exact system has been presented elsewhere (71Apl) with the exception that a 26 cm^3 Ge(Li) detector has been replaced with one of larger volume. The detectors used with this system were true coaxial Ge(Li) detectors with active volumes of 55 cm^3 and 65 cm^3, both having a FWHM energy resolution of 2.1 keV for the 1332-keV ^{60}Co γ-ray. The timing criteria between the energy signals and the gating signals were much less stringent with this system, hence this system did not require either the restorer/rejectors or the delay amplifiers. This fact, along with the location of the system in a thermally stabilized room, resulted in no appreciable deterioration in detector energy resolution under experimental conditions. The use of ORTEC 453 Constant Fraction Timing Discriminators instead of ORTEC 463 modules resulted in an energy acceptance range of approximately 50 keV to 3000 keV and a timing resolution of ~11 nsec FWHM and ~23 nsec FW.1M. With the SCA timing gate set at the FW.1M limits, a singles count rate of ~10,000 counts/sec. and a coincidence rate (for $^{131}Te^{m+g}$) of ~2600 coincidences/min., the real-to-random coincidence ratio was measured to be ~27 to one.

D. Analysis of Data

The large amounts of data acquired in γ-ray spectroscopic studies virtually necessitate some form of computerized data analysis. In this investigation, a typical γ-ray singles spectrum had 150-300 γ-ray peaks in it, many of which were close multiplets. Hence, the γ-ray singles spectra and the Compton-suppressed spectra were analyzed on the LLL CDC 7600 computer systems using the LLL spectrum analysis computer code, "GAMANAL," which has been described in detail elsewhere (71Gu) . This code processes the raw spectral data, finding γ-ray peaks, fitting them to a skewed-Gaussian function, and integrating them. In determining γ-ray energies and intensities it takes into consideration a large variety of possible experimental configurations (e.g., source-detector geometry, source self-absorption, any absorbers present, detector dead-time etc.) and a variety of detector-analyzer characteristics which have been previously determined (e.g., ADC non-linearity, detector efficiency as a function of energy, Ge(Li) crystal configurations, etc.). Its output includes a listing of γ-rays observed which gives energies, energy uncertainties, absolute γ-ray intensities in photons/min, intensity uncertainties, and a measure of the quality of the peak fit, and may include, at the user's option, a

wide variety of spectrum plots ranging from labeled plots of the entire spectrum to detailed plots of the fitting of each peak. Some singles spectra taken at UM were analyzed on the UM UNIVAC 1108 computer system using computer codes developed at UM (7 Go , 73Vi) or written by myself (see Appendix I).

A typical two-parameter γ-γ coincidence experiment involved the acquisition of several millions of address pairs (coincidence events). Analysis of this data entailed the determination of the γ-ray spectra in one detector (e.g., the "stop" detector, labeled "Y") which were coincident with specific energy regions (gates or slices) in the other detector (e.g., the "start" detector, labeled "X"). The γ-γ coincidence data taken with the UM two-parameter coincidence system were processed on the UM UNIVAC 1108 computer system, employing computer codes which I developed. The principles of these programs and the mechanics of their use are described in Appendix I, Section B. Similar computer codes were developed by Dr. J. T. Larsen (75La2) to process data from the LLL two-parameter coincidence system using the LLL CDC 7600 computer systems.

Gamma-ray energies were determined by obtaining spectra simultaneously from samples and known γ-ray standards on one or more of the detector-analyzer

systems. A high-order polynomial energy calibration curve was fit by the method of least-squares to the energy versus peak centroid data by using either "GAMANAL" (71Gu) or "CALIB4" (see Appendix I). Energies of low-intensity γ-rays were determined from long counts in which the previously determined energies of strong γ-rays were used as internal standard energies. Quoted uncertainties in energies are statements of the standard deviation and include the uncertainty in the system non-linearity which was determined from the energy calibration curve. The γ-ray energy standards used included ^{22}Na, ^{24}Na, ^{56}Co, ^{57}Co, ^{60}Co, $^{110}Ag^{m}$, ^{113}Sn, ^{125}Sb, ^{133}Ba, ^{137}Cs, ^{182}Ta, ^{192}Ir, ^{203}Hg, ^{207}Bi, ^{228}Th, and ^{241}Am. The precision energy values of Tirsell and Multauf (72Ti), Greenwood et al. (70Gr, 71He), and Meyer (74Me2) were used.

Relative and absolute γ-ray intensities were determined by "GAMANAL" by correcting peak areas for source-detector geometry, sample self-absorption, detector characteristics (e.g., the thickness of the "dead" region on the Ge(Li) crystal surface), and the relative photopeak efficiency of the Ge(Li) detector. The determination of the relative efficiency curves for Ge(Li) detectors has been described in detail elsewhere (e.g., 71Gu , 71Apl , 69Zo). It involves the analysis of spectra from γ-ray standards of known absolute intensity as well as from radioactive species

emitting many γ-rays with well-known intensity ratios. Quoted uncertainties in intensity values are one standard deviation as determined from the peak fit and integration. To obtain uncertainties in absolute intensities an uncertainty of 2%, representing the uncertainty in the detector relative efficiency curves, must be added in quadrature.

III. DECAY SCHEMES OF 30-hr $^{131}Te^{m}$ AND 25-min $^{131}Te^{g}$

A. Introduction.

The iodine nuclei, with three protons beyond the closed shell at Z=50 and neutron number approaching the closed shell at N=82, offer the opportunity to examine the structure of nuclei with limited seniority. There has been much recent experimental work on the level structures of ^{127}I and ^{129}I. This has included the study of the decay of $^{127}Te^{m+g}$ (70Apl, 71Apl), the study of the decay of $^{129}Te^{m+g}$ (72Wa, 74Mal), the study of γ-ray angular correlations in ^{129}I (74De), the study of the $^{126,128}Te(^{3}He, d)$ $^{127,129}I$ reactions (68Au), and the study of the Coulomb excitation of ^{127}I and ^{129}I (73Re). In addition there have been several recent theoretical studies which have dealt with single particle plus phonon (68Ru), three quasi-particle plus phonon (73Al, 73Pa, 74Ci, 74Va), and dressed three quasi-particle (71Ku, 72Ku, 74Kul, 74Ku2, 74Ku3, 74Ku4, 74Ma3) states near the Z=50 closed shell. The decays of $^{131}Te^{m}$ and $^{131}Te^{g}$ to levels in ^{131}I are of particular interest because of the increased Q_{β} values (relative to ^{127}Te and ^{129}Te) which allow the observation of levels at higher excitation energies. A knowledge of the levels of ^{131}I allows the extension of the systematics of the level structures of the odd-mass neutron excess iodine isotopes. The systematics of the energy levels and their

electromagnetic decay properties provide both a valuable check of the theoretical work as well as a guide to further theoretical development.

The structure and properties of the high spin ($J \geq 7/2$) excited states of ^{131}I observed in the decay of 30-hr $11/2^-$ $^{131}Te^m$ were first studied by Hebb (55He) and by Badescu et al. (59Ba, 61Ba). More recent studies, employing Ge(Li) detectors and Ge(Li)- NaI(Tl) coincidence spectrometers, were performed by Devare, Singru, and Devare (65De) and by Beyer, Berzins, and Kelly (67Be1). The multipolarities of several of the transitions were established by studies of the internal conversion electron spectrum associated with the decay of $^{131}Te^m$ (65De, 67Be2). Two isomeric states have been observed in ^{131}I, one at 149.7 keV and the other at 179? keV, with half-lives of 0.75- nsec (71Ma1) and 6.0- nsec (65De, 70Ap2), respectively. In addition, the g-factors of these two states were measured and found to be +1.11 and -0.16, respectively (67Ta). The resulting decay scheme for $^{131}Te^m$, however, contained many ambiguities as to spin and parity assignments of the ^{131}I levels. To a large extent, these ambiguities resulted from the use of small volume, low resolution Ge(Li) detectors and the use of a NaI(Tl) detector in the γ-γ coincidence measurements.

For the purpose of elucidating the high-spin level structure of ^{131}I, I investigated the decay of 30-hr $11/2^-$ $^{131}Te^m$, making extensive use of large volume, high

resolution Ge(Li) detectors for both γ-ray singles and γ-γ coincidence measurements. I have been able to identify 190 γ-rays associated with the decay of 30-hr $^{131}Te^{m}$ and have placed 174 of these in a ^{131}I level scheme. The study was complicated by the observation of numerous important γ-ray multiplets, many of which were resolvable only through the use of the Ge(Li)-Ge(Li) γ-γ coincidence data; and by the interferences from the decays of 25-min $^{131}Te^{g}$ and 8.0-day ^{131}I.

The structure of the low-spin ($\leq 5/2$) excited states of ^{131}I seen in the decay of 25-min $3/2^{+}$ $^{131}Te^{g}$ was first studied using low-resolution NaI(Tl) detectors (55Ma, 61Fe, 63De, 67Ah), however these studies provided inconsistent data. More recently, this decay has been studied in detail, using Ge(Li) detectors and a Ge(Li)-Ge(Li) coincidence spectrometer, by Walters, Bemis, and Gordon (65Wa) and by Macias and Walters (71Ma1). In addition, the ^{131}I level structure has been studied, using the (^{3}He,d) reaction on ^{130}Te, by Auble, Ball, and Fulmer (68Au). I performed an independent investigation of the decay of 25-min $^{131}Te^{g}$ to aid in the assignment of weak γ-rays and to reduce the uncertainties in the measured β^{-}, γ^{-}, and isomeric-transition (IT) branches of the isomeric decay. I have been able to identify 80 γ-rays associated with the decay of 25-min $^{131}Te^{g}$ and have placed 77 of these in a level scheme for ^{131}I.

The total resultant ^{131}I level scheme consists of 52

excited states below 2333 keV. Of these, 38 were observed in the decay of 30-hr $11/2^-$ $^{131}Te^m$, and 19 were observed in the decay of 25-min $5/2^+$ $^{131}Te^g$.

B. Experimental Procedure and Results.

1. Source Preparation.

The samples of $^{131}Te^m$ were produced by irradiating 10-50 mg of tellurium metal enriched to 99.5% ^{130}Te (purchased from Isotopes Division, Oak Ridge National Laboratory, Oak Ridge, Tennessee) for several hours in either the Lawrence Livermore Laboratory (LLL) pool-type reactor or the National Bureau of Standards (NBS) reactor at thermal neutron fluxes of 0.5 - 5.0 x 10^{13} neutrons - cm^{-2} - sec^{-1}. The sources were allowed to decay for several hours until the 25-min $^{131}Te^g$ was in transient equilibrium with the 30-hr $^{131}Te^m$. At that point the principal activities present were ~1-2 mCi of $^{131}Te^m$, ~0.2 - 0.4 mCi of $^{131}Te^g$ and ~15-30 mCi of 8.0-day ^{131}I. A chemical separation was performed to remove this large amount of ^{131}I activity.

The following chemical procedure was developed to insure that the ^{131}I activity was retained in solution and not released to the atmosphere. The irradiated Te metal sample, in powder form, was placed in a flask along with 0.5 mℓ of 6 M NaOH and 0.5 mℓ of a KI solution equivalent to 0.5 mg of iodine. Then, 2 mℓ of fresh 30% H_2O_2 was slowly added while gently agitating the flask. When the sample was completely dissolved (~10 min), the solution

was chilled in an ice water bath and 6-8 drops of conc. HNO_3 were added to form I_2. The contents of the flask were then transferred to a separatory funnel and extracted with three 5-7 mℓ portions of cold CCl_4, each time discarding the CCl_4 fraction (which contains the ^{131}I activity) in the liquid radioactive waste. The water fraction was then transferred to a flask along with ~1-2 mℓ of H_2O used to rinse the separatory funnel. Approximately 2 mℓ of conc. formic acid (88% HCOOH) was then added, and the flask was heated in a boiling water bath until the NO_3^- was completely destroyed (~5-8 minutes). At this time the solution was made basic (pH ≥ 13-14) with 6M NaOH, and SO_2 was bubbled through the solution to precipitate the tellurium as the metal. The black metallic Te precipitate was then filtered out and mounted on a sample card for counting or redissolved to repeat the chemical separation. One separation was usually sufficient to remove nearly all of the ^{131}I. The degree of purification was somewhat difficult to determine as two of the principal ^{131}I γ-rays (80.183- and 364.480-keV) are doubleted with $^{131}Te^m$ γ-rays (81.14- and 364.98-keV), however at the end of one typical separation step the 364-keV doublet was approximately one-fifteenth as intense as the principal $^{131}Te^m$ transition (773.67-keV). [See Appendix II, Part C.] The chemical yield of Te, as determined gravimetrically, was ~85-92% per purification cycle.

The sources of $^{131}Te^{g}$ were produced by neutron irradiation of ^{130}Te in the LLL pool-type reactor. Large samples ($\geq$50 mg) and short irradiation times (30 sec.) were employed to minimize the production of $^{131}Te^{m}$ and ^{131}I. No chemical separations were performed, and counting began ~5 min. after irradiation. Each sample was replaced with a fresh sample every 25 min., and a total of nineteen 25-min counts were summed to achieve good statistics.

2. Gamma-Ray Singles Spectroscopy.

Direct γ-ray spectra of 30-hr $^{131}Te^{m}$ samples were taken using a large variety of detector-pulse-height analyzer systems at LLL and at UM. These systems included a 0.6 cm^3 Ge(Li) x-ray detector with FWHM energy resolution of 480 eV at 60 keV as well as a large number of Ge(Li) detectors ranging in size from 7 cm^3 to 65 cm^3 and in FWHM from 1.9 keV to 2.4 keV for the 1332-keV ^{60}Co γ-ray. In addition, extensive use was made of the LLL Compton Suppression Spectrometer (69Ca). Spectra were taken through various absorbers, including 1/2" of Al, 1/2" of Pb, 1" of Pb, 1/2" of Cd, and several combinations of these. Source to detector distances ranged from $\leq$1 cm to ~50 cm. The absorber and distance variations allowed the determination of summing contributions to the spectra. Sum peaks, being the result of simultaneous observation of intense coincident pairs of γ-rays, tended to vanish at smaller solid-angle counting configurations. Also, since

they were higher energy peaks resulting from two lower energy γ-rays, their intensities decreased with increasing absorber thickness at approximately the same rate as the intensities of the lower energy γ-rays. Spectra were taken over a period of ~5 half-lives (~150 hours), and counting times ranged from ~1 hr to ~62 hr. In all, over 40 different spectra were taken of the $^{131}Te^{m}$ sources.

The γ-ray spectrum of an equilibrium source of $^{131}Te^{m+g}$ observed with the 7 cm^3 Ge(Li) detector in the Compton Suppression Spectrometer is shown in Figures 16 through 20 with insets from large volume Ge(Li) detectors to clarify certain features and show the high energy portion of the spectrum. A portion of the low-energy spectrum of $^{131}Te^{m+g}$ observed with the 0.6 cm^3 Ge(Li) detector is shown in Figures 21 and 22. From all spectra, a total of 260 peaks were observed, including single-escape (SE), double-escape (DE), x-ray escape, x-ray, and sum (SUM) peaks. Fifteen additional transitions were established on the basis of coincidence information, and their intensities were calculated from coincidence spectra.

The 275 peaks are tabulated in Table I. 190 γ-rays were attributed to the decay of 30-hr $^{131}Te^{m}$, although 16 of these were not placed in the decay scheme. A majority of the remaining γ-rays were assigned to either $^{131}Te^{g}$ decay (based on the present work and the work of Macias and Walters (71Mal)) or to ^{131}I decay (based on the work

Figures

16. Compton supressed γ-ray spectrum (CSS) of $^{131}Te^{m+g}$ between 0 and 400 keV.

17. Compton supressed γ-ray spectrum of $^{131}Te^{m+g}$ between 400 and 800 keV.

18. Compton supressed γ-ray spectrum of $^{131}Te^{m+g}$ between 800 and 1200 keV.

19. Compton supressed γ-ray spectrum of $^{131}Te^{m+g}$ between 1200 and 1600 keV.

20. Compton supressed γ-ray spectrum of $^{131}Te^{m+g}$ between 1600 and 2000 keV and γ-ray spectrum from 19 cm^3 detector (M) between 1600 and 2400 keV.

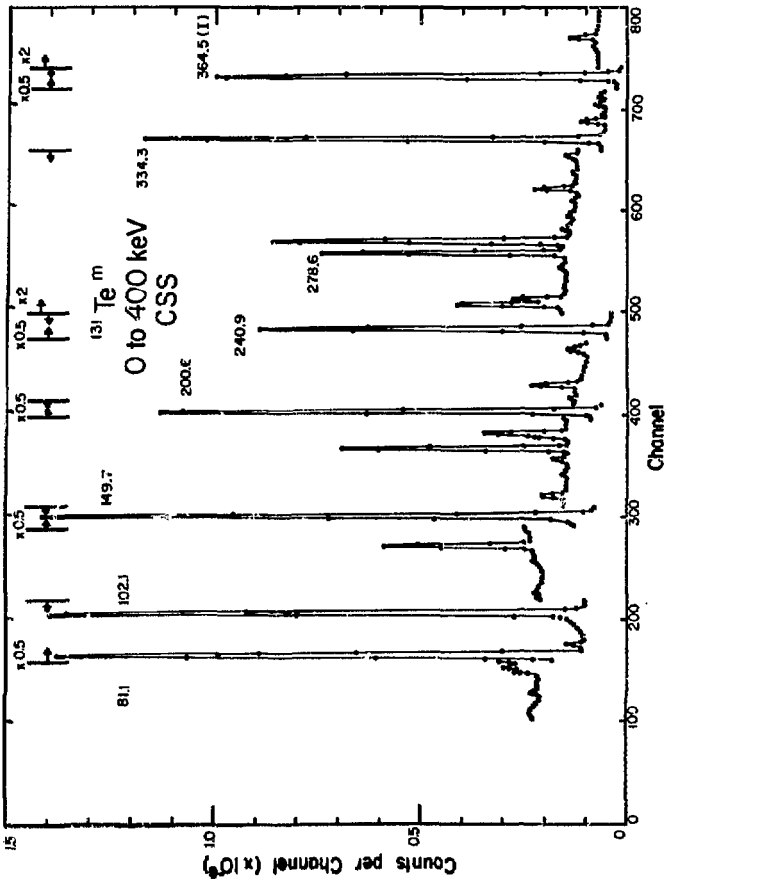
131 Te m
0 to 400 keV
CSS
81.1
102.1
149.7
200.6
240.9
278.6
334.3
364.5 (1)
x0.5
x2
Counts per Channel (x 10⁶)
Channel
0
100
200
300
400
500
600
700
800
0.5
1.0
1.5

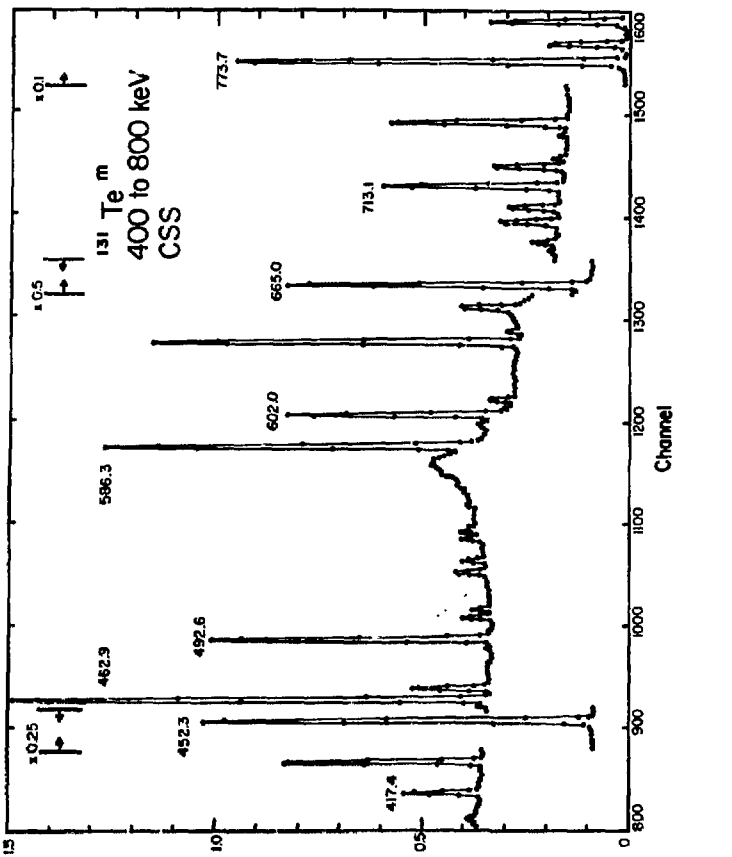
131 Te m
400 to 800 keV
CSS
x0.25
x0.5
x0.1
462.9
452.3
492.6
417.4
586.3
602.0
665.0
713.1
773.7
Counts per Channel (x10^3)
Channel
0
0.5
1.0
1.5
800
900
1000
1100
1200
1300
1400
1500
1600

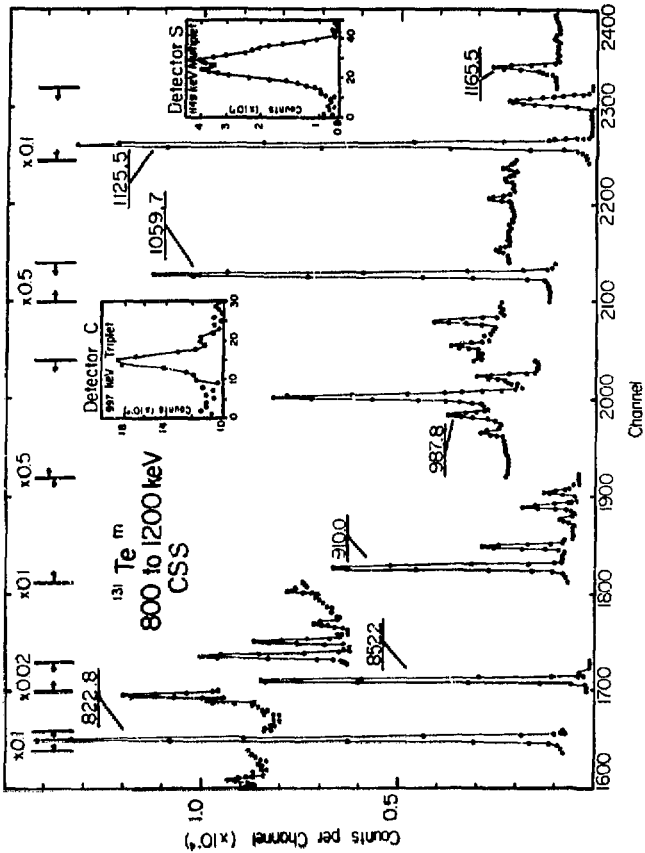
131 Te m
800 to 1200 keV
CSS
822.8
8522
2100
987.8
1059.7
1125.5
1165.5
Detector C
997 keV Triplet
Detector S
x0.01
x0.002
x0.1
x0.5
x0.05
Counts per Channel (x10⁴)
Channel
1600
1700
1800
1900
2000
2100
2200
2300
2400

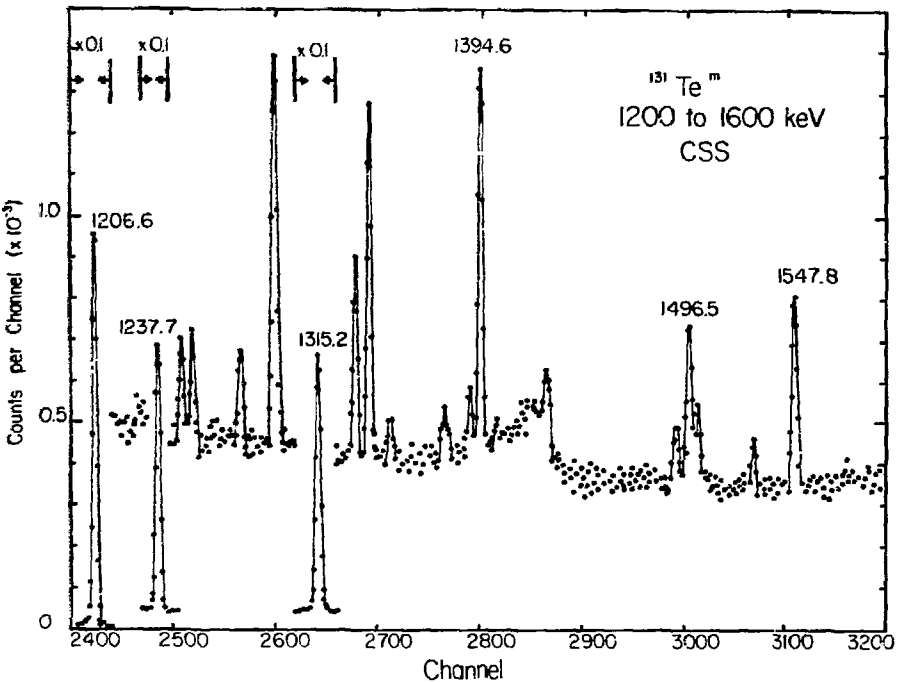
x0.1
x0.1
x0.1
1394.6
^{131}Te^{m}
1200 to 1600 keV
CSS
1206.6
1237.7
1315.2
1496.5
1547.8
Counts per Channel (x 10^{-3})
1.0
0.5
0
2400
2500
2600
2700
2800
2900
3000
3100
3200
Channel

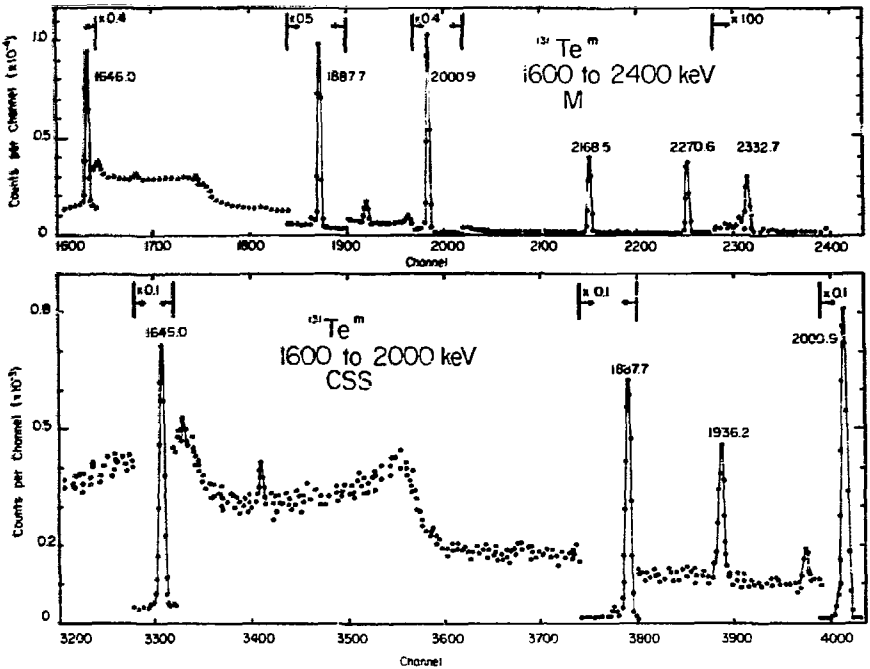
x0.4
x0.5
x0.4
x100
1646.0
1887.7
2000.9
2168.5
2270.6
2332.7
$^{131}Te^{m}$
1600 to 2400 keV
M
Counts per Channel (x10^{-4})
Channel
x0.1
x0.1
x0.1
1645.0
2000.9
1887.7
1936.2
$^{131}Te^{m}$
1600 to 2000 keV
CSS
Counts per Channel (x10^{-3})
Channel

Figures

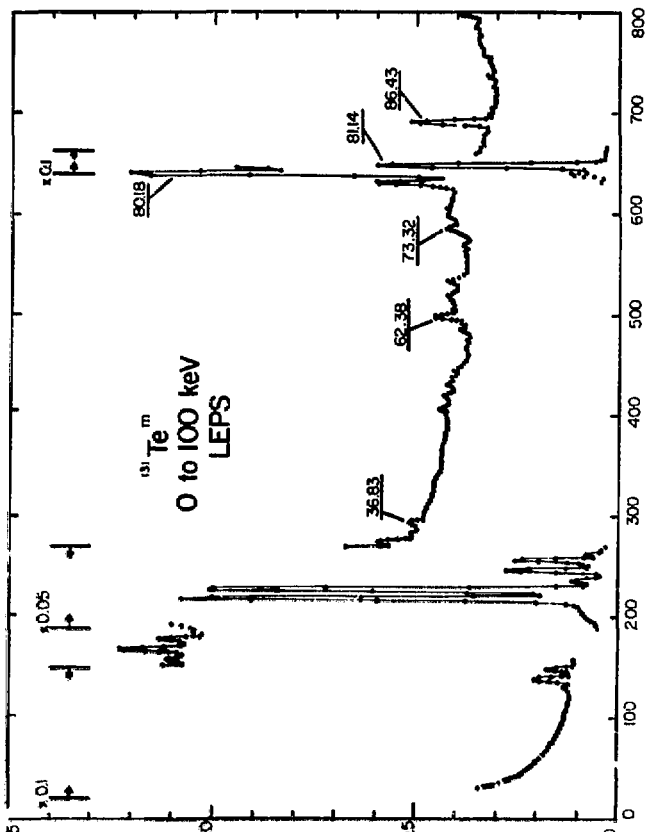
$^{131}Te^{m}$
0 to 100 keV
LEPS
36.83
62.38
73.32
80.18
81.14
86.43
x.01
x.05
x.01
Counts per Channel (x10^{3})
Channel
0
0.5
1.0
1.5
0
100
200
300
400
500
600
700
800

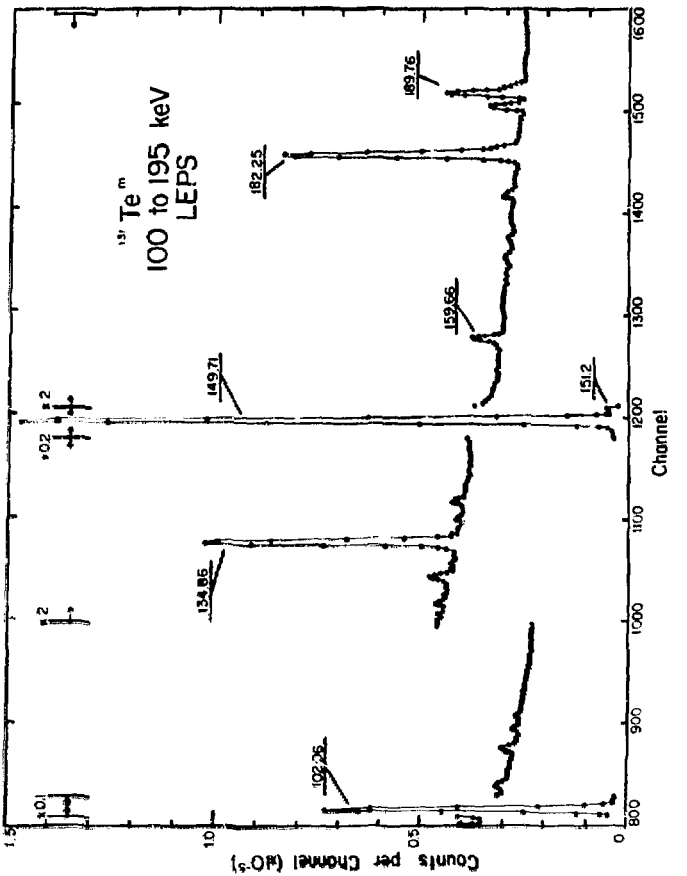
^{131}Te^{m}
100 to 195 keV
LEPS
149.71
182.25
159.66
189.76
134.86
192.36
151.2
Counts per Channel (x10^{-3})
Channel
800
900
1000
1100
1200
1300
1400
1500
1600
0
05
10
1.5
x1
x2
x02
x2

TABLE I.

Gamma Rays Observed in the Decay of 30-hr 11/2- $^{131}Te^{m}$.

Energy[a] (key)	Intensity[a,b]	Note	Transition[c] (from/ to)	Coincident Gamma Rays in $^{131}Te^{m}$ Decay or Identification[d]
16.2	(1)			Ge x-ray escape peak
17.3	(1)			Ge x-ray escape peak
17.6	(1)			Ge x-ray escape peak
18.4	(1)			Ge x-ray escape peak
18.7	(1)			Ge x-ray escape peak
19.6	(1)			Ge x-ray escape peak
19.9	(1)			Ge x-ray escape peak
21.1	(1)			Ge x-ray escape peak
21.8	(1)			Ge x-ray escape peak
22.4	(1)			Ge x-ray escape peak
23.1	(1)			Ge x-ray escape peak
23.7	(1)			Ge x-ray escape peak
24.5	(1)			Ge x-ray escape peak

TABLE I (cont.)

Energy[a] (keV)		Intensity[a,b]	Note	Transition[c] (from/to)	Coincident Gamma Rays in $^{131}Te^{m}$ Decay or Identification[d]
27.2	(1)				Te x-ray
27.5	(1)				Te x-ray
28.3	(1)				I x-ray
28.6	(1)				I x-ray
29.5	(1)				Xe x-ray
29.8	(1)				Xe x-ray
31.0	(1)				Te x-ray
31.7	(1)				Te x-ray
32.3	(1)				I x-ray
33.0	(1)				I x-
33.6	(1)				Xe x-ray
34.4	(1)				Xe x-ray
35.55	(8)				$^{125}Te^{m}$
36.83	(3)	0.31 (4)		(1924/1887)	
51.00	(5)	0.16 (4)		(1697/1646)	

TABLE I (cont.)

Energy[a] (keV)	Intensity[a,b]	Note	Transition[c] (from / to)	Coincident Gamma Rays in $^{131}Te^{m}$ Decay or Identification[d]
52.59 (6)	0.14 (4)			Not placed
54.1 (1)	0.05 (2)		1059/1005	
55.8 (1)	0.07 (3)			Not placed
57.50 (7)				^{127}Te
60.84 (7)	0.15 (4)			Not placed
62.38 (2)	0.34 (6)		(2063/2001)	
63.2 (1)	0.11 (4)			Not placed
65.05 (8)	0.21 (5)		(2001/1936)	
66.95 (5)	0.6 (1)			Not placed
68.8 (1)				Au x-ray
70.3 (1)				Ge x-ray escape peak
71.2 (1)				Ge x-ray escape peak
72.8 (1)				Pb x-ray
73.32 (5)	0.69 (3)		(2001/1936)	
75.0 (1)				Pb x-ray

Energy[a] (keV)		Intensity[a,b]		Level Energies (keV)	Comments and Possible ^{131}I Decay Scheme Assignments
78.57	(8)	0.40	(8)	[illegible]	
79.19	(3)	3.3	(1)	2011/1931	154, 53
80.18	(2)				^{191}I [25.0]
81.14	(2)	105	(2)	1980/1899	102, 149.7, 151, 158, 196, 208, 240, 273, 342, 744, 773, 782, 795, 802, 814, 1023, 1125, 1646
84.9	(1)				Pb x-ray
86.43	(2)	3.8	(1)	2011/1924	149.7, 278, 773, 1150
87.3	(1)				Pb x-ray
92.2	(1)				Ge x-ray escape peak
95.00	(12)	0.10	(5)		Not placed
96.4	(2)	0.15	(6)		Not placed
98.3	(1)	0.35	(8)	1646/1547	
100.0	(1)	1.9	(1)	1980/1880	
101.6	(3)	4.4	(4)	2001/1899	102

TABLE I (cont.)

Energy[a] (keV)		Intensity[a,b]		Note	Transition[c] (from/ to)	Coincident Gamma Rays in $^{131}Te^{m}$ Decay or Identification[d]
102.06	(1)	205	(4)		1899/1797	81, 101, 111, 149.7, 151, 200, 240, 744, 773, 782, 793, 822, 852, 1023
103.3	(3)	1.2	(2)		(2114/2011)	
105.0	(2)	0.7	(1)		(2168/2063)	
109.4	(2)	1.3	(1)	T, 125m		$^{131}Te^{g}$, $^{131}Te^{m}$, $^{125}Te^{m}$
		0.4	(1)	G		$^{131}Te^{g}$ [602/492]
		0.9	(2)	M, 125m		$^{131}Te^{m}$, $^{125}Te^{m}$
		0.2	(1)	MF	602/492	492
111.9	(2)	0.8	(2)		2011/1899	102, 342
113.5	(1)	0.3	(1)		2011/1887	
123.7	(5)	0.10	(5)	Q		Not placed
125.2	(3)	0.22	(8)	Q		Not placed
126.1	(3)	0.15	(8)		1887/1761	
127.4	(4)	0.6	(2)		(1924/1797)	
130.5	(1)	1.8	(2)	D		Not placed
132.2	(1)	0.12	(8)	Q		Not placed

TABLE I (cont.)

Energy[a] (keV)		Intensity[a,b]		Note	Transition[c] (from/to)	Coincident Gamma Rays in $^{131}Te^{m}$ Decay or Identification[d]
134.86	(2)	18.3	(6)		1931/1797	79, 182, 200, 240, 744, 773, 782, 822, 852
137.6	(2)	2	(1)		1899/1761	
139.8	(1)					Ge x-ray escape peak
149.3	(3)	2.0	(5)	GG	1697/1547	283, 773, 774
149.71	(1)	533	(5)	T		$^{131}Te^{g}$, $^{131}Te^{m}$
		402	(12)	G		$^{131}Te^{g}$ [149/ GS]
		131	(17)	M		$^{131}Te^{m}$
		125	(6)	MF	149/ GS	81, 86, 102, 151, 189, 200, 253, 255, 278, 309, 334, 342, 351, 354, 364, 452, 462, 586, 609, 665, 685, 702, 713, 744, 793, 852, 856, 865, 910, 920, 941, 995, 999, 1127, 1148, 1165, 1254, 1323, 1496
151.2	(2)	3.0	(4)	T		$^{131}Te^{g}$, $^{131}Te^{m}$
		1.0	(4)	G		$^{131}Te^{g}$ [1298/1146]
		2.0	(8)	MD	1797/1646	81, 102, 149.7, 183, 586, 793, 852, 1646
155.4	(2)	1.0	(5)		(2270/2114)	
159.66	(4)	3.3	(4)	123m	2170/2011	$^{123}Te^{m}$: 213, 364, 793, 1237, 1646

TABLE I (cont.)

Energy[a] (keV)		Intensity[a,b]		Note	Transition[c] (from/ to)	Coincident Gamma Rays in $^{131}Te^{m}$ Decay or Identification[d]
169.7	(2)	0.8	(2)		2170/2001	1148, 2001
172.0	(2)	0.3	(1)			Not placed
177.2	(2)	1.7	(3)	131-I	(1974/1797)	^{131}I [2.68] :
182.25	(2)	41	(4)	T		$^{131}Te^{m}$
		20	(4)	IT		Internal transition
182.25	(2)	19	(5)	GG	2114/1931	134, 200, 240, 335, 375, 773, 822
183.11	(8)	4.0	(5)		1980/1797	151, 200, 240, 744, 773, 782, 822, 852
188.13	(5)	5.5	(3)		2168/1980	81, 283, 334, 773, 793, 852, 910, 1059, 1127, 1206
189.76	(4)	13	(1)		2114/1924	149.7, 278, 773, 793, 865, 1150, 1646, 1887
190.52	(6)	3.0	(4)		2170/1980	81, 283, 334, 773, 793, 852, 910, 1059, 1127, 1206
200.63	(2)	195	(3)		1797/1596	81, 102, 134, 149.7, 182, 183, 213, 744, 773, 822, 852
203.4	(4)	0.5	(2)	Q	(2001/1797)	
207.5	(1)	1.0	(3)		1059/852	852

TABLE I (cont.)

Energy[a] (keV)		Intensity[a,b]		Note	Transition[c] (from/ to)	Coincident Gamma Rays in ^{131}Te^{m} Decay or Identification[d]
210.3	(3)	0.4	(1)			Not placed
211.9	(4)	0.3	(1)	Q, 121m	(1974/1761)	
213.98	(3)	11.0	(5)		2011/1797	159, 200, 230, 240, 744, 773, 782, 822, 852
227.7	(4)	0.4	(3)	Q	(1924/1697)	
230.65	(5)	5.0	(3)		2241/2011	213, 364, 773, 793, 1237, 1646
232.3	(1)	2.4	(3)		2168/1936	1333, 1936
235.0	(2)	0.4	(3)	Q	(2170/1936)	
240.93	(1)	196	(2)		1797/1556	81, 102, 134, 182, 183, 213, 773, 782
25[illegible].17	(2)	16.8	(3)		1899/1646	81, 149.7, 586, 793, 852, 910, 1059, 1646
255.44	(7)	8.0	(3)		1315/1059	149.7, 665, 910, 1059
261.4	(2)	0.4	(1)		2241/1980	
267.2	(3)	0.4	(3)	Q, N	(2241/1974)	
269.2	(3)	2.8	(6)		(2168/1899) or (1646/1376)	
272.4	(3)					^{131}I [0.56]

TABLE I (cont.)

Energy[e] (keV)	Intensity[a,b]	Note	Transition[c] (from/ to)	Coincident Gamma Rays in $^{131}Te^{m}$ Decay or Identification[d]
278.56 (2)	46.5 (9)	T		$^{131}Te^{m}$, $^{131}Te^{g}$
	0.6 (1)	G		$^{131}Te^{g}$ [1427/1148]
278.56 (2)	46 (1)	MD	1924/1646	86, 149.7, 189, 345, 586, 793, 852, 910, 1059, 1646
281.4 (3)	0.9 (5)		2168/1887	1887
283.2 (2)	10 (1)		1980/1697	149.3, 188, 190, 844, 852, 923
284.30 (8)				^{131}I [61.5]
290.3 (2)	2.0 (3)		2270/1980	
296.8 (3)	1.3 (2)	X	1148/852	852
298.8 (2)	0.6 (4)	T		$^{131}Te^{g}$ [1444/1146] ; $^{131}Te^{g}$ [1800/1500]
	0.6 (1)	G		$^{131}Te^{g}$ [1444/1146] ; $^{131}Te^{g}$ [1800/1500]
302.7 (2)	1.0 (3)	131-I, GG	1899/1596	^{131}I [0.045] ; 822
303.9 (2)	1.0 (2)		2001/1697	
309.47 (6)	9.7 (9)		1315/1005	149.7, 665, 856, 1005
317.9 (1)				^{131}I [0.79]
323.7 (4)	0.4 (2)			Not placed

TABLE I (cont.)

Energy[a] (keV)		Intensity[a,b]		Note	Transition[c] (*from*/ to)	Coincident Gamma Rays in $^{131}Te^{m}$ Decay or Identification[d]
324.8	(2)					^{131}I [0.22]
325.8	(2)					^{131}I [2.49]
331.2	(6)	0.8	(3)		1646/1315	
334.27	(1)	247	(3)		1980/1646	149.7, 188, 190, 586, 702, 773, 793, 852, 872, 910, 1059, 1646
335.44	(7)	3.5	(6)		1931/1596	79, 182, 744, 822
342.92	(5)	14	(2)	T		$^{131}Te^{m}$, $^{131}Te^{g}$
		4	(1)	G		$^{131}Te^{g}$ [492/149]
		0	(2)	MF	492/149	149.7
342.92	(5)	10	(3)	GG, MD	1899/1556	81, 111, 773, 792
345.9	(3)	2.5	(8)	N	2270/1924	278, 1150
351.3	(1)	5.4	(5)	N	1899/1547	149.7, 695, 773, 774, 852
353.5	(3)	2.1	(8)	T		$^{131}Te^{m}$, $^{131}Te^{g}$
		0.1	(1)	G		$^{131}Te^{g}$ [1500/1146]
		2.0	(9)	MD	2241/1887	1887
354.7	(1)	5.9	(3)		2001/1646	149.7, 793, 852, 1646

TABLE I (cont.)

Energy[a] (keV)		Intensity[a,b]		Note	Transition[c] (from/ to)	Coincident Gamma Rays in $^{131}Te^{m}$ Decay or Identification[d]
357.4	(3)	0.5	(2)		(2980/1622)	
362.3	(4)	2	(1)	Q	1646/1284	
364 48	(2)					^{131}I [806]
364.98	(10)	31	(4)	GG	2011/1646	149.7, 159, 230, 586, 702, 773, 793, 852, 910, 1059, 1646
375.8	(3)	0.3	(1)		1931/1556	182
377.8	(3)	1.0	(7)	Q	(1974/1596) or (2001/1622)	
379.3	(3)	0.5	(2)		2176/1797	
383.90	(7)	10.4	(5)	T		$^{131}Te^{m}$, $^{131}Te^{g}$
		5.2	(3)	G		$^{131}TE^{g}$ [876/492]
		5.2	(8)	MD	1980/1596	744, 773, 822, 852
401.5	(5)	0.10	(5)	T		$^{131}Te^{g}$ [1500/1098]
		0.06	(9)	G		$^{131}Te^{g}$ [1500/1098]
403.3	(4)	0.8	(5)	N	1005/602	
404.5	(2)					^{131}I [0.56]
408.2	(3)	1.6	(8)	Q	2332/1924	

TABLE I (cont.)

Energy[a] (keV)		Intensity[a,b]		Note	Transition[c] (from/ to)	Coincident Gamma Rays in $^{131}Te^{m}$ Decay or Identification[d]
417.4	(2)	7.2	(5)	127	2063/1646	586, 793, 852, 1646
421.8	(5)	0.2	(1)	T		$^{131}Te^{g}$ [1427/1005]
		0.2	(1)	G		$^{131}Te^{g}$ [1427/1005]
432.40	(7)	17.1	(7)		1980/1547	695, 773, 774, 852, 1547
452.30	(4)	147	(3)	T		$^{131}Te^{m}$, $^{131}Te^{g}$
		107	(7)	G		$^{131}Te^{g}$ [602/149]
		40.	(10)	M		$^{131}Te^{m}$
		33	(2)	MF	602/149	149.7, 546, 665, 685, 713, 1333
462.92	(5)	47	(1)		1315/852	149.7, 609, 665, 685, 702, 852
468.16	(9)	8.1	(8)		2114/1646	793, 852, 1646
492.65	(5)	30	(1)	T		$^{131}Te^{m}$, $^{131}Te^{g}$
		28	(3)	G		$^{131}Te^{g}$ [492/GS]
		2	(4)	M		$^{131}Te^{m}$
		0.2	(1)	MF	492/ GS	109
503.0	(1)					^{131}I [3.58]
506.8	(2)	2.3	(4)			Not placed

TABLE I (cont.)

Energy[a] (keV)		Intensity[a,b]		Note	Transition[c] (from/ to)	Coincident Gamma Rays in $^{131}Te^{m}$ Decay or Identification[d]
524.8	(1)	3.5	(4)		2170/1646	793
530.7	(1)	2.7	(5)		2176/1646	793
541.4	(1)	2.9	(6)		1315/773	665
544.8	(2)	3.0	(7)	T		$^{131}Te^{g}$ [1146/602]
		2.5	(3)	G		$^{131}Te^{g}$ [1146/602]
546.7	(2)	1.0	(2)	X	1148/602	452, 602
551.1	(4)	0.10	(8)	T		$^{131}Te^{g}$ [1427/876]
		0.11	(10)	G		$^{131}Te^{g}$ [1427/876]
558.1	(2)	0.6	(2)		(2114/1556)	
567.2	(3)	0.6	(3)	T		$^{131}Te^{g}$ [1444/876]
		0.6	(1)	G		$^{131}Te^{g}$ [1444/376]
572.7	(2)	1.3	(4)	T		$^{131}Te^{m}$, $^{131}Te^{g}$
		0.2	(2)	G		$^{121}Te^{g}$ [1427/853]
		1.1	)6)	MD	1887/1315	
579.8	(3)	2.0	(6)		2176/1596	
586.30	(3)	51	(2)		1646/1059	149.7, 151, 253, 278, 334, 544, [illegible]

TABLE I (cont.)

Energy[a] (keV)		Intensity[a,b]		Mode	Transition (from/to)	Coincident Gamma Rays in $^{131}Te^{m}$ Decay or Identification[c]
597.0	(2)	1.3	(5)		2001/1403	
602.09	(4)	32	(1)	T		$^{131}Te^{m}$, $^{131}Te^{g}$
		24	(2)	G		$^{131}Te^{g}$ [602/ GS]
		8	(5)	M		$^{131}Te^{m}$
		8	(1)	MF	602/ GS	546, 665, 713, 1333
609.4	(1)	3.6	(4)		1924/1315	140.7, 462, 713, 1315
(637.3)	(2)	(≤0.8)	(8)	131-I	(1697/1059)	^{131}I [72.1]
642.73	(9)					^{131}I [2.18]
654.2	(1)	11	(2)	T		$^{131}Te^{g}$ [1146/492]
		9	(2)	G		$^{131}Te^{g}$ [1146/492]
657.2	(2)	0.8	(4)	Q		Not placed
665.05	(3)	112	(2)		1980/1315	140.7, 255, 309, 452, 462, 541, 602, 702, 713, 852, 856, 910, 1059, 1165, 1315
681.95	(30)	0.8	(2)		1284/602	
685.9	(1)	4.0	(3)		2001/1315	140.7, 452, 462, 713, 852, 1315

TABLE I (cont.)

Energy[a] (keV)	Intensity[a,b]	Note	Transition[c] (from/ to)	Coincident Gamma Rays in $^{131}Te^{m}$ Decay or Identification[d]
695.62 (8)	11.2 (6)	T		$^{131}Te^{m}$, $^{131}Te^{g}$
	0.9 (2)	G		$^{131}Te^{g}$ [1298/602]
	10.3 (8)	MD	1547/852	351, 432, 852
702.50 (7)	10.1 (5)	N	852/149	149.7, 334, 364, 462, 665, 744, 793, 1127, 1148
713.10 (4)	37 (4)		1315/602	149.7, 452, 602, 609, 665, 685
722.90 (7)				^{131}I [17.0]
727.0 (2)	3.0 (3)	T		$^{131}Te^{g}$ [876/149]
	2.8 (4)	G		$^{131}Te^{g}$ [876/149]
738.8 (2)	1.7 (3)	X	1887/1148	902, 1148
744.20 (4)	41 (1)	N	1596/852	81, 102, 134, 149.7, 183, 200, 213, 335, 583, 702, 852
749.0 (8)	0.4 (2)	Q	(2063/1315)	
773.67 (3)	1000. (8)	T		$^{131}Te^{m}$ + ublet
	986 (10)	DG	773/ 00	81, 84, 102, 134, 149.3, 182, 183, 188, 190, 200, 213, 250, 340, 334, 335, 342, 354, 364, 383, 432, 774, 786, 788, 902, 1053, 1114, 1128, 1150, 1206, 1237, 1340, 1344

80

TABLE I (cont.)

Energy[a] (keV)		Intensity[a,b]		Note	Transition[c] (from/ to)	Coincident Gamma Rays in $^{131}Te^{m}$ Decay or Identification[d]
774.1	(1)	14	(2)	GG	1547/773	149.3, 351, 432, 773
782.49	(4)	201	(5)		1556/773	81, 102, 134, 183, 213, 240, 342, 773
793.75	(3)	358	(5)		1646/852	81, 102, 149.7, 151, 159, 188, 189, 190, 230, 253, 278, 334, 364, 417, 468, 524, 530, 702, 852
801.6	(2)	0.5	(2)		1403/602	
822.78	(4)	158	(2)		1596/773	81, 102, 134, 182, 183, 200, 213, 302, 335, 383, 773
842.1	(2)	1.3	(4)	T		$^{131}Te^{g}$ [1444/602]
		1.2	(2)	C		$^{131}Te^{g}$ [1444/602]
844.9	(2)	4	(1)		1697/852	283, 852
848.9	(2)	1.0	(3)		(1622/773)	
852.21	(3)	543	(6)	T, N		$^{131}Te^{m}$ doublet
		533	(11)	DG, N	852/ GS	81, 102, 134, 151, 188, 190, 200, 207, 213, 253, 278, 283, 296, 334, 351, 354, 364, 383, 417, 432, 462, 468, 665, 685, 695, 744, 793, 844, 1035, 1127, 1148, 1211, 1316

TABLE I (cont.)

Energy[a] (keV)		Intensity[a,b]		Note	Transition[c] (fr.m/ to)	Coincident Gamma Rays in $^{131}Te^{m}$ Decay or Identification[d]
852.21	(3)	10	(5)	GG, X	2001/1148	149.7, 999, 1148
856.05	(6)	16	(1)	T		$^{131}Te^{m}$, $^{131}Te^{g}$
		0.5	(1)	G		$^{131}Te^{g}$ [1005/149]
		16	(1)	M	1005/149	149.7, 309, 665, 995
865.1	(2)	5	(1)	-DE	1924/1059	DE [1887.70] : 149.7, 189, 910, 1059
872.3	(3)	2.6	(3)		1646/773	334
881.6	(3)	0.9	(3)	N	1887/1005	
898.6	(3)	0.9	(3)	T		$^{131}Te^{g}$ [1500/602]
		0.8	(2)	G		$^{131}Te^{g}$ [1500/602]
910.00	(3)	85	(2)		1059/149	149.7, 189, 190, 253, 256, 278, 334, 364, 586, 665, 805, 920, 941
920.62	(5)	31	(2)		1080/1059	149.7, 910, 1059
923.4	(2)	3.0	(6)		1697/773	283, 773
930.0	(4)	0.5	(3)	Q	1939/1059	
934.5	(1)	4.9	(4)	T		$^{131}Te^{g}$ [1437/433]
		5.1	(4)	G		$^{131}Te^{g}$ [1437/433]

TABLE I (cont.)

Energy[a] (keV)		Intensity[a,b]		Note	Transition[c] (from/to)	Coincident Gamma Rays [illegible] or Identification[d]
941.27	(5)	20.2	(7)		2001/1059	149.7, [illegible], [illegible]
948.57	(5)	13.3	(6)	T		^{131}Te[illegible] [1098/149]
		13.2	(6)	G		^{131}Te[illegible] [1098/149]
951.3	(1)	2.0	(4)	T		^{131}Te^{E} [1444/492]
		1.9	(3)	G		^{131}Te^{E} [1444/492]
979.0	(1)					DE [2000-[illegible]]
987.8	(1)	4.0	(3)		1761/773	
995.1	(3)	2.3	(4)		2001/1005	149.7, 856, 1005
997.16	(6)	19.5	(9)	T		^{131}Te^{E} [1146/149]
		19.5	(9)	G		^{131}Te^{E} [1146/149]
999.2	(1)	4.4	(5)	X, N	1148/149	149.7, 738, [illegible]
1003.6	(2)	0.7	(4)	Q	2063/1059	
1005.7	(2)	1.9	(4)	N	1005/ GS	309, 995
1007.7	(1)	4.9	(4)	T		^{131}Te^{E} [1500/492]
		4.8	(3)	G		^{131}Te^{E} [1500/492]
1023.6	(2)	1.6	(2)		1797/773	81, 102, 773

TABLE I (cont.)

Energy[a] (keV)		Intensity[a,b]		Note	Transition[c] (from/ to)	Coincident Gamma Rays in $^{131}Te^{m}$ Decay or Identification[d]
1027.8	(4)	0.2	(1)	Q	1880/852	
1035.4	(2)	2.7	(2)	N	1887/852	852
1059.69	(4)	40.	(1)		1059/ GS	188, 190, 253, 255, 278, 334, 364, 586, 665, 865, 920, 941
1072.3	(2)	0.6	(1)		1924/852	
1098.3	(2)	1.1	(2)	T		$^{131}Te^{g}$ [1098/ GS]
		1.1	(2)	G		$^{131}Te^{g}$ [1098/ GS]
1108.3	(3)	0.6	(2)		2168/1059	
1114.1	(3)	0.3	(1)		1887/773	773
1125.46	(4)	295	(6)		1899/773	81, 773
1127.96	(6)	25	(2)		1980/852	149.7, 188, 190, 702, 852
1134.2	(4)	0.2	(1)	Q	1284/149	
1146.97	(6)	30.	(3)	T, -DE		DE [2168.54] : $^{131}Te^{g}$ [1146/ GS]
		29	(3)	G		$^{131}Te^{g}$ [1146/ GS]
1148.89	(7)	44	(2)	T, N		$^{131}Te^{m}$ doublet
		39	(8)	DG	2001/852	149.7, 169, 702, 852

TABLE I (cont.)

Energy[a] (keV)		Intensity[a,b]		Note	Transition[c] (from/ to)	Coincident Gamma Rays in $^{131}Te^{m}$ Decay or Identification[d]
1148.89	(7)	5	(6)	CG, X, MF	1148/ GS	738, 852
1150.90	(9)	17	(2)		1924/773	86, 189, 345, 773
1162.7	(2)	0.7	(2)		2168/1005	
1165.5	(1)	3.6	(3)		1315/149	149.7, 665
1181.4	(4)	0.3	(2)		2241/1059	
1206.60	(4)	252	(4)		1980/773	188, 190, 773
1211.0	(2)	1.6	(3)		2063/852	852
1227.8	(5)	0.2	(1)	Q	(2001/773) or (1376/149)	
1237.32	(5)	17.0	(8)		2011/773	159, 230, 773
1248.5	(3)					DE [2270.65]
1254.2	(4)	0.7	(1)		1403/149	149.7
1277.7	(3)	0.8	(2)	T		$^{131}Te^{g}$ [1427/149]
		0.7	(2)	G		$^{131}Te^{g}$ [1427/149]
1294.47	(7)	2.9	(2)	T		$^{131}Te^{g}$ [1444/149]
		2.8	(3)	G		$^{131}Te^{g}$ [1444/149]

TABLE I (cont.)

Energy[a] (keV)		Intensity[a,b]		Note	Transition[c] (from/ to)	Coincident Gamma Rays in $^{131}Te^{m}$ Decay or Identification[d]
1315.16	(8)	20	(1)	T		$^{131}Te^{m}$ doublet
		18	(2)	DG	1315/ GS	609, 665, 685
1316.2	(2)	2.5	(9)	GG	2168/852	852
1318.3	(2)	1.0	(2)		2170/852	
1333.8	(3)	1.4	(2)		1936/602	149.7, 232, 452, 602
1340.6	(1)	2.6	(3)		2114/773	773
1350.9	(4)	0.3	(1)	T		$^{131}Te^{g}$ [1500/149]
		0.3	(2)	G		$^{131}Te^{g}$ [1500/149]
1376.8	(4)	1.1	(2)		1376/ GS	
1389.6	(3)	0.4	(1)		2241/852	
1394.83	(9)	2.8	(2)		2168/773	773
1403.6	(6)	0.3	(2)		1403/ GS	
1426.8	(3)	0.4	(1)	T		$^{131}Te^{g}$ [1427/ GS]
		0.6	(2)	G		$^{131}Te^{g}$ [1427/ GS]
1490.0	(3)					SE [2000.94]
1496.5	(4)	1.5	(2)		1646/149	149.7

TABLE I (cont.)

Energy[a] (keV)		Intensity[a,b]		Note	Transition[c] (from/ to)	Coincident Gamma Rays in $^{131}Te^{m}$ Decay or Identification[d]
1500.4	(2)	0.8	(2)	T		$^{131}Te^{g}$ [1500/ GS]
		0.7	(2)	G		$^{131}Te^{g}$ [1500/ GS]
1527.7	(3)	0.3	(1)	T		$^{131}Te^{g}$ [1677/149]
		0.3	(1)	G		$^{131}Te^{g}$ [1677/149]
1547.75	(9)	1.8	(2)	N	1547/ GS	432
1556.2	(5)					SUM [773+782]
1596.4	(5)					SUM [773+822 and 852+744]
1646.01	(5)	32	(1)		1646/ GS	81, 151, 159, 189, 230, 253, 278, 334, 354, 364, 417, 468
1657.5	(5)					SE [2168.54]
1696.8	(5)	0.4	(1)		1697/ GS	283
1759.6	(5)					SE [2270.65]
1830.6	(4)	0.2	(1)	Q	1980/149	
1880.1	(3)	1.6	(2)		1880/ GS	
1887.70	(7)	35	(1)		1887/ GS	189, 281, 353
1899.1	(5)					SUM [1127+852]

TABLE I (cont.)

Energy[a] (keV)	Intensity[a,b]	Note	Transition[c] (from/ to)	Coincident Gamma Rays in $^{131}Te^{m}$ Decay or Identification[d]
1924.1 (3)	0.10 (5)	N	1924/ GS	
1936.15 (9)	1.9 (2)		1936/ GS	232
1980.3 (3)	0.8 (2)		1980/ GS	
2000.94 (6)	52 (1)		2001/ GS	169
2168.54 (9)	9.0 (5)		2168/ GS	
2270.65 (9)	9.9 (5)		2270/ GS	
2332.75 (40)	0.07 (1)		2332/ GS	

[a] Value shown as 16.2 (1) means 16.2 ± 0.1 for example. The uncertainties are one standard deviation.

[b] The intensity values are relative to a value of 1000 for the combined 773.67 and 774.1-keV transitions. To convert to absolute intensities (per 1000 decays) multiply the relative intensity value by 0.384_6. This includes the absolute beta branch direct to ground of 5.2 %. Since this table consists of peaks seen under a wide variety of counting conditions, intensity values are given only for transitions assigned to $^{131}Te^{m+g}$ decay. Transitions not placed in the decay scheme are thought to come from $^{131}Te^{m}$ decay as their intensity values were consistent under all counting conditions and they were not observed in $^{131}Te^{g}$ decay.

TABLE I (cont.)

[c] Transition assignments are made for $^{131}Te^{m}$ decay. Assignments in parentheses are dotted in the decay scheme and were placed on the basis of sums and differences and on being consistent with being monopole or dipole transitions. Double assignments are both shown in the decay scheme, with the sums and differences giving no preference for the placement.

[d] Assignments to other Te isotope decays are based on variations in relative intensity values with length of irradiation and with time after irradiation. Assignments to $^{131}Te^{g}$ decay are based on the present work and on the work of Maclas and Walters (71Mal). Assignments to ^{131}I decay are based on the work of Meyer et al. (74Mel) On the intensity scale of this table, the most intense ^{131}I gamma-ray (364.48-keV) had a relative intensity value ranging from about 100 to about 700 depending on the length of the count and the time after chemical separation. For ^{131}I gamma-rays, the absolute intensity value (per 1000 decays) from the work of Meyer et al. (74Mel) is given.

The letters in the table mean the following :

T - The relative intensity value is that measured for the total peak.

G - The relative intensity value is the contribution to the peak from $^{131}Te^{g}$ decay. The value is calculated based on the 997.16-keV transition being a pure $^{131}Te^{g}$ gamma-ray and using the relative intensity values for $^{131}Te^{g}$ decay from this work.

M - The relative intensity value is the result of subtracting the contribution to the peak from $^{131}Te^{g}$ decay.

N - The contribution to the intensity from a transition in $^{131}Te^{g}$ decay was negligible.

TABLE I (cont.)

MF - The relative intensity value is the result of balancing input to the level and output from the level and assuming no direct beta feeding to the level.

125m (etc) - The decay of this Te isotope may contribute to the intensity of this peak.

Q - The presence of this transition is in some doubt. Generally this is a weak peak with large uncertainty and may not have been observed in all of the singles spectra.

D - This transition is possibly a doublet.

GG - This transition was observed solely in gamma-gamma coincidence spectra.

IT - This is the internal transition 131m to 131g. The relative intensity value is calculated from the measured IT branch and the theoretical conversion coefficients.

MD - The relative intensity value is the result of subtracting the contribution from $^{131}Te^{g}$ decay, however the placement of t is transition is different from the placement in $^{131}Te^{g}$ decay.

X - Coincidence information supports the assignment of this transition either into or out of the level at 1148.9 keV.

131-I - An ^{131}I gamma-ray of this energy may contribute to the relative intensity.

DG - The relative intensity is the result of subtracting the contribution of an unresolvable transition seen only in coincidence spectra.

-DE - The relative intensity value has been corrected for the contribution from a double escape peak.

TABLE II

Gamma Rays Observed in the Decay of 25-min $^{131}Te^{g}$

Energy[a] (keV)	Intensity[a,b]	Note	Transition (from/ to)
109.40 (4)	0.9 (1)	n	602/492
141.20 (4)	0.41 (7)		1146/1005
149.716 (5)	1000. (-)	n	149/ GS
151.1 (1)	2.5 (9)	n	1298/1146
221.57 (5)	0.48 (7)		1098/876
267.5 (3)	0.06 (5)	n	---------
274.68 (15)	<0.1		876/602
278.17 (2)	1.43 (7)	n	1427/1148
280.17 (12)	0.25 (7)		1427/1146
294.75 (15)	<0.07		1146/852
297.09 (5)	0.72 (7)	d	1444/1146
299.94 (6)	0.57 (7)		1800/1500
342.945 (4)	10.2 (1)	n	492/149
345.6 (1)	0.20 (6)		1444/1098
351.48 (7)	0.34 (6)	n	1500/1148
353.58 (9)	0.28 (6)		1500/1146
384.059 (3)	13.0 (1)	n	876/492
402.36 (14)	0.10 (5)		1500/1098
403.3 (--)	0.10 (5)	n	1005/602
421.32 (7)	0.61 (12)		1427/1005
438.3 (2)	0.10 (5)		1444/1005
452.323 (2)	264.5 (7)	n	602/149
469.7 (1)	0.22 (8)		1346/876
492.66 (1)	70.2 (3)	n	492/ GS
494.85 (5)	1.1 (1)		1500/1005
496.23 (8)	0.5 (1)		1098/602
544.88 (1)	6.2 (2)		1146/602
550.4 (1)	0.4 (1)		1427/876
567.33 (4)	1.49 (9)		1444/876
574.9 (1)	0.45 (7)	n	1427/852

TABLE II (cont.)

Energy[a] (keV)	Intensity[a,b]	Note	Transition (from/ to)
602.039 (5)	60.0 (5)	n	602/ GS
605.55 (2)	1.7 (1)		1098/492
654.26 (1)	22.2 (2)		1146/492
696.19 (2)	2.6 (2)		1298/602
702.7 (3)	0.11 (8)	-m	1800/1098
727.00 (3)	6.8 (1)		876/149
744.4 (3)	0.11 (6)	-m	1376/602
805.57 (20)	0.20 (8)		1298/492
825.0 (3)	3.4 (1)		1427/602
841.93 (2)	9.3 (1)		1444/602
852.21 (6)	0.64 (7)	-m	852/ GS
853.85 (5)	1.40 (7)		1346/492
856.08 (3)	1.1 (1)	n	1005/149
881.15 (7)	0.57 (6)	n	1757/876
898.54 (5)	2.0 (1)		1500/602
934.483 (5)	10.7 (2)		1427/492
948.542 (4)	32.8 (4)		1098/149
951.39 (3)	4.8 (1)		1444/492
997.25 (.)	48.5 (2)		1146/149
999.26 (15)	0.4 (1)	n	1148/149
1003.76 (15)	0.9 (1)	-m	1005/ GS
1007.8 (3)	11.6 (1)		1500/492
1035.5 (5)	0.04 (3)	-m	2040/1005
1042.2 (3)	0.09 (5)		2042/1005
1098.35 (2)	2.5 (1)		1098/ GS
1146.76 (1)	12.0 (4)		1146/ GS
1148.51 (6)	1.6 (1)		1298/149
1148.9 (--)	0.1 (1)		1148/ GS
1255.8 (3)	0.06 (3)		1757/602
1298.7 (3)	0.08 (3)		1677/492
1298.9 (3)	0.08 (3)		1900/602

TABLE II (cont.)

Energy[a] (keV)	Intensity[a,b]	Note	Transition (from/ to)
1265.2 (2)	0.07 (2)		1757/492
1277.44 (1)	1.71 (7)		1427/149
1294.34 (2)	7.0 (1)		1444/149
1297.98 (16)	0.07 (3)		1298/ GS
1308.1 (2)	0.10 (1)		1800/492
1350.91 (4)	0.88 (5)		1500/149
1427.14 (2)	1.53 (5)		1427/ GS
1500.62 (3)	1.67 (5)		1500/ GS
1527.73 (2)	0.83 (4)		1677/149
1548.0 (5)	0.013 (7)	-m	2040/492
1579.94 (9)	0.12 (1)		2072/492
1650.97 (9)	0.18 (1)		1800/149
(1765.2 (5))	(0.02 (7))		--------
1800.68 (20)	0.05 (1)		1800/ GS
1891.1 (3)	0.04 (2)		2040/149
1923.6 (2)	0.05 (1)	n	2072/149
(1973.1 (4))	(0.03 (1))		--------
2040.8 (1)	0.10 (1)		2040/ GS
2072.5 (3)	0.04 (2)		2072/ GS

[a] A value shown as 109.40 (4) means 109.40 ± 0.04 for example. The uncertainties are one standard deviation.

[b] The intensity values are relative to 1000 for the 149.716-keV transition. To convert to absolute intensities (per 1000 decays) multiply the relative intensity value by 0.681$_4$.

[c] This includes a total conversion coefficient of 0.257 for the 149-keV transition and the assumption of a ? E2 character for the 140-keV transition (taken from ^{128}Te → ^{128}I data).

TABLE II (cont.)

[d] Part of the 297-keV transition is 1148 to 852. I = 0.1 as calculated from $^{131}Te^{m}$ decay and the measured 999-keV intensity in $^{131}Te^{g}$ decay.

[e] The 1148.9-keV transition intensity was calculated from known ratios in $^{131}Te^{m}$ decay and the measured 999-keV intensity in $^{131}Te^{g}$ decay.

[n] The contribution to the peak from the isomer decay impurity was negligible.

[m] The contribution from the isomer decay impurity has been deleted using the intensity ratios from $^{131}Te^{m}$ decay.

of Meyer, Momyer, and Walters (74Mel)).

In the case of $^{131}Te^{g}$, the direct γ-ray spectrum was observed, as described above, with a new sample produced every 25 minutes and the old source moved on to the next detector-pulse-height analyzer system in sequence. In this manner nineteen 25 minute counts were summed on each of the several systems. This method had the advantage of achieving good counting statistics while maintaining a relatively constant count rate on each system. In addition, any contaminating activities could be identified on a half-life basis as each additional system counted the samples approximately one half-life (~25 min) later than the preceding system.

In the $^{131}Te^{g}$ spectra, 80 γ-rays were attributed to the decay of 25-min $^{131}Te^{g}$. These are tabulated in Table II, and 77 of them are placed in a decay scheme for $^{131}Te^{g}$. In Table I, ground-state decay contributions were determined based on the 997.25-keV transition, and in Table II the isomeric-state decay contributions were determined based on the 773.67-keV and 774.1-keV transitions.

By observing the growth and decay of daughter ^{131}I in an equilibrium $^{131}Te^{m+g}$ source initially free of ^{131}I and by employing the intensity and transition assignment data in Tables I and II, I determined the direct ground state β-branch and the 182.2-keV M4 I.T. branch for $^{131}Te^{m}$ by an iterative technique. The details of this determination are presented in Appendix II. I determined the direct

ground-state β-branch to be (5.2 ± 3.0)% which is in good agreement with the previous value of 6% (65De). I determined the 182.2-keV I.T. branch to be (22.2 ± 1.6)%. This is in fair agreement with the previous value of 18% (65De) which was obtained by comparison of the total β-spectrum with the K- and L-electron conversion lines due to the 182.2-keV M4 I.T. In $^{131}Te^{g}$ decay, Devare, Tandon, and Devare (63De) were unable to detect any measureable direct β-decay to the ground state of ^{131}I.

Recently, Fujiwara, Imanishi, and Nishi (74Fu) measured absolute γ-ray intensities for the decay of ^{131}Te isomers. For the 149.72-keV γ-ray, they reported values of 0.21 ± 0.02 and 0.87 ± 0.04 γ-rays per decay for $^{131}Te^{m}$ and $^{131}Te^{g}$, respectively. Using my γ-ray data (Table I) and the ground-state β-branch value of 5.2% for $^{131}Te^{m}$, I arrived at a value of 0.205 ± 0.008 γ-rays per decay for the 149.72-keV transition in the decay of $^{131}Te^{m}$ which is in good agreement with the recently reported value. For the $^{131}Te^{g}$, the internal conversion of the 149.72-keV transition must be included in determining the total decay intensity. The α_K and K/L values have been measured (67De2) to be 0.21 ± 0.01 and 7.9 ± 0.4, respectively. My γ-ray data (Table II) combined with the α_K, α_L, and a theoretical α_M (68Ha) resulted in a value of 0.68 ± 0.03 γ-rays per decay for the 149.72-keV γ-ray in the decay of $^{131}Te^{g}$. This is in marked disagreement with the recently reported value, which is

clearly in error as the measured internal conversion coefficients in themselves imply an absolute upper limit of 0.77 for 149.72-keV γ-rays per decay, assuming that there are no other transitions to the ^{131}I ground state in $^{131}Te^{g}$ decay.

3. Gamma-Gamma Coincidence Spectroscopy.

The γ-γ coincidence measurements were carried out at UM using two large volume true-coaxial Ge(Li) detectors (55 cm^3 and 65 cm^3, both having a FWHM energy resolution of 2.1 keV at 1332 keV) in conjunction with a multiparameter pulse-height analyzer and associated electronics described in Section II and elsewhere (71Ap1). The coincidence time gate was approximately 23-25 nsec which resulted in a real-to-random coincidence ratio of ~27 to one. The coincidence events were recorded on magnetic tape in an 8192 by 8192 channel format for later analysis using the UM UNIVAC 1108 computer along with computer codes already described (Section II and Appendix I). Approximately 3 million coincidence events recorded on magnetic tape were scanned, and coincidence spectra were extracted for 60 peak regions as well as for neighboring regions to account for Compton backgrouns. The Compton-gate spectra were subtracted from the photopeak-gate spectra to obtain net coincidence spectra. Energy gates were set on the spectrum obtained with the 65 cm^3 detector, and the spectrum in coincidence with the gated region was

retrieved for the 55 cm^3 detector. The results obtained are tabulated in Table III which lists all photopeak gates which were set and all γ-rays which were observed in true coincidence in the gates. Random coincidences, as determined by looking for peaks from intense non-coincident γ-rays, were essentially negligible (e.g., see Figure 26). All coincidences observed are also listed in Table I, although the coincidence information obtained on $^{131}Te^{g}$ decay is not shown there as it was less complete and in agreement with the work of Macias and Walters (71Mal).

Due to the unique nature of coincidence relationships, the γ-γ coincidence data revealed the presence of 15 peak doublets which had been unresolved in singles spectra. In ten of these cases the doublets consisted of one transition which could be assigned to $^{131}Te^{m}$ β-decay on the basis of coincidences and another which could be assigned elsewhere, such as to ^{131}I or $^{131}Te^{g}$ decay. For example, Table III indicates that a gate on the 362-367 keV region resulted in the observation of numerous $^{131}Te^{m}$ decay γ-rays. In singles spectra, the only major transition observed in this gated region was the 364.48-keV γ-ray in ^{131}I decay, yet many of the coincident γ-rays were much too weak in singles spectra to have merely been random coincidences. Thus, the 364.48-keV peak must have included an unresolved component arising from $^{131}Te^{m}$ β-decay. In the other five cases, the coincidence data required that the one peak observed in singles spectra consist of two components,

TABLE III

Gamma-Gamma Coincidences in $^{131}Te^{m+g}$ Decay

Ge(Li) Gate (keV)	Gated Photopeak[a] (keV)	Coincident Gamma Rays Observed (keV)
78.0 - 82.8	78.57 79.19 80.18 (X) 81.14	102, 134, 149-151, 188-189-190, 200, 240, 253, 284 (X), 335, 342, 744, 773, 782, 793, 822, 852, 1023, 1125, 1646
99.4 - 103.8	100.0 101.6 102.06 103.3	81, 101-102, 111, 149, 151, 200, 240, 744, 773, 782, 793, 822, 852, 1023
132.2 - 136.3	132.2 134.86	79, 182, 200, 240, 744, 773, 782, 822, 852
146.6 - 154.2	149.3 149.71 (+) 151.1 (*) 151.2	81, 86, 102, 151, 183, 189, 200, 253, 255, 278, 283, 309, 334, 342(*), 351, 354, 364, 452, 462, 586, 609, 654(*), 665, 685, 695(*), 702, 713, 727(*), 744, 773-774, 793, 842(*), 852, 856, 865, 898(*), 910, 920, 941, 948(*), 995, 997(*), 999, 1007(*), 1127, 1148, 1165, 1254, 1294(*), 1338, 1496, 1646
157.9 - 161.7	159.66	213, 364, 793, 1237, 1646
180.1 - 184.4	182.25 (IT) 182.25 183.11	134, 151, 200, 240, 337, 375, 744, 773, 782, 822, 852
186.2 - 192.0	188.13 189.76 190.52	81, 149, 278, 283, 334, 744, 773, 793, 852, 865, 910, 1059, 1127, 1150, 1206, 1646

TABLE III (cont.)

Ge(Li) Gate (keV)	Gated Photopeak[a] (keV)	Coincident Gamma Rays Observed (keV)
198.1 - 202.2	200.63	81, 102, 134, 149, 182-183, 213, 744, 773, 822, 852
211.7 - 215.5	211.9 213.98	159, 200, 230, 240, 744, 773, 782, 822, 852
227.8 - 234.0	227.7 230.65 232.3	364, 773, 793, 1237, 1333, 1646, 1936
238.6 - 242.8	240.93	81, 102, 134, 182-183, 213, 773, 782
250.8 - 257.6	253.17 255.44	81, 149, 586, 665, 793, 852, 910, 1059, 1646
276.7 - 280.2	278.17 (*) 278.56 280.2 (*)	86, 149, 189, 345, 586, 793, 852, 910, 1059, 1146-1148(*), 1646
281.2 - 285.4	281.4 283.2 284.30 (X)	80.18(X), 149, 188-190, 844, 852, 925
307.4 - 311.6	309.47	149, 665, 856, 1005
332.3 - 337.3	334.27 335.44	79, 149, 182, 188-190, 586, 702, 744, 773, 793, 822, 852, 872, 910, 1059, 1646
340.4 - 345.0	342.92 (+)	81, 111, 149, 384(*), 654(*), 773, 792, 934(*)
348.5 - 353.2	351.3 351.48 (*) 353.5	149, 695, 773-774, 852, 1887

TABLE III (cont.)

Ge(Li) Gate (keV)	Gated Photopeak[a] (keV)	Coincident Gamma Rays Observed (keV)
353.0 - 356.7	353.5 353.5 (*) 354.7	149, 793, 852, 1646, 1887
362.1 - 366.8	362.3 364.48 (X) 364.98	149, 159, 230, 586, 702, 773, 793, 852, 910, 1059, 1646
381.8 - 386.1	383.90 384.059 (*)	149(*), 342(*), 492(*), 744, 773, 822, 852
414.4 - 419.4	417.4	586, 793, 852, 1646
430.1 - 434.5	432.40	695, 773-774, 852, 1547
450.1 - 454.5	452.30 (+)	149, 544(*), 546, 654(*), 665, 685, 696(*), 713, 841(*), 898(*), 1333
460.5 - 464.9	462.92	609, 665, 685, 702, 852
467.4 - 470.1	468.16 469.23 (*)	793, 852, 1646
490.7 - 494.5	492.65 (+)	109, 384(*), 654(*), 853(*), 934(*), 951(*), 1007(*), 1294(*)
584.0 - 588.5	586.30	149, 151, 253, 278, 334, 364, 910, 1059
599.7 - 604.1	602.05 (+)	544(*), 546, 665, 713
662.7 - 667.2	665.05	149, 255, 309, 452, 462, 541, 602, 702, 713, 852, 856, 910, 1059, 1165, 1315

TABLE III (cont.)

Ge(Li) Gate (keV)	Gated Photopeak[1] (keV)	Coincident Gamma Rays Observed (keV)
683.5 - 687.6	686.1	140, 482, 488, 514, 701, 1272
693.1 - 697.5	695.42 696.13 (+)	811, 943, 1[illegible] (+), [illegible]
700.4 - 704.8	702.80 702.7 (+)	140, 634, 814, 867, 1[illegible], [illegible], 1[illegible], 1[illegible], 1145
710.5 - 715.5	713.16	140, 482, 488, 695, 1[illegible], 1[illegible]
741.8 - 746.5	744.20	81, 102, 134, 143, 188, 200, 213, 253, 383, 702, 852
770.6 - 776.2	773.67 774.1	81, 82, 102, 134, 143, 149-151, 188-190, 200, 213, 230, 240, 254, 334, 364, 383, 432, 773-774, 782, 827, 1[illegible], 1125, 1150, 1206, 1237, 1640, 1814
779.9 - 785.1	782.49	81, 102, 134, 183, 213, 240, 343, 773
790.8 - 796.4	793.75	81, 102, 149-151, 159, 188-189-190, 230, 253, 278, 334, 364, 417, 468, 524, 530, 702, 852
819.9 - 825.4	822.78 825.0	81, 102, 134, 182-183, 200, 213, 302, 335, 383, 773
849.6 - 854.2	852.21 (+) 852.21	81, 102, 134, 151, 188, 190, 200, 207, 213, 253, 278, 283, 296, 334, 351, 354, 364, 383, 417, 432, 462, 468, 665, 685, 695, 744, 793, 844, 999, 1035, 1127, 1148, 1211, 1316
854.7 - 857.9	856.05 (+)	149, 309, 665, 995

TABLE III (cont.)

[illegible] (keV)	[illegible] peak[a] (keV)	Coincident Gamma Rays Observed (keV)
[illegible]	[illegible]	[illegible], 920, [illegible]
[illegible]	[illegible] [illegible]	[illegible], 1059
[illegible]	[illegible]	[illegible], 1059
[illegible]	[illegible] (*) [illegible] (*)	[illegible](*), [illegible](*)
[illegible]	[illegible] [illegible] (*) [illegible]	[illegible], 1005
[illegible]	[illegible]	[illegible], 773
[illegible] – 10[illegible]	[illegible] [illegible] (*)	[illegible]
[illegible]	[illegible]	[illegible], 190, [illegible]–255, 278, 334, 364, [illegible], [illegible], 920, 941
[illegible] – 11[illegible]	[illegible] [illegible]	[illegible], 702, 773, 852
114[illegible].5 – 1153.[illegible]	114[illegible] (*) 1148.51 (*) [illegible] 114[illegible]	[illegible], 140–151, 169, 189, 345, 353(*), 702, 738, 773, 852
1204.[illegible] – 1209.4	120[illegible]	188, 190, 773

TABLE III (cont.)

Ge(Li) Gate (keV)	Gated Photopeak[a] (keV)	Coincident Gamma Rays Observed (keV)
1235.2 - 1240.7	1237.32	159, 230, 773
1310.6 - 1318.5	1315.16 1316.2 1318.3	609, 665, 685, 852
1331.4 - 1337.5	1333.8	149, 232, 452, 602
1338.1 - 1344.2	1340.6	773
1643.7 - 1649.3	1646.01	151, 159, 189, 230, 253, 278, 334, 354, 364, 468
1885.6 - 1890.0	1887.70	189, 281, 353
1933.5 - 1940.8	1936.15	232
1997.0 - 2003.3	2000.94	169

[a] When more than one photopeak appears in a gate, the principal ^{131}Te decay peak is underlined.

(X) - This is a transition assigned to ^{131}I decay.

(*) - This is a transition assigned to $^{131}Te^{g}$ decay.

(+) - This transition is assigned to both $^{131}Te^{m}$ and $^{131}Te^{g}$ decay.

clearly in error as the measured internal conversion coefficients in themselves imply an absolute upper limit of 0.77 for 149.72-keV γ-rays per decay, assuming that there are no other transitions to the ^{131}I ground state in $^{131}Te^{g}$ decay.

3. Gamma-Gamma Coincidence Spectroscopy.

The γ-γ coincidence measurements were carried out at UM using two large volume true-coaxial Ge(Li) detectors (55 cm^3 and 65 cm^3, both having a FWHM energy resolution of 2.1 keV at 1332 keV) in conjunction with a multiparameter pulse-height analyzer and associated electronics described in Section II and elsewhere (71Apl). The coincidence time gate was approximately 23-25 nsec which resulted in a real-to-random coincidence ratio of ~27 to one. The coincidence events were recorded on magnetic tape in an 8192 by 8192 channel format for later analysis using the UM UNIVAC 1108 computer along with computer codes already described (Section II and Appendix I). Approximately 3 million coincidence events recorded on magnetic tape were scanned, and coincidence spectra were extracted for 60 peak regions as well as for neighboring regions to account for Compton backgrouns. The Compton-gate spectra were subtracted from the photopeak-gate spectra to obtain net coincidence spectra. Energy gates were set on the spectrum obtained with the 65 cm^3 detector, and the spectrum in coincidence with the gated region was

retrieved for the 55 cm^3 detector. The results obtained are tabulated in Table III which lists all photopeak gates which were set and all γ-rays which were observed in true coincidence in the gates. Random coincidences, as determined by looking for peaks from intense non-coincident γ-rays, were essentially negligible (e.g., see Figure 26). All coincidences observed are also listed in Table I, although the coincidence information obtained on $^{131}Te^{g}$ decay is not shown there as it was less complete and in agreement with the work of Macias and Walters (71Mal).

Due to the unique nature of coincidence relationships, the γ-γ coincidence data revealed the presence of 15 peak doublets which had been unresolved in singles spectra. In ten of these cases the doublets consisted of one transition which could be assigned to $^{131}Te^{m}$ β-decay on the basis of coincidences and another which could be assigned elsewhere, such as to ^{131}I or $^{131}Te^{g}$ decay. For example, Table III indicates that a gate on the 362-367 keV region resulted in the observation of numerous $^{131}Te^{m}$ decay γ-rays. In singles spectra, the only major transition observed in this gated region was the 364.48-keV γ-ray in ^{131}I decay, yet many of the coincident γ-rays were much too weak in singles spectra to have merely been random coincidences. Thus, the 364.48-keV peak must have included an unresolved component arising from $^{131}Te^{m}$ β-decay. In the other five cases, the coincidence data required that the one peak observed in singles spectra consist of two components,

TABLE III

Gamma-Ray[a] Coincidences in $^{131}Te^{m+g}$ Decay

Energy Gate (keV)	Gamma Ray Peak[b] (keV)	Coincident Gamma Rays Observed (keV)
[illegible]	[illegible]	[illegible]
100.0 - 103.8	100.0	81, 101-103, 111, 149, 151, 200, 240, 744, 773, 782, 793, 822, 852, 1023
	103.8	
130.2 - 146.3	130.2	79, 182, 200, 240, 744, 773, 782, 822, 852
146.3 - 154.2	147.3	81, 86, 102, 151, 183, 189, 200, 253, 255, 278, 283, 309, 334, 342(*), 351, 354, 364, 452, 462, 586, 609, 654(*), 665, 685, 695(*), 702, 713, 727(*), 744, 773-774, 793, 842(*), 852, 856, 865, 898(*), 910, 920, 941, 948(*), 995, 997(*), 999, 1007(*), 1127, 1148, 1165, 1254, 1294(*), 1338, 1496, 1646
	149.71 (+)	
	151.1 (*)	
	151.2	
157.9 - 161.7	159.66	213, 364, 793, 1237, 1646
180.1 - 184.4	182.25 (IT)	134, 151, 200, 240, 337, 375, 744, 773, 782, 822, 852
	182.25	
	183.11	
186.2 - 192.0	188.13	81, 149, 278, 283, 334, 744, 773, 793, 852, 865, 910, 1059, 1.27, 1150, 1206, 1646
	189.76	
	190.52	

TABLE III (cont.)

Ge(Li) data (keV)	Gated Photopeak[a] (keV)	Coincident Gamma Rays Observed (keV)
198.[illegible] - 203.[illegible]	200.03	81, 102, 134, 140, 182-185, 213, 744, 774, 828, 852
211.[illegible] - 215.5	211.0 213.08	150, 200, 250, 340, 744, 774, 852, 852
227.[illegible] - 234.[illegible]	227.7 230.65 232.5	304, 773, 805, 1284, 1653, 1681, 1850
238.6 - 242.8	240.03	81, 102, 134, 140-185, 216, 773, 792
250.8 - 257.0	253.17 255.44	81, 140, 580, 665, 773, 852, 910, 1059, 1646
276.7 - 280.2	278.17 (*) 278.56 280.2 (*)	86, 140, 189, 345, 580, 705, 852, 910, 1059, 1146-1148(*), 1646
281.2 - 285.4	281.4 283.2 284.30 (X)	80.18(X), 149, 188-190, 804, 852, 923
307.4 - 311.6	309.47	140, 665, 856, 1005
332.3 - 337.3	334.27 335.44	79, 149, 182, 188-190, 580, 702, 744, 773, 793, 822, 852, 872, 910, 1059, 1646
340.4 - 345.0	342.92 (+)	81, 111, 149, 384(*), 654(*), 773, 792, 934(*)
348.5 - 353.2	351.3 351.48 (*) 353.5	149, 695, 773-774, 852, 1887

TABLE III (cont.)

Σ (L.I.) Gate (keV)	Gated Photopeak[1] (keV)	Coincident Gamma Rays Observed (keV)
348.6 - 356.7	353.5 353.5 (*) 354.7	149, 793, 852, 1646, 1887
360.1 - 368.8	362.3 364.48 (X) 364.98	149, 159, 230, 586, 702, 773, 793, 852, 910, 1059, 1646
378.5 - 386.1	383.90 384.059 (*)	149(*), 342(*), 492(*), 744, 773, 822, 852
414.4 - 419.4	417.4	586, 793, 852, 1646
430.1 - 434.5	432.40	695, 773-774, 852, 1547
450.1 - 454.5	452.30 (+)	149, 544(*), 546, 654(*), 665, 685, 696(*), 713, 841(*), 898(*), 1333
460.5 - 464.9	462.92	609, 665, 685, 702, 852
467.4 - 470.1	468.16 469.23 (*)	793, 852, 1646
490.7 - 494.5	492.65 (+)	109, 384(*), 654(*), 853(*), 934(*), 951(*), 1007(*), 1294(*)
584.0 - 588.5	586.30	149, 151, 253, 278, 334, 364, 910, 1059
599.7 - 604.1	602.05 (+)	544(*), 546, 665, 713
662.7 - 667.2	665.05	149, 255, 309, 452, 462, 541, 602, 702, 713, 852, 856, 910, 1059, 1165, 1315

TABLE III (cont.)

Ge(Li) Gate (keV)	Gated Photopeak[a] (keV)	Coincident Gamma Rays Observed (keV)
683.5 - 687.6	685.9	149, 452, 462, 713, 852, 1315
693.1 - 697.5	695.62 696.19 (*)	351, 432, 452(*), 852
700.4 - 704.8	702.50 702.7 (*)	149, 334, 364, 462, 665, 744, 793, 1127, 1148
710.5 - 715.5	713.10	149, 452, 602, 609, 665, 685
741.8 - 746.5	744.20	81, 102, 134, 149, 183, 200, 213, 335, 383, 702, 852
770.6 - 776.2	773.67 774.1	81, 86, 102, 134, 149, 182-183, 188-190, 200, 213, 230, 240, 334, 335, 342, 351, 364, 383, 432, 773-774, 782, 822, 1114, 1125, 1150, 1206, 1237, 1340, 1394
779.9 - 785.1	782.49	81, 102, 134, 183, 213, 240, 342, 773
790.8 - 796.4	793.75	81, 102, 149-151, 159, 188-189-190, 230, 253, 278, 334, 364, 417, 468, 524, 530, 702, 852
819.9 - 825.4	822.78 825.	81, 102, 134, 182-183, 200, 213, 302, 335, 383, 773
849.6 - 854.2	852.21 (+) 852.21	81, 102. 134, 151, 188, 190, 200, 207, 213, 253, 278, 283, 296, 334, 351, 354, 364. 383, 417, 432, 462, 468, 665, 685, 695, 744, 793, 844, 999, 1035, 1127, 1148, 1211, 1316
854.7 - 857.9	856.05 (+)	149, 309, 665, 995

TABLE III (cont.)

Ge(Li) Gate (keV)	Gated Photopeak[a] (keV)	Coincident Gamma Rays Observed (keV)
907.6 - 912.6	910.00	149, 188, 190, 253, 255, 278, 334, 364, 586, 665, 865, 920, 941
918.4 - 926.3	920.62 923.4	149, 283, 773, 910, 1059
939.0 - 944.3	941.27	149, 910, 1059
946.3 - 951.2	948.57 (*) 951.3 (*)	149(*), 492(*)
994.7 - 1001.0	995.1 997.16 (*) 999.2	149, 738, 852, 856, 1005
1021.4 - 1026.4	1023.6	81, 102, 773
1033.6 - 1037.7	1035.4 1035.5 (*)	852
1057.6 - 1062.6	1059.69	188, 190, 253-255, 278, 334, 364, 586, 665, 865, 920, 941
1122.9 - 1129.6	1125.46 1127.96	81, 149, 702, 773, 852
1146.5 - 1153.6	1146.97 (*) 1148.51 (*) 1148.89 1148.89	86, 149-151, 169, 189, 345, 353(*), 702, 738, 773, 852
1204.1 - 1209.4	1206.60	188, 190, 773

TABLE III (cont.)

Ge(Li) Gate (keV)	Gated Photopeak[a] (keV)	Coincident Gamma Rays Observed (keV)
1235.2 - 1240.7	1237.32	159, 230, 773
1312.6 - 1318.5	<u>1315.16</u> 1316.2 1318.3	609, 665, 685, 852
1331.4 - 1337.5	1333.8	149, 232, 452, 602
1338.1 - 1344.2	1340.6	773
1643.7 - 1649.3	1646.01	151, 159, 189, 230, 253, 278, 334, 354, 364, 468
1885.6 - 1890.0	1887.70	189, 281, 353
1933.5 - 1940.8	1936.15	232
1997.0 - 2003.3	2000.94	169

[a] When more than one photopeak appears in a gate, the principal ^{131}Te decay peak is underlined.

(X) - This is a transition assigned to ^{131}I decay.

(*) - This is a transition assigned to ^{131}Te^{g} decay.

(+) - This transition is assigned to both ^{131}Te^{m} and ^{131}Te^{g} decay.

each having a separate placement in the $^{131}Te^{m}$ decay scheme. It must be noted that in these cases the evidence for an unresolved doublet was based in large part on the level scheme which had been constructed from a large amount of additional coincidence data, and it was required that the two separate placements be consistent with all observed coincidence relationships. The transition energies were determined from coincidence spectra for the four cases in which one of the components was very weak relative to the other and hence could differ significantly in energy from the energy determined for the singles γ-ray peak (149.3-, 364.98-, 774.1-, and 1316.3-keV). All other energy values reported are those from γ-ray singles measurements. The γ-ray transition intensities of the $^{131}Te^{m}$ β-decay components of the doublets were determined from the coincidence spectra. In the six cases where the doublet involved a $^{131}Te^{g}$ γ-ray (178.56-, 342.92-, 353.5-, 383.92-, 695.62-, and 856.05-keV), however, more precise intensity values were obtained by subtracting the $^{131}Te^{g}$ decay contribution based on the 997.16-keV $^{131}Te^{g}$ decay transition and the data in Table II.

Before discussing the intensity results in detail, it is important to note that the determination of relative intensity values from coincidence spectra is not particularly straightforward and is strongly dependent on the proposed level scheme. This is illustrated in Figure 23.

Figure

23. A portion of a sample level scheme illustrating some possible coincidence relationships.

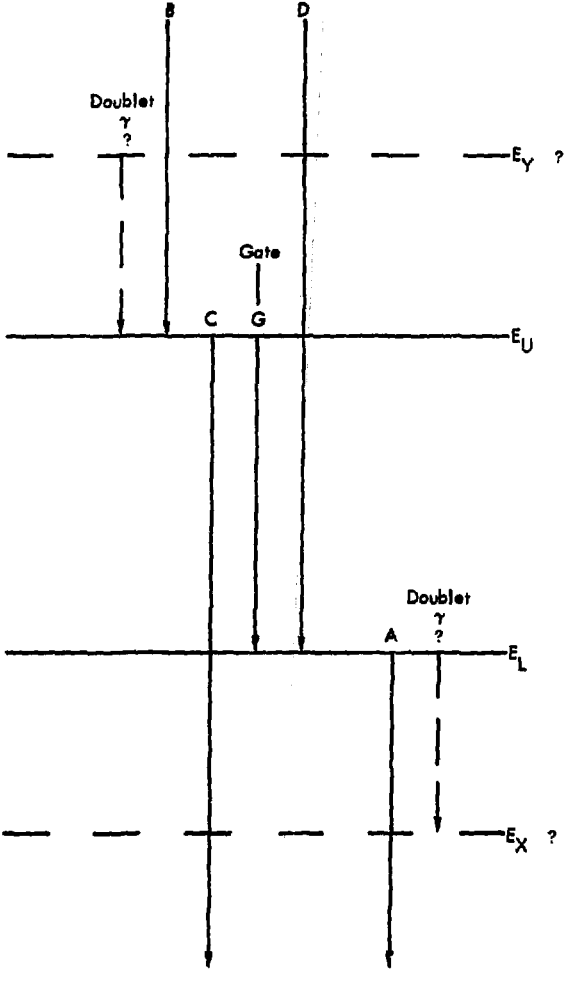
B
D
Doublet
γ
?
E_Y ?
Gate
C
G
E_U
Doublet
γ
?
A
E_L
E_X ?

Assume that a coincidence gate was set on the γ-ray labeled "G" and that the doublet γ-ray was observed in the resultant coincidence spectrum along with the γ-rays labeled "A" and "B". "G" has been placed between the levels, "E_U" and "E_L", and the doublet γ-ray has energy, E_γ. Before a relative intensity may be determined, the γ-ray must be placed in the level scheme. Assuming that other coincidence relationships have determined that the doublet γ-ray is not in indirect coincidence with "G" (e.g., the γ-rays "A" and "B" are in indirect coincidence), there are still two possible placements involving possible levels at "E_Y" or "E_X". The following factors might lead to the upper placement from "E_Y" to "E_U": (1.) "E_L" is the ground state or within E_γ of ground; (2.) the doublet γ-ray is also coincident with "C" and possibly "A"; (3.) the doublet γ-ray is not coincident with "B"; (4.) there exists firm coincidence information establishing a level, "E_Y", but not a level, "E_X"; or (5.) the intensity balances for the levels, "E_U" and "E_L", require the upper placement. Similar factors might lead to the lower placement, although the first energy argument would involve the Q_β value and the energy of "E_U" rather than the energy of "E_L". The placement of the doublet γ-ray is of importance as, to determine its relative intensity, it is necessary to compare its peak area with that of either "A" or "B" in the coincidence spectrum, correcting for the detector efficiency as a

function of γ-ray energy. The upper placement requires comparison with "B", and the lower placement requires comparison with "A". It should be noted, also, that the chosen placement is required to be consistent with all observed coincidence relationships.

Three of the observed doublets are of particular interest or involved special problems in determining the transition relative intensities. In the first, the 182.25-keV M4 I.T. transition of $^{131}Te^{m}$ was found to be a doublet with a transition between ^{131}I levels. This doublet greatly complicated the determination of the I.T. branch (see Appendix II). A gate on the 180-184 keV region resulted in observed coincidences which required two placements in the ^{131}I level scheme, one for a 182.25-keV transition (2114 to 1931 keV) and the other for the 183.11-keV transition (1980 to 1797 keV). The optimum gate for observing the 182.25-keV transition and determining its relative intensity was the 132-136 keV gate (134.86-keV γ-ray, placed 1931 to 1797 keV), a portion of which is shown in Figure 24. The 182.25-keV peak was compared to the 79.19-keV peak (2011 to 1931 keV), and a relative intensity of 19 ± 5 was deduced. The total singles intensity was 41 ± 4 resulting in an I.T. intensity of 22 ± 7. This is in excellent agreement with the value of 20 ± 4 which was calculated from the measured I.T. branch and the theoretical conversion coefficients (68Ha) for a 182.25-keV M4 transition.

Figures

24. A portion of the $^{131}Te^{m}$ γ-ray spectrum coincident with the 132-136 keV gate showing the 134- by 79-keV and 134- by 182-keV coincidences.

25. A portion of the $^{131}Te^{m}$ γ-ray spectrum coincident with the 1643-1650 keV and 791-796 keV gates. The 791-796 keV gate, having much better statistics, was used to determine the 364-keV γ-ray relative intensity.

26. A portion of the $^{131}Te^{m}$ γ-ray spectrum coincident with the 770-776 keV gate. The 773- by 774-keV, 773- by 782-keV, and 773- by 822-keV coincidences are shown as well as the 773- by 852-keV random coincidence.

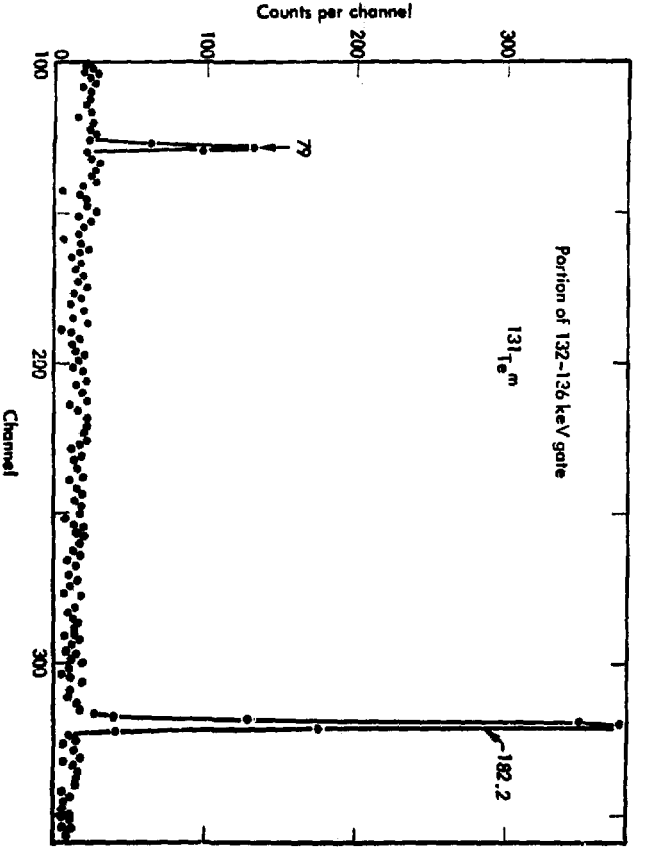
Counts per channel
100
200
300
0
100
200
300
Channel
79
182.2
Portion of 132-136 keV gate
131mTe

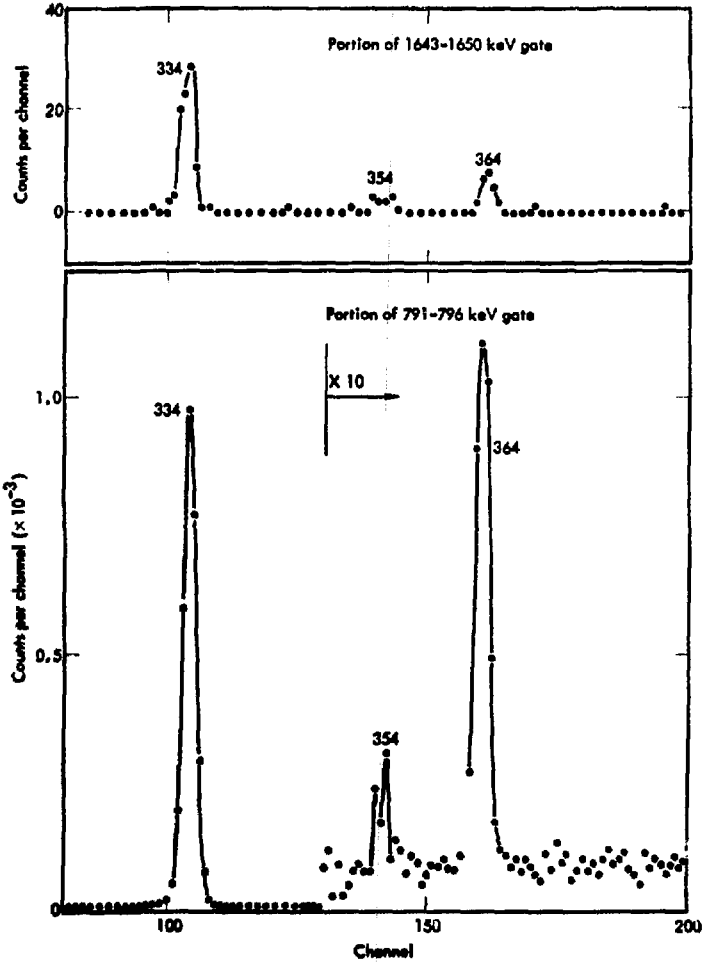
Portion of 1643-1650 keV gate
334
354
364
40
20
0
Counts per channel
Portion of 791-796 keV gate
X 10
334
364
354
1.0
0.5
0
Counts per channel (× 10⁻³)
100
150
200
Channel

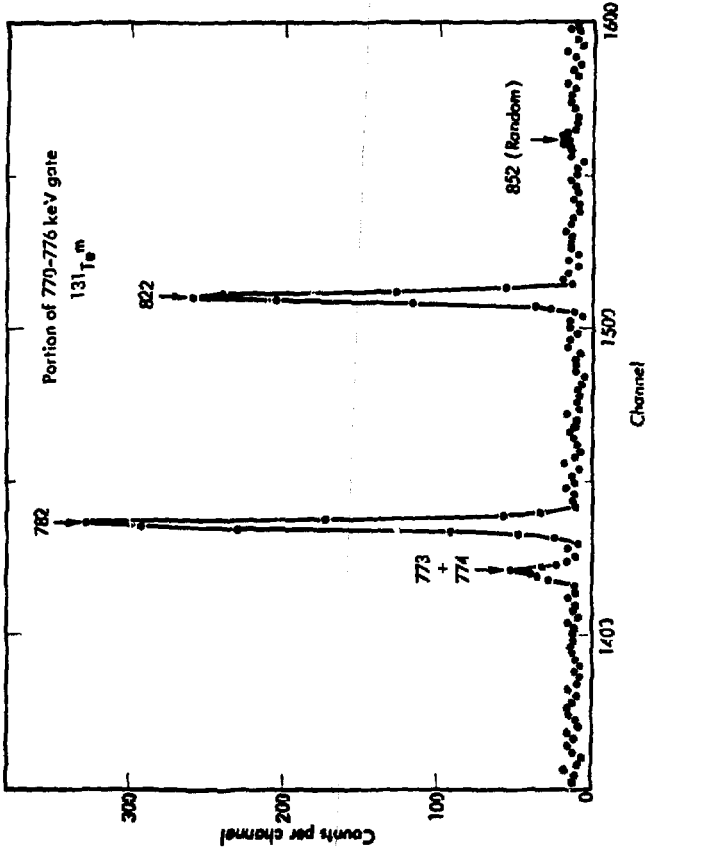
Portion of 770-776 keV gate
$^{131}Te^{m}$
782
822
773
+
774
852 (Random)
Counts per channel
Channel
0
100
200
300
1400
1500
1600

Coincidence spectra revealed the presence of a 364.98-keV transition in $^{131}Te^{m}$ decay which was not resolved from the principal ^{131}I decay γ-ray (364.48-keV) in singles spectra. Coincidence relationships placed this transition from a level at 2011 keV to one at 1646 keV. Figure 25 shows a portion of the spectra arising from 1643-1650 keV (1646.01-keV γ-ray, placed 1646 keV to ground) and 791-796 keV (793.75-keV γ-ray, placed 1646 to 852 keV) gates. The 364.98-keV peak in the 791-796 keV gate was compared to the 334.27-keV peak (1980 to 1646 keV), and a relative intensity of 31 ± 4 was deduced. When determining the ground state β-branch of $^{131}Te^{m}$ by observing growth and decay of ^{131}I in a $^{131}Te^{m}$ sample, it was necessary to correct the 364-keV peak area for contribution from this $^{131}Te^{m}$ decay transition (see Appendix II).

The third doublet of special interest is the 773.67-774.1 keV doublet. Figure 26 shows that a peak at 773.9-keV was observed in the spectrum from the 770-776 keV coincidence gate. Comparison with the 852.21-keV random coincidence peak revealed that the 773.9-keV peak was not the result of 773.67-773.67 keV random coincidences. Other coincidence relationships established levels at 773.67 and 1547.75 keV. Since the coincidence gate included both members of the two γ-ray cascade, the peak consisted of equal parts from both γ-rays. The measured energy of 773.9-keV along with the singles energy of 773.67-keV resulted in an energy for the other member of the doublet of 774.1-keV.

The relative intensity of the 774.1-keV γ-ray was determined by correcting the peak for random coincidence contributions (on the basis of the 852.21-keV random peak), dividing by two, and comparing it to the 782.49-keV (1556 to 773 keV) and 822.78-keV (1596 to 773 keV) peaks, correcting for detector relative efficiency differences. The value thus determined was 14 ± 2 which, when subtracted from the singles value of 1000 ± 8, resulted in a relative intensity of 986 ± 10 for the 773.67-keV transition (733 keV to ground).

The remaining doublets were split in a manner similar to the three cases just described. A γ-ray of 149.3-keV was observed in the 281-285 keV coincidence gate (283.2-keV γ-ray, placed 1980 to 1697 keV) and placed from 1697 to 1547 keV. Comparison with the 844.9-keV (1697 to 852 keV) and 923.4-keV (1697 to 773 keV) peaks yielded a relative intensity value of 2.0 ± 0.5. A 302.7-keV γ-ray was observed in the 820-825 keV coincidence gate (822.78-keV γ-ray, placed 1596 to 773 keV), and a 302.41-keV γ-ray appears in the decay of ^{131}I (74Me1). The 302.7-keV transition was placed from 1899 to 1596 keV, and its relative intensity was determined to be 1.0 ± 0.3 by comparison to the 200.63-keV transition (1797 to 1596 keV). The 865.3-keV peak in singles spectra consisted of components from a double escape peak and from an 865.1-keV transition which coincidence relationships placed from 1924 to 1059 keV. The 907-912 keV gate (910.00-keV γ-ray, placed 1059 to 149 keV)

resulted in the observation of an 865.1-keV transition with relative intensity of 5 ±1 determined by comparison to the 920.62-keV peak (1980 to 1059 keV). The 1316.2-keV transition was observed in the spectrum from the 849-854 keV gate (852.21-keV γ-ray, predominantly placed 852 keV to ground) and placed from 2168 to 852 keV. Its relative intensity was determined to be 2.5 ± 0.9 through comparison with the 1127.96-keV transition (1980 to 852 keV) whic' resulted in a net relative intensity of 18 ± 2 for the 1315.16-keV transition (1315 keV to ground). The splitting of the 852.21-keV and 1148.89-keV doublets was accomplished together. Coincidence spectra established a definite 1148-852 keV cascade de-exciting a level at 2001 keV. Additional coincidence relationships along with data from $^{131}Te^{g}$ decay established levels at both 852.21 and 1148.89 keV. (See Section III.C for details of the evidence for these level placements.) The 995-1001 keV gate (999.2-keV γ-ray, placed 1148 to 149 keV) determined the 852.21-keV γ-ray (2001 to 1148 keV) relative efficiency as 10 ± 5 by comparison to the 738.8-keV peak (1887 to 1148 keV). The relative intensity of the 1148.89-keV γ-ray (1148 keV to ground) was calculated to be 5 ± 6 by performing an intensity balance on the 1148 keV level assuming no direct β-feeding to the level.

C. Construction of Level Schemes.

1. Levels of ^{131}I Populated in ^{131}Te^{m} β-Decay.

In Figures 27, 28, 29, and 30, I present the level scheme of ^{131}I as determined in this investigation of the decay of 30-hr 11/2^{-} ^{131}Te^{m}. The levels along with their properties are tabulated in Table IV. The notation on Figures 27-30 is the same as in Table IV. Energies and relative intensities of the γ-rays are tabulated in Table I and presented on the figures vertically above the γ-ray transition line with the relative intensity value in parentheses. Intensities given on the figures as (205 + 145), for example, indicate γ-ray intensity plus theoretical conversion electron intensity (68Ha), respectively. Energy gates were set in the γ-γ coincidence experiment on those γ-rays depicted with a dot on their upper end, whereas those γ-rays observed in the resulting coincidence spectra are indicated by a dot at their lower end. Dashed transitions signify tentative placement and are indicated in Table I by parentheses placed around the transition assignment. Dashed levels are placed solely on the basis of dashed transitions. In making intensity balances to determine direct β-decay feeding to the levels, I assumed that there was no direct β-decay from the isomer to the levels at 149, 492, 602, and 1140 keV. The Q_{β} for ^{131}Te^{m} is 2424 ± 13 keV, calculated based on the masses of ^{130}Te and ^{131}Xe (71Wa), the Q-value for the ^{130}Te (d,p) reaction (67Grl), the measured Q_{β} of ^{131}I (51Ve, 52Ro), and the

Figures

27. The partial decay scheme of 30-hr $^{131}Te^{m}$ including β feedings to the levels between ground and 1404 keV.

28. The partial decay scheme of 30-hr $^{131}Te^{m}$ including β feedings to the levels from 1547 to 1899 keV.

29. The partial decay scheme of 30-hr $^{131}Te^{m}$ including β feedings to the levels from 1924 to 2001 keV.

30. The partial decay scheme of 30-hr $^{131}Te^{m}$ including β feedings to the levels from 2010 to 2333 keV.

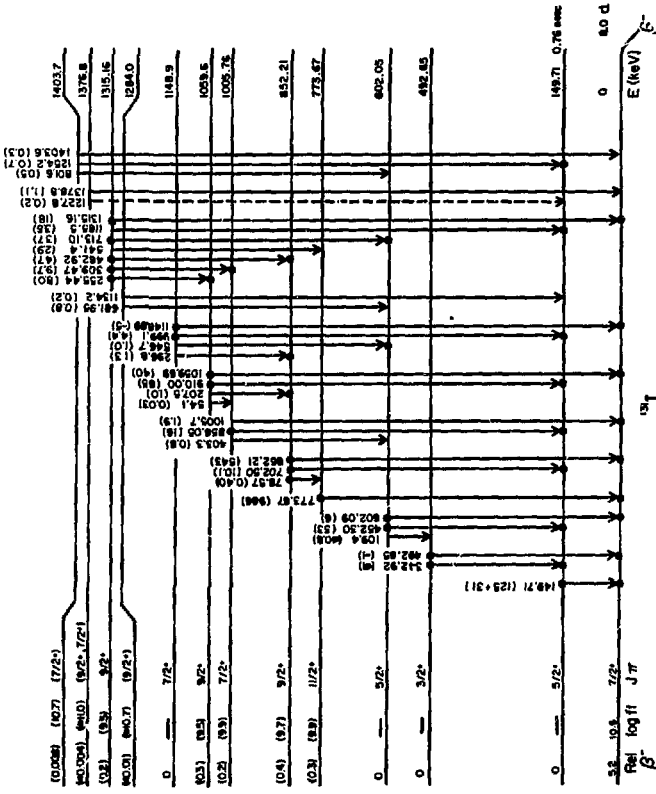
E (keV)
8.0 d
0.76 msec
149.71
492.45
602.05
773.67
852.21
1005.76
1059.5
1148.9
1315.16
1376.8
1403.7
Rel log ft
Jπ
β⁻
53⁻⁷⁸
131

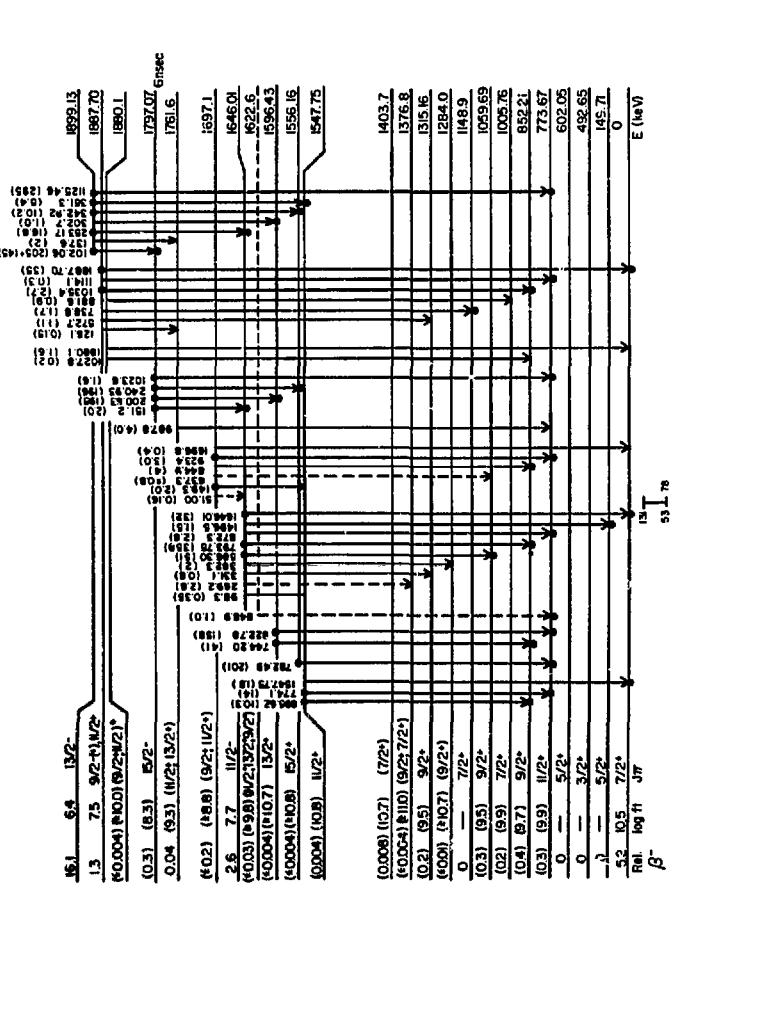
β⁻
Rel. log ft
E (keV)
1899.13
1887.70
1880.1
1797.07 Gnsec
1751.6
1697.1
1646.01
1622.6
1596.43
1556.16
1547.75
1403.7
1376.8
1315.16
1284.0
1148.9
1059.69
1005.76
852.21
773.67
602.05
492.65
145.71
0

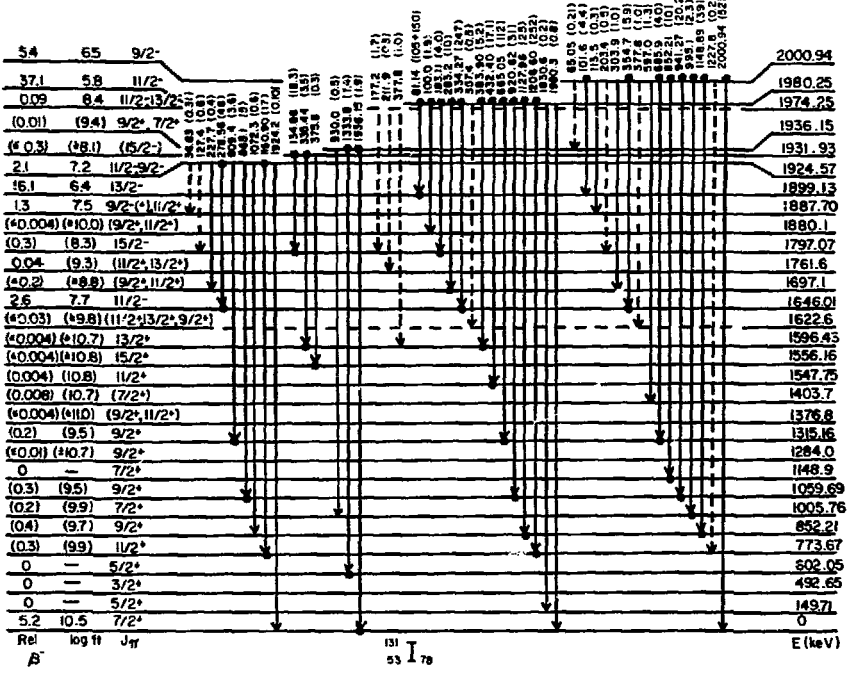
Rel
log ft
$J_{\pi f}$
E(keV)
β^-
$^{131}_{53}I_{78}$
2000.94
1980.25
1974.25
1936.15
1931.93
1924.57
1899.13
1887.70
1880.1
1797.07
1761.6
1697.1
1646.01
1622.6
1596.45
1556.16
1547.75
1403.7
1376.8
1315.16
1284.0
1148.9
1059.69
1005.76
852.21
773.67
602.05
492.65
149.71
0

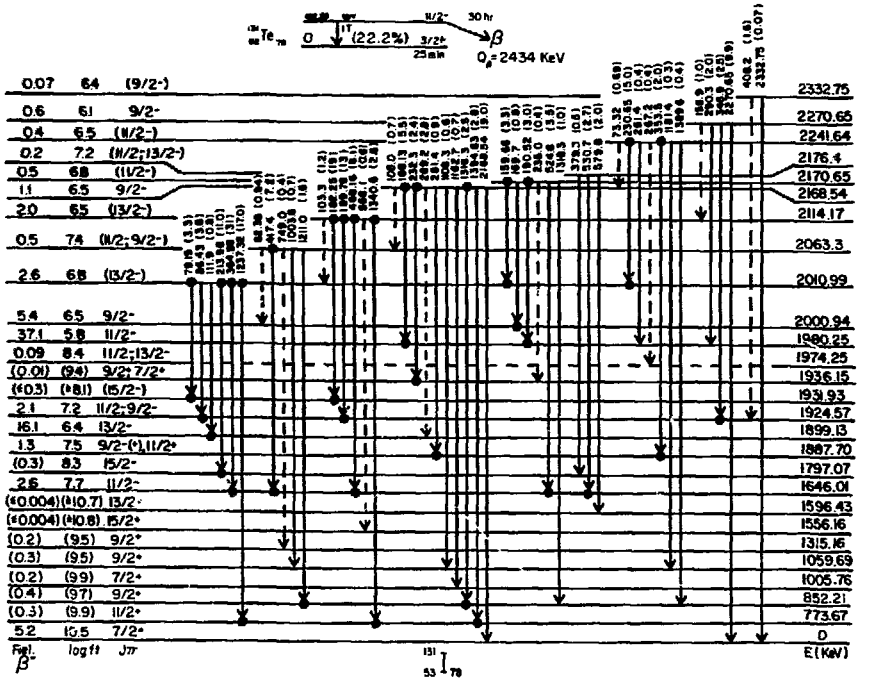
$^{131}_{52}Te_{79}$
0
11
(22.2%)
3/2+
25 min
11/2⁻
30 hr
β
Q_β=2434 KeV
Fed. β⁻
log ft
Jπ
E(KeV)
$^{131}_{53}I_{78}$
0.07 64 (9/2⁻)
0.6 61 9/2⁻
0.4 6.5 (11/2⁻)
0.2 7.2 (11/2;13/2⁻)
0.5 6.8 (11/2⁻)
1.1 6.5 9/2⁻
2.0 6.5 (13/2⁻)
0.5 7.4 (11/2;9/2⁻)
2.6 6.8 (13/2⁻)
5.4 6.5 9/2⁻
37.1 5.8 11/2⁻
0.09 8.4 11/2;13/2⁻
(0.01) (9.4) 9/2;7/2⁺
(≤0.3) (≥8.1) (15/2⁻)
2.1 7.2 11/2;9/2⁻
16.1 6.4 13/2⁻
1.3 7.5 9/2⁻(;)11/2⁺
(0.3) 8.3 15/2⁻
2.6 7.7 11/2⁻
(≤0.004) (≥10.7) 13/2⁻
(≤0.004) (≥10.8) 15/2⁺
(0.2) (9.5) 9/2⁺
(0.3) (9.5) 9/2⁺
(0.2) (9.9) 7/2⁺
(0.4) (9.7) 9/2⁺
(0.3) (9.9) 11/2⁺
5.2 10.5 7/2⁺
2332.75
2270.65
2241.64
2176.4
2170.65
2168.54
2114.17
2063.3
2010.99
2000.94
1980.25
1974.25
1936.15
1931.93
1924.57
1899.13
1887.70
1797.07
1646.01
1596.43
1556.16
1315.16
1059.69
1005.76
852.21
773.67
0

TABLE IV

^{131}I Levels Observed in the Beta Decay of 30-hr ^{131}Te^{m}.

Energy (keV)	σ^{*} (keV)	Absolute Beta**	σ^{*}	log ft	Note	Jπ Assignment
0	-	5.2	3.0	10.5	f	$7/2^{+}$
149.71	0.01	0	-	-	a	$5/2^{+}$
492.65	0.05	0	-	-	a	$3/2^{+}$
602.05	0.06	0	-	-	a	$5/2^{+}$
773.67	0.03	0.3	1.3	(9.9)	b	$11/2^{+}$
852.21	0.03	0.4	1.3	(9.7)	b	$9/2^{+}$
1005.76	0.07	0.2	0.2	(9.9)	b	$7/2^{+}$
1059.69	0.04	0.3	0.4	(9.5)	b	$9/2^{+}$
1148.9	0.1	0	-	-	a	$7/2^{+}$
1284.0	0.4	-0.04	0.05	($\geq$10.7)	c	$(9/2^{+})$
1315.16	0.08	0.2	0.4	(9.5)	b	$9/2^{+}$
1376.8	0.4	-0.06	0.04	($\geq$11.0)	d	$(9/2^{+}, 7/2^{+})$
1403.7	0.3	0.008	0.04	(10.7)	b	$7/2^{+}$
1547.75	0.10	0.004	0.2	(10.8)	b	$11/2^{+}$
1556.16	0.07	-0.3	0.2	($\geq$10.8)	d	$15/2^{+}$
1596.43	0.07	-0.5	0.3	($\geq$10.7)	d	$13/2^{+}$
1622.6	0.2	-0.02	0.05	($\geq$9.8)	c	$(11/2^{+}, 13/2^{+}, 9/2^{+})$
1646.01	0.08	2.6	0.9	7.7		$11/2^{-}$
1697.1	0.2	-0.01	0.2	($\geq$8.8)	c	$(9/2^{+}, 11/2^{+})$

TABLE IV (cont.)

Energy (keV)	σ^* (keV)	Absolute Beta**	σ^*	Log ft	Note	J^π Assignment
1761.6	0.2	0.04	0.06	(9.3)	b	$(11/2^+, 13/2^+)$
1797.07	0.08	0.3	0.7	(8.3)	b	$15/2^-$
1880.1	0.3	~0.02	0.024	(≥10.0)	c	$(9/2^+, 11/2^+)$
1887.70	0.07	1.3	0.2	7.5		$9/2^-$ (+), $11/2^+$
1899.13	0.07	16.1	0.2	6.4		$13/2^-$
1924.57	0.11	2.1	0.5	7.2		$11/2^-$, $9/2^-$
1931.93	0.10	~0.05	0.3	(≥8.1)	c	$15/2^-$
1936.15	0.09	0.01	0.05	(9.4)	b	$9/2^+$, $7/2^+$
1974.25	0.20	0.09	0.05	8.4		$11/2^-$, $13/2^-$
1980.25	0.10	37.1	1.9	5.8		$11/2^-$
2000.94	0.06	5.4	0.6	6.5		$9/2^-$
2010.99	0.08	2.6	0.3	6.8		$13/2^-$
2063.3	0.2	0.5	0.08	7.4		$(11/2^-, 9/2^-)$
2114.17	0.14	2.0	0.4	6.5		$(13/2^-)$
2168.54	0.09	1.1	0.2	6.5		$9/2^-$
2170.65	0.12	0.5	0.1	6.8		$(11/2^-)$
2176.4	0.2	0.2	0.04	7.2		$(11/2^-, 13/2^-)$
2241.64	0.13	0.4	0.1	6.5		$(11/2^-)$
2270.65	0.09	0.6	0.1	6.1		$9/2^-$
2332.75	0.40	0.07	0.04	6.4		$(9/2^-)$

TABLE IV (cont.)

* All uncertainties are one standard deviation.

** This is the number of beta rays directed to this level per 100 decays of $^{131}Te^{m}$.

a A zero beta feeding to this level was assumed.

b The intensity balance results in a positive beta branch, but due to the large uncertainty a zero beta branch cannot be ruled out.

c The intensity balance results in a negative beta branch. The log ft limit is the result of adding the uncertainty value to the calculated value.

d The intensity balance results in a negative beta branch larger in magnitude than the uncertainty value. The log ft limit was made from assuming a maximum beta feeding of 0.1 relative gamma-ray units.

f The log ft value in this case is the log f_1t.

isomer being at 182 keV. The Q_β value for $^{131}Te^m$ of 2434 ± 6 of Wapstra and Gove (71Wa) and the logf_o^- tables of Gove and Martin (71Go) were used to calculate log*ft* values.

The positions of the first three excited states have been firmly established by $^{131}Te^g$ decay scheme studies (71Mal, 65Wa) and by ^{130}Te (^3He,d) ^{131}I reaction studies (68Au). The two states at 773.67 and 852.21 keV are established by the strong intensities of the two γ-rays of these energies, the absence of any coincidence between them, as well as a 149.71- by 702.50-keV coincidence.

The level at 1005.76 keV is placed on the basis of a γ-ray of this energy and a 149.71- by 856.05-keV coincidence. In addition, these transitions are observed in $^{131}Te^g$ decay, and several weak γ-rays observed in $^{131}Te^g$ decay fit between established low-spin ^{131}I levels and a level at 1005.76 keV. The level at 1059.69 keV is placed on the basis of a γ-ray of this energy as well as 149.71- by 910.00- and 852.21- by 207.5-keV coincidences. The level at 1315.16 keV is established on the basis of a γ-ray of this energy as well as numerous coincidences including 1059.69- by 255.44- , 1005.7- by 309.45- , 852.21- by 462.92- , and 602.05- by 713.10-keV. The level at 1403.7 keV is established on the basis of a γ-ray of this energy and a 149.71- by 1254.2-keV coincidence. The level at 1547.75 keV is established by a γ-ray of this energy as well as 773.67- by 774.1- and 852.21- by 695.62-keV coincidences. For all five of these levels

the transition to ground does not appear in coincidence with any transitions originating at levels of lower energy.

The levels of 1556.16 and 1596.43 keV are placed by strong 773.67- by 782.49- and 773.67- by 822.78-keV coincidences as well as a strong 852.21- by 744.20-keV coincidence. The level at 1646.01 keV is placed by a strong γ-ray of this energy as well as 852.21- by 792.75- 1059.69- by 586.30- , and 149.71- by 1496.5-keV coincidences. In addition, a high-spin level at 1638 ± 10 keV was observed in the (^{3}He,d) reaction work (68Au). The level at 1697.1 keV is established on the basis of a γ-ray of this energy as well as coincidences indicating feeding to the levels at 773.67 and 852.21 keV. The level at 1797.07 keV is placed on the basis of coincidences between the 200.63-keV γ-ray and the 822-773 keV cascade as well as coincidences between the 240.93-keV γ-ray and the 782-773 keV cascade. This level has been observed to have a half-life of 6 nsec (70Ap2).

The 1887.70, 1924.57, 1980.25, and 2168.54 keV levels are all placed on the basis of γ-rays of these values, coincidences indicating feeding to the level at 773.67 keV, as well as numerous other coincidences indicating feeding to other established levels. The level at 1899.13 keV is established on the basis of numerous coincidences, including 773.67- by 1125.46- , 782.49- by 342.92- , 1646.01- by 253.17- , and 200.63- and 240.93- by 102.06-keV. The level at 1931.93 keV is placed on the basis of coin-

cidences, including 773.67- by 1125.46- , 782.49- by 342.92- , 1646.01- by 253.17-, and 200.63- and 240.93- by 102.06-keV. The level at 1931.93 keV is placed on the basis of coincidences indicating feeding to the levels at 1596.43 and 1797.07 keV. The level at 1936.15 keV is placed on the basis of a γ-ray of this energy as well as 602.05- and 452.30- by 1333.8-keV coincidences.

The level at 2000.94 keV is placed on the basis of a strong γ-ray of this energy as well as numerous coincidences, including 1005.7- by 995.1- , 1059.69- by 941.27- , 1315.16- by 685.9- , and 1646.01- by 354.7-keV. The levels at 2010.99, 2063.3, and 2170.65 keV are all established on the basis of coincidences indicating feeding to the 1646.01 keV level as well as to numerous other previously established levels. The level at 2241.64 keV is placed on the basis of 1887.70- by 353.5- and 1237.32- by 230.65-keV coincidences. The level at 2270.65 keV is placed on the basis of a γ-ray of this energy as well as coincidences between the 345.9-keV γ-ray and the two strongest transitions out of the level at 1924.57 keV.

The coincidence spectra indicate a strong 1148.89- by 852.21-keV coincidence, and this cascade is a major mode of deexcitation of the level at 2000.94 keV. I have, however, placed levels at both 852.21 and 1148.9 keV. A level at 852.21 keV is established by numerous coincidences between the 852.21-keV γ-ray and other γ-rays (such as; 1127.96- , 1035.4- , 844.9- , and 792.75-keV) which

when added to 2000.94-keV result in a value greater than Q_{β^-} and which cannot deexcite a level at 1148.9 keV. The level at 1148.9 keV is established on the basis of the following coincidences: 1) 149.71- by 999.2-keV (= 1148.91 keV); 2) 1148.89- by 738.8-keV (= 1887.69 keV); 3) 999.2- by 852.21-keV (deexciting 2000.94 keV level); 4) 602.05- by 546.7-keV (= 1148.75 keV); and, 5) 999.2- by 738.8-keV. In addition, the $^{131}Te^{g}$ decay data indicates the presence of the 999.2-keV transition as well as two doublets (278-280 and 351-353 keV) which may be placed from established low-spin levels to an established level at 1146.95 keV and a new level at 1148.9 keV. The splitting of the 852.21 and 1148.89-keV doublets in $^{131}Te^{m}$ decay given in Table I is based on relative intensities from coincidence spectra and on calculating an intensity balance assuming no direct β-decay from the isomer to the 1148.9 keV level.

Of the remaining eight levels shown in Figures 27-30, and in Table IV, the levels at 1376.8, 1880.1, and 2332.75 keV are established on the basis of γ-rays of these energies which were not observed in any coincidence spectra. In addition, each level is the result of one or more sums involving γ-rays not assigned to previously established levels. The remaining five levels, 1284.0, 1622.6, 1761.6, 1974.25, and 2176.4 keV, are placed solely on the basis of a number of sums and differences involving γ-rays not assigned to previously established levels.

2. Levels of ^{131}I Populated in ^{131}Te^{g} β-Decay.

In Figures 31 and 32, I present the level scheme of ^{131}I as observed in the β-decay of 25-min $3/2^{+}$ ^{131}Te^{g}. The levels along with their properties are tabulated in Table V. The notation is the same as that used in Figures 27-30 and in Table IV. The energies and intensities of the γ-rays are tabulated in Table II and presented on Figures 31 and 32 as on Figures 27-30. The Q_{β} for ^{131}Te^{g} is 2242 ± 13 keV, calculated as described in the preceding section. (The value of 2252 ± 6 keV of Wapstra and Gove (71Wa) was used in logft calculations.) The β-branch values are based on a zero direct β-feeding from ^{131}Te^{g} to the ^{131}I ground state (63De), and the logft values were calculated using the $\log f_{o}^{-}$ tables of Gove and Martin (71Go).

For the ground state decay of ^{131}Te, most of the levels were established by the decay scheme work of Macias and Walters (71Mal) and the (^{3}He,d) reaction work of Auble et al. (68Au). I have observed a number of previously unobserved weak γ-transitions and have placed six new levels. Three of these, 852.21, 1005.76, and 1148.9 keV, were also observed in ^{131}Te^{m} β-decay. The level at 1757.9 keV is placed on the basis of two γ-rays which may feed the levels at 492.66 and 149.716 keV. The levels at 2040.8 and 2072.6 keV are placed on the basis of γ-rays of these energies as well as three additional transitions apiece. In addition, the (^{3}He,d) work placed a level at 2040 ± 15 keV (68Au). The newly observed weak γ-rays were placed on

Figures

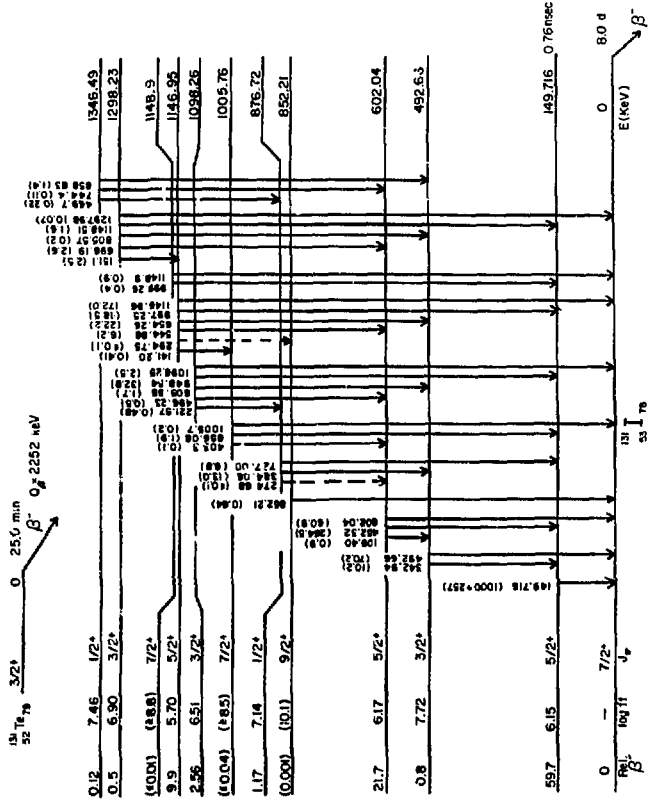
131 52 Te 79
3/2+
0
25.0 min
β⁻
Qβ = 2252 keV
131 53 I 78
8.0 d
0.76nsec
E(keV)
Rel. β⁻
log ft
Jπ
1346.49
1298.23
1148.9
1146.95
1098.26
1005.76
876.72
852.21
602.04
492.63
149.716
0
1/2+
3/2+
7/2+
5/2+
3/2+
1/2+
9/2+
5/2+
3/2+
7/2+
5/2+

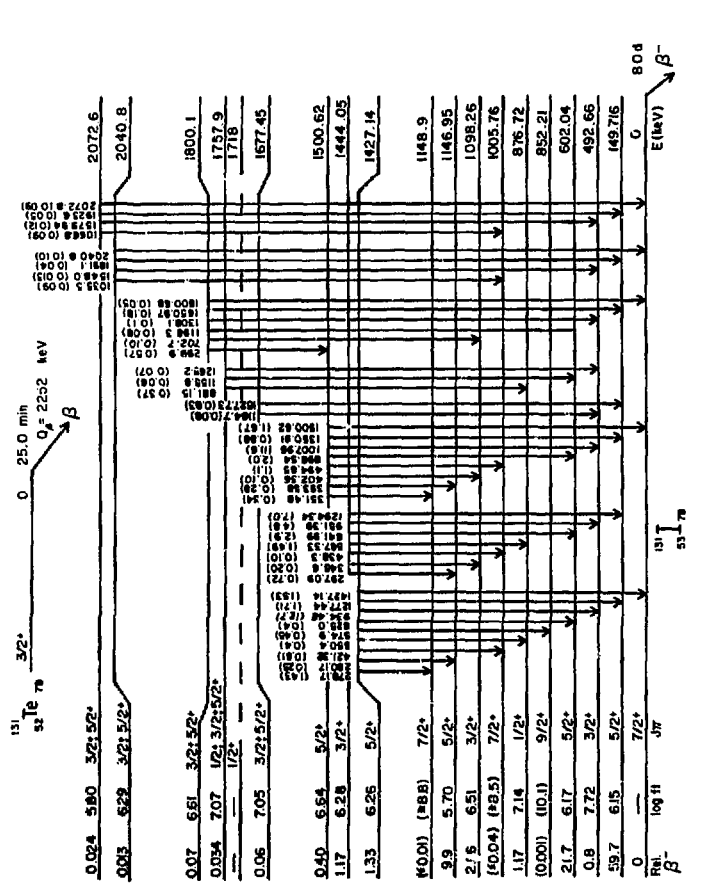
131 52 Te 79
3/2+
0
25.0 min
Q_β = 2252 keV
β
2072.6
2040.8
1800.1
1757.9
1718
1677.45
1500.62
1444.05
1427.14
1148.9
1146.95
1098.26
1005.76
876.72
852.21
602.04
492.66
149.716
0
804
E(keV)
β⁻
131 53 I 78

TABLE V

^{131}I Levels Observed in the Beta Decay of 25-min ^{131}Te^{g}.

Energy (keV)	σ[a] (keV)	Absolute Beta[b]	σ[a]	log ft	Note	J π Assignment
0	---	0	---	---	c	$7/2^+$
149.716	0.005	59.7	0.6	6.15		$5/2^+$
492.66	0.01	0.8	0.1	7.72		$5/2^+$
602.04	0.01	21.7	0.2	6.17		$5/2^+$
852.21	0.06	0.001	0.020	(10.1)	d	$9/2^+$
876.72	0.02	1.17	0.05	7.14		$1/2^+$
1005.76	0.04	-0.01	0.05	(≥8.5)	e	$7/2^+$
1098.26	0.02	2.56	0.04	6.51		$3/2^+$
1146.95	0.02	9.9	0.2	5.70		$5/2^+$
1148.9	0.1	-0.02	0.03	(≥8.8)	e	$7/2^+$
1298.23	0.03	0.5	0.1	6.90		$3/2^+$
1346.49	0.06	0.12	0.02	7.46		$1/2^+$
1427.14	0.03	1.33	0.07	6.26		$5/2^+$
1444.05	0.03	1.17	0.06	6.28		$3/2^+$
1500.62	0.03	0.40	0.04	6.64		$5/2^+$
1677.45	0.05	0.06	0.01	7.05		$3/2^+$, $5/2^+$
1718	10.	---	---	----	f	$1/2^+$
1757.9	0.1	0.034	0.007	7.07		$1/2^+$, $3/2^+$, $5/2^+$

TABLE V (cont.)

Energy (keV)	σ[a] (keV)	Absolute Beta[b]	σ[a]	log ft	Note	J^π Assignment
1800.7	0.1	0.07	0.02	6.61		$3/2^+$, $5/2^+$
2040.8	0.1	0.013	0.005	6.29		$3/2^+$, $5/2^+$
2072.6	0.1	0.024	0.006	5.80		$3/2^+$, $5/2^+$

[a] All uncertainties are one standard deviation.

[b] This is the number of betas direct to this level per 100 decays of $^{131}Te^g$.

[c] A zero beta feeding to this level was assumed.

[d] The intensity balance gives a positive beta branch, but due to the large uncertainty value a zero beta branch cannot be ruled out.

[e] The intensity balance gives a negative beta branch. The log ft limit is the result of adding the uncertainty value to the calculated value.

[f] This level was seen in (^{3}He,d) reaction studies, however there was no definite evidence for this level in this study of $^{131}Te^g$ decay.

the basis of precise sums and differences.

I have reassigned the 1579.94-keV transition which was used by Macias and Walters (71Mal) to place a level at 1729 keV. Their observation of a 149- by 1579-keV coincidence was marginal, and I was unable to detect this coincidence. A search for any other possible transitions deexciting a level of this energy proved unsuccessful. The (^{3}He,d) reaction work placed a level at 1718 ± 10 keV with an assignment of $1/2^+$ and a relatively large spectroscopic factor (0.31). The most probable transitions from such a level would be to the 149 keV level (1569 ± 10 keV) or the 493 keV level (1226 ± 10 keV). A close examination of the singles spectra resulted in upper limits for such transitions of I_γ (1569) $\leq$0.02 (in two spectra) and I_γ (1226) $\leq$0.01 (in all spectra).

D. Spin and Parity Assignments.

The spin and parity assignments of the ^{131}I levels seen in the decay of 25-min $3/2^+$ ^{131}Te^g are presented in Figures 31 and 32 and in Table V. These assignments are essentially taken from the work of Macias and Walters (71Mal). The assignments of the three newly observed levels seen also in the ^{131}Te^m decay study will be discussed in the context of the decay scheme of the $11/2^-$ isomer. The level at 1757.9 keV is assigned as $1/2^+$, $3/2^+$, or $5/2^+$ based on a logft value of 7.07, indicative of allowed β-decay. With logft values $\leq$6.3 and direct transitions to the $7/2^+$ ground

state, the levels at 2040.8 and 2072.6 keV are assigned as $3/2^+$ or $5/2^+$. The levels at 1146.95 and 1427.14 keV ($3/2^+$ or $5/2^+$ in Macias and Walters) are assigned as $5/2^+$ based on the observation of transitions to the $9/2^+$ state at 852.21 keV. The remaining levels previously assigned as $3/2^+$ or $5/2^+$ have been given one or the other assignment based on branching ratios to $1/2^+$ and $7/2^+$ states and on systematic considerations. These levels may well have either assignment however.

The spin and parity assignments of the levels of ^{131}I observed in the β-decay of 30-hr $11/2^-$ $^{131}Te^m$ are presented in Figures 27-30 and in Table IV. These assignments are based on log*ft* values for the β-decay of the $11/2^-$ isomer (Nota bene: A survey of 29 first-forbidden transitions in the β-decays of the nearby nuclei; ^{125}Sb, $^{125}Sn^g$, $^{127}Sn^g$, $^{127}Te^m$, and $^{129}Te^m$ reveals no log*ft* values less than 8.0 (72Au2, 71Ka, 70Apl, 71Apl, 74Ap, 72Wa, 74Mal).), the γ-ray deexcitation patterns between levels, and the earlier conversion electron measurements (65De, 67Be2). The assignments for the ground state and the states at 149.71, 492.65, and 602.05 keV are taken from the $^{131}Te^g$ decay scheme work (65Wa, 71Mal).

All of the levels from 773.67 to 1403.7 keV are limited to spin and parity values of $7/2^+$, $9/2^+$, and $11/2^+$ by their prompt γ transitions to the $7/2^+$ ground state, the lack of observed direct β-feeding in the decay of 25-min $3/2^+$ $^{131}Te^g$, and their γ feeding from numerous high-lying levels

with spin values of 9/2, 11/2, and 13/2. The even parity assignments are consistent with the log*ft* values ranging from 9.5 to ≥11.0 reflecting first-forbidden β-decay. The levels at 852.21, 1059.69, 1315.16, and 1376.8 keV are assigned as $9/2^+$ based on their prompt decay to the $5/2^+$ state at 149.71 keV and their γ-feeding from the $11/2^-$ state at 1646.01 keV (although the 1376.8 keV level may be $7/2^+$ as the 269.2-keV γ-transition is dashed in and is placed twice). The state at 1284.0 keV is assigned as $9/2^+$ based on decay to $5/2^+$ states and feeding from the $11/2^-$ level at 1646.01 keV. The states at 1005.76, 1148.9, and 1403.7 keV are assigned as $7/2^+$ based on γ-feeding from $9/2^-$ states, the lack of feeding from $11/2^-$ states, and their pattern of strong decay branches to the $5/2^+$ 602.05 keV level. In addition the 1005.76 and 1148.9 keV levels are fed by several $3/2^+$ or $5/2^+$ levels in $^{131}Te^g$ decay. The level at 773.67 keV is assigned as $11/2^+$ based on the absence of any transitions from or to any $3/2^+$ or $5/2^+$ levels, and on the systematic presence of an $11/2^+$ level in ^{127}I and ^{129}I firmly established by (n,n' γ), γγ', and Coulomb excitation studies (72Au, 72Ho).

The state at 1646.01 keV was observed in the (^{3}He,d) work of Auble *et al.* (68Au). They reported an *ℓ* value of 5 and a spectroscopic factor (C^2S_J) of 0.70. They assigned the state as $11/2^-$ and interpreted it as being predominantly $h_{11/2}$ single particle in character. The log*ft* value of 7.7 is somewhat high for an allowed β-transition but is considerably

lower than the values for the first forbidden β-transitions. Allowed β-transitions with logft values as high as 9.7 have been found in the decay of 9.4-hr $^{127}Te^{g}$ (70Ap1, 71Ap1).

The ten states, 1899.13, 1980.25, 2000.94, 2010.99, 2114.17, 2168.54, 2170.65, 2241.64, 2270.65, and 2332.75 keV, all have logft values ≤ 6.8 and are assigned spin and parity values of $9/2^-$, $11/2^-$, or $13/2^-$ consistent with allowed β-decay from $11/2^-$ $^{131}Te^{m}$. The four states with large γ branches to the $7/2^+$ ground state, 2000.94, 2168.54, 2270.65, and 2332.75 keV, are assigned as $9/2^-$. The states at 1980.25, 2170.65, and 2241.64 keV lack or have very weak branches to the ground state, lack branches to any of the $7/2^+$ excited states, and have strong branches to various of the low-energy $9/2^+$ states. They are assigned spin and parity of $11/2^-$. The remaining three states, 1899.13, 2010.99, and 2114.17 keV, are assigned spin and parity of $13/2^-$ on the basis of a lack of observed branches to any $7/2^+$ or $9/2^+$ states and the presence of strong branches to the 773.67 keV $11/2^+$ state. These assignments are all consistent with the conversion electron measurements (65De, 67Be2) which indicate the 81.14-keV transition (1980 to 1646 keV) to be M1 + E2.

The conversion electron measurements have shown the 102.06-keV transition (1899 to 1797 keV) to be pure M1 and the 200.63-keV (1797 to 1596 keV) and 240.93-keV (1797 to 1556 keV) transitions to be E1. Thus, the level at 1797.07 keV must be of odd parity while the levels at 1556.16 and

1596.43 keV must be of even parity. The assignment of $13/2^-$ to the 1899.13 keV level restricts the 1797.07 keV level to spin values of 11/2, 13/2, and 15/2. The half-life of the 1797.07 keV level has been measured to be 6 nsec (70Ap2). The upper limit for the intensity of a 1797.07-keV transition to ground was determined to be $\leq$0.1 intensity units. This results in a partial half-life for the 1797.07-keV transition of $\geq$25 μsec. The theoretical single-particle half-lives (with statistical factor omitted) (67Le) for an M2 ($11/2^-$ to $7/2^+$) or E3 ($13/2^-$ to $7/2^+$) transition of this energy are 1.2×10^{-11} sec and 5.9×10^{-9} sec. respectively. Thus, the hindrances would be $\geq 2 \times 10^6$ and $\geq$4200, respectively. The partial half-life of the 1023.6-keV transition to the $11/2^+$ level at 773.67 keV is 1.5 μsec. The theoretical single-particle half-lives (67Le) for an E1 ($11/2^-$ to $11/2^+$ or $13/2^-$ to $11/2^+$), M2 ($15/2^-$ to $11/2^+$), or E3 ($15/2^-$ to $11/2^+$), transition of this energy are 1.6×10^{-16} sec, 2.0×10^{-10} sec, and 3.1×10^{-7} sec, respectively. The E1 hindrance would be $\approx 10^{10}$, whereas the M2 hindrance would be $\approx$7500, and the E3 hindrance would be $\approx$5. We, therefore, propose a spin and parity assignment of $15/2^-$ for the 1797.07 keV isomeric level as being most consistent with known trends of observed and theoretical γ-transition rates (65Go, 65Mo). I take the logft value of 8.3 as a lower limit due to the large uncertainty involved in the intensity balance for this level.

The level at 1547.75 keV is assigned as $11/2^+$ on the basis of transitions to $7/2^+$, $9/2^+$, and $11/2^+$ levels, feeding from $11/2^-$ and $13/2^-$ levels, and a logft value of 10.8. I favor assignment of $11/2^+$ to the levels at 1622.6 and 1761.6 keV on the basis of logft values and transitions to only the $11/2^+$ level at 773.67 keV, although $9/2^-$ and $13/2^+$ assignments are not ruled out. The level at 1697.1 keV feeds levels with assignments $11/2^+$, $11/2^-$, $7/2^+$, and $9/2^+$ and is fed from $9/2^-$ and $11/2^-$ levels. I favor an assignment of $9/2^+$ but cannot rule out $11/2^+$. With a logft value of $\geq$10.0 and transitions to $7/2^+$ and $9/2^+$ and feeding from an $11/2^-$ level, I assign a value of $9/2^+$ or $11/2^+$ to the 1880.1 keV level. The logft value of 7.5 and strong transitions to $7/2^+$, $9/2^+$, and $11/2^+$ levels as well as feeding from $9/2^-$ and $11/2^-$ levels leads to a preferred assignment of $9/2^-$ for the 1887.70 keV level. However, I cannot rule out $9/2^+$ or $11/2^+$, although these two assignments are unlikely in view of the logft values for first forbidden β-transitions already observed in $^{131}Te^m$ decay.

The logft value of 9.4 and strong transitions to $5/2^+$ and $7/2^+$ states as well as feeding from a $9/2^-$ state leads to assigning the 1936.15 keV state as $9/2^+$ or $7/2^+$. The state at 1931.93 keV is assigned as $15/2^-$ on the basis of observing transitions only to levels with spin and parity $15/2^-$, $15/2^+$ or $13/2^+$ and feeding only from $13/2^-$ levels. The states at 1924.57 and 2063.3 keV are assigned as $11/2^-$ or $9/2^-$ on the basis of logft values suggesting allowed

β-decay and γ-transitions only to levels with spin and parity values of $11/2^-$, $11/2^+$, or $9/2^+$. The levels at 1974.25 and 2176.4 keV feed $15/2^-$ and $13/2^+$ levels and are fed reasonably strongly in β-decay. I, therefore, assigned these levels spin and parity values of $11/2^-$ or $13/2^-$.

E. Discussion.

The excited states of ^{131}I may be separated into several major categories: single quasi-particle proton states, single proton plus Te core collective excitation states (large, even parity), proton three quasi-particle states, three proton quasi-particle plus Sn core collective excitation states, and three quasi-particle states constructed from one-proton-two-neutron ($\pi\nu_1\nu_2$) configurations (largely odd parity). This study of the decays of the $11/2^-$ and $3/2^+$ isomers of ^{131}Te has offered the opportunity to examine the character of a large number of states of ^{131}I. Including the results of the earlier ^{130}Te (^{3}He,d) reaction work (68Au), there are now a total of 55 excited states placed in ^{131}I below 2.4 MeV. These levels have spin and parity (J^π) values ranging from $1/2^+$ to $15/2^+$ and from $9/2^-$ to $15/2^-$.

In Figure 33, I compare the levels of ^{131}I below ~1.9 MeV with the levels of ^{129}I observed in the decays of 69-min $3/2^+$ ^{129}Te^g (72Wa) and 34.1-day $11/2^-$ ^{129}Te^m (74Mal) and in the ^{128}Te(^{3}He,d) reaction (68Au). Also shown are the low-lying even parity excited states observed in the

Figure

33. The levels of ^{131}I (this work and 68Au) compared to the levels of ^{129}I (72Wa, 74Ma1). Also shown are the even-even Te core states (71Se, 72Ke1, 72Ke2, 73Au1, 74Hi, 74Ke).

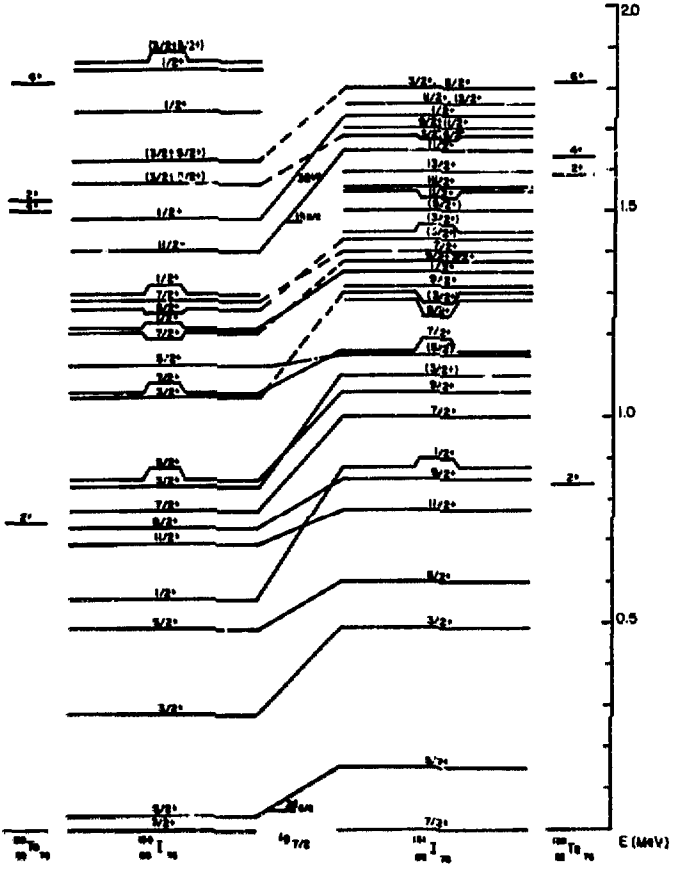
2.0
1.5
1.0
0.5
E (MeV)

even-even cores, ^{128}Te and ^{130}Te (71Se, 72Kel, 72Ke2, 73Aul, 74Hi, 74Ke). The notation of the $1g_{7/2}$, $2d_{5/2}$, $1h_{11/2}$, and $3s_{1/2}$ single quasi-particle levels is made for the levels of the appropriate spin and parity having the largest spectroscopic factors in the (^{3}He,d) reaction. The $2d_{3/2}$ state in both ^{129}I and ^{131}I remains uncertain as the single particle strength is split between a large number of $3/2^+$ states (68Au). The single quasi-particle levels are seen to rise in energy from ^{129}I to ^{131}I. This continues a similar behavior seen when going from ^{127}I (70Apl, 71Apl, 68Au, 72Aul) to ^{129}I. Qualitatively, the level structures of ^{129}I and ^{131}I are seen to be quite similar. The ^{129}I level structure is lacking in observed high-spin ($\geq$13/2) states and in odd parity states, but this is understandable as the Q_β of ^{129}Te^m is only 1602 keV (71Wa).

There is a general increase in energy of all of the positive parity levels from ^{129}I to ^{131}I which parallels the increase in energy of the collective core excitations (2^+ one-phonon and 4^+, 2^+ two-phonon states) from ^{128}Te to ^{130}Te. This systematic behavior is presented in greater detail in Figure 34 which shows the lowest lying $5/2^+$, $7/2^+$, $9/2^+$, and $11/2^+$ levels in ^{127}I (68Au, 70Apl, 71Apl), ^{129}I (72Wa, 74Mal), ^{131}I, and ^{133}I (75Lal) along with the appropriate Te core 2_1^+ spacing (73Aul, 73Au2, 74Hi, 74Ke) above the $1g_{7/2}$ and $2d_{5/2}$ single quasi-particle levels. The positive parity states appear to behave as if they result from the coupling of the core excitations to the single

Figure

34. Even parity level systematics of the odd-mass iodine nuclei (this work, 68Au, 70Ap1, 71Ap1, 72Wa, 74Ma1, 75La1). Also shown is the appropriate Te core 2_1^+ spacing (73Au1, 73Au2, 74Hi, 74Ke) above the $1g_{7/2}$ and $2d_{5/2}$ single quasi-particle levels in each nucleus.

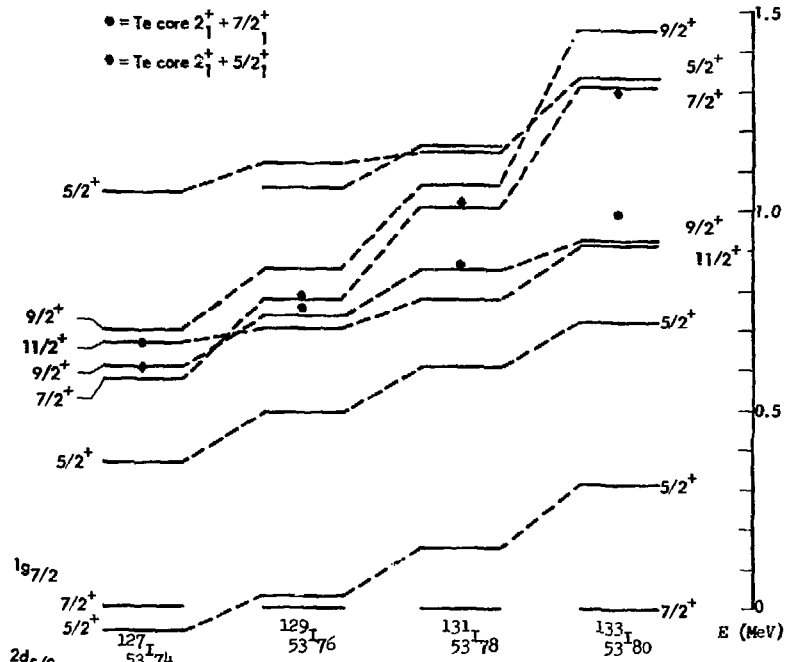
● = Te core $2_1^+ + 7/2_1^+$
● = Te core $2_1^+ + 5/2_1^+$
$5/2^+$
$9/2^+$
$11/2^+$
$9/2^+$
$7/2^+$
$5/2^+$
$1g_{7/2}$
$7/2^+$
$5/2^+$
$2d_{5/2}$
$^{127}_{53}I_{74}$
$^{129}_{53}I_{76}$
$^{131}_{53}I_{78}$
$^{133}_{53}I_{80}$
$9/2^+$
$5/2^+$
$7/2^+$
$9/2^+$
$11/2^+$
$5/2^+$
$5/2^+$
$7/2^+$
1.5
1.0
0.5
0
E (MeV)

quasi-particle states. It may be noted in particular that the $11/2^+$ and $9/2^+$, levels appear to be phonon-plus-$1g_{7/2}$ states and that the $7/2_2^+$ and $9/2_2^+$ levels appear to be phonon-plus-$2d_{5/2}$ states. The $5/2^+$ levels also appear to follow the general trend, but, as will be shown later, no single-particle-plus-phonon calculation predicts a $5/2^+$ state lying within 400-500 keV of the $2d_{5/2}$ state as is observed experimentally.

The general features of the level structure of ^{131}I may be understood in terms of the single quasi-particle proton states coupling to core excitations or to two quasi-particle states in the ^{130}Te core. In Table VI,I show the spins, parities, and configurations expected in the low-lying ^{130}Te level structure along with the energies of those states which have been observed. Not all of these states have been observed and identified in ^{130}Te; however, an examination of the structure of the even-even Sn isotopes for A = 122, 124, and 126 and the even-even Te isotopes for A= 122, 124, 126, 128, and 130 (72Be, 73Au1, 73Au2, 73Be, 74Hi) indicates that most of these states are present. The coupling of these core states to the single quasi-particle proton states results in a large number of states of even parity ranging from spins of 1/2 to 27/2 and of odd parity ranging from 1/2 to 21/2.

In ^{130}Te, the one phonon and two phonon excitations both lie lower than the lowest observed two quasi-particle level, a 6^+ state at 1815 keV (see Figures 33 and 36).

TABLE VI.

Possible Low-lying States in ^{130}Te

and the Energies (in keV) of those States Observed in ^{130}Te.

Type of excitation or Particle configuration	J^{π} of resultant states						
One phonon		2^+(839)					
Two phonon	0^+	2^+(1588)	4^+(1632)				
Octupole			3^-(2732)				
$\nu(1h_{11/2})^2$	0^+	2^+	4^+	6^+	8^+	10^+	
$\nu(2d_{3/2})^2$	0^+	2^+					
$\nu(3s_{1/2})^2$	0^+						
$\nu(1h_{11/2}, 2d_{3/2})$			4^-	5^-, 6^- (2100)	7^-(2147)		
$\nu(1h_{11/2}, 3s_{1/2})$				5^-, 6^- (2100)			
$\nu(2d_{3/2}, 3s_{1/2})$		1^+, 2^+ (1880)					
$\pi(1g_{7/2}, 2d_{5/2})$		1^+, 2^+ (1880)	3^+	4^+	5^+	6^+ (1815)	
$\pi(1g_{7/2})^2$	0^+	2^+	4^+		6^+ (1815)		
$\pi(2d_{5/2})^2$	0^+	2^+	4^+				

TABLE VII.

The distribution of even parity states of ^{131}I below ~2 MeV predicted by zeroth-order coupling of the one-phonon and two-phonon excitations in ^{130}Te with the $1g_{7/2}$ and $2d_{5/2}$ shell model orbitals, and by the $(1g_{7/2})^3$ configuration and the coupling of the particular configuration, $(1g_{7/2})^3\ 5/2^+$, to the one-phonon excitation in ^{128}Sn. The $3s_{1/2}$ and $2d_{3/2}$ single proton shell model orbitals are also included. The number of observed levels of each J^π is also shown (this work and 68Au).

J^π	Theor. One Phonon	Obs. One Phonon	Theor. $(1g_{7/2})^3$	Obs. $(1g_{7/2})^3$	Theor. $(1g_{7/2})^3 5/2^+$ + Sn Phonon	Theor. Two Phonon	Observed High Energy Even Parity States
$1/2^+$	1	1	---	---	1	3[a]	2
$3/2^+$	2	2	1	0	1	4[b]	2
$5/2^+$	2	2	1	1	1	5	1
$7/2^+$	2	2	1	0	1	5	1
$9/2^+$	2	2	1	0	1	4	2
$11/2^+$	1	1	1	0	---	3	1
$13/2^+$	---	---	---	---	---	2	1
$15/2^+$	---	---	1	0	---	1	1

[c] 5[c], 1[c], 2[c], 3[c], 1[c], 1[c]

[a] Includes the $3s_{1/2}$ shell-model orbital.

[b] Includes the $2d_{3/2}$ shell-model orbital.

[c] Indicates states which are assigned more than one possible J^π value.

Figure

35. The even parity levels of ^{131}I (this work and 68Au). On the left are the even parity ^{130}Te core states (72Ke2, 74Hi, 74Ke); and in the center are the states arising from a zeroth-order coupling of the Te core to the $1g_{7/2}$ and $2d_{5/2}$ states in ^{131}I, and of the Sn core 2_1^+ to the $(1g_{7/2})^3$ $5/2^+$ in ^{131}I.

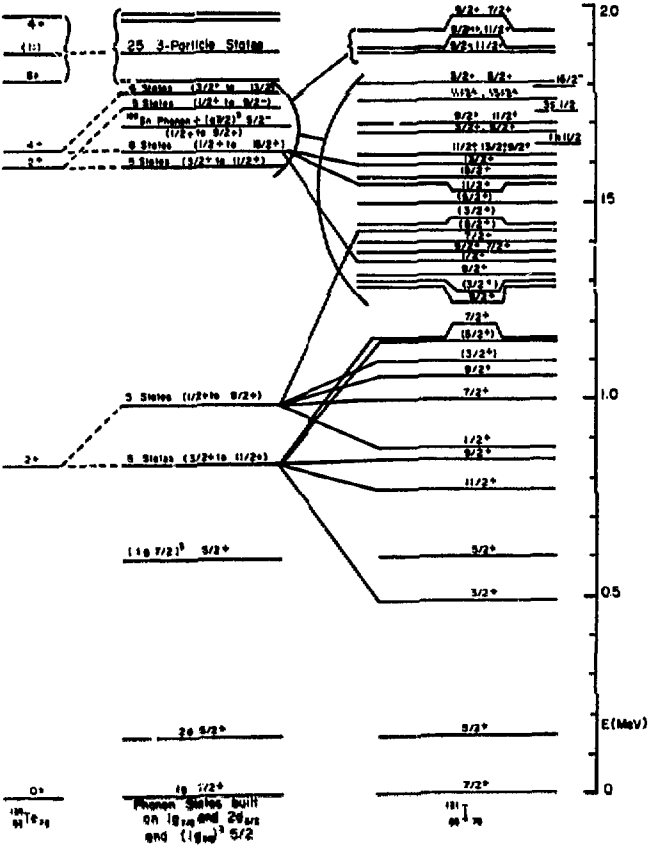
4+
(1)
8+
4+
2+
25 3-Particle States
3 States (1/2+ to 9/2+)
5 States (3/2+ to 11/2+)
Phonon + (g9/2)3 5/2−
(1/2+ to 9/2+)
8 States (1/2+ to 15/2+)
5 States (3/2+ to 11/2+)
3 States (1/2+ to 9/2+)
5 States (3/2+ to 11/2+)
(1g 7/2)3 5/2+
2d 5/2+
1g 7/2+
0+
Phonon States built on 1g7/2 and 2d5/2 and (1g7/2)3 5/2
2.0
1.5
1.0
0.5
E(MeV)
0

Thus, although one expects a certain amount of configuration mixing at higher energies, it appears probable that the phonon states in ^{131}I should be identifiable, particularly the one-phonon excitations. In Table VII I show the distribution of states resulting from coupling the Te one- and two-phonon excitations to the $1g_{7/2}$ and $2d_{3/2}$ single quasi-particle states and from a $(\pi 1g_{7/2})^3 5/2$ configuration and its coupling to the 2^+ one-phonon state in ^{128}Sn, along with a count of the number of states of each spin and parity observed in ^{131}I below 2.0 MeV. This is illustrated schematically in Figure 35 which shows the observed even parity states in ^{130}Te (72Ke2, 74Hi, 74Ke), the result of a zeroth-order coupling of these states with the $7/2^+$ and $5/2^+$ states (ground and 149.71 keV) in ^{131}I, the result of a zeroth-order coupling of the observed $(\pi 1g_{7/2})^3$ $5/2^+$ state (602.05 keV) with the ^{128}Sn one-phonon state, and the observed levels in ^{131}I below 2.0 MeV. The connections between states are made on the basis of possible spin values, level systematics (Figure 34), and on the de-excitation branchings of the observed states to the $7/2^+$ and $5/2^+$ single quasi-particle states. It may be observed that all ten states resulting from the coupling of the two single quasi-particle states to the 2^+ one-phonon ^{130}Te core state have been identified and that the second phonon excitation can account for the remaining observed even parity states. Most of the "missing" states are

$7/2^+$ which are very difficult to observe in the β decay of $3/2^+$ or $11/2^-$ isomers or in the ^{130}Te (^3He,d) reaction.

In Figure 36 I show a comparison of the experimental even parity levels of ^{131}I with the detailed calculations of Rustgi, Lucas, and Mukherjee (68Ru: proton plus ^{130}Te core), Kisslinger and Sorenson (63Ki: quasi-particle plus Te phonon), and Almar, Civitarese, and Krmpotic (73Al: three-proton cluster plus Sn core phonon). The agreement between theory and experiment is reasonable, however the positions of some states are not identified in the theoretical calculations, namely the $13/2^+$ and $15/2^+$ states and some of the $9/2^+$ or $11/2^+$ states. Some of these states were not calculated, as the core states used included only first and second phonon states and the models used are not very realistic at high excitation energies (68Ru, 63Ki). The three-proton cluster plus Sn core model clearly gives the best explanation of the observed density of even parity states, and presumably extensions of this model to higher spin states and higher excitation energies would improve the fit to the experimental levels.

Only the three-proton cluster plus Sn phonon model predicts a $5/2^+$ level in the vicinity of 500-600 keV. Such a level is observed experimentally at 602.05 keV and is thought to be predominantly $(1g_{7/2})^3 5/2$ in character (as labeled in Figure 34). The three-proton cluster models predict that the $5/2^+$ coupling will be

Figure

36. Comparison between the experimental even parity states in ^{131}I (this work and 68Au) and three different theoretical calculations (63Ki, 68Ru, 73Al).

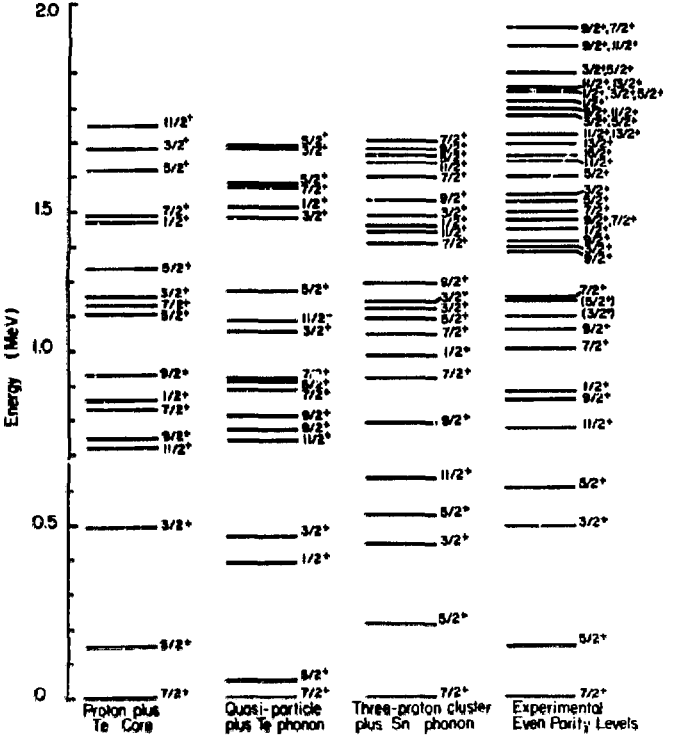
2.0
1.5
1.0
0.5
0
Energy (MeV)
Proton plus Te Core
Quasi-particle plus Te phonon
Three-proton cluster plus Sn phonon
Experimental Even Parity Levels

the lowest lying of all the states arising from a $(1g_{7/2})^3$ three-proton configuration (73Al, 73Pa, 73Va, 74Ku2, 74Va). In odd-A iodine nuclei the $5/2^+$ states, in particular, seem to exhibit behavior suggesting coupling between a three-proton state and the Sn core phonon. This is illustrated in Figure 37 which presents the first four $5/2^+$ states in ^{127}I (68Au, 70Apl, 71Apl), ^{129}I (72Wa, 74Mal), ^{131}I, and ^{133}I (75Lal) with the energy base (E = 0 keV) being the first $5/2^+$ state. For comparison, the first-phonon 2^+ state in the appropriate Te and Sn core (73Au1, 73Au2, 73Be, 74Hi, 74Ke) is also indicated. The upper two $5/2^+$ states clearly follow the systematic behavior of the Sn core phonon rather than that of the Te core phonon, suggesting that the Sn core excitation is of importance in their configurations. In contrast with the behavior of the $5/2^+$ states, the first $1/2^+$ state in the iodine nuclei is seen to correlate better with the Te core phonon, suggesting that it results from the coupling between the $2d_{5/2}$ single proton state and the Te core phonon. Finally, it may be noted that, using this energy scale based on the first $5/2^+$ state, the first $11/2^+$ state does not correlate with either core phonon. This is understandable, as the maximum spin which can result from a $5/2^+$ to 2^+ coupling is 9/2. For the $11/2^+$ state to be a vibrational excitation it must involve the $1g_{7/2}$ single proton configuration, and, in fact, this appears to be the case (see Figure 34).

Figure

37. The systematics of the $5/2^+$ states observed in the odd-mass iodine nuclei (data from this work and 68Au, 70Ap1, 71Ap1, 72Wa, 74Ma1, 75La1). The first $5/2^+$ state is taken to be zero keV on the energy scale. For comparison, the first 2^+ states in the appropriate Sn and Te cores are also shown. The position of the $1/2^+$ and of the first $11/2^+$ state is also indicated.

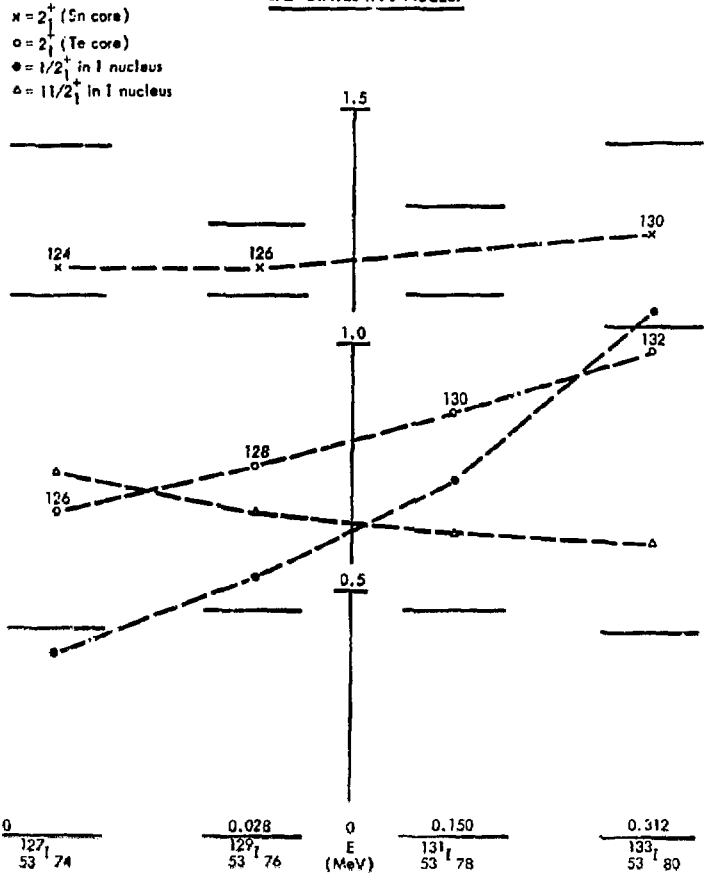
5/2⁺ STATES IN I NUCLEI
x = 2₁⁺ (Sn core)
o = 2₁⁺ (Te core)
● = 1/2₁⁺ in I nucleus
△ = 11/2₁⁺ in I nucleus
1.5
1.0
0.5
124
126
130
132
128
0
0.028
0
0.150
0.312
E
(MeV)
127 I 74
53
129 I 76
53
131 I 78
53
133 I 80
53

In contrast with the even parity levels, the odd parity levels observed in ^{131}I have not been the subject of any detailed theoretical calculations to predict level properties and configurations. It may be noted, however, that low-lying odd parity states may arise from only three types of possible couplings. First, the $1g_{7/2}$ or $2d_{5/2}$ single proton state may couple with the collective 3^- octupole excitation of the Te core. Second, the $1h_{11/2}$ single proton state may couple with the 2^+ one-phonon Te core excitation. And third, the $1g_{7/2}$ or $2d_{5/2}$ single proton state may couple with the odd parity two-neutron states in the Te core, resulting in odd parity levels having $\pi\nu,\nu_2$ three quasi-particle configurations. The distribution of all possible resulting odd parity states is tabulated in Table VIII. Figure 38 depicts this schematically for couplings involving only the observed odd parity excitations in the ^{130}Te core (72Ke2, 73Aul, 74Ke, 75Ma). The observed odd parity states in ^{131}I are also presented. An examination of Table VIII and Figure 38 indicates that the phonon and octupole states, alone, cannot account for the observed density of odd parity states, and furthermore that they would be expected to occur at considerably higher excitation energies than the observed levels. Thus, although some configuration mixing undoubtedly occurs, the observed odd parity levels in ^{131}I are primarily describable as $\pi\nu,\nu_2$ three quasi-particle configurations. Couplings

TABLE VIII.

Distribution of the odd-parity states of ^{131}I predicted by zeroth-order coupling between the odd-parity ^{130}Te core states in Table VI and the $1g_{7/2}$ and $2d_{3/2}$ shell-model orbitals and by the coupling of the one-phonon excitation (in ^{130}Te) with the $1h_{11/2}$ orbital.

J^{π}	$\pi\nu_1\nu_2$ States	Octupole States	Phonon States
$1/2^-$	1	2	
$3/2^-$	4	2	
$5/2^-$	8	2	
$7/2^-$	10	2	1
$9/2^-$	11	2	1
$11/2^-$	11	2	1
$13/2^-$	11	1	1
$15/2^-$	10		1
$17/2^-$	8		
$19/2^-$	4		
$21/2^-$	1		

Figure

38. The odd parity states of ^{131}I (this work. On the left are the odd parity states observed in the ^{130}Te core (72Ke2, 74Hi, 74Ke); and in the center are the possible states resulting from a zeroth-order coupling of the core to the $1g_{7/2}$ and $2d_{5/2}$ states as well as the 2^+ one-phonon Te core excitation to the $1h_{11/2}$ state.

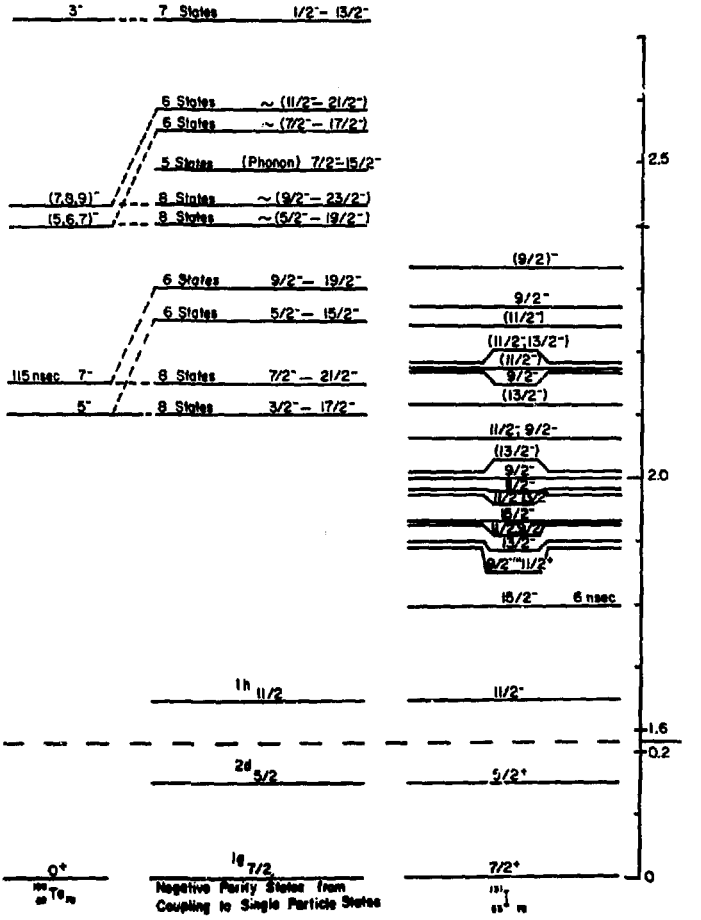
3⁻
7 States 1/2⁻ - 13/2⁻
6 States ~ (11/2⁻ - 21/2⁻)
6 States ~ (7/2⁻ - 17/2⁻)
5 States (Phonon) 7/2⁻-15/2⁻
(7,8,9)⁻
8 States ~ (9/2⁻ - 23/2⁻)
(5,6,7)⁻
8 States ~ (5/2⁻ - 19/2⁻)
6 States 9/2⁻ - 19/2⁻
6 States 5/2⁻ - 15/2⁻
115 nsec 7⁻
8 States 7/2⁻ - 21/2⁻
5⁻
8 States 3/2⁻ - 17/2⁻
(9/2)⁻
9/2⁻
(11/2⁻)
(11/2;13/2⁻)
(11/2⁻)
9/2⁻
(13/2⁻)
11/2; 9/2⁻
(13/2⁻)
9/2⁻
15/2⁻
6 nsec
1h 11/2
11/2⁻
2d 5/2
5/2⁺
1g 7/2
7/2⁺
0⁺
Negative Parity States from Coupling to Single Particle States
2.5
2.0
1.6
0.2
0

using only the observed 5^- (2100.8 keV) and 7^- (2146.0 keV) states in the ^{130}Te core can account for the observed density of states, and many more high-spin odd parity states could result from the unobserved 4^-, 5^-, and 6^- states, as shown in Table VIII.

Of the odd parity levels observed in ^{131}I, the $15/2^-$ 6-nsec isomeric state at 1797.07 keV is of particular interest. A $15/2^-$ isomer has been reported in ^{127}Sb (an isodiosphere of ^{131}I) by Apt and Walters (71Ap1, 71Ap2, 74Ap). That isomer has an 11 μsec half-life and decays by two transitions of nearly equal intensity (805.9- and 824.7-keV) to levels with spin and parity values of $9/2^+$ and $11/2^+$. The partial half-life of the 1035.4-keV transition in ^{131}I ($15/2^-$ to $11/2^+$) is 1.5 μsec. The equivalent transition in ^{127}Sb, corrected for energy differences, has a partial half-life of ≈5.0-8.0 μsec (pure M2) or of ≈3.0-6.0 μsec (pure E3). As in ^{130}Te, both a 5^- and a 7^- excited state have been observed near 2 MeV in excitation energy in ^{126}Sn (70F1). Thus, it seems highly likely that the $15/2^-$ isomers in ^{131}I and ^{127}Sb are very similar in configuration.

Some light is shed on the interpretation of the $15/2^-$ isomer in ^{131}I by the work of Tandon and Devare (67Ta). They measured the g-factor of this isomeric level to be -0.16 ± 0.05. In Table IX I show the result of calculating the g-factor for each of the eleven possible $\pi\nu,\nu_2$ configurations resulting in a $15/2^-$ state. (The

TABLE IX.

Calculated g-Factors for the Possible One-proton-two-neutron Configurations Which Result in a Spin and Parity Value of $15/2^-$.

Configuration		Calculated g-factor
Proton	Neutrons	
$[1g_{7/2}, (1h_{11/2}, 3s_{1/2})\ 5^-]\ 15/2^-$		+ 0.16
$[1g_{7/2}, (1h_{11/2}, 3s_{1/2})\ 6^-]\ 15/2^-$		- 0.32
$[1g_{7/2}, (1h_{11/2}, 2d_{3/2})\ 4^-]\ 15/2^-$		- 0.17
$[1g_{7/2}, (1h_{11/2}, 2d_{3/2})\ 5^-]\ 15/2^-$		- 0.06
$[1g_{7/2}, (1h_{11/2}, 2d_{3/2})\ 6^-]\ 15/2^-$		- 0.01
$[1g_{7/2}, (1h_{11/2}, 2d_{3/2})\ 7^-]\ 15/2^-$		+ 0.01
$[2d_{5/2}, (1h_{11/2}, 3s_{1/2})\ 5^-]\ 15/2^-$		+ 0.60
$[2d_{5/2}, (1h_{11/2}, 3s_{1/2})\ 6^-]\ 15/2^-$		- 0.04
$[2d_{5/2}, (1h_{11/2}, 2d_{3/2})\ 5^-]\ 15/2^-$		+ 0.40
$[2d_{5/2}, (1h_{11/2}, 2d_{3/2})\ 6^-]\ 15/2^-$		+ 0.30
$[2d_{5/2}, (1h_{11/2}, 2d_{3/2})\ 7^-]\ 15/2^-$		+ 0.15

details of this calculation are presented in Appendix III.) It is seen that only two configurations,

$$[\pi 1g_{7/2}, (\nu_1{}^{1}h_{11/2}, \nu_2{}^{2}d_{3/2})4-] \quad 15/2^-$$

and

$$[\pi 1g_{7/2}, (\nu_1{}^{1}h_{11/2}, \nu_2{}^{2}d_{3/2})5-] \quad 15/2^-$$

result in a calculated g-factor within two standard deviations of the measured value. I favor the second configuration as the 4^- state has not been observed and identified in ^{130}Te. I note, also, that this second configuration is the same as that proposed by Apt and Walters (71Ap1, 71Ap2, 74Ap) for the $15/2^-$ isomeric level in ^{127}Sb.

The deexcitation of the $15/2^-$ isomer in ^{131}I proceeds via transitions to the $11/2^-$ single-proton state at 1646.01 keV, to the two-phonon coupled to $1g_{7/2}$ states at 1596.43 and 1556.13 keV ($13/2^+$ and $15/2^+$), and to the one-phonon coupled to $1g_{7/2}$ state at 773.67 keV ($11/2^+$). The first of these transitions is a 151.2-keV pure E2 transition with a partial half-life of ~1.2 μsec. The theoretical single-particle half-life (67Le) is 84 nsec. The E2 hindrance of ~14 is indicative of the great difference in configuration between the two states. The transition very likely proceeds as a result of a small amount of configuration mixing of $\pi\nu_1\ \nu_2$ character into the 1646.01 keV state and/or of one-phonon plus $1h_{11/2}$ character into the isomeric state. The other

three transitions can be interpreted as merely the decay of the 5^- two-neutron core state (2100.8 keV) to the 4^+ two-phonon (1632.8 keV) or to the 2^+ one-phonon (839.4 keV) core state.

The quantitative question of why the $15/2^-$ state is lower in energy than the other possible $\pi\nu_1\nu_2$ configurations is something which must be answered by any detailed theoretical treatment of the odd parity levels of ^{131}I. A set of predictions has been devised (69Pe) to predict the lowest lying member of the multiplet resulting from a strong coupling between three nucleons, all occupying different orbitals. This technique fails for ^{131}I (and also for ^{127}Sb) in that it predicts the most stable member of the $\pi(1g_{7/2})\ \nu_1(1h_{11/2})\ \nu_2\ (2d_{3/2})$ multiplet to be $19/2^-$, whereas $15/2^-$ is the lowest state observed. Apparently it is more realistic to treat the $15/2^-$ state as the result of a weak coupling between the single proton state and the 5^- core two-neutron state. In this case, however, any theoretical treatment must explain why the $15/2^-$ state is the most stable coupling, in particular why it is more stable than the parallel ($17/2^-$) or the anti-parallel ($3/2^-$) couplings. It is possible that this is the result of admixture of the $15/2^-$ one-phonon plus $1h_{11/2}$ configurations, as there are no possible $17/2^-$ or $3/2^-$ one-phonon states. Apt and Walters have suggested that the admixture of $[\pi 2d_{5/2},\ (\nu_1\ \nu_2)5^-]\ 15/2^-$ configurations may be responsible.

I have observed major β-decay branches to four $9/2^-$, three $11/2^-$, and three $13/2^-$ states in ^{131}I. The mechanism for β-decay to three-nucleon $\pi\nu_1\nu_2$ states from $11/2^-$ $^{131}Te^m$ may be viewed as a single-particle transition from a core neutron orbital (ν_2) near the Fermi level to the final state proton orbital (π), with the valence $1h_{11/2}$ neutron (ν_1) remaining unchanged. In this case the strongest β transitions should be the allowed transitions from an initial state with the configuration $[\nu_2 2d_{3/2}, \nu_2 2d_{3/2})\ 0^+, \nu_1 1h_{11/2}]\ 11/2^-$ to the twelve odd parity states with configurations, $[\pi 2d_{5/2}, (\nu_1 1h_{11/2}, \nu_2 2d_{3/2})^{4^-,5^-,6^-,7^-}]_{9/2^-,11/2^-,13/2^-}$. This lends additional weight to the interpretation of the negative parity states as being $\pi\nu_1\nu_2$ states, although it would be somewhat presumptuous to identify the 10 states observed to be strongly fed in β-decay as having the exact configurations given above.

The β-decay of $11/2^-$ $^{131}Te^m$ to the $1h_{11/2}$ single quasi-particle proton state in ^{131}I (1646.01 keV) is relatively hindered (log*ft* = 7.7) when compared to the β-decay to the $\pi\nu_1\nu_2$ states (log*ft* = 5.8 - 6.8). Similar hindrances have been observed in the β-decays of $11/2^-$ $^{129}Te^m$ (72Wa, 74Mal) and $11/2^-$ ^{125}Sn (70Ma) where the equivalent $\nu(1h_{11/2})$ to $\pi(1h_{11/2})$ β-transitions were observed to have log*ft* values of 8.4 and 7.4, respectively. The electron capture of the $\nu(1h_{11/2})$ isomer of ^{119}Te (67Gr) to the $\pi(1h_{11/2})$ state at 1365.8 keV in ^{119}Sb, with a log*ft* of 6.4, is

somewhat faster but still is slower than the decay to the $\pi\nu,\nu_2$ states in ^{119}Sb near 2 MeV. The hindrance of this β-transition between single particle states is not easily understood, particularly in view of the occupancy of the parent $\nu(1h_{11/2})$ orbital, the emptiness of the daughter $\pi(1h_{11/2})$ orbital, and the relative purity of both parent and daughter states as exhibited in the (^{3}He,d) and (d,p) reactions. This is certainly something which must be explained in any theoretical treatment of the negative parity states of ^{131}I as observed in the β-decay of $^{131}Te^m$.

My inability to observe a β-decay branch from $3/2^+$ $^{131}Te^g$ ($\nu 2d_{3/2}$) to the $1/2^+$ state which was observed at 1718±10 keV in the (^{3}He,d) study is consistent with the earlier observations of very hindered β transitions to the $1/2^+$ levels in $^{127,129,131}I$ from the respective $^{127,129,131}Te$ $3/2^+$ isomers (70Apl,71Apl,71Mal,74Ma). Although the β transition is ℓ-forbidden ($\Delta\ell = 2$), the observed logft values are much higher than ℓ-forbiddenness is expected to contribute (e.g. the logft of 6.4 for decay of $7/2^+$ ^{131}I to the $5/2^+$ 364-keV state in ^{131}Xe (74Mel)). The hindrance is also surprising in view of the single-particle character of the states involved and, in fact, appears to be directly correlated with the amount of single particle character. As with $\nu(1hr_{11/2})$ to $\pi(1h_{11/2})$ β-transition just discussed, this hindrance of β-transitions involving single particle

states offers a challenge to any theoretical treatment of ^{131}I levels.

In conclusion, I note that the three-proton cluster plus quadrupole vibrator (Sn core) model results in the best fit to the even parity levels of ^{131}I (Figure 36). It seems to be of particular importance in describing the $5/2^+$ levels in iodine nuclei (Figures 36 and 37). There is evidence, however, that the positive parity levels have a large amount of single proton plus Te core character. This is seen in the odd-A iodine level systematics (Figures 33 and34) which show a general rise in the level positions paralleling the rise of the 2^+ state of the even-even Te nuclides with increasing neutron number. The Sn core 2^+ states, in contrast, change very little with neutron number (Figure 37). In addition, the theoretical three-proton cluster work has placed a $15/2^+$ level near 800 keV with a sizeable $(1g_{7/2})$ $15/2^+$ component (73Va). It may be noted that there can be no $(1g_{7/2})^3$ $13/2^+$ state (62Pr); and, as the $13/2^+$ and $15/2^+$ states lie close to each other and near the position of the 4^+ state in the ^{130}Te core (Figure 35), I suggest that the $(1g_{7/2})^3$ $15/2^+$ configuration is not important below ~2 MeV, and that the observed $15/2^+$ and $13/2^+$ levels might be better described in terms of a single proton coupled to the Te core two-phonon excitation. Thus, a model based on both three-particle-plus-Sn-core and single-particle-plus-Te-core

configurations might be expected to give the most accurate fit to ^{131}I levels. To fit the odd parity levels, this model would undoubtedly have to include a wider basis of states than have so far been considered, specifically the $1h_{11/2}$ proton state, the octupole states, and the $\nu_1\nu_2$ configurations.

IV. THE DECAY OF 55.5-min $5/2^+$ ^{105}Cd TO LEVELS OF ^{105}Ag.

A. Introduction.

The silver nuclei, with three holes in the proton closed shell at Z = 50, have recently been the subject of several theoretical calculations (73Pa, 71Ku, 72Ku, 74Kul, 74Ku2, 74Ku3, 74Ku4, 74Ma3) concerned with three-hole states and their properties. These theoretical investigations have been particularly successful in describing the low-lying $7/2^+$ excited state (anomalous coupling state) which has been observed in the odd-mass silver isotopes from A = 103 to A = 113. Detailed theoretical calculations for other levels have only been performed for ^{107}Ag and ^{109}Ag, however; and recent experimental investigations have dealt primarily with the levels of ^{107}Ag and ^{109}Ag as observed in radioactive decay (74Pa, 69Sc) and in the ^{106,108}Pd (^{3}He,d) ^{107,109}Ag reactions (72Ku, 73Au3, 75Ku, 75An2). These two nuclei, however, provide a somewhat limited check of the theoretical work due to the relatively low radioactive decay Q values involved. The decay of $5/2^+$ ^{105}Cd to levels of ^{105}Ag is thus of interest because the increased Q_{EC} value allows the observation of levels at higher excitation energies. In addition, knowledge of the levels of ^{105}Ag allows the extension of the systematics of the level structures of the odd-mass silver isotopes. The systematics of the energy levels and their electromagnetic

decay properties provide both a valuable check of the theoretical work and a guide to further theoretical development.

Studies of the decay of 55.5-min $5/2^+$ ^{105}Cd have thus far been limited to half-life determinations (50Gu, 53Jo, 61Ra, 68Bo, 69St), γ-ray singles measurements (69Ok, 69St, 71Be, 72Pr, 74Bu), and a measurement of the conversion electrons from a 25.5-keV transition (53Jo). Two ^{105}Ag level schemes have been proposed; however, the first (69St) was not intended to establish the existence of any excited states but merely to illustrate the additive properties of the γ-ray energies, and the second (74Bu) was not consistent with γ-ray energy sums and intensity balances. When this investigation of the decay of ^{105}Cd was initiated, only one excited state of ^{105}Ag had been established, the $7/2^+$ 7.23-min isomeric state at 25.5 keV (69Ho). While this study was in progress, the results of a study of the excited states of ^{105}Ag seen in the ^{104}Pd (^{3}He,d) ^{105}Ag reaction were reported (74An, 75An1).

By making extensive use of large volume, high resolution Ge(Li) detectors for both γ-ray singles and γ-γ coincidence measurements, I have been able to identify 274 γ-transitions associated with the decay of ^{105}Cd. I have placed 248 of these in a ^{105}Ag level scheme involving 50 excited states. This study was complicated by the observation of numerous γ-ray multi-

plets, most of which were resolvable only through the use of Ge(Li)-Ge(Li) γ-γ coincidence data. The ^{105}Cd sources were produced via the ^{106}Cd (n,2n)^{105}Cd reaction, and the γ-ray measurements were complicated by the presence of several interfering activities, principally ^{105}Ag^{g}, ^{105}Ag^{m}, ^{106}Ag^{m}, and ^{111}Cd^{m}.

B. Experimental Procedure and Results.

1. Source Preparation.

The samples of 55.5-min ^{105}Cd were produced via the ^{106}Cd (n,2n) ^{105}Cd reaction by irradiating 50-100 mg of enriched 82.09% ^{106}Cd as the oxide (purchased from Isotopes Division, Oak Ridge National Laboratory, Oak Ridge, Tennessee) with 14 MeV neutrons from the LLL Insulated Core Transformer (ICT) accelerator with Rotating Target Neutron Source (RTNS). This accelerator produces 14 MeV neutrons via the $d(^{3}H,\alpha)N$ reaction and can attain a maximum neutron flux of approximately 6×10^{12} neutrons-sec^{-1} into 4π. It has been described in detail elsewhere (72Bo, 73Ba). (Nota bene: The quoted energy value of 14 MeV is the nominal value for the neutron energy. The actual energy depends on source-sample geometry and can range from ~13.2 to ~15.5 MeV.)

The enriched CdO target material was heat sealed in polyethylene capsules and transported to the RTNS using a pneumatic rapid sample transport system ("rabbit" system). Irradiation times ranged from approximately

ten minutes to one hour, and the neutron flux at the target position was estimated to be approximately 1-5 x 10^{10} neutrons - cm^{-2} - sec^{-1}. After irradiation, the samples were allowed to decay for 10-20 minutes to reduce the contributions from the contaminating activities, 122-sec ^{15}O, 7.1-sec ^{16}N, and 24.1-min $^{106}Ag^{g}$. No chemical separations were performed, and when counting began the principal activity present was 55.5-min ^{105}Cd. The following contaminating activities were identified on the basis of γ-ray energy, intensity, and half-life data: 41-day $^{105}Ag^{g}$, 7.23-min $^{105}Ag^{m}$, 24.1-min $^{106}Ag^{g}$, 8.4-day $^{106}Ag^{m}$, 6.5-hr ^{107}Cd, 48.6-min $^{111}Cd^{m}$, and 53.5-hr $^{115}Cd^{g}$ (74Be1, 74Ba2, 72Be2, 71Be, 71Ra, 66Gr). Five CdO targets were employed, and an irradiation was performed approximately every hour for 16 hours for γ-ray singles spectroscopy and for 13 hours for γ-γ coincidence spectroscopy.

2. Gamma-Ray Singles Spectroscopy.

Direct γ-ray spectra of 55.5-min ^{105}Cd samples were taken using the following detector-pulse-height analyzer systems at LLL: (1.) the LLL Compton Suppression Spectrometer (described in Section II and 69Ca), (2.) a 50 cm^3 Ge(Li) detector having a FWHM energy resolution of 1.9 keV at 1332 keV, (3.) an 80 cm^3 Ge(Li) detector having a FWHM energy resolution of 2.1 keV at 1332 keV, and (4.) a 1.5 cm^3 Ge(Li) x-ray detector having a FWHM energy resolution of 500 eV at 60 keV. Source to detector

distances ranged from ~35 cm to ~1 cm, and a 1" Pb absorber was used with the 80 cm^3 detector. The distance variations and the Pb absorber allowed the determination of summing contributions to the spectra. A new ^{105}Cd sample was produced every hour and the old sources moved on to the next detector-analyzer system in sequence. In this manner a total of sixteen one-hour counts were summed on each of the systems. Contaminating activities could be identified on a half-life basis as each successive system counted the samples approximately one ^{105}Cd half-life (55.5 minutes) later than the preceding system. In addition, two of the samples were combined and then counted for ~12 hour periods for eight days with the 80 cm^3 detector (without absorber) to aid in the identification of long-lived contaminating activities.

The γ-ray spectrum of the ^{105}Cd samples from 0-2.0 MeV as observed with the 50 cm^3 Ge(Li) detector is shown in Figures 39 through 43 . The high energy portion (2.0 to 2.8 MeV) of the γ-ray spectrum, as observed through 1" of Pb with the 80 cm^3 Ge(Li) detector, is shown in Figure 44. From all spectra, a total of 250 peaks were observed which decayed with a half-life of about one hour and which were not single escape (SE), double escape (DE), x-ray escape, x-ray, or sum peaks.

The 250 peaks are tabulated in Table X along with 18 additional transitions which were established on the basis of γ-γ coincidence data and 11 transitions for

which intensity limits were determined from either γ-ray singles or γ-γ coincidence spectra. Of these 279 transitions, five were assigned to the EC-decay of 7.23-min $^{105}Ag^{m}$ on the basis of my coincidence data and the recent study of the EC-decay branch of $^{105}Ag^{m}$ (72Kr). The remaining 274 transitions were assigned to the decay of 55.5-min ^{105}Cd, although 26 of these could not be placed in the decay scheme. Peak intensity corrections for contributions to the singles spectra from the decay of $^{105}Ag^{g}$ or $^{106}Ag^{m}$ were based on the recent decay scheme studies of these isomers (70Ka, 73In).

The absolute β^{+}/EC decay branch of $5/2^{+}$ ^{105}Cd to the $7/2^{+}$ state at 25.5 keV in ^{105}Ag (7.23-min $7/2^{+}$ $^{105}Ag^{m}$) was determined to be (51.4 ± 4.0) %. A source of ^{105}Cd was produced in a short irradiation (10 minutes). The decay of the principal ^{105}Cd γ-ray (961,84-keV) was followed for approximately two half-lives, and an activity at end of irradiation (t=0) was determined by extrapolation of the decay curve. The amount of ^{105}Ag was determined ~32 days later by counting the sample at a known geometry and using the ^{105}Ag decay scheme of Kawakami and Hisatake (70Ka). Then the β^{+}/EC branch was determined by using the decay scheme data in Table X and the equations of radioactive growth and decay. The details of this determination are presented in Appendix IV. The results of attempting this determination by observing 7.23-min $^{105}Ag^{m}$ in transient equilibrium with ^{105}Cd and

Figures

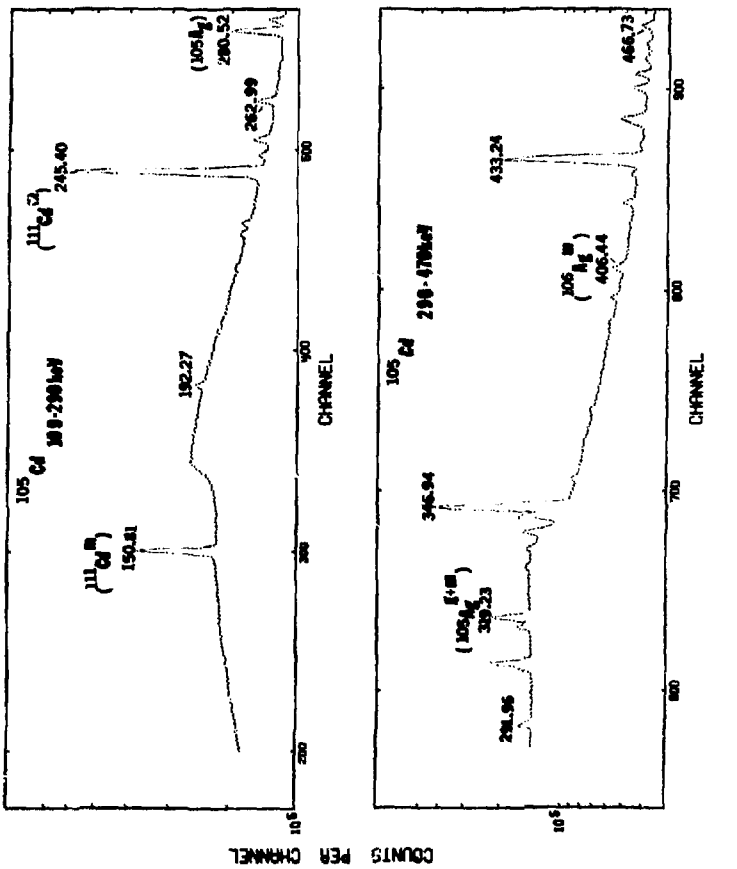
COUNTS PER CHANNEL
CHANNEL
CHANNEL
105 Cd
245.40
282.99
280.52
192.27
150.81
345.94
433.24
406.44
466.73
298.96
339.23

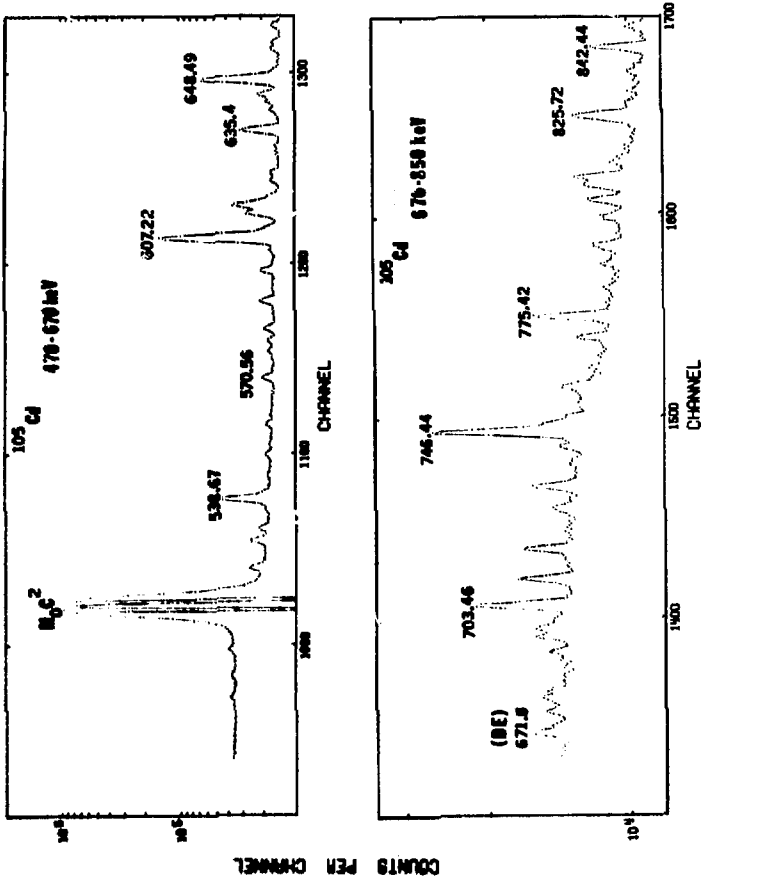
105 Cd
470-670 keV
538.67
570.56
607.22
635.4
648.49
CHANNEL
105 Cd
670-850 keV
703.46
746.44
775.42
825.72
842.44
(BE)
671.8
CHANNEL
COUNTS PER CHANNEL

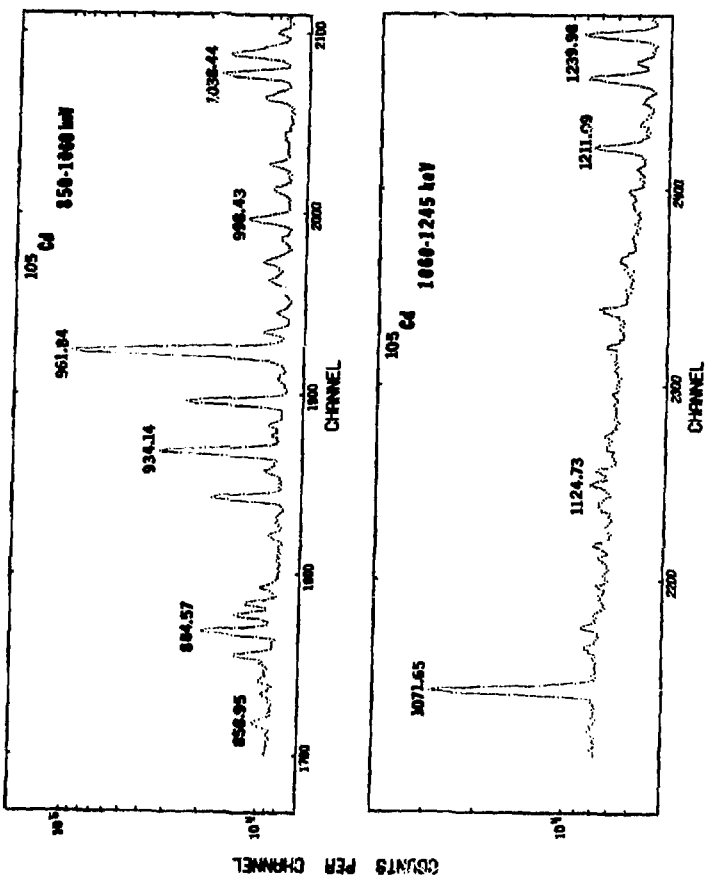
105 Cd
850-1060 keV
961.84
934.14
884.57
858.95
998.43
1038.44
1700
1800
1900
2000
2100
CHANNEL
105 Cd
1060-1245 keV
1077.65
1124.73
1211.59
1239.98
2200
2300
2400
CHANNEL
COUNTS PER CHANNEL

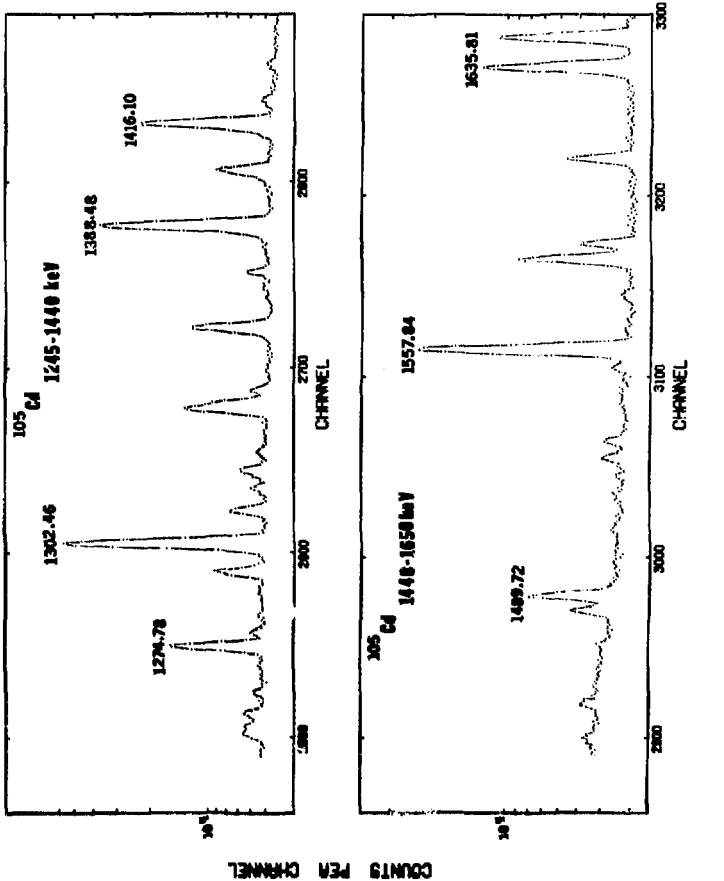
105 Cd
1245-1440 keV
1302.46
1274.78
1388.48
1416.10
CHANNEL
105 Cd
1440-1650 keV
1557.84
1635.81
1489.72
CHANNEL
COUNTS PER CHANNEL

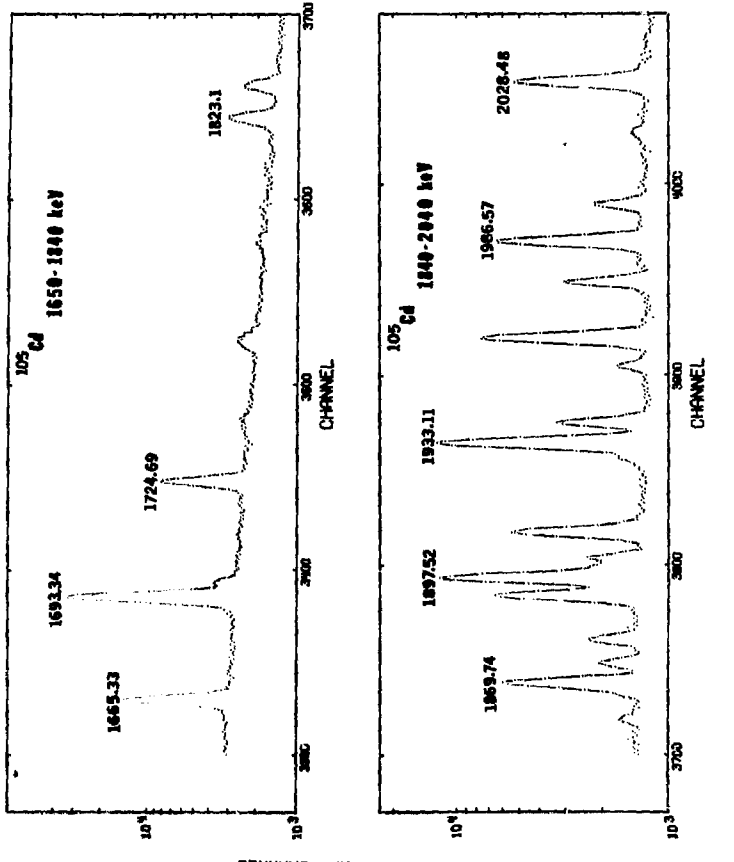
^{105}Cd
1650-1840 keV
1693.34
1665.33
1724.69
1823.1
^{105}Cd
1840-2040 keV
1869.74
1897.52
1933.11
1986.57
2026.48
COUNTS PER CHANNEL
CHANNEL

Figure

44. γ-ray spectrum of ^{105}Cd between 1950 and 2760 keV observed with the 80 cm^3 Ge(Li) detector through a 1" Pb absorber.

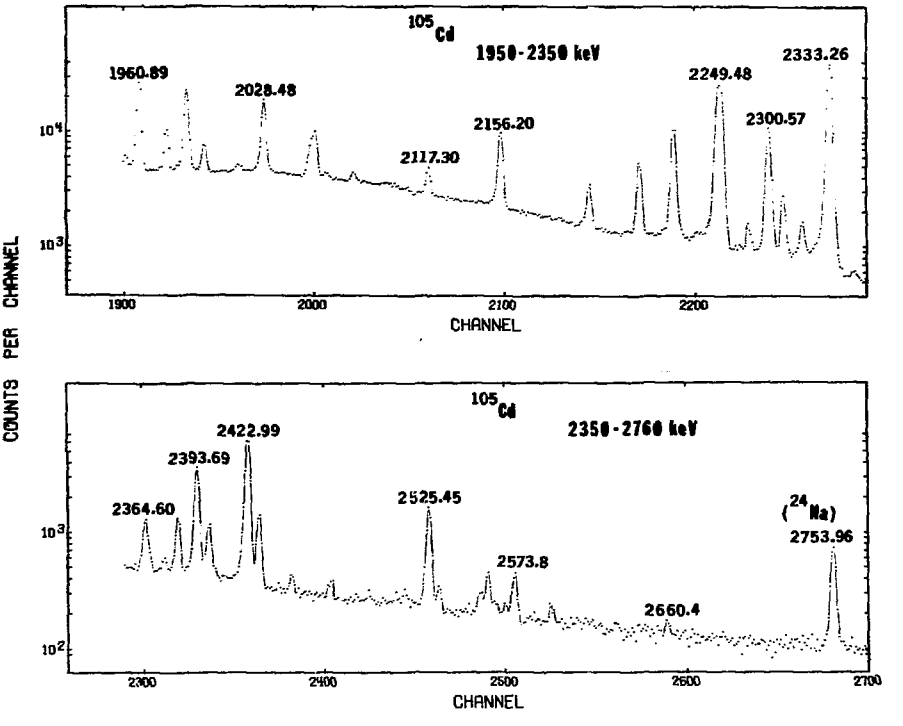
105Cd
1950-2350 keV
1960.89
2028.48
2117.30
2156.20
2249.48
2300.57
2333.26
COUNTS PER CHANNEL
CHANNEL
105Cd
2350-2760 keV
2422.99
2393.69
2364.60
2525.45
2573.8
2660.4
(24Na)
2753.96
CHANNEL

Table X. γ-rays Observed in the Decay of 55.5-min ^{105}Cd

Energy[a] (keV)		Intensity[a,b]		Note	Transition[c] (from/to)	Coincident[d] γ-rays in ^{105}Cd Decay or Identification[e]
27.70	(6)	45	(5)		53/25	
51.7	(2)	4	(2)	Q	2308/2256	
86.33	(7)	21	(2)		433/346	
107.6	(3)	1.2	(7)	Q		Not placed
128.6	(2)	1.6	(6)		(1923/1794) or (1294/1166)	
132.9	(2)	4	(2)		1690/1557	
171.34	(16)	12	(4)		1557/1386	
172.82	(13)	16	(3)		1923/1750	(1403)
192.27	(9)	19	(2)		1750/1557	1557
221.76	(12)	7	(1)			Not placed
229.82	(9)	15	(2)		1557/1327	1302
232.37	(8)	18	(2)		1923/1690	1665
249.41	(6)	14	(2)	T	Multiplet	1360, 1388
		5	(3)	C	1690/1441	
		10	(4)	C	1635/1386	
253.42	(3)	31	(2)		1923/1669	283, 1644
262.99	(3)	39	(2)		1557/1294	307, 346, (775), 948, 1294
283.29	(4)	33	(2)		1669/1386	253, 316, 1360
291.96	(4)	47	(2)		1586/1294	307, 346, 662, 746, (842), 948, 1294

TABLE X (cont.)

Energy[a] (keV)		Intensity[a,b]		Note	Transition[c] (from/to)	Coincident[d] γ-rays in ^{105}Cd Decay or Identification[e]
295.7	(3)	3	(2)		1986/1690	
306.35	(5)	29	(15)	105		$^{105}Ag^{m}$ Decay [21]
307.83	(3)	192	(7)	T	Multiplet	262, 291, 340, 613, (640), (697), 934, 961, 1038, 1274, 1302
		12	(5)	C	1294/987	
		180	(12)	MC	1635/1327	
316.82	(5)	53	(2)		1986/1699	283, (1322), 1644
319.23	(3)	189	(4)	105		$^{105}Ag^{m}$ Decay [100]
325.0	(2)	5	(2)			Not placed
340.66	(4)	97	(3)	T	Multiplet	304, 934, 948, 961, (1294)
		14	(6)	C	1635/1294	
		83	(9)	MC	1327/987	
343.4	(2)	≤6		SL , 105	(1586/1243)	
346.87	(2)	896	(9)		346/GS	262, 292, 530, 640, 695, 746, 896, 948, (1006), 1038, (1039), 1211, 1239, 1322, 1343, 1403, 1902, 1909, (1953), 1960, 1986, 2053, (2076), 2203
353.91	(12)	9	(2)			Not placed
362.9	(3)	4	(2)		(1386/1023) or (1690/1327) or (2081/1718)	

TABLE X (cont.)

Energy[a] (keV)		Intensity[a,b]		Note	Transition[c] (from/to)	Coincident[d] γ-rays in ^{105}Cd Decay or Identification[e]
371.28	(10)	9	(2)			Not placed
398.[illegible]	(8)	12	(1)		1386/987	961
403.3	(4)	3	(2)		2326/1923	
417.1	(2)	3	(2)		1294/877	
422.27	(6)	19	(1)		1750/1327	1302
433.24	(3)	600.	(5)		433/GS	590, 609, (613), 733, 810, 1124, (1159), 1360, 1489, (1552), 1823, (1867), (1874), 1881, 1892, (1894), 1900, 1938, 1995, 2117
442.3	(2)	18	3	105		^{105}Ag^{m} Decay [9.4]
443.9	(2)	≤4		SL, L, 105	(1885/1441)	
444.6	(2)	≤4		SL, L, 105	(877/433)	
454.38	(7)	23	(2)		1441/987)	934, 961
458.30	(11)	11	(2)			Not placed
461.96	(11)	10.	(2)		2256/1794	
466.73	(7)	11	(2)		1794/1327	1302
486.73	(10)	14	(2)	105	(2473/1986) or (2156/1669)	
499.45	(8)	14	(2)	T	(Multiplet)	(1360)
		8	(4)	C	1885/1386	
		6	(6)	MC	(2249/1750)	

TABLE X (cont.)

Energy[a] (keV)	Intensity[a,b]	Note	Transition[c] (from/to)	Coincident[d] γ-rays in ^{105}Cd Decay or Identification[e]
520.54 (5)	24 (1)		2314/1794	
530.95 (8)	16 (1)		877/346	346
538.67 (6)	151 (5)		1635/1097	(613), 1043, 1071
545.0 (2)	3 (1)		1986/1441	
550.17 (11)	8 (1)		(2300/1750) or (2473/1923)	
558.14 (10)	8 (1)		2308/1750 or (1885/1327)	(1403), (1724)
560.9 (3)	2 (1)			^{105}Ag^{m} Decay [0.5]
570.56 (6)	23 (2)		1557/987	(934), 961
576.1 (5)	3 (2)	Q	2326/1750	
577.4 (2)	9 (2)		2371/1794	
579.97 (9)	12 (1)		2249/1669	1644
583.17 (6)	18 (1)		2333/1750	1403, (1724)
590.44 (5)	25 (1)		1023/433	433, 1302
598.54 (5)	25 (2)		2156/1557	1557
607.22 (2)	798 (7)		2326/1718	1665, 1693
609.45 (5)	23 (2)		1042/433	433, 613
613.50 (4)	73 (2)	T	Multiplet	307, (433), 538, 609, (648), 1043, (1665)
	21 (13)	C	2249/1635	
	52 (15)	MC	1656/1042	

TABLE X (cont.)

Energy[a] (kev)		Intensity[a,b]		Note	Transition[c] (from/to)	Coincident[d] γ-rays in ^{105}Cd Decay or Identification[e]
617.41	(9)	16	(6)	105, 105m	2308/1690	(703), (1665)
623.7	(2)	14	(1)		2314/1690	1665
630.8	(3)	8	(3)		2300/1669	
635.4	(3)	102	(2)		2326/1690	703, 1343, 1665
640.46	(8)	13	(2)		987/346	(307), 346, (648)
642.80	(6)	20.	(2)		2333/1690	1665
648.49	(2)	335	(5)	105m	1635/987	(613), (640), (697), 934, 961
656.53	(7)	15	(1)	105m	2326/1669	1644
658.27	(8)	13	(1)	T	Multiplet	(1302)
		7	(6)	C	1986/1327	
		6	(7)	?C	(2328/1669)	
662.79	(7)	17	(2)		2249/1986	202
676.88	(12)	10.	(1)		1023/346	
681.97	(16)	7	(2)	105, 106	1669/987	(961)
691.88	(13)	9	(2)		(2249/1557) or (2328/1636)	
695.76	(10)	16	(2)		1042/346	346
697.7	(2)	19	(1)		2333/1635	(307), (648), (1665)
700.07	(16)	9	(1)		2419/1718	1669
703.46	(8)	64	(2)	106m	1690/987	(617), 635, 934, 961
709.87	(8)	27	(2)		2430/1690	1665
714.8	(6)	4	(3)	C	2186/1441	

Table 4 (cont.)

Energy[a] (keV)		Intensity[a,b]		Note	Transition[c] (from/to)	Coincident[d] γ-rays in ^{106}Cd decay or Identification[e]
721.6	(4)	4	(2)	Q	2306/1556	
727.54	(13)	12	(2)		2314/1586	
733.03	(9)	24	(2)		1166/433	433, (1159), (1296)
738.8	(3)	4	(2)		2324/1586	
746.44	(7)	114	(2)		2332/1586	292, 346
749.7	(3)	8	(2)		2419/1669	
755.9	(3)	6	(2)		2550/1794	
758.07	(15)	18	(2)		1635/877	877
762.8	(3)	4	(2)		1750/987	
770.18	(12)	12	(2)		2156/1386	(1360)
775.41	(7)	41	(2)		2333/1557	(262), 1557
782.4	(3)	4	(2)	105m	2473/1690	
788.7	(2)	6	(2)		1885/1097	
800.23	(16)	10.	(2)		2550/1750	
810.10	(8)	26	(1)		1243/433	433
813.9	(2)	8	(2)		(2400/1586) or (2371/1557)	
825.72	(15)	26	(3)	106m	1923/1097	1044, 1071
827.7	(6)	2	(2)	Q	2156/1327	
836.3	(3)	5	(2)		2422/1586	
842.44	(8)	23	(1)	T	Multiplet	(292), 1557

TABLE X (cont.)

Energy[a] (keV)		Intensity[a,b]		Note	Transition[c] (from/to)	Coincident[d] γ-rays in ^{105}Cd Decay or Identification[e]
		14	(4)	C	2400/1557	
		7	(5)	MC	2429/1586	
858.95	(12)	21	(2)	T	2300/1441	1388
		≤ 5		L	2494/1635	
866.9	(2)	10.	(1)		2308/1441	(1388), (1416)
870.88	(14)	10.	(3)		2429/1557	1557
877.81	(9)	46	(2)		877/GS	758
884.57	(8)	126	(2)		2326/1441	(454), 1388, 1416
889.13	(8)	54	(2)		1986/1097	1044, 1071
892.21	(8)	38	(2)	T	2308/1416	1416
		≤ 6		L	2333/1441	
896.61	(9)	18	(2)		1243/346	346
921.62	(5)	102	(2)		2249/1327	340, 1274, 1302
928.8	(2)	7	(4)	105m	2256/1327	
934.14	(4)	271	(3)		987/53	307, 340, 454, (570), 648, 703, (998), (1169), 1338, 1340, 1413, 1485
941.60	(11)	13	(2)		2328/1386	1360
948.04	(4)	182	(3)		1294/346	262, 291, 340, 346, (746), 1013, (1031), 1038
954.53	(12)	6	(2)		2249/1294	

TABLE X (cont.)

Energy[a] (keV)		Intensity[a,b]		Note	Transition[c] (from/to)	Coincident[d] γ-rays in ^{109}Cd Decay or Identification[e]
961.84	(3)	1000.	(7)		987/25	327, 348, 398, 454, 570, (635), 681, (682), 703, 998, 1159, 1252, 1327, 1388, 1340, 1413, 1485
967.23	(6)	26	(2)			Not placed
972.48	(10)	12	(2)		2309/1337	(1341)
978.22	(15)	12	(2)		2419/1441	
981.50	(9)	29	(3)		2422/1441	(1337), 1416
984.58	(17)	15	(4)		2081/1097	1071
986.91	(10)	35	(3)		2314/1327	1302
992.93	(14)	9	(2)		2550/1557	(1557)
998.43	(5)	63	(3)	T	Multiplet	(948), 961, 1302
		20	(6)	C	1966/987	
		31	(8)	C	2325/1327	
		12	(17)	MC	(1023/25)	
1006.25	(9)	16	(3)		2249/1243	(346)
1013.51	(8)	22	(2)		2308/1294	948
1021.5	(2)	7	(3)			Not placed
1031.86	(13)	30.	(4)	T	Multiplet	(948), 1388, 1416
		10.	(7)	C	2326/1294	
		15	(10)	C	2473/1441	
1033.1	(2)	15	(4)		2419/1386	(1360)

TABLE X (cont.)

Energy[a] (kev)		Intensity[a,b]		Note	Transition[c] (from/to)	Coincident[d] γ-rays in ^{105}Cd Decay or Identification[e]
1038.44	(6)	125	(2)		2333/1294	307, 346, 948, 1294
1039.4	(2)	≤6		L	1386/346	(346)
1043.46	(7)	105	(3)	T	Multiplet	538, 614, 825, 889, 1228
(1042.7	(1))	45	(17)	DC	1042/GS	
(1044.0	(1))	60	(14)	C	1097/52	
1061.4	(3)	4	(2)		2447/1386	
1071.65	(5)	273	(4)		1097/25	538, 825, 889, 984, 1228, 1332, 1375
1082.56	(16)	13	(3)		2326/1243	
1091.0	(3)	6	(2)		2419/1327	
1095.7	(4)	3	(2)		2422/1327	
1098.5	(3)	3	(2)			^{105}Ag^{m} Decay [3.7]
1105.8	(2)	6	(1)		2400/1294	
1109.16	(13)	10.	(1)	T	(Multiplet)	
		8	(4)	C	2550/1441	(1388), (1416)
		≤6		L	(2494/1386)	
1119.7	(2)	13	(2)		2447/1327	1302
1124.73	(8)	20.	(2)		1557/433	433
1137.2	(2)	8	(2)			Not placed
1144.7	(3)	3	(1)		2473/1327	
1147.9	(4)	2	(1)		2314/1166	

TABLE X (cont.)

Energy[a] (keV)		Intensity[a,b]		Note	Transition[c] (from/to)	Coincident[d] γ-ray in [1]Cl Decay or Identification[e]
1159.75	(16)	14	(3)	T	2326/1166	(1167), (1795)
		≤7		L	(2326/1167)	
1169.09	(8)	24	(2)		2156/987	(987), 1169
1196.3	(3)	5	(1)			Not placed
1205.4	(3)	4	(2)		2371/1166	
1211.09	(7)	42	(3)		1557/346	346
1217.5	(2)	4	(1)		(2314/1097) or (1243/25)	
1228.74	(6)	52	(4)		2326/1097	1044, 1071
1232.84	(13)	14	(2)		2256/1023	
1239.98	(5)	61	(2)		1586/346	346
1256.50	(10)	23	(2)	T	2422/1166	(733)
		≤6		L	(2584/1327)	
1262.24	(14)	8	(2)		2249/987	961
1274.78	(4)	175	(3)		1327/52	307
1283.60	(3)	5	(2)		2326/1042	
1289.6	(4)	6	(2)		2584/1294	
1294.89	(4)	66	(2)		1294/GS	262, 291, (340), 1038
1302.46	(2)	868	(6)	T	Multiplet	229, 307, 422, 466, 590, (658), 921, (972), 986, 998, 1119
		20	(10)	C	2326/1023	

TABLE X (cont.)

Energy[a] (keV)		Intensity[a,b]		Note	Transition[c] (from/to)	Coincident[d] γ-rays in ^{105}Cd Decay or Identification[e]
		848	(16)	MC	1327/25	
1317.41	(11)	16	(2)			Not placed
1322.20	(10)	36	(4)	T	Multiplet	(316), 346, 1071
		13	(8)	C	2419/1097	
		24	(7)	C	1669/346	
1327.20	(17)	10.	(2)		2314/987	961
1338.69	(4)	139	(4)		2326/987	934, 961
1340.50	(6)	66	(4)		2328/987	934, 961
1343.82	(10)	19	(2)		1690/346	346, 645
1350.0	(3)	4	(2)	106	2447/1097	
1360.79	(4)	145	(4)	T, E	Multiplet	249, (253), 259, 423, ([illegible]), ([illegible]), 941, (1033)
(1361.5	(2))	26	(11)	C	1794/433	
		119	(15)	MC	1386/25	
1375.77	(8)	24	(2)		2472/1097	1071
1388.48	(3)	575	(5)		1441/52	249, 650, (666), 884, (991), 1031, (1139)
1403.10	(6)	83	(3)		1750/346	(172), 346, (556), 583
1413.24	(18)	30	(7)		2400/987	934, 961

TABLE X (cont.)

Energy[a] (keV)		Intensity[a,b]		Note	Transition[c] (from/to)	Coincident[d] γ-rays in ^{152}Gd Decay or Identification[e]
1416.10	(10)	350	(10)	T	Multiplet	(936), 694, 792, 961, 1271, (1138)
		40	(15)	C	1415/GS	
		310	(25)	MC	1441/25	
1422.19	(15)	6	(2)	E	2300/877	
1431.85	(16)	9	(2)		2419/987	
1459.62	(13)	16	(3)		2447/987	961
1465.1	(4)	3	(2)			Not placed
1469.1	(6)	2	(2)	Q		Not placed
1485.71	(8)	36	(2)		2472/987	(934), 961
1489.72	(5)	95	(2)		1923/433	433
1507.8	(3)	5	(1)		(2550/1042) or (2494/987)	
1522.9	(3)	4	(2)		2400/877	
1532.32	(12)	14	(2)		1557/25	
1552.8	(3)	7	(2)		1986/433	(433)
1557.84	(4)	437	(4)		1557/GS	192, 598, 775, 842, 866, (992)
1582.56	(7)	135	(2)		1635/52	
1586.84	(8)	44	(2)		1586/GS	
1610.30	(6)	56	(3)		1635/25	
1635.81	(6)	223	(4)		1635/GS	(613), (697)

TABLE X (cont.)

Energy[a] (keV)		Intensity[a,b]		Note	Transition[c] (from/to)	Coincident[d] γ-rays in ^{105}Cd Decay or Identification[e]
1644.03	(7)	186	(3)		1669/25	253, 316, 579, 656
1665.33	(6)	278	(4)	T	Multiplet	232, 607, (617), 623, 635, 642, 709
(1665.20	(8))	75	(14)	C	1713/52	
(1665.65	(10))	203	(18)	MC	1690/25	
1693.34	(5)	755	(5)		1718/25	607, 700
1697.2	(2)	2	(3)		1750/53	
1724.69	(7)	148	(3)		1750/25	(558), (583)
1741.8	(4)	7	(2)		1794/53	
1797.5	(4)	5	(2)			Not placed
1809.0	(4)	5	(1)		2156/346	
1823.1	(2)	33	(7)		2256/433	433
1831.67	14)	33	(2)		(1884)/25	
1853.6	(8)	1	(1)	Q		Not placed
1860.1	(2)	8	(2)		1885/25	
1867.3	(3)	10.	(2)		2300/433	(433)
1869.74	(9)	136	(3)		1923/53	
1874.99	(14)	19	(2)		2308/433	(433)
1881.36	(12)	28	(2)		2314/433	433
1892.89	(8)	151	(2)		2326/433	433

TABLE X (cont.)

Energy[a] (keV)		Intensity[a,b]		Note	Transition[c] (from/to)	Coincident[d] γ-rays in ^{105}Cd Decay or Identification[e]
1894.8	(3)	10.	(8)	C	2328/433	(433)
1897.52	(7)	308	(3)		1923/25	
1900.21	(13)	25	(2)		2333/433	433
1902.79	(13)	28	(2)		2249/346	346
1909.69	(8)	130.	(3)		2256/346	346
1929.1	(2)	10.	(2)			Not placed
1933.11	(8)	339	(3)		1986/52	
1938.50	(9)	63	(2)		2371/433	433
1953.51	(16)	13	(1)		2300/346	(346)
1960.89	(9)	200.	(3)	T	Multiplet	346
		11	(7)	C	2308/346	
		189	(10)	MC	1986/25	
1975.66	(10)	52	(7)	A		Not placed
1986.57	(7)	161	(2)		2333/346	346
1995.97	(10)	29	(3)		2429/433	433
2014.0	(3)	7	(2)	E	2447/433	
2028.48	(7)	135	(4)		2081/53	
2053.60	(14)	34	(2)		2400/346	346
2056.06	(13)	52	(2)		2081/25	

TABLE X (cont.)

Energy[a] (keV)		Intensity[a,b]		Note	Transition[c] (from/to)	Coincident[d] γ-rays in ^{105}Cd Decay or Identification[e]
2061.5	(3)	5	(1)		2494/433	
2076.5	(4)	8	(1)		2422/346	(346)
2095.2	(6)	2	(1)	Q		
2117.30	(15)	19	(2)		2550/433	433
2156.20	(11)	80.	(3)		2156/GS	
2203.58	(14)	21	(1)	T	(Multiplet)	346
		20	(8)	C	2550/346	
		≤8		MC	(2256/52)	
2230.88	(12)	42	(2)		2256/25	
2249.48	(10)	105	(4)		2249/GS	
2272.85	(15)	220.	(12)		2326/52	
2274.83	(15)	180.	(12)		(2300/25) or (2328/52)	
2288.9	(2)	6.4	(7)		2314/25	
2300.57	(9)	110.	(4)		(2300/GS) or (2326/25)	
2308.30	(12)	22	(1)		2308/GS	
2318.50	(14)	10.4	(9)		2371/53	
2333.26	(5)	422	(14)		2333/GS	
2345.7	(7)	0.8	(5)	Q	2371/25	
2364.60	(13)	10.5	(6)	A		Not placed

TABLE X (cont.)

Energy[a] (keV)		Intensity[a,b]		Note	Transition[c] (from/to)	Coincident[d] γ-rays in ^{105}Cd Decay or Identification[e]
2375.2	(3)	1.6	(5)		2400/25	
2382.66	(12)	10.2	(6)	A		Not placed
2393.69	(9)	38	(1)		(2447/53) or (2419/25)	
2400.27	(15)	9.4	(7)		2400/GS	
2422.99	(10)	75	(3)		2422/GS	
2429.19	(14)	13.0	(6)		2429/GS	
2447.5	(3)	≤0.1		106	(2473/25)	
2469.5	(5)	1.3	(3)		2494/25	
2512.1	(5)	0.7	(3)	A		Not placed
2525.45	(18)	16.7	(7)		2550/25	
2530.8	(3)	1.3	(3)		2584/53	
2554.3	(4)	1.2	(3)	A		Not placed
2558.8	(2)	3.2	(3)		2584/25	
2568.5	(8)	0.5	(3)	A		Not placed
2573.8	(2)	3.2	(3)	A		Not placed
2594.5	(5)	0.7	(2)	A		Not placed
2665.4	(6)	0.4	(2)	A		Not placed

TABLE X (cont.)

[a]Value shown as 27.70(6) means 27.70 ± 0.06 for example. The uncertainties are one standard deviation.

[b]The intensity values are relative to a value of 1000 for the 961.84-keV transition. To convert to absolute intensity (per 1000 decays), multiply the relative intensity value by 0.0469 ± 0.0029. This includes the absolute branch to the 7/2+ 25.5-keV state of 51.4%. An uncertainty of 2% must be added in quadrature to reflect the uncertainty in the Ge(Li) detector efficiency.

[c]Assignments are made on the basis of energy sums and coincidence relationships. Multiple assignments and assignments of transitions with intensity limits are in parentheses and are dotted in the level scheme. These assignments are consistent with being dipole or electric quadrupole in character and the energy sums involved give no preference for placement.

[d]Coincidences in parentheses are marginal. These are indicated in the level scheme by the use of open circles to indicate the coincidence.

[e]The assignments to the decay of 7.23-min $^{105}Ag^{m}$ are based on the work of Krien et al. The values in parentheses are the relative intensity values from that work. Transitions not placed are thought to come from ^{105}Cd decay on the basis of half-lives and/or consistent values for relative intensity.

The notes to the table mean the following:

Q - The presence of this transition is in some doubt. Generally this is a weak peak with large uncertainty and may not have been observed in all singles spectra.

T - The transition intensity is that observed for the single peak in singles spectra.

C - The transition intensity was obtained from coincidence measurements.

TABLE X (cont.)

MC - The transition intensity is the result of subtracting the intensities noted "C" from the total intensity (noted "T").

105(etc.)-The transition intensity has been corrected for contributions from the decay of this Ag isotope.

SL - Intensity limit is from singles spectra.

L - Intensity limit is from coincidence measurements.

E - The intensity has been corrected for the presence of an escape peak.

A - This γ-ray determines a level at (E)-, (E + 25.5)-, or (E + 53.2)-keV. It is either not coincident with the 346- or 433-keV γ-rays or Q_{EC} considerations preclude its placement into any level but G.S., 25.5-, or 53.2-keV.

by observing the positrons associated with ^{105}Cd decay (correcting the singles spectra for positrons from ^{106}Ag^{g} decay (67Ra)) are also presented in Appendix IV.

A balance of the intensities of the γ-rays placed into and out of the 53.2 keV level of ^{105}Ag resulted in a value for the total conversion coefficient (α_{total}) of the 27.7-keV γ-transition of $(49 \pm 6) \leq \alpha_{Total} \leq (56 \pm 6)$. I assumed that there was no direct β-decay to the 53.2 keV level. The two values resulted from the double placements of the 2274.83- and 2393.69-keV γ-rays. A comparison with the theoretical α_{Total} of a 27.7-keV transition indicates that this transition is M1 + (25 ± 4) % E2.

3. Gamma-Gamma Coincidence Spectroscopy.

The γ-γ coincidence measurements were carried out at LLL using two large volume true-coaxial Ge(Li) detectors (both ~50-60 cm^3, having effective FWHM energy resolutions in the two-parameter system of 3.0 and 3.3 keV at 1332 keV) in conjunction with a multiparameter pulse-height analyzer system and associated electronics as described in Section II. The coincidence time gate was approximately 35 nsec which resulted in a real-to-random coincidence ratio of about 15 to one. As in the ^{131}Te^{m} γ-γ coincidence study, the random coincidences were found to be essentially negligible. The coincidence events were recorded on magnetic tape in an 8192 by 8192 channel format for later analysis using the LLL CDC 7600

computer system along with computer codes developed at LLL (75La2). Approximately 2.3 million coincidence events were recorded on magnetic tape, and during analysis, coincidence spectra were extracted for 39 peak regions as well as for neighboring regions to account for Compton backgrounds. The Compton-gate spectra were subtracted from the photopeak-gate spectra to obtain net coincidence spectra. Energy gates were set on the spectrum obtained with the "stop" detector (FWHM = 3.3 keV) and the spectrum in coincidence with the gated region was retrieved for the "start" detector (FWHM = 3.0 keV). The results obtained are tabulated in Table XI which lists all photopeak gates which were set and all γ-rays which were observed to be in true coincidence in the resulting coincidence spectra. Marginal coincidences are indicated in parentheses. (These were doubtful peaks in the coincidence spectra which, however, agreed in energy with transitions seen in γ-ray singles spectra. These transitions could be placed between established levels on the basis of energy sums such that the placement was consistent with the observation of a coincidence.) All coincidences observed are also listed in Table X.

As in the case of the $^{131}Te^{m}$ γ-γ coincidence study, evidence for many γ-ray transitions was obtained solely from coincidence data. For example, the γ-ray singles spectra showed a single peak at 1665.33 keV, however, the coincidence data revealed this peak to be a doublet. Part of the evidence for this is shown in Figure 45 which shows the same

TABLE XI

Gamma-Gamma Coincidences in ^{105}Cd Decay

Ge(Li) Gate (keV)	Gated Photopeak[a] (keV)	Coincident Gamma Rays Observed[b] (keV)
250.4 - 256.4	253.42	283, 1644
260.0 - 266.0	262.99	(307), 346, (775), 948, 1294
288.7 - 295.0	291.96	307, 346, 662, 746, (842), 948, 1294
303.5 - 310.7	306.35(*) 307.83	182(*), 262, 291, 340, 420(*), 613, (640), (697), 934, 961, (1038), 1274, 1302
314.8 - 322.0	316.82 319.23(*)	283, 331(*), (1322), 1644
343.0 - 350.0	344.58(*) 346.87	262, 292, 306(*), 328(*), 530, 617(*), 640, 695, 746, 896, 948, (1006), 1038, (1039), 1211, 1239, 1322, 1343, 1403, 1902, 1909, (1953), 1961, 1986, 2053, (2076), 2203
429.8 - 436.5	433.24	590, 609, (613), 733, 810, 1124, (1159), 1360, 1489, (1552), 1823, (1867), (1874), 1881, 1892, (1894), 1900, 1938, 1995, 2117
535.6 - 541.8	538.67	(613), 1043, 1071

TABLE XI (cont.)

Ge(Li) Gate (keV)	Gated Photopeak[a] (keV)	Coincident Gamma Rays Observed[b] (keV)
555.0 - 561.0	<u>558.14</u> 560.9	(1403), (1724)
580.0 - 586.4	583.17	(1403), (1724)
586.4 - 594.8	590.44	433, (1302)
603.8 - 611.9	<u>607.22</u> 609.45	433, 1665, 1693
610.6 - 620.0	<u>613.50</u> 616.1(+) 617.41 617.8(*)	307, 344(*), 429(+), 511(+), (538), 609, (648), (695), (703), 804(+), 1043, (1635), (1665)
631.6 - 639.2	635.4	703, 1343, 1665
643.8 - 651.4	644.62(*) <u>648.49</u>	443(*), (613), (640), (697), 934, 961
729.0 - 737.0	733.03	433, (1159), (1256)
822.2 - 829.0	824.7(+) <u>825.72</u>	616(+), 703(+), 804(+), 1044, 1071
874.5 - 880.1	877.81	758
881.3 - 887.9	884.57	(454), 1388, 1416
887.5 - 895.0	<u>889.13</u> 892.21	1044, 1071, 1416

TABLE XI (cont.)

Ge(Li) Gate (keV)	Gated Photopeak[a] (keV)	Coincident Gamma Rays Observed[b] (keV)
918.0 - 925.2	921.62	340, 1274, 1302
930.0 - 938.2	934.14	(307), 340, 454, 511, (570), 648, 703, (998), (1169), 1338, 1340, (1413), 1485
943.9 - 952.1	948.04	262, 291, 340, 346, (746), 1013, (1031), 1038
957.6 - 966.0	961.84	307, 340, 398, 454, 511, 570, (635), 648, (681), 703, 998, 1169, 1262, 1327, 1338, 1340, 1413, 1485
1034.5 - 1041.5	1038.44	307, 948, 1294
1041.5 - 1047.6	1043.46 1045.9(+)	538, 613, 748(+),(793)(+), (808)(+), (825), 889, (1199)(+), 1228
1067.4 - 1075.8	1071.65	538, 825, 889, 984, 1228, 1322, 1375
1290.9 - 1298.9	1294.89	262, 291, (340), 1038
1298.0 - 1307.0	1302.46	229, 307, 422, 466, 590, (658), 921, (972), 986, 998, 1119
1356.8 - 1365.2	1360.79	249, (253), 283, 433, (499), (770), 941, (1033)

TABLE XI (cont.)

Ge(Li) Gate (keV)	Gated Photopeak[a] (keV)	Coincident Gamma Rays Observed[b] (keV)
1384.8 - 1392.8	1388.48	249, 858, (866), 884, 981, 1031, (1109)
1398.7 - 1407.1	1403.10	(172), 346, (558), 583
1410.7 - 1419.8	1413.24 1416.10	(866), 884, 892, 934, 961, 981, 1031, (1109)
1553.0 - 1562.9	1557.84	192, 598, 775, 842, 866, (992)
1631.5 - 1639.8	1635.81	(613), (697)
1639.8 - 1648.1	1644.03	253, 316, 579, 656
1660.0 - 1670.0	1665.33	232, 607, (617), 623, 635, 642, 709
1687.2 - 1698.8	1693.34 1697.2	607, 700
1905.0 - 1914.0	1909.69	346

[a] When more than one photopeak appears in a gate the principal ^{105}Cd decay peak is underlined.

[b] Coincidences in parentheses were marginal.

(*) - This is a transition in $^{105}Ag^{g}$ or $^{105}Ag^{m}$ decay.

(+) - This is a transition in $^{106}Ag^{g}$ or $^{106}Ag^{m}$ decay.

Figure

45. A portion of the ^{105}Cd γ-ray spectrum coincident with the 632- 639 keV and 604- 612 keV gates. The 607- by 1665-keV and 635- by 1665-keV coincidences indicate the 1665.33-keV peak observed in γ-ray singles spectra to be a doublet.

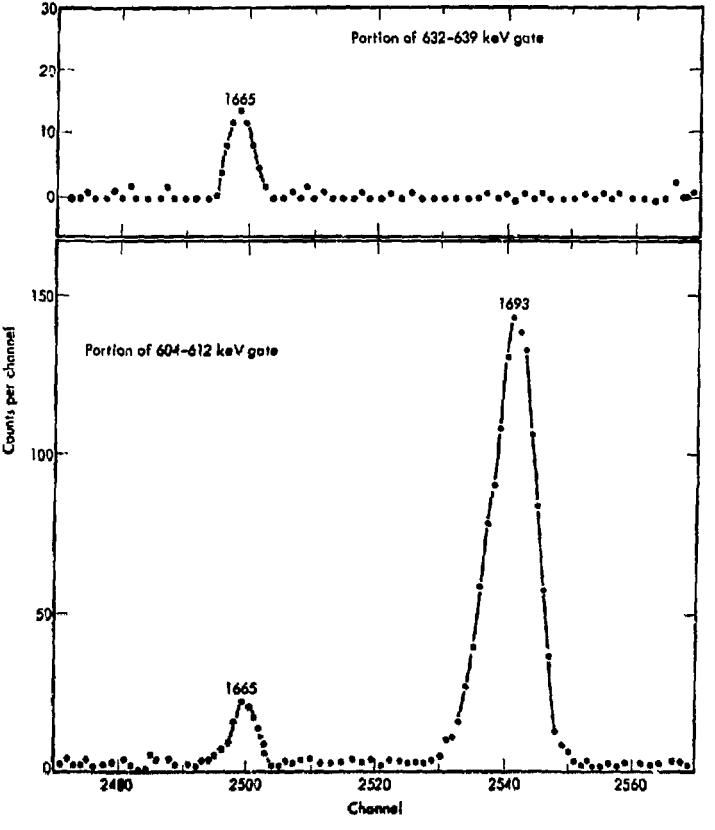
Portion of 632–639 keV gate
1665
Portion of 604–612 keV gate
1693
1665
Counts per channel
Channel
30
20
10
0
150
100
50
0
2480
2500
2520
2540
2560

portion of both the 632-639 keV gate (635.4-keV γ-ray, placed 2326 to 1690 keV) and the 604-612 keV gate (607.22-keV γ-ray, placed 2326 to 1718 keV). The two members of the 1665-keV doublet were found to have energies of 1665.20- and 1665.65-keV (in the upper and lower spectrum, respectively), and the relative intensity of the 1665.65-keV transition was found to be 75 ± 14 through comparison with the 1693.34-keV peak in the lower spectrum. This left a net relative intensity value of 203 ± 18 for the 1665.20-keV transition.

Through techniques as described above and in Section III.B.3., eighteen multiplets were resolved and the relative intensities, as determined from singles spectra, were split between the members of the multiplets. These cases are indicated by the note "C" or "MC" in Table X. In addition, energy sums and differences between established levels indicated the possibility of eleven doublets, although no evidence was found for these in any coincidence spectra. In these cases, limiting relative intensity values were determined from γ-ray singles and/or γ-γ coincidence spectra. These limiting values are listed in Table X and noted by the transition assignment being placed in parentheses and by the note "L" or "SL".

C. Construction of the ^{105}Ag Level Scheme.

In Figures 46, 47, 48, 49, 50, and 51, I present the level scheme of ^{105}Ag as determined in this investigation

Figures

see p. 251

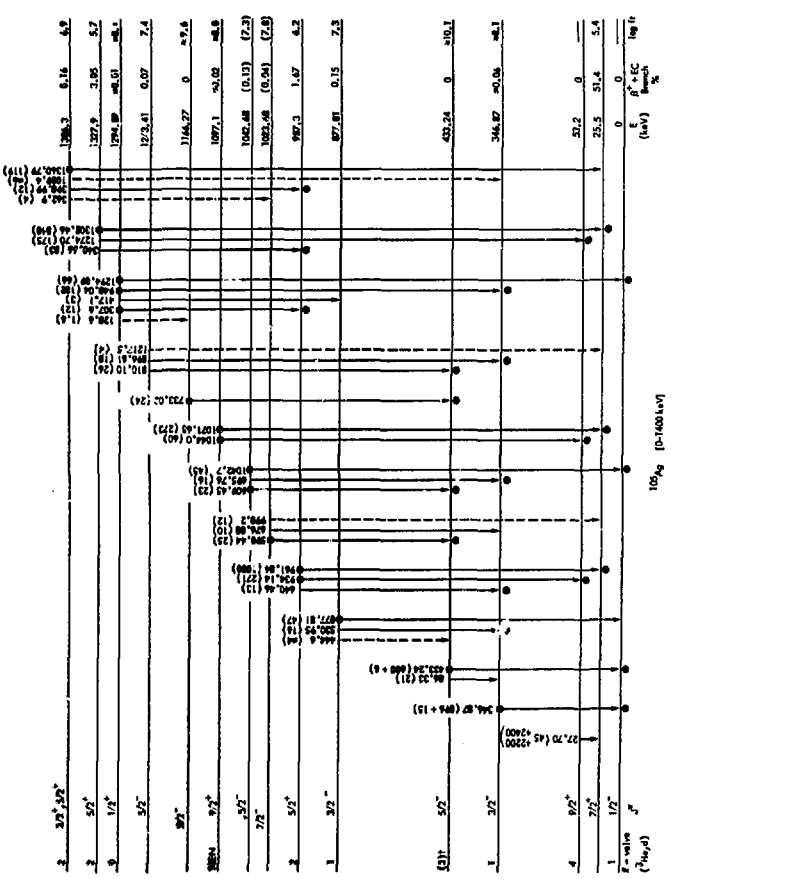
^{109}Ag [0-1400 keV]
E (keV)
β⁺+EC Branch %
log ft
E - value (^{3}He,d)
J$^\pi$

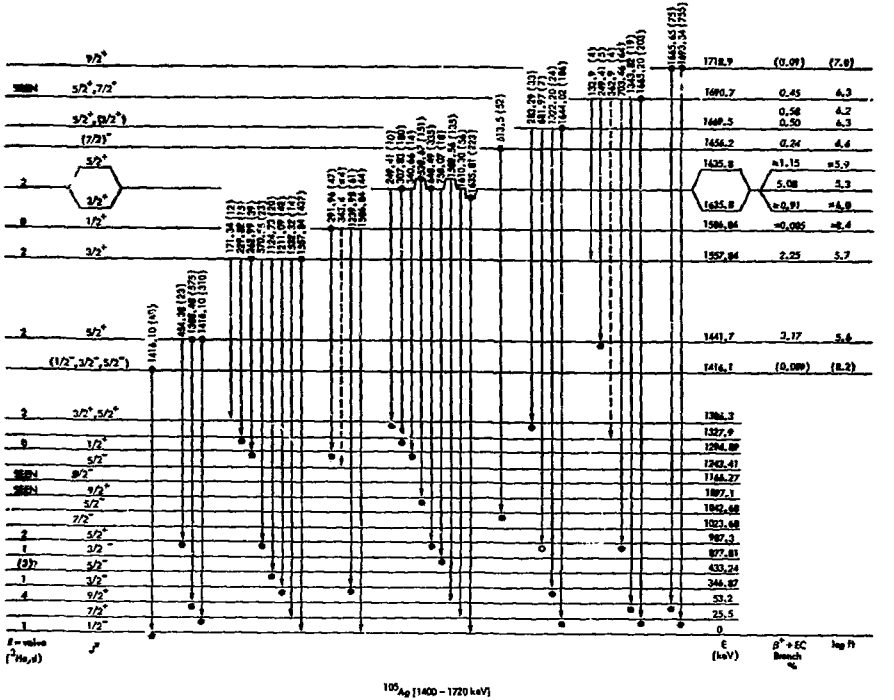
9/2+
5/2+,7/2+
3/2+,(9/2+)
(7/2)-
3/2-
3/2+
1/2+
3/2+
5/2+
(1/2-,3/2-,5/2-)
3/2+,5/2+
1/2+
5/2+
9/2-
9/2+
5/2+
7/2+
5/2+
3/2-
(3)+
5/2+
3/2+
9/2+
7/2+
1/2-
1718.9 (0.09) (7.9)
1690.7 0.45 6.3
1669.5 0.58 6.2
0.50 6.3
1656.2 0.24 6.4
1635.8 ≤1.15 ≤5.9
5.08 5.3
1635.8 ≤0.91 ≤6.8
1586.84 ≤0.085 ≤8.4
1557.84 2.25 5.7
1441.7 2.17 5.6
1416.1 (0.089) (8.2)
1386.3
1327.9
1294.89
1243.41
1166.27
1097.1
1062.68
1023.68
987.3
877.81
433.24
346.87
53.2
25.5
0
E (keV)
β+ + EC Branch %
log ft
E - value (3He,d)
Jπ
105Ag [1400 – 1720 keV]

SEEN 3/2+
SEEN 5/2-,7/2-
2 5/2-
4 7/2-
(4-) 5/2-,7/2-
(4-) (7/2-)
4 7/2-
2 5/2-
SEEN 9/2-
SEEN 5/2-,7/2-
SEEN (7/2-)
2 5/2-
2 9/2-
2 3/2-,5/2-
2 5/2-
0 1/2-
SEEN 9/2-
2 5/2-
(3)- 5/2-
1 3/2-
4 7/2-
1 7/2-
192.27(19)
422.27(19)
762.8(4)
1403.10(83)
1697.21(25)
1724.69(148)
466.72(21)
1361.5(26)
1741.8(7)
?1801.67(33)
443.9(4.4)
499.45(8)
558.14(8)
788.70(6)
1860.1(8)
128.6(1.6)
172.82(16)
232.37(18)
253.42(31)
825.72(26)
1489.77(95)
1869.74(136)
1897.52(308)
295.7(3)
316.82(153)
545.0(3)
658.27(7)
699.13(54)
998.1(20)
1552.8(7)
1933.11(339)
1960.79(189)
362.8(4)
984.58(15)
2028.48(135)
2056.06(52)
486.73(11)
598.54(25)
714.9(4)
770.18(12)
827.7(2)
1169.09(24)
1809.0(5)
2156.20(80)
2081.7 0.95 5.6
2156.3 0.74 5.4
1986.3 2.17 5.2
1923.0 2.94 5.3
1885.6 0.12 6.7
(1884.91)? 0.16 6.6
1794.4 (0.02) (7.5)
1750.03 1.11 (5.0)
1718.9
1690.7
1609.5
1557.84
1441.7
1396.3
1327.9
1294.89
1097.1
987.3
433.24
346.07
53.2
25.5
0
$^{105}_{49}In_{56}$ (1720 - 2200 keV)
Energy (keV)
J^π - EC
β^+ Branch %

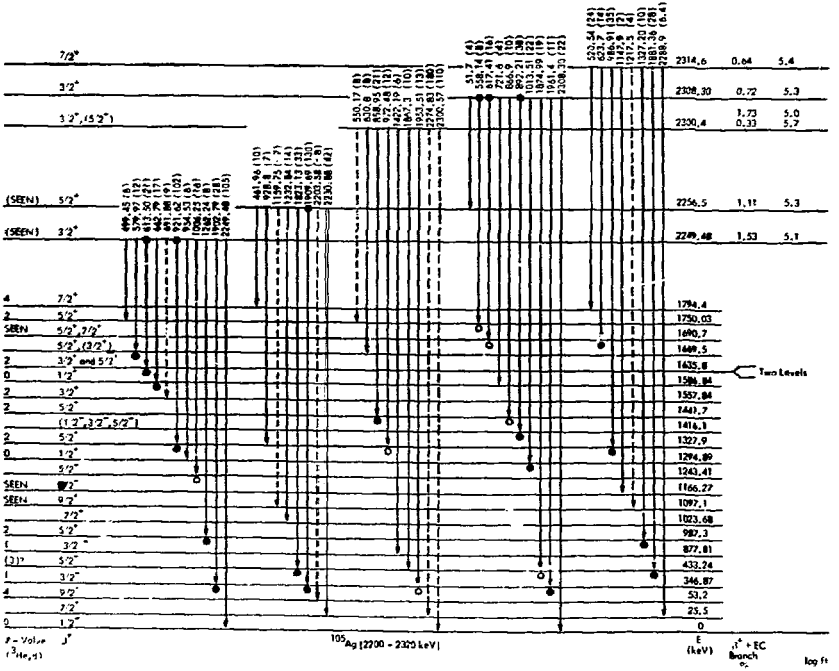
7/2+
3/2+
3 2+,(5 2+)
(SEEN) 5/2+
(SEEN) 3/2+
4 7/2+
2 5/2+
SEEN 5/2+,7/2+
5/2+,(3/2+)
2 3/2+ and 5/2+
0 1/2+
2 3/2+
2 5/2+
(1 2+,3/2+,5/2+)
2 5/2+
0 1/2+
5/2+
SEEN 7/2+
SEEN 9/2+
7/2+
2 5/2+
1 3/2+
(3)+ 5/2+
1 3/2+
4 9/2+
7/2+
0 1/2+
499.45 (61)
579.97 (12)
613.50 (21)
691.2 (8)
921.86 (102)
934.23 (18)
1256.5 (10)
1282.24 (81)
1995.2 (28)
2249.6 (105)
981.96 (10)
1159.75 (-7)
1222.84 (14)
1827.4 (13)
2230.58 (-9)
2230.88 (42)
550.17 (81)
658.8 (8)
858.95 (121)
972.48 (12)
1422.19 (6)
1492.2 (10)
1953.51 (13)
2274.83 (180)
2300.57 (110)
51.7 (4)
515.41 (16)
615.4 (8)
721.6 (42)
865.7 (10)
1013.51 (22)
1824.99 (19)
1951.4 (11)
2288.3 (125)
503.54 (26)
623.7 (14)
986.91 (35)
1217.5 (2)
1327.20 (10)
1881.36 (28)
2288.9 (6.4)
2314.6 0.64 5.4
2308.30 0.72 5.3
2300.4 1.73 5.0
0.33 5.7
2256.5 1.11 5.3
2249.48 1.53 5.1
1794.4
1750.03
1690.7
1669.5
1635.8
1586.84
1557.84
1441.7
1416.1
1327.9
1294.89
1243.41
1166.27
1097.1
1023.68
987.3
877.81
433.24
346.87
53.2
25.5
0
Two Levels
β- Value (3He,t)
J+
105Ag (2200 - 2325 keV)
E (keV)
J+ + EC Branch %
log ft

105Ag (2320 + 2410 keV)
E (keV)
Jπ
Two Levels
MULTIPLET
2400.37
2331.74
2233.26
2229.03
2226.72
0.49
0.45
4.44
0.42
0.53
5.2
5.4
4.5
5.0
4.3

$^{105}_{Ag}$(2410 - 2600 keV)
Log ft
Energy (keV)
Branch %
Total Levels

TABLE XII. ^{105}Ag Levels Observed in the β^+/EC Decay of 55.5-min $5/2^+$ ^{105}Cd

Energy (keV)	Absolute β^++ EC Branch[a]	σ^b	log ft	Note	J^π Assignment	L-Value[1] (^{3}He,d)	C^2S_{fj}
0	0	-	-	c	$1/2^-$	1	0.46
25.5	51.4	4.0	5.4		$7/2^+$		
53.2	0	-	-	c	$9/2^+$	4	1.57
346.87	$\leq$0.06	-	$\leq$8.1	d	$3/2^-$	1	0.21
433.24	0	-	$\leq$10.1	d	$5/2^-$	(3)?	
877.81	0.15	0.03	7.3		$3/2^-$*	1	0.19
987.3	1.67	0.14	6.2		$5/2^+$	2	0.52
1023.68	0.042	0.094	(7.8)	e	$7/2^-$*		
1042.68	0.13	0.13	(7.3)	e	$5/2^-$*	Seen	
1097.1	$\leq$0.02	-	$\leq$8.0	d	$9/2^+$	Seen	
1166.7	0	-	$\leq$9.6	d	$9/2^-$*	Seen	
1243.41	0.070	0.042	7.4		$5/2^-$		
1294.89	$\leq$0.01	-	$\leq$8.1	d	$1/2^+$	0	0.17
1327.9	3.05	0.23	5.7		$5/2^+$	2	0.86
1386.3	0.16	0.09	6.9		$3/2^+$, $5/2^+$	2	0.08 , 0.06
1416.1	0.009	0.009	(8.2)	e	($1/2^-$, $3/2^-$, $5/2^-$)		
1441.7	3.17	0.24	5.6		$5/2^+$	2	0.03
1557.84	2.25	0.16	5.7		$3/2^+$	2	0.12
1586.84	$\leq$0.005	-	$\leq$8.4	d	$1/2^+$	0	0.04
1635.8	5.08	0.33	5.3	f	$3/2^+$ and $5/2^+$	2	0.16 , 0.12

TABLE XII (cont.)

Energy (keV)	Absolute β^+ + EC Branch[a]	σ^b	log ft	Note	J# Assignment	L-Value[1] (^{3}He,d)	$C^2S_{l_j}$
	⩾0.91		⩽6.0	g	$3/2^+$		
	⩾1.15		⩽5.9	g	$5/2^+$		
1656.2	0.24	0.07	6.6		$(7/2)^-$		
1669.5	0.58	0.07	6.2	h	$5/2^+$, $(3/2^+)$		
	0.50	0.07	6.3	i	$5/2^+$, $(3/2^+)$		
1690.7	0.45	0.10	6.3		$5/2^+$, $(3/2^+)$	Seen	
1718.9	0.089	0.09	(7.0)	e	$9/2^+$		
1750.03	1.11	0.09	5.8		$5/2^+$	2	0.08
1794.4	0.02	0.05	(7.5)	e	$7/2^+$	4	0.45
(1884.9)	0.16	0.01	6.6		$(7/2^+)$?	4 (2)	1.21
1885.6	0.12	0.03	6.7		$5/2^+$, $7/2^+$		
1923.0	2.94	0.19	5.3		$7/2^+$	4	0.67
1986.3	3.17	0.21	5.2		$5/2^+$	2	0.05
2081.7	0.95	0.07	5.6		$5/2^+$, $7/2^+$	Seen	
2156.3	0.74	0.07	5.6		$3/2^+$	Seen	
2249.48	1.53	0.12	5.1		$3/2^+$	Seen	
2256.5	1.11	0.09	5.3		$5/2^+$		
2300.4	1.73	0.12	5.0	h	$3/2^+$, $(5/2^+)$		
	0.33	0.03	5.7	i	$3/2^+$, $5/2^+$		
2308.30	0.72	0.07	5.3		$3/2^+$		
2314.6	0.64	0.05	5.4		$7/2^+$ *		

TABLE XII (cont.)

Energy (keV)	Absolute β^+ + EC Branch[a]	α^b	log ft	Note	J^π Assignment	L-Value[1] (^{3}He,d)	C^2S_{lj}
2326.13	8.53	0.53	4.2	h	$5/2^+$		
	8.01	0.59	4.3	i	$5/2^+$		
2328.03	1.33	0.11	5.0	h	$5/2^+$, $7/2^+$	Multiplet	
	0.42	0.05	5.5	i	$3/2^+$, $5/2^+$, $7/2^+$		
2333.26	4.44	0.28	4.5		$3/2^+$		
2371.74	0.45	0.04	5.4		$5/2^+$, $7/2^+$		
2400.37	0.61	0.06	5.2		$3/2^+$		
2419.2	0.52	0.06	5.3	h	$5/2^+$, $7/2^+$		
	0.34	0.05	5.4	i	$5/2^+$, $7/2^+$	Seen	
2422.99	0.67	0.05	5.1		$3/2^+$		
2429.19	0.52	0.06	5.3		$3/2^+$		
2447.20	0.39	0.03	5.3	h	$5/2^+$, $7/2^+$		
	0.22	0.03	5.6	i	$5/2^+$, $7/2^+$		
2473.0	0.45	0.06	5.2		$5/2^+$, $7/2^+$		
2494.8	0.056	0.038	6.0		$3/2^+$, $5/2^+$, $7/2^+$		
2550.47	0.45	0.04	4.9		$3/2^+$, $5/2^+$	(Seen)	
2584.1	0.052	0.014	5.7		$5/2^+$		

Energy (keV)	Absolute β^+ + EC Branch[a]	σ^b	log ft	Note	J^π Assignment	Level[f] (MeV)	σ^2[f]
~2000	≥0.24	-	≤6.2	k	Probably all $3/2^+$, $5/2^+$, $7/2^+$	(Seen)	
~2390	≥0.049	-	≤6.3	k			
~2410	≥0.048	-	≤6.3	k			
~2535	≥0.003	-	≤7.1	k			
~2580	≥0.006	-	≤6.7	k			
~2590	≥0.002	-	≤7.0	k		Multiplet	
~2600	≥0.015	-	≤6.2	k			
~2620	≥0.003	-	≤6.7	k			
~2685	≥0.002	-	≤6.5	k			

[a] This is the number of decays to this level per 100 decays of ^{105}Cd.

[b] All uncertainties are one standard deviation.

[c] A zero β^+/EC branch to this level was assumed.

[d] The intensity balance results in a negative β^+/EC feeding. The log ft limit is the result of adding the uncertainty value to the calculated value. If this resulting feeding was still negative, the log ft limit was obtained by assuming a maximum feeding of 0.1 relative gamma-ray units.

[e] The intensity balance results in a positive β^+/EC feeding, but due to the large uncertainty a zero beta branch cannot be ruled out. The log ft value is regarded essentially as a lower limit.

[f] This level is thought to be two separate levels. This feeding and log ft value represent decay to both levels. The log ft value, then, is a lower limit for each level.

* see p. 251

[g]The log ft limits arise from performing the intensity balance using only the transitions which can unambiguously be assigned to the level of the given J^{π}.

[h]This feeding and log ft are the limits resulting from performing the intensity balance using all multiply assigned (dotted) transitions.

[i]This feeding and log ft are the limits resulting from performing the intensity balance omitting all multiply assigned (dotted) transitions.

[k]These are levels which may be placed at E- , (E+ 25.5)- , or (E+ 53.2)-keV. The approximate energy value is the γ-ray energy (these are labeled "A" in the γ-ray list) plus ~25 keV.

[l]The (^{3}He,d) data is from the work of Anderson and Kraushaar (7cAn).

of the decay of 55.5-min $5/2^+$ ^{105}Cd. The levels along with their properties as determined in this study and in the ^{104}Pd (^{3}He,d) ^{105}Ag reaction study (75An) are tabulated in Table XII. The notation in Figures 46-51 is the same as in Table XII. Energies and relative intensities of the γ-rays are tabulated in Table X and presented on the figures vertically above the γ-ray transition line with the relative intensity value in parentheses. Intensities given on the figures as (896 + 15), for example, indicate γ-ray intensity plus theoretical conversion electron intensity (68Ha), respectively (except in the case of the 27.70-keV transition for which the conversion electron intensity was determined from an intensity balance assuming no direct β^+/EC feeding to the 53.2 keV level). Energy gates were set in the γ-γ coincidence experiment on those γ-rays depicted with a dot on their upper end, whereas those γ-rays observed in the resulting coincidence spectra are indicated by a filled dot at their lower end. Marginal coincidences are indicated by open circles at the lower end of the transition. Dashed transitions signify either transitions for which the relative intensity value is an upper limit or transitions which are also placed elsewhere in the level scheme with no evidence to support one placement over the other. These transitions are indicated in Table X by parentheses placed around the transition assignment.

In making intensity balances to determine direct β^+/EC decay feeding to the levels of ^{105}Ag, I assumed that

there was no direct β^+/EC decay from $5/2^+$ ^{105}Cd to the ground state ($1/2^-$) or to the 53.2 keV excited state ($9/2^+$). The Q_{EC} value for ^{105}Cd of 2800 ± 100 keV of Wapstra and Gove (71Wa) and the log(f^{ε}_{o} + $^{\varepsilon^+}_{o}$) tables of Gove and Martin (71Go) were used to calculate log$\underline{ft}$ values. As noted in Table XII, when two log$\underline{ft}$ values are given for a level, one value arises from performing the intensity balance for the level without including any dashed transitions, and the other arises from including them.

At the time this investigation of the decay of ^{105}Cd was initiated, only one excited state was firmly established in ^{105}Ag (74Bel). This was the 7.23-min isomeric level at 25.5 keV which decays principally by a highly converted transition to the ground state of ^{105}Ag and by a 0.34% EC-branch to ^{105}Pd (53Jo, 69Ho, 72Kr). During the course of this investigation, the excited states of ^{105}Ag were studied via the ^{104}Pd (^{3}He,d) ^{105}Ag reaction by Anderson and Kraushaar (75Anl). Their data were used to aid in the placement of levels and the assignment of spin and parity values.

The second excited state of ^{105}Ag was observed in the (^{3}He,d) reaction and is placed at 53.2 keV on the basis of a 27.70-keV transition (to the 25.5 keV level) as well as the observation of numerous 27.7 keV differences between strong γ-rays. The levels at 346.87, 433.24, and 877.81 keV were observed in the (^{3}He,d) reaction, and their energies are based on observed γ-transitions to the ground state. In addition, the placement of the level at 877.81 keV is

substantiated by a 346.87- by 530.95-keV coincidence.

The level at 987.3 keV was observed in the (^{3}He,d) reaction and is placed on the basis of a 346.87- by 640.46-keV coincidence as well as transitions to the levels at 25.5 and 53.2 keV. The level at 1023.68 keV is placed by a 433.24- by 590.44-keV coincidence. The levels at 1042.68, 1097.1, and 1166.27 keV were all populated in the (^{3}He,d) reaction. The first and third of these are placed by coincidences indicating transitions from them to the 433.24 keV level. The 1097.1 keV level is placed on the basis of transitions to the 25.5 and 53.2 keV levels.

The level at 1243.41 keV is placed by 346.87- by 896.61-keV and 433.24- by 810.10-keV coincidences. The level at 1294.89 keV was observed in the (^{3}He,d) reaction and is placed on the basis of a γ-ray of this energy as well as several coincidences. The levels at 1327.9, 1386.3, and 1441.7 keV were observed in the (^{3}He,d) reaction and are placed by coincidences indicating feeding to the level at 987.3 keV. The level at 1416.1 keV was placed on the basis of a strong 1416.10- by 892.21-keV coincidence (= 2308.31 keV) indicating a cascade from a level at 2308.30 keV which is established by other coincidences. The level placement at 1416.1 keV rather than at 892.2 keV is supported by the failure to observe any coincidences higher in energy than 1416 keV in the 887-895 keV coincidence gate, although the background above 1416 keV was virtually nil. The levels at 1557.84 and 1586.84 keV were seen in the (^{3}He,d) reaction

study and are placed on the basis of γ-rays of these energies as well as numerous coincidences indicating feeding to established lower-lying levels.

The two levels at 1635.8 keV are placed on the basis of numerous coincidences including 1071.65- and 1044.0- by 538.67-keV, 1302.46- by 307.83-keV, and 877.81- by 758.07-keV. The (^{3}He,d) reaction study observed an excited state at 1635 ± 4 keV. My proposal that there are actually two excited states is based on the observation of strong γ-transitions to lower-lying levels having spin and parity values of $9/2^+$ and $1/2^-$. (This will be discussed in more detail in the next section, dealing with the assignment of spin and parity values.)

The level at 1656.2 keV is established on the basis of 609.45- and 1042.7- by 613.5-keV coincidences as well as a marginal 695.76- by 613.5-keV coincidence. The level at 1669.5 keV is placed by 1360.79- by 283.29-keV and 346.87- by 1322.20-keV coincidences. The excited state at 1690.7 keV was seen in the (^{3}He,d) reaction and is placed by 1388.49- by 249.41-keV and 961.84- by 703.46-keV coincidences. The level at 1718.9 keV is placed on the basis of transitions to the 25.5 keV and 53.2 keV levels (1693.34- and 1665.65-keV, respectively). These transitions were both observed in the coincidence spectrum from the 604- 612 keV coincidence gate.

The levels at 1750.03 and 1794.4 keV were both seen in the (^{3}He,d) reaction and are placed on the basis of coin-

cidences indicating feeding to the level at 1327.9 keV as well as several additional coincidences. The tentative level at 1884.9 keV is placed on the basis of the observation of a high-spin (ℓ = 4) level at 1880 ± 6 keV in the (^{3}He,d) reaction and the observation of a relatively intense 1831.67-keV γ-ray which was not observed in any of the coincidence spectra. The level at 1885.6 keV was placed on the basis of several energy sums involving otherwise unassigned γ-rays as well as a marginal 1360.79- by 499.45-keV coincidence. The levels at 1923.0, 1986.3, and 2081.7 keV were all observed in the (^{3}He,d) reaction study and were placed on the basis of coincidences indicating transitions from all three to the 1097.1 keV level as well as several additional coincidences and numerous precise energy sums. The level at 2156.3 keV is placed by 1557.84- by 598.54-keV and 961.84- by 1169.09-keV coincidences and was observed in the (^{3}He,d) reaction study.

The level at 2249.48 keV is established by numerous coincidences, including 346.87- by 1902.79-keV, 961.84- by 1262.24-keV, and 1644.02- by 579.97-keV. The level at 2256.5 keV is established by coincidences indicating transitions to the levels at 433.24 and 346.87 keV. A level was seen at 2255 ± 7 keV in the (^{3}He,d) reaction and undoubtedly is one of these two states. The excited state at 2300.4 keV is placed by one good coincidence, 1388.48- by 858.95-keV, as well as by two marginal coincidences and several precise energy sums. The level at 2308.30 keV is

placed by several coincidences indicating transitions to the levels at 346.87 keV and 1294.89 keV. The excited state at 2314.6 keV is established by several coincidences, including 433.24- by 1881.36-keV, 961.84- by 1327.20-keV, and 1302.46- by 986.91-keV.

The level at 2326.13 keV is established by eight good coincidences and three marginal coincidences. The level at 2328.03 keV is established unambiguously by a 1360.79- by 941.60-keV coincidence. The level at 2333.26 keV is placed on the basis of eight coincidences and an intense γ-ray of this energy. In the (^{3}He,d) reaction a multiplet of excited states was observed at 2332 ± 6 keV. The excited state at 2371.74 keV is placed by a strong 433.24- by 1938.50-keV coincidence. The level at 2400.37 keV is placed by several coincidences, including 346.87- by 2053.60-keV and 961.84- by 1413.24-keV.

The level at 2419.2 is placed by 1693.34- by 700.04-keV and 1071.65- by 1322.20-keV coincidences. The level at 2422.99 keV is established by a 1388.48- by 981.50-keV coincidence as well as by two additional marginal coincidences. The level at 2429.19 keV is placed by two good coincidences, 1557.84- by 870.88-keV and 433.24- by 1995.97-keV. One of these three levels is undoubtedly the same as the excited state observed at 2420 ± 7 keV in the (^{3}He,d) reaction.

The levels at 2447.20 and 2473.0 keV are placed by coincidences indicating transitions to the 987.3 keV level as well as by additional coincidences and several good

energy sums. The excited state at 2550.47 keV is placed by coincidences indicating transitions to the levels at 346.87 and 433.24 keV. The levels at 2494.8 and 2584.1 keV are placed solely on the basis of energy sums involving lower-lying excited states and otherwise unassigned γ-rays.

Nine additional excited states are listed at the end of Table XII, two or three of which may have been observed in the (^{3}He,d) reaction study. These nine levels involve unassigned γ-rays which either cannot be placed into levels above 433 keV because of Q_{EC} and are not coincident with the 346.87-keV or the 433.24-keV transition or cannot be placed into any levels above the 53.5 keV level because of Q_{EC}. These γ-rays are noted in Table X by the note, "A". The level energy given in Table XII is approximately E_γ plus 25.5 keV, however any one of three level energies is possible as is noted in a footnote to Table XII. No other γ-transitions listed in Table X could be placed from these nine levels, (27 different possible level energies) to any established levels, hence the calculated log*ft* values are given as upper limits.

D. Spin and Parity Assignments.*

The spin and parity (J^π) assignments of the levels of ^{105}Cd observed in the β^+/EC decay of 55.5-min $5/2^+$ ^{105}Cd are presented in Figures 46-51 and in Table XII. These assignments are based on log*ft* values for the β^+/EC decay of ^{105}Cd, the *l*-transfer values determined in the ^{104}Pd

*see p.251

(^{3}He,d) ^{105}Ag reaction study (75Anl), the γ-ray de-excitation patterns between levels, and some systematic considerations. The ground states of ^{105}Cd and ^{105}Ag have been measured to be $5/2^{+}$ and $1/2^{-}$, respectively (69Fu). The 25.5 keV isomeric state in ^{105}Ag has been assigned as $7/2^{+}$ based on L-conversion subshell ratios of the 25.5-keV transition which favored an E3 transition (53Jo, 74Bel). The $7/2^{+}$ assignment is also suggested by analogy with the ^{107}Ag and ^{109}Ag $7/2^{+}$ E3 isomeric states (69Ho, 74Bel).

The 53.2 keV level was observed in the (^{3}He,d) reaction with an ℓ-transfer value of 4, limiting its spin and parity assignment to $7/2^{+}$ or $9/2^{+}$. The large $C^{2}S_{\ell j}$ spectroscopic factor obtained, indicative of strong single particle character, together with general shell model considerations favor the $9/2^{+}$ assignment. The $9/2^{+}$ assignment is also suggested by analogy with ^{107}Ag and ^{109}Ag, both of which possess a $9/2^{+}$ excited state lying just above the $7/2^{+}$ isomeric state in energy (71Be, 72Be2). The $9/2^{+}$ assignment is consistent with the lack of any observed transitions from the eight definite $3/2^{+}$ excited states of ^{105}Ag to the 53.2 keV level.

The excited states at 1294.89 and 1586.84 keV were observed in the (^{3}He,d) reaction, each with an ℓ-transfer value of zero. Hence, they are both assigned as $1/2^{+}$ states. The logft limits of $\geq$8.1 and $\geq$8.4, respectively, are consistent with second forbidden β^{+}/EC decay. All transitions placed out of each of these levels are con-

sistent with being M1, E1, or E2 transitions deexciting a $1/2^+$ state.

The eight excited states, 1557.84, 2156.3, 2249.48, 2308.30, 2333.26, 2400.37, 2422.99, and 2429.19 keV, all have log*ft* values ≤5.7 and have strong γ-branches to the $1/2^-$ ground state. Thus, they are all assigned as definite $3/2^+$ states, consistent with allowed β^+/EC decay from a $5/2^+$ parent and E1 γ-transitions to a $1/2^-$ state. The $3/2^+$ assignment of the 1557.84 keV level is also consistent with the *l*-value of 2 determined for this level in the (^{3}He,d) reaction study. All transitions placed as deexciting these eight levels are consistent with being M1, E1, or E2 (*e.g.* none of these levels is observed to decay to any $9/2^+$ states).

The five levels, 987.3, 1327.9, 1441.7 1750.03, and 1986.3 keV were all observed in the (^{3}He,d) reaction via strong *l*= 2 transitions, limiting their J^π assignment to $3/2^+$ or $5/2^+$. All five levels are observed to decay via strong γ-branches to the $9/2^+$ state at 53.2 keV, hence they are all assigned as definite $5/2^+$ states. Their log*ft* values, all ≤6.2, are consistent with this assignment.

The excited states at 346.87 and 877.81 keV were observed via *l*= 1 transitions in the (^{3}He,d) reaction, limiting their J^π assignments to $1/2^-$ or $3/2^-$. The observation of a strong γ-transition from $5/2^+$ 1750.03 keV level to the 346.87 keV level requires a $3/2^-$ assignment for the 346.87 keV level. It has been suggested (75An) that the 877.81 keV level is $3/2^-$. This is also suggested by

analogy with ^{107}Ag and ^{109}Ag which have known $3/2^-$ excited states at 786.7 keV (74Pa) and 701.9 keV (71Be), respectively. This assignment is supported by my observation of feeding from two levels which are possibly $5/2^+$ (1635.8 and 2300.4 keV), although I cannot completely rule out a $1/2^-$ assignment.

The excited state at 433.24 keV was observed in the (^{3}He,d) reaction and an ℓ-value of 3 was suggested (74An). The large log*ft* value ($\geq$10.1), the observation of a prompt γ-transition to the $1/2^-$ ground state, and the observation of a strong feeding from the $3/2^+$ 1557.84 keV level suggest possible assignments of $1/2^+$, $1/2^-$, $3/2^-$, or $5/2^-$. The observation of strong transitions to the 433.24 keV level from $\ell = 4$ states at 1794.4 and 1923.0 keV requires that the assignment be $5/2^-$ and, further, that the 1794.4 and 1923.0 keV levels be assigned as definite $7/2^+$ states.

The three states, 2256.5, 2326.13, and 2584.1 keV, must be $3/2^+$, $5/2^+$, or $7/2^+$ based on having log*ft* values 5.7, indicating allowed β^+/EC decay. The 2256.5 keV level is assigned as $5/2^+$ based on the observation of strong γ-branches to the $3/2^-$ 346.87 keV level and to the $5/2^-$ 433.24 keV level. The 2326.13 and 2584.1 keV levels are assigned as $5/2^+$ based on observed transitions to both $9/2^+$ and $1/2^+$ states.

The states at 1097.1 and 1718.9 keV deexcite via transitions solely to the $7/2^+$ 25.5 keV and the $9/2^+$ 53.2 keV states. They are not directly fed by β^+/EC decay and

are not fed from any $3/2^+$ states. They are fed by γ-transitions from established $5/2^+$ states. Hence, they are both assigned spin and parity of $9/2^+$.

The nine levels, 2081.7, 2300.4, 2314.6, 2328.03, 2371.74, 2419.2, 2447.20, 2473.0, and 2550.47 keV, all have log*ft* values 5.6 and are hence limited to J^π values of $3/2^+$, $5/2^+$, or $7/2^+$. Five of these (2081.7, 2371.74, 2419.2, 2447.20, and 2473.0 keV) are further limited to $5/2^+$ or $7/2^+$ as they have strong γ-ray branches to $9/2^+$ states. The 2300.4 keV level is limited to $3/2^+$ or $5/2^+$ by a transition to the $3/2^-$ 346.87 keV level, with the $3/2^+$ assignment favored by the possible placement of the 2300.57-keV transition to the $1/2^-$ ground state. The 2314.6 keV level is limited to $3/2^+$ or $5/2^+$ by a transition to the $1/2^+$ 1586.84 keV level, with the $5/2^+$ assignment favored by a possible (dashed) transition to the $9/2^+$ 1097.1 keV level. The 2550.47 keV level is limited to $3/2^+$ or $5/2^+$ by a transition to the $3/2^-$ 346.87 keV level. The 2328.03 keV level is limited to $5/2^+$ or $7/2^+$ only if the 2274.83-keV dashed transition may be placed to the $9/2^+$ 53.2 kev level.

In the (^{3}He,d) reaction a strong $\ell = 2$ transition was observed at an energy of 1635 ± 4 keV. I have placed two excited states at 1635.8 keV, one with $J^\pi = 5/2^+$ and the other with $J^\pi = 3/2^+$, on the basis of transitions to the lower-lying $9/2^+$ states (one of which was confirmed by coincidence data) and a strong transition to the $1/2^-$

ground state. The evidence for the placement of two levels is as follows: (1.) a 1071.65- by 538.67-keV coincidence (1097.1 + 538.7 = 1635.8 keV), (2.) a 1582.56-keV transition placed to the 53.2 keV level (1582.6 + 53.2 = 1635.8 keV), (3.) a 1635.81-keV transition placed to the $1/2^-$ ground state, (4.) a marginal 538.67- by 613.50-keV coincidence, and (5.) a marginal 1635.81- by 613.50-keV coincidence. The first two points place an $\ell=2$ $5/2^+$ level at 1635.8 keV; the third point places an $\ell=2$ $3/2^+$ level at 1635.8 keV; and the final two points place a transition from the 2249.48-keV level to both the $3/2^+$ and the $5/2^+$ levels at 1635.8 keV. The log*ft* limits for each of these two levels result from using only the transitions which can be unambiguously placed as deexciting one or the other level. The log*ft* value of 5.3 is the result for the two levels considered simultaneously and must be regarded as a lower limit for each level.

Of the remaining twelve excited states, eight are fed directly by the β^+/EC decay, having log*ft* values ranging from 6.0 to 7.4. These are the levels at 1243.41, 1386.3, 1656.2, 1669.5, 1690.7, 1884.9, 1885.9, and 2494.8 keV. All are limited to spin values of 3/2, 5/2 or 7/2, consistent with allowed or first forbidden β^+/EC decay. A J^π value of $5/2^-$ is suggested for the 1243.41 keV level as it deexcites to levels with J^π of $3/2^-$, $5/2^-$, and (possibly) $7/2^+$ and is fed from $3/2^+$ and $5/2^+$ levels. Values of $3/2^+$, $3/2^-$, and $5/2^+$ cannot be ruled out, but seem unlikely in view of the

lack of observed transitions to $1/2^-$ or $9/2^+$ states. The 1386.3 keV level is limited to $3/2^+$ or $5/2^+$ by its ℓ-value of 2 determined in the (^{3}He,d) reaction. A $7/2^-$ assignment is suggested for the 1656.2 keV level as its only transition is to a level of negative parity with $J \geq 3/2$. A J^π value of $5/2^+$ is suggested for the 1669.5 keV level on the basis of the relatively low log$\underline{ft}$ value (~6.2), transitions to $7/2^+$ and $3/2^-$ levels, and the lack of an observed transition to the $1/2^-$ ground state. The 1690.7 keV level is suggested to be even parity because of its relatively low log$\underline{ft}$ value (6.3). The strong transition to the $9/2^+$ 53.2 keV state limits it to being $5/2^+$ or $7/2^+$. The levels at 1884.9 and 1885.6 keV are assigned as $7/2^+$ (?) and $5/2^+$ or $7/2^+$, respectively, based on the (^{3}He,d) reaction study which observed an $\ell = 4$ transition with some possible $\ell = 2$ component at 1880 ± 6 keV (74An). The 2494.8 keV level is assigned even parity based on the logft value of 6.0 (indicating a probable allowed β^+/EC transition).

The four remaining states (1023.68, 1042.68, 1166.7, and 1416.1 keV), which may have no direct β^+/EC feeding, are all assigned odd parity and $3/2 \leq J \leq 7/2$, consistent with first forbidden β^+/EC decay and with the lack of any observed transitions to any lower-lying even parity states. The 1023.68 keV level is suggested to be $5/2^-$ or $7/2^-$ on the basis of a possible (dashed) transition to the $7/2^+$ 25.5 keV state. The 1166.27 keV state is suggested to be $3/2^-$ or $5/2^-$ as it was observed in the (^{3}He,d) reaction.

The nine additional states listed at the end of Table XII and having no definite energy placement are suggested to be positive parity states with $3/2 \leq J \leq 7/2$. With only a single transition apiece placed out of them, they each still have logft values ≤ 7.1, suggestive of being fed in allowed β^+/EC decay.

E. Discussion.

This investigation of the decay of $5/2^+$ 55.5-min ^{105}Cd has offered the opportunity to examine the character of a large number of excited states in ^{105}Ag. There are now 49 excited states firmly established in ^{105}Ag below 2.7 MeV and an additional ten states which are known to exist but cannot be definitely placed. On the basis of the γ-ray deexcitation patterns and the logft values observed in this study, and using the ℓ-transfer values of the ^{104}Pd(^{3}He,d)^{105}Ag reaction study (75An1), I have been able to assign unique spin and parity values to over half of these excited states. No detailed theoretical calculations of the levels of ^{105}Ag have ever been reported. The general features of the low-energy ($\leq$2 MeV) level structure of ^{105}Ag may be understood, however, by examining the level energy systematics of the nearby odd-mass nuclei and by comparing the ^{105}Ag level structure with the results of a recent calculation of ^{107,109}Ag levels by Parr (73Pa) who used a three-proton hole plus quadrupole vibrator model.

The levels of ^{105}Ag provide an extension of both the

isotonic, N=58, and the isotopic, Z=47, odd-A level systematics. In Figure 52, I show the level systematics below 1 MeV for the N=58 odd-mass nuclei from Z=41 to Z=47 (73Jo, 74Ko, 74Me3). Also shown is the position of the one-phonon excitation in each appropriate even-even core (Z-1, A-1) and in the Sn-core (^{108}Sn) in the case of ^{105}Ag (69Bl, 69Ya, 70Fi, 701a, 72Si2). The unfilled proton shell model orbitals for these odd-A nuclei are the $2p_{1/2}$ and $1g_{7/2}$ orbitals. Thus, the low-lying $1/2^-$ and $9/2^+$ states may be understood as being single (quasi-)proton states. The $1/2^-$ state falls to become the ground state in ^{103}Rh and ^{105}Ag as a consequence of the pairing energy being greater in the higher-J $1g_{9/2}$ orbital (63Ki). The low-lying $3/2^-_1$ and $5/2^-_1$ states may be explained as being the states expected from the coupling of the $2p_{1/2}$ single proton state with the one-phonon core excitation. The systematics of the $5/2^+_1$ and $7/2^+_1$ states are of special interest, however. The $5/2^+_1$ level drops dramatically to just 15.6 keV in ^{101}Tc. As the first $7/2^+$ state in ^{99}Nb is not known, the fall of the $7/2^+_1$ level is not shown, however, the first $7/2^+$ state in $^{107}_{49}In_{58}$ does not occur until at least 1 MeV (75Me). The behavior of these states cannot be explained in terms of a quasi-particle-plus-phonon model or an intermediate coupling model. The nearest $5/2^+$ and $7/2^+$ single proton orbitals are located in the next major shell, and no particle-phonon coupling calculation sufficiently brings down the $5/2^+$ state in Tc or the $7/2^+$ state in Tc, Rh, and Ag (63Ki).

Figure

52. The low-energy ($\lesssim$1 MeV) level systematics of the N = 58 odd-mass nuclei (this work and 73Jo, 74Ko, 74Me3). Also shown is the position of the one-phonon excitation in each appropriate even-even core (69Bl, 69Ya, 70Ei, 70Ta, 72Se2).

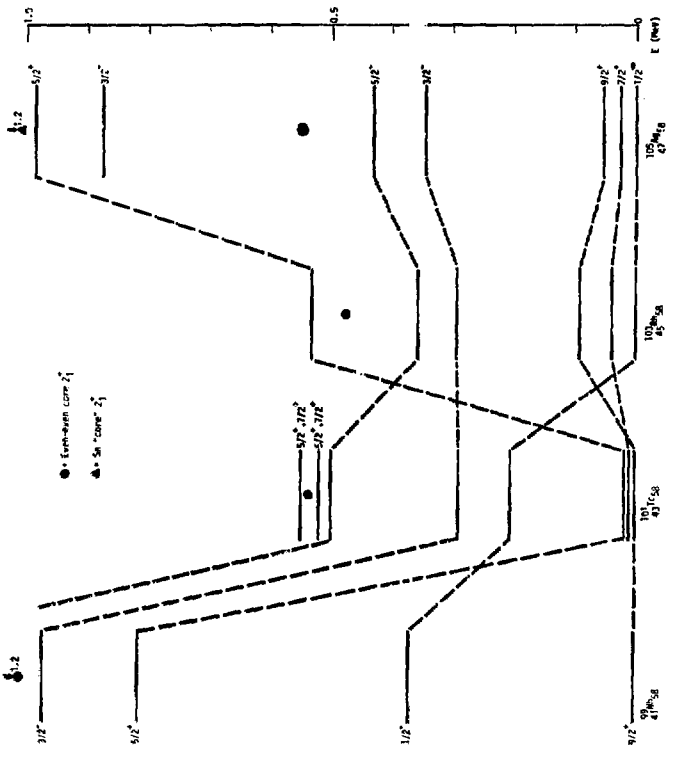
1.0
0.5
0
E (MeV)
● = Even-even core 2_1^+
▲ = Sn "core" 2_1^+
$5/2^+ \otimes 3/2^+$
$5/2^+ \otimes 3/2^+$
$3/2^+$
$5/2^+$
$1/2^+$
$9/2^+$
$^{99}_{43}Tc_{56}$
$^{101}_{43}Tc_{58}$
$^{103}_{45}Rh_{58}$
$^{105}_{47}Ag_{58}$

The $7/2^+$ state has been interpreted as being a three-proton-hole state. This was first suggested by Talmi and Unna (60Ta) who proposed the configuration $(1g_{9/2})^{-3}_{7/2}$ for the state. In ^{105}Ag, experimental evidence supporting this configuration is provided by the measured magnetic moment of the $7/2^+$, state of ±4.31 nuclear magnetons (69Fu). It has been noted (69Ho) that, based on the empirical magnetic moment of +5.53 nm for a $(\pi 1g_{9/2})^{-1}$ configuration determined from the odd-A indium nuclei, a pure $(1g_{9/2})^{-3}_{7/2}$ state is expected to have a magnetic moment of +4.30 nuclear magnetons. Recent theoretical calculations of the odd-mass silver nucle by Parr (73Pa) using a three-hole plus quadrupole vibration model and of odd-mass silver, rhodium, and technetium nuclei by Kuriyama et al. (72Ku, 74Kul) using a dressed-three-quasi-particle model have also interpreted the $7/2^+$, state as having the principal configuration, $(1g_{9/2})^{-3}_{7/2}$. In both calculations, the explicit treatment of the Pauli principle in the valence shell results in the $[(J^{-2})_2\ J^{-1}]$ multiplet being split, with the J-1 coupling being brought down and the other four couplings (J-2, J, J+1, and J+2) being raised. This effect is particularly strong in the case of the $1g_{9/2}$ orbital, as the configuration $(\pi 1g_{9/2})^{-2}_2$makes a large contribution to the one phonon excitation in this region. Thus, a low-lying $7/2^+$ state with the configuration $(1g_{9/2})^{-3}_{7/2}$ is predicted for Tc, Rh, and Ag nuclei. The low-lying $5/2^+$ state in Tc (and Rh) has not been treated in detail, although Kuriyama et al. (72Ku, 74Kul) have suggested that the five

quasi-particle $[(J^2)_2\ (J^2)_2\ J']$ configuration, which results in the lowering of the J-2 coupling, might be responsible. Kuriyama et al. have also demonstrated (74Kul) that the coupling between a $[(J^{-2})_2\ J^{-1}]$ configuration and the single quasi-particle J-2 state from the next shell ($2d_{5/2}$) results in the lowering of the J-2 state.

Detailed calculations of levels other than the $7/2^+$ anomolous coupling state have been reported (73Pa) only for an "average" ^{107,109}Ag nucleus. In Figure 53, I present the systematics of the odd parity levels observed in the odd-mass silver nuclei (69Be, 69Sc, 71Be, 73Au3, 74Pa, 75An2) along with the calculated odd parity levels (73Pa). Also shown are the first and second 2^+ state in each appropriate even-even (palladium) core nucleus (69Ro, 70Pi, 72Si2, 74Be2) and the first 2^+ state in each appropriate tin "core" (69Co, 69Ya, 70Br). The theoretical calculation appears to reproduce the level ordering and spacing very well up to at least 1 MeV. It may be noted however, that an intermediate coupling model calculation might well result in an equally good fit to the experimental data. In that model, a pair $2p_{1/2}$ plus one-phonon states with $J^\pi = 3/2^-$ and $5/2^-$ are expected near the first core phonon energy, and five $2p_{1/2}$ plus two-phonon states ranging from $J^\pi = 1/2^-$ to $J^\pi = 9/2^-$ are expected in the vicinity of the two-phonon energy. In point of fact, the three-hole plus quadrupole model determines configurations for these states which are largely $[(1g_{9/2})_0^{-2}\ 2p_{1/2}^{-1}]$ plus one phonon (or two phonons) in character.

Figure

53. The systematics of the odd parity levels observed in the odd-mass silver nuclei (this work and 69Be, 69Sc, 71Be, 73Au3, 74Pa, 75An2). Also shown are the calculated odd parity levels (73Pa) for an "average" ^{107,109}Ag nucleus and the positions of the phonon excitations in each appropriate palladium core (69Ro, 70Pi, 72Si2, 74Be2) and each appropriate tin "core" (69Co, 69Ya, 70Br).

▲ = Sn "core" 2_1^+
● = Even-even core 2_1^+
■ = Even-even core 2_2^+
2.0
1.5
1.0
0.5
0
E (MeV)
Shell Model Calculation

In Figure 54, I present the low-energy systematics of the even parity levels in the odd-mass silver nuclei (69Be, 69Sc, 71Be, 73Au3) along with the levels calculated for an "average" ^{107,109}Ag nucleus. As in Figure 53, the Pd and Sn core quadrupole vibration excitations are also indicated. The energy scale has been adjusted so that zero energy corresponds to the $7/2^+$ anomolous coupling state. It is clear from the lack of states near the Pd core one-phonon excitation energy that an intermediate coupling model calculation would fail to account for the observed level structures. The three-hole plus phonon model, however, appears to explain the two major features of the level structures. The first of these is the low-lying $7/2^+$ anomolous coupling state. The second is the large gap between the $9/2^+_1$ level and the next even parity level, generally a $5/2^+$ state. This latter characteristic is particularly evident in ^{105}Ag and ^{107}Ag and becomes less apparent as the phonon energy decreases, reflecting a "softer" nucleus. All of the possible states resulting from a three-hole plus quadrupole vibration calculation have not been calculated, therefore, it is not possible to make a more detailed comparison between the experimental data and the theoretical predictions in the case of the even parity excited states.

I have observed major electron capture branches (log$ft \leq 5.5$) from $5/2^+$ ^{105}Cd to 17 levels in ^{105}Ag between 2300 keV and 2600 keV. In the cases of three levels in particular,

Figure

54. The low-energy ($\lesssim$2 MeV) systematics of the even parity levels observed in the odd-mass silver nuclei (this work and 69Be, 69Sc, 71Ba, 73Au3). Also shown are the calculated even parity levels (73Pa) for an "average" ^{107,109}Ag nucleus and the positions of the phonon excitations in each appropriate palladium core (69Ro, 70Pi, 72Si2, 74Be2) and each appropriate tin "core" (69Co, 69Ya, 70Br).

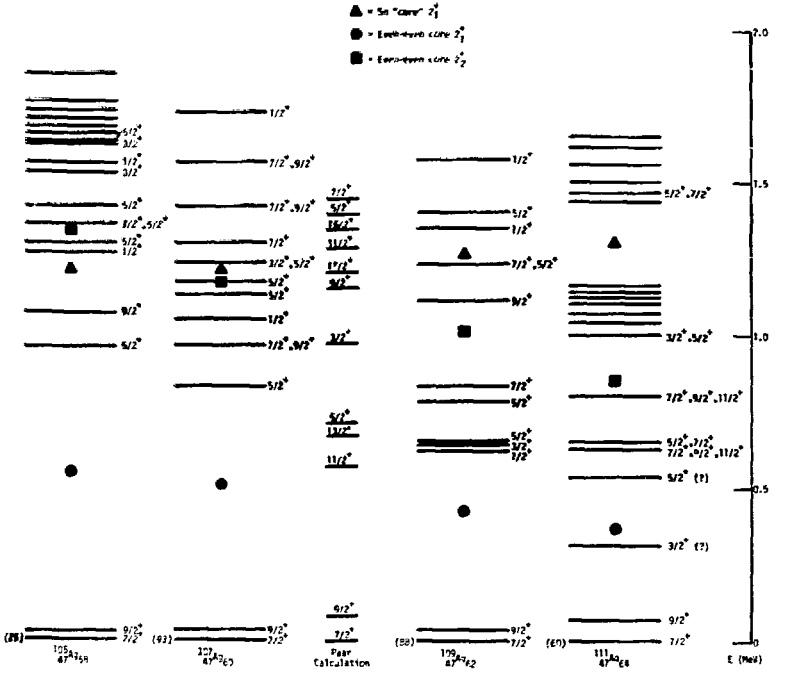
▲ = Sn "core" 2_1^+
● = Even-even core 2_1^+
■ = Even-even core 2_2^+
2.0
1.5
1.0
0.5
0
E (MeV)
$^{105}_{47}Ag_{58}$
$^{107}_{47}Ag_{60}$
Pear Calculation
$^{109}_{47}Ag_{62}$
$^{111}_{47}Ag_{64}$

2326.13, 2333.26, and 2550.47 keV, the decay branches are especially strong, having log*ft* values of 4.2, 4.5, and 4.9, respectively. The shell model valence states for ^{105}Cd and ^{105}Ag are $1f_{7/2}$, $2p_{3/2}$, and $1g_{9/2}$ for protons and $1g_{7/2}$, $2d_{5/2}$, $2d_{3/2}$, $3s_{1/2}$, and $1h_{11/2}$ for neutrons. The only single nucleon EC-transition which is not ℓ-forbidden is $\pi 1g_{9/2}$ to $\nu 1g_{7/2}$. In ^{111}Sn decay this transition has been observed to have a log*ft* of 4.8 (71Ra), and the β^- transition in ^{117}In decay, $\nu 1g_{7/2}$ to $\pi 1g_{9/2}$, has been observed to have a log*ft* of 4.4 (70Ba). The electron capture decay data for ^{105}Cd, therefore, suggest that the strongly fed states (log*ft* $\leq$ 5.5) above the neutron pairing energy (~2.1 MeV) are principally one-proton-two-neutron states. The EC-decay mechanism would then involve the transition from $5/2^+$ ^{105}Cd, assumed to be in the $[\pi(1g_{9/2})^2_0\ \nu,\ (2d_{5/2})]_{5/2}$ configuration, to one of the many $3/2^+$, $5/2^+$, or $7/2^+$ states in ^{105}Ag resulting from the configuration:

$$[\pi\ 1g^{-1}_{9/2}\ \ (\nu_1\ 2d_{5/2},\ \nu_2\ 1g_{7/2})]_{1,2,3,4,5,6}\,3/2,\ 5/2,\ 7/2.$$

In the ^{104}Pd core, a large number of even parity states with $1 < J < 6$ have been observed in the vicinity of 1.8 to 2.7 MeV, and several of these have been suggested as condidates for being two quasi-particle states (69Di, 71Do, 71Mu, 72Si2). It seems likely that several of these are two neutron states, and that the $\pi\nu^2$ states in ^{105}Ag may be explained by a coupling between the $1g_{9/2}$ hole state in ^{105}Ag and the two-neutron states in the ^{104}Pd core.

The strong β^+/EC-decay branch from $5/2^+$ ^{105}Cd to the

$7/2^+$ anomolous coupling state, with log*ft* = 5.4, is somewhat difficult to understand in view of the predicted $(1g_{9/2})^{-3}_{7/2}$ configuration for the $7/2^+$ state. The single nucleon β^+/EC transition, $\pi 1g_{9/2}$ to $\nu 2d_{5/2}$, is second forbidden, leading one to expect a much higher log*ft* value ($\geq$10). In light of the preceding discussion of β^+/EC-decay mechanisms it seems likely that this transition must involve a $\pi 1g_{9/2}$ to $\nu 1g_{7/2}$ transition. Thus, the ground state of ^{105}Cd must have some amount of the seniority three configuration

$$[(\pi 1g_{9/2})^2_0 \ (\pi 1g_{9/2})^{-2}_2 \ \nu 1g_{7/2}]_{5/2}$$

mixed into it. The $\pi 1g_{9/2}$ to $\nu 1g_{7/2}$ β^+/EC transition would then result in leaving ^{105}Ag in the

$$[(\pi 1g_{9/2})^{-2}_2 \ (\pi 1g_{9/2})^{-1} \ (\nu 1g_{7/2})^2_0]_{7/2}$$

configuration, the proton part of which is just the $(1g_{9/2})^{-3}_{7/2}$ configuration suggested for the $7/2^+$ anomolous coupling state. If the "bare" $\pi 1g_{9/2}$ to $\nu 1g_{7/2}$ transition is assumed to have a log*ft* value of 3.8-4.0, then the observed log*ft* value of 5.4 could be accounted for by a mixing of only 2.5-4.0% seniority three configuration into the ^{105}Cd ground state configuration. This is not unreasonable in view of the expected occupancy of the $\nu 1g_{7/2}$ orbital in N = 57 nuclei (^{105}Cd) and in view of the predicted prevalence of the $(\pi 1g_{9/2})^{-2}_2$ two-proton hole configuration in the silver nuclei.

In conclusion, it is clear that a three-hole model of

some type is necessary in order to explain the $7/2^+$ anomolous coupling state observed in the odd-mass silver nuclei. The three-hole plus quadrupole vibrator model of Parr successfully explains many of the characteristics of the low-energy level structures in the odd-mass silver nuclei, however further theoretical calculations are needed in order to make more detailed comparison between theory and experiment. More detailed level calculations using the dressed three quasi-particle model of Kuriyama et al. are also needed. ving a large number of well chara zed excited states, e level structure of ^{105}Ag can now provide a good test of this theoretical work. It should be noted, however, that any theoretical model must include $\pi\nu^2$ configurations among its basis states in order to explain all of the observed even parity levels in ^{105}Ag.

NOTE ADDED IN PROOF

Just before the final printing of this manuscript, a preprint reporting the results of a study of the ^{107}Ag (p,t) ^{105}Ag reaction (R. M. Del Vecchio, I. C. Oelrich and R. A. Naumann, J. Henry Laboratory and Frick Chemical Laboratory, Princeton University, Princeton, New Jersey 08540 and to appear in Phys. Rev. C12 (1975)) was brought to my attention. This study along with reexamination of the results of my work provides the following definite J^π assignments (E(J^π)): 877.81 ($3/2^-$), 1023.68 ($7/2^-$), 1042.68 ($5/2^-$), 1166.27 ($9/2^-$), (2276 ($5/2^+$)), and 2314.6 ($7/2^+$) keV. These assignments have been indicated in Figs. 46 to 54 although the text still indicates the assignments originally made without any knowledge of the (p,t) reaction study.

APPENDIX I

COMPUTER PROGRAMS

In order to facilitate the handling of both one- and two-parameter nuclear decay scheme data, several computer programs were written for operation on the University of Maryland UNIVAC 1108 computer system. All of the programs are written in either UNIVAC Assembly Language or in RALPH (which is FORTRAN as compiled by the U. of Md. FORTRAN/MAD Compiler). All of the programs operate under the current U. of Md. UNIVAC 1108 system with Exec 8 and conform to the current specifications as described in the U. of Md. Computer Notes (70UM, 71Ci, 71Re, 73UM) and the UNIVAC Systems Reference Manuals (70UN, 73UN1, 73UN2, 74UN).

Most of the programs deal with either the reading of data from magnetic tape, or the output of spectral data in special formats, or the processing of two-parameter coincidence data. Generally, these programs are specific to the UNIVAC 1108 system with RALPH compiler and to the specific primary data acquisition systems (Northern Scientific coincidence system (71Ap1) and Packard multi-channel analyzer). Thus the computer codes will not be given here, however descriptions of the basic subroutines and main programs, along with their uses, follows.

A. Subroutines.

1. TAPRD

This is a RALPH subroutine which reads tapes, writes

tapes, and writes end-of-file (EOF) marks on tape. It employs the Executive Request, IOW$ (73UN1), to do all of this. All tape handling errors (parity, power-drop, etc.) are handled by the computer operator. The routine is called as follows:

```
To read:        CALL TAPRD(NAME,BUF,SIZ,NWD,NCH,RET)
To write:       CALL TAPWT(NAME,BUF,SIZ)
To write EOF:   CALL TAPEF(NAME)

   NAME = Filename (max. of 6 characters).
   BUF  = Array to be read or written.
   SIZ  = Number of words to read or write.
   NWD  = Actual number of complete words read.
   NCH  = Number of excess characters read.
   RET  = Statement number for return if EOF read.
```

2. YREAD

YREAD is an assembly language subroutine developed at the University of Maryland (73Si). I modified it so that its sole function is to read magnetic tape regardless of density, parity, or tape condition. To do this it employs the UNIVAC arbitrary device handler (73UN1). The calling program is informed of any tape reading errors and has full discretion on how to handle them. The routine is called as follows:

```
CALL XREAD(UNIT,ARRAY,NWD,STATUS,PARITY,DENS,REC)

   UNIT   =  FORTRAN logical unit number of tape.
```

ARRAY = Array to be read (integer).

MWD = Maximum size of ARRAY.

STATUS = Returned status of read.

PARITY = Parity to assume during the read.

DENS = Density to assume during the read.

REC = Logical variable for attempting recovery or not.

3. READER (primary)

This is a RALPH subroutine designed to read magnetic tapes regardless of parity errors. It employs the Executive Request, IOWI$ (73UN1), to do this. At the end of each read a status word is returned by the tape drive. This word is then examined bit by bit in order to determine if any errors occurred (73UN2). Before calling this routine from a main program for the first time, an alternate entry point must be called to set up the handling of any error recovery. Before swapping tapes on a multi-tape job, this error recovery must be cleared and then re-established after the swap. For most tape reading errors (particularly parity errors), the data is returned to the calling program as read along with a CODE variable specifying the nature of the error. The calling program then has full discretion on how to handle the data. The routine is called as follows:

To set up: CALL SETUPR(FILE,DATA,MAX,DECK)

To clear: CALL CLEAR(FILE,DATA,MAX,DECK)

To read: CALL READER(NW,NC,CODE,RET1,RET2)

FILE = 2-word array for filename (max. 12 char.).

DATA = Integer array to be read.

MAX = Max. record size (one more than expected).

DECK = Logical variable to determine 7-track or 9-track tape.

NW = Actual number of complete words read.

NC = Number of excess characters read.

CODE = Code to inform about special errors.

RET1 = Statement number for return if EOF read.

RET2 = " " " " in case of parity error.

4. READER (modified)

This RALPH subroutine is identical with the primary version of READER except that it initiates messages to the computer operator's console in the event of a tape drive power-drop. It tells the operator to just restart the drive without worrying about the tape position. It then returns to the calling program through the parity error return. This version must be used only with a main program which 1.) is able to find the start of the next block of data without making an error handling a partial record, 2.) can afford to lose a complete data record, and 3.) is not engaged in a search for a particular tagged data record. All calling sequences for this version are the same as for the primary version of READER.

5. STORA1

In the operation of both versions of READER, the tape-drive status word is returned to accumulator A1 in the computer. This accumulator cannot be directly accessed in RAI'H (73UN1, 71Re). Thus the purpose of this assembly language subroutine is to fetch the contents of accumulator A1 and return it to READER. It is called as follows:

CALL STORA1(STAT)

STAT = Status word from tape drive.

[NOTE: This routine must be included when using either version of READER.]

6. MOVE

This is an assembly language subroutine for the manipulation of magnetic tapes. It will move tapes forward either by an integral number of records (stopping if an EOF mark is encountered) or by an integral number of files. Any errors or bad spots on the tape have no effect on the move. The routine is called as follows:

Files: CALL XSKIPF(FILE,N,DECK)

Records: CALL XSKIPR(FILE,N,DECK)

FILE = 2-word array for the filename (maximum of 12 characters).

N = Number of files or records to skip.

DECK = Logical variable indicating a 7-track or 9-track tape.

[NOTE: This subroutine must be used for skipping files/ records when also making use of YREAD or either of the two versions of READER.]

7. WRITER

This is a RALPH subroutine which uses the Executive Request, IOW$ (73UN1), to write on tape, write EOF marks on tape, or to rewind tape. It is called as follows:

To write: CALL TAPWT(FILE,BUF,MAX)

To write EOF: CALL TAPEF(FILE)

To rewind: CALL REW(FILE)

FILE = 2-word array for the filename (maximum of 12 characters).

BUF = Array to be written.

MAX = Number of words to write.

8. WCRNCH

This is a RALPH subroutine which outputs an integer array (eg. spectrum) in a compressed format on punched cards. The maximum allowed value is 999,999,999; and all values must be greater than or equal to zero. An average 4096-channel spectrum will need approximately 200-250 cards. The last three columns of each card contain a sequencing number. The

routine is called as follows:

```
CALL WCRNCH(NSPEC,N,TAG)
```

NSPEC = Spectrum array.

N = Number of channels in spectrum.

TAG = 8-digit octal tagword of spectrum.

9. RCRNCH

This is a RALPH subroutine which reads data output by WCRNCH. It will check to be sure the cards are in order and will return information on where the disorder occurred. If the spectrum is not complete, RCRNCH will return the channel number of the first missing channel. The routine is called as follows:

```
CALL RCRNCH(NSPEC,N,TAG,NFLAG)
```

NSPEC = Spectrum array.

N = Number of channels expected.

TAG = 8-digit octal tagword.

NFLAG = 0, for successful read.

.GT. 0, for incomplete spectrum.

.LT. 0, for disordered data deck.

10. LPLOT

This is a RALPH subroutine which uses the line printer to plot a spectrum array linearly along the length of the

computer paper. The full scale value of the plot is maximized at regular intervals as specified by the calling program. The plot will consist of 66 or 88 channels per page depending on which of the following control cards is inserted at the beginning of the run deck (respectively):

```
@HDG,N .M,66,0,0
```

or

```
@HDG,N .M,88,0,0 .S,'PLEASE RESET PRINTER TO 8 LINES
                     PER INCH'
```

The output should be sent to one of the low-speed printers using the control card

```
@SYM PRINT$,,PR
```

The first ten channels and the last four channels of the spectrum are not plotted. The routine is called as follows:

```
CALL LPLOT(NSPEC,N,NGROUP,LABEL)
```

NSPEC	=	Spectrum array.
N	=	Number of channels in spectrum.
NGROUP	=	Size of groups in which the full scale is to be maximized.
LABEL	=	8-digit octal tagword.

11. HPLOTL

This is a RALPH subroutine which uses the line printer to plot an integer spectrum array either linearly or

logarithmically horizontally on the computer paper. The plot is done at 120 channels per page with the first 20 channels of each page overlapping the last 20 channels of the previous page. The full scale value is optimized on each page. The routine requires the insertion of the following two control cards at the start of the computer run stream:

```
@SYM PRINT$,,PR
@HDG,N .M,88,0,0 .S,'PLEASE RESET PRINTER TO 8 LINES
                    PER INCH'
```

The first ten channels and the last four channels of the spectrum are not plotted. The routine is called as follows:

```
CALL HPLOTL(NSPEC,N,LABEL,LG)
```

NSPEC = Spectrum array.

N = Number of channels in spectrum.

LABEL = 8-digit octal tagword.

LG = Logical variable to specify log or linear plot.

12. ADDER

This is an assembly language subroutine which increments or decrements a particular channel of a 4096-word spectrum. It is used in particular when the input channel number is from an 8192-channel spectrum and references a channel in a 4096-word spectrum stored as half-words in a 2048-word array. Instead of performing several divide operations (integer divide

by 2, at 10.125 μsec per divide) it uses one bit logical shifts (at 0.75 μsec per operation). It also maintains the proper sign convention in half-word arithmetic by performing half-word operations with sign fill (7JCi). The routine is called as follows:

CALL ADDER

All variables are passed back and forth through a labeled common block. (The 8192-channel original spectrum is converted to a 4096-channel spectrum stored as half-words in a 2048-word array in order to conserve storage in the computer memory.)

B. Main Programs for Coincidence Analysis.

There are four main programs employed in the reduction and analysis of two-parameter coincidence data. All are written in RALPH and involve several of the subroutines just described. They are designed to be used sequentially, each program performing a specific phase of the data analysis. Thus any errors or problems which develop (computer malfunction, bad tape, run-time limitations, etc.) will result in a minimal waste of computer time. In the event of minor errors, specifically tape reading errors, these programs are designed to discard data rather than risk processing incorrect data, the philosophy being that the loss of several hundred coincidence events is of little consequence when dealing with several million events.

1. ANYOUT

This program is the first step in the reduction of coincidence data. It employs the following subroutines: READER (modified), STORA1, MOVE, and HPLOTL. Its principle purpose is to read the raw coincidence data tapes (written by the Northern Scientific coincidence system), find all valid coincidence pairs, and output these pairs in a compressed format in standard UNIVAC 1108 36-bit binary to a master magnetic tape.

The original raw data tapes are written as odd parity, 7-track, medium density (556 BPI) binary. The coincidence pairs are written as pairs of 24-bit binary words, with one parameter (X) written as a channel number (0 to 8191) and the other parameter (Y) tagged by being written as a channel number plus 8192 (8192 to 16,383). A file on this tape consists of a 24-bit tagword, a record gap, 256 pairs of 24-bit words, a record gap, and finally a file gap. In the 256 pairs, a valid pair is indicated by an "X" event followed by a "Y" event (eg. YXXYXYYXY contains the three valid pairs which are underlined).

This tape format is inconvenient for total processing of the data for a number of reasons, most of which involve computer time considerations. In future analysis all of the valid data must be scanned and gates set on one or both of the parameters. However in the raw data format the data are in code, contain invalid events, and are on tape at a relatively low density. This last is of importance due to the time

needed merely to run through a tape. Each record gap involves 3/4" of blank tape, and each file gap involves 3 $^{3}/_{4}$ " of blank tape. Thus a 2400' raw data tape will contain only about 700,000-800,000 valid coincidence pairs.

ANYOUT reads the raw data tapes (modified READER) ignoring any files in which any type of tape reading error occurs. It finds all valid pairs, decodes the Y-event, and stores each pair as one 36-bit word. It then outputs the data in 500-word records as 9-track, odd parity, high density (800 BPI) magnetic tape. In typical operation, 4 to 4.5 raw data tapes are condensed to one master tape (limited to 3.1 million words). Along with the tape output, both any-coincidence spectra are are stored in memory and are printed in both 8192-channel and 4096-channel format. These spectra may also be plotted (using HPLOTL) at the user's option. In case of computer malfunction, this program has the option of being rerun starting with the raw data tape which was being processed at the time of malfunction.

The following specifications are necessary when running this program:

a.) Computer time estimate --- 6-7 minutes per input raw data tape, plus 8 minutes if the plots are requested.

b.) Page estimate --- 150 pages without plots; 900 pages with the plots.

c.) Input tape file control cards ---

```
@ASG,TMO COINC,8C,NC__N,NC__N.....
@USE 12,COINC
```

(NC__ are tape numbers. It is usually optimal to process only 4 raw data tapes per run.)

d.) Output tape file control cards ---

```
@ASG,T OUTANY,8C9,NC__R,NC__R.....
@USE 13,OUTANY
```

(There must be at least 1 tape per 4 input tapes.)

e.) Data cards ---

CARD 1 --- I2,I2,I5,I2,I2

NTAPES	=	Number of input tapes.
ENDFL	=	Normally left blank.
	=	1, if one or more tapes end early.
STOUT	=	Number of good 500 word blocks on first output tape. Leave blank unless rerunning the job.
PLTFLG	=	Blank if plots are desired.
	=	1, to suppress plots (Do this on reruns to save time.)
EFFLAG	=	Blank, then input tapes end with >3 EOF marks.
	=	1, then input tapes end with only 2 EOF marks.

CARD 2 --- 16I5 (optional)

This card is used only when ENDFL = 1. Then each value indicates when that input tape (in sequence) is to end (by file #).

2. ALLCON

ALLCON is an optional program which is used primarily when a rerun was necessary for ANYOUT or when ANYOUT was run

several times, processing the raw data tapes four at a time. In these cases, ANYOUT will not yield the complete any-coincidence spectra for the two parameters, but only that portion which was processed in each run or rerun. ALLCON scans the master tapes output by ANYOUT and produces the any-coincidence spectra. These are printed and plotted both as 8192-channel and 4096-channel spectra.

The run specifications are as follows:

a.) Computer time estimate --- 6-7 minutes per input master tape, plus 8 minutes for plots.

b.) Page estimate --- 900 pages.

c.) Input tape file control cards ---

```
@ASG,T VALIDPAIRS,8C9,NC__N,NC__N.....
@USE 12,VALIDPAIRS
```

d.) Data cards ---

CARD 1 --- I2,1X,I4

NTAPES = Number of input tapes.
LSTBLK = Number of 500 word records on last tape.

3. GATES

This is the principle program used in the analysis of coincidence data. It scans the master tapes produced by ANYOUT setting one to ten gates (restrictions) on one of the parameters. For each gate, a 4096-channel spectrum of coincident events is produced. This spectrum is printed,

plotted (HPLOTL), and written on magnetic tape. The limit of ten gates per run is the result of computer storage and run time limitations, as is the fact that the output spectra are compressed to 4096 channels even though the gates are applied to the original 8192-channel spectrum. These 4096-channel spectra are stored internally in half-word format in a 2048 word array and are accessed by the routine, ADDER.

In each run, the gates must be set on only one of the two parameters (X or Y). Each gate is specified by six numbers which must be monotonically increasing:

$$G_1 < G_2 < G_3 < G_4 < G_5 < G_6 .$$

G_1 and G_2 specify the low-energy background gate; G_3 and G_4 specify the peak gate; G_5 and G_6 specify the high-energy background gate. All gate limits are included in the specific gate. Two separate gates may overlap on background gates, but no part of any other gate may overlap any peak gate. An error in setting up a gate will result in that gate being ignored. If the total number of background channels in a gate is more than two different from the number of peak channels, a warning that the gate may be in error will be printed.

This program takes a large amount of computer time and results in a large number of output pages for each run, thus extreme care should be exercised in its use. In the event of a computer malfunction, the program may be rerun starting with the tape which was being processed at the time

of the malfunction by inputting a value for the number of completed input tapes.

The run specifications are as follows:

a.) Computer time estimate --- approximately 15 minutes per input tape for 10 gates, plus 15 minutes for plots.

b.) Page estimate --- 1500 pages.

c.) Input tape file control cards ---

```
@ASG,T VALIDPAIRS,8C9,NC__N,N__N.....
@USE 12,VALIDPAIRS
```

d.) Output tape file control cards ---

```
@ASG,T SPECTRATOTAL,8C9,NC__R
@USE 13,SPECTRATOTAL
```

e.) Data cards ---

CARD 1 --- I2,A1,I2

NTAPES = Number of input tapes.

SIDE = X , if gates to be set on X-side.
= Y , if gates to be set on Y-side.

TDONE = Normally left blank except in the event of a rerun when it equals the number of already completed tapes.

CARDS 2 - 11 (MAX.) --- 6I4

One card for each gate giving the six channel numbers specifying the gate. (Maximum of 10 gates.)

4. NETSPC

This program reads the spectrum tape output by GATES. The spectra are printed and at the user's option may be plotted (HPLOTL) and/or output on punched cards (WCRNCH). The program also has the option of reading spectral data from punched cards (RCRNCH), however in this mode there will be no punched card output. This program is designed so that with minor modifications it can be interfaced with the peak finding and integrating routines currently in use (72Go, 73Vi).

The input specifications are as follows:

a.) Computer time estimate --- 2 minutes, plus 25 sec. per plot, 20 sec. per punched spectrum, and 20 sec. per input spectrum from cards.

b.) Page estimate --- 50 pages, plus 100 pages per plot.

c.) Output card estimate --- 250 cards per spectrum.

d.) Input tape file control cards --- Same as output tape for gates.

e.) Data cards ---

CARD 1 --- 3I2

SOURCE = Blank if reading tape.
= 1 , if reading cards.
PLTFLG = Blank if no plots desired.
= 1 , if plots are desired.
PNCHFL = Blank for no punched output.
= 1 , if punched output is desired.

CARD 2 and Following as Needed

Tape --- Data cards from run of GATES.
Cards --- Up to 20 spectrum decks as produced by this program.

C. Miscellaneous Main Programs.

1. BCDRD

This program uses TAPRD to read spectrum tapes produced by the Packard Analyzer system. It translates the Packard BCD type format to UNIVAC 1108 binary format and then prints the spectra. The user may specify a number of spectra to skip and then a number to read.

The input specifications are as follows:

a.) Computer time estimate --- about 4 sec. per spectrum.

b.) Page estimate --- 12 pages per spectrum.

c.) Input tape file control cards ---

```
@ASG,TMO SPECT,8C,NC__N
@USE 12,SPECT
```

d.) Data cards ---

CARD 1 --- I4,I4

SKIP = Number of EOF marks to skip.
READ = Number of spectra to read.

(Note --- More than one data card may be used so that one proceeds down a tape alternately skipping and reading spectra.)

2. NORRD

This program uses TAPRD to read spectrum tapes produced by the Northern Scientific Analyzer system. It translates the Northern Scientific 24-bit binary word format to UNIVAC 1108 36-bit binary format. The spectra along with any timing

data are printed. The user has the options of skipping spectra, printing a specified number of spectra, and searching the tape for a spectrum of a given tagword.

The input specifications are as follows:

a.) Computer time estimate --- about 4 sec. per spectrum read, plus 6-8 seconds per tagword search.

b.) Page estimate --- 12 pages per spectrum.

c.) Input tape file control cards ---

```
@ASG,TMO SPECT,8C,NC__N
@USE 12,SPECT
```

d.) Data cards ---

CARD 1 --- I4,I4,O8,I4,I4

SKIP	=	Number of EOF marks to skip.
READ	=	Number of spectra to read.
ITAG	=	Blank, if there is no tagword search.
	=	8 digit octal tagword to be searched for through the number of spectra specified by READ.
MODE	=	Blank, then print only the spectrum with the given ITAG.
	>	0, then print this many spectra starting with the tagged spectrum.
IPASS	=	Blank, then each spectrum of given ITAG will be printed (but only if MODE=0).
	>	0, then search will continue until this many spectra of a given tagword are found.

More than one data card may be used. The tape will be rewound each time if ITAG ≠ blank and IPASS > 0 and IMODE = blank. Otherwise, the program will continue down the tape, applying each data card in turn.

3. CALIB4

This program uses several UNIVAC Math-Pack Library subroutines (70UM) to fit a set of orthogonal polynomials to channel-energy data in order to obtain a spectrum energy calibration. The method of orthogonal polynomials has been found to be faster and more accurate than the standard matrix inversion (using Gauss-Jordan reduction) technique for performing least-squares polynomial fits (69Wa).

The input channel-energy data is fit by polynomials of first through twelfth order when possible. If the number of input data points, N1, is less than 16 then the maximum order fit is N1-3. The best fit is found subject to the conditions that it be monotonically increasing over the total spectrum and that it be a significantly better fit than the first-order (linear) fit. The formula for this best fit polynomial as a power series is output along with the formula for the linear fit.

The rest of the output consists of the calculated energies for the input centroids, the mean standard deviation of these values, the calculated energies for centroids from unknown peaks, and a table of energies corresponding to each channel number in the spectrum. All of this is output for the best fit as well as for the linear fit (provided that the linear fit is not the best fit). The linear fit is of interest when extrapolating far away from the portion of the spectrum covered by the input centroid-energy pairs. The range over which the best fit is interpolated is also output.

The input specifications are as follows:

a.) Computer time estimate --- 30-40 seconds.

b.) Page estimate --- 50 pages.

c.) Control cards needed before the data deck ---

```
@MAP,I
LIB UOM*MSLIB.
@XQT,FS
```

d.) Data cards ---

CARD 1 --- I5,I5,I5

- N1 = Number of input centroid-energy pairs.
- NCH = Number of channels in spectrum (fit must be monotonically increasing over this range).
- N2 = (optional) Number of centroids of unknown peaks input.

CARD 2 to X (as needed) --- 8F10.3

These cards contain input data pairs as centroid, energy, centroid, energy, etc

CARD X+1 to Y (as needed) --- 8F10.3 (optional)

These cards contain the centroid values for the unknown peaks.

(Note --- More than one complete data deck (as above) may be processed per run. In this case, time and page estimates must be increased.)

APPENDIX II

CALCULATION OF THE I.T. BRANCH AND THE GROUND STATE β-BRANCH IN $^{131}Te^{m}$ DECAY

The determination of the 182.2-keV M4 I.T. branch for $^{131}Te^{m}$ is complicated by the fact that the 182.25-keV transition was discovered to be an unresolved doublet with one component being the I.T. and the other being a transition in ^{131}I (2114 to 1931 keV). Thus the total decay intensities for both $^{131}Te^{m}$ and $^{131}Te^{g}$ in transient equilibrium must be determined. To arrive at a value for the first of these, it is necessary to know the intensity of the $^{131}Te^{m}$ β-decay branch directly to the ground state of ^{131}I. As this ground state β-branch is determined by observing the growth and decay of ^{131}I activity in a $^{131}Te^{m+g}$ sample initially chemically purified to remove iodine, a value for the $^{131}Te^{m}$ I.T. branch is needed to calculate the ground state β-branch. Thus these two calculations are linked, and an iterative technique must be used to arrive at the two branching values.

A. The I.T. Branch.

The total $^{131}Te^{g}$ β-decay activity of a transient equilibrium $^{131}Te^{m+g}$ source is determined from: 1.) the intensity of a pure $^{131}Te^{g}$ γ-ray in the equilibrium source, I_e (Table I), 2.) the intensity of this same γ-ray in a pure $^{131}Te^{g}$ source, I_g (Table II), and 3.) the total β-decay intensity of the pure $^{131}Te^{g}$ source, T_g, in relative γ-ray

units. This last quantity is obtained by summing the intensities of all γ transitions to the ground state of ^{131}I observed in the decay of the pure $^{131}Te^{g}$ source (Table II). These intensities must be corrected for internal conversion, and the total sum must be corrected for direct β-decay to the ground state of ^{131}I (which in this case is zero (63De)). The total $^{131}Te^{g}$ activity, T_e, in equilibrium with $^{131}Te^{m}$ is then given as

$$T_e = I_e T_g / I_g \ . \qquad \text{(II-A1)}$$

The most intense pure $^{131}Te^{g}$ γ-ray with the least uncertainty in intensity is the 997.16-keV transition. For this transition the right-hand quantities in eq. II-A1 are (in relative units):

$$\begin{aligned} I_e &= 19.5 \pm 0.9 \\ I_g &= 48.5 \pm 0.2 \\ T_g &= 1467.8 \pm 1.6 \end{aligned} \qquad \text{(II-A2)}$$

resulting in a value for T_e of

$$T_e = 590. \pm 27 \ . \qquad \text{(II-A3)}$$

To determine the total $^{131}Te^{m}$ β-decay activity, it is first assumed that there is no direct β-decay to the three low spin levels at 149.71, 492.65, and 602.05 keV. Then the intensities of all transitions from the levels above 602.05 keV to these three levels and ground are summed (Table I)to get a total γ intensity, S_m. The total β-decay intensity of $^{131}Te^{m}$,

T_m, is related to S_m and to the fraction of $^{131}Te^m$ β-decay directly to the ground state of ^{131}I, X, as

$$T_m = S_m / (1-X) \quad . \qquad \text{(II-A4)}$$

The value of S_m is

$$S_m = 1893 \pm 45 \quad . \qquad \text{(II-A5)}$$

Assuming that $^{131}Te^g$ is in transient equilibrium with $^{131}Te^m$ results in an expression for the total $^{131}Te^m$ activity (β-decay plus I.T.) of

$$T = T_m + T_e(1- t_{1/2,g}/t_{1/2,m}) \quad , \qquad \text{(II-A6)}$$

where the half-lives ($t_{1/2}$) are

$$\begin{aligned} t_{1/2,g} &= 25 \text{ minutes} \\ t_{1/2,m} &= 30 \text{ hours} \quad . \end{aligned} \qquad \text{(II-A7)}$$

The I.T. activity is then given by the expression

$$T_{IT} = T\, B_{IT} \qquad \text{(II-A8)}$$

in which B_{IT} is the I.T. branch value (ie. the fraction of total $^{131}Te^m$ decay resulting in $^{131}Te^g$). The assumption of transient equilibrium results in the expression

$$T_{IT} / T_e = 1 - t_{1/2,g} / t_{1/2,m} \quad . \qquad \text{(II-A9)}$$

Using eqs. II-A3 through II-A8 to substitute into eq. II-A9 and solving for B_{IT} results in the expression:

$$B_{IT} = 582 / [1893/(1-X) + 582] , \quad \text{(II-A10)}$$

in which "X" is as in eq. II-A4.

B. The Ground State β-Branch.

The growth and decay of ^{131}I activity was observed in a transient equilibrium $^{131}Te^{m+g}$ source initially chemically purified to remove iodine. The decay chain which was observed is:

$$\begin{array}{ccccc} ^{131}Te^{m} & \xrightarrow{\lambda_\beta} & & & \\ \Big\downarrow{\scriptstyle \lambda_\gamma} & & & & \\ ^{131}Te^{g} & \xrightarrow{\lambda_g} & & & \end{array} \qquad ^{131}I \xrightarrow{\lambda_I} {}^{131}Xe \qquad \text{(II-A11)}$$

in which the following variables are defined:

$$\begin{aligned} M &= \text{the amount of } ^{131}Te^{m} \\ G &= \text{the amount of } ^{131}Te^{g} \\ I &= \text{the amount of } ^{131}I \\ \lambda_\beta &= \text{the decay constant for } ^{131}Te^{m} \ \beta\text{-decay} \\ \lambda_\gamma &= \text{the decay constant for } ^{131}Te^{m} \text{ I.T. decay} \\ \lambda_g &= \text{the decay constant for } ^{131}Te^{g} \\ \lambda_I &= \text{the decay constant for } ^{131}I. \end{aligned} \qquad \text{(II-A12)}$$

The change in I with respect to time is given as

$$\frac{dI}{dt} = \lambda_\beta M + \lambda_g G - \lambda_I I . \qquad \text{(II-A13)}$$

The amount of $^{131}Te^{m}$ present at any time, t, is

$$M(t) = M_o e^{-\lambda_\gamma t} e^{-\lambda_\beta t} = M_o e^{-\lambda_T t} \qquad \text{(II-A14)}$$

where λ_T is the total decay constant for $^{131}Te^{m}$ and the subscript, "o", indicates the amount present at some initial zero time.

The change in G with respect to time is given by the expression

$$\frac{dG}{dt} = \lambda_\gamma M - \lambda_g G . \qquad \text{(II-A15)}$$

Solution of this differential equation for G as a function of time yields the familiar equation for the growth and decay of a daughter activity,

$$G(t) = \frac{\lambda_\gamma}{\lambda_g - \lambda_\gamma} M_o (e^{-\lambda_\gamma t} - e^{-\lambda_g t}) + G_o e^{-\lambda_G t} . \qquad \text{(II-A16)}$$

Using eqs. II-A14 and II-A16 to substitute into eq. II-A13 results in the differential equation:

$$\frac{dI}{dt} = \lambda_\beta M_o e^{-\lambda_T t} + \lambda_g G_o e^{-\lambda_g t} - \lambda_I I + \frac{\lambda_\gamma \lambda_g M_o}{\lambda_g - \lambda_\gamma} (e^{-\lambda_\gamma t} - e^{-\lambda_g t}) \qquad \text{(II-A17)}$$

This is solved by assuming a solution of the form

$$I = u e^{-\lambda_I t} , \qquad \text{(II-A18)}$$

where "u" is to be determined. Differentiating eq. II-A18 gives

$$\frac{dI}{dt} = -u\lambda_I e^{-\lambda_I t} + \left(\frac{du}{dt}\right) e^{-\lambda_I t} . \quad \text{(II-A19)}$$

Substituting for I and (dI/dt) in eq. II-A17 results in the following differential equation for u :

$$\frac{du}{dt} = \lambda_\beta M_o e^{-(\lambda_T-\lambda_I)t} + \lambda_g G_o e^{-(\lambda_g-\lambda_I)t} + \frac{\lambda_\gamma\lambda_g M_o}{(\lambda_g-\lambda_\gamma)} e^{-(\lambda_\gamma-\lambda_I)t} + \frac{\lambda_\gamma\lambda_g M_o}{(\lambda_g-\lambda_\gamma)} e^{-(\lambda_g-\lambda_I)t} , \quad \text{(II-A20)}$$

which upon integration yields

$$u = \frac{\lambda_\beta}{(\lambda_I-\lambda_T)} M_o e^{-(\lambda_T-\lambda_I)t} + \frac{\lambda_\gamma\lambda_g M_o}{(\lambda_g-\lambda_\gamma)(\lambda_I-\lambda_\gamma)} e^{-(\lambda_\gamma-\lambda_I)t} - \frac{\lambda_\gamma\lambda_g M_o}{(\lambda_g-\lambda_\gamma)(\lambda_I-\lambda_g)} e^{-(\lambda_g-\lambda_I)t} + \frac{\lambda_g}{(\lambda_I-\lambda_g)} G_o e^{-(\lambda_g-\lambda_I)t} + C \quad \text{(II-A21)}$$

where "C" is a constant of integration to be determined at zero time. Substitution for u in eq. II-A18 gives

$$I(t) = \frac{\lambda_\beta M_o}{(\lambda_I-\lambda_T)} e^{-\lambda_T t} + C e^{-\lambda_I t}$$

$$+ \frac{\lambda_\gamma \lambda_g M_o}{(\lambda_g-\lambda_\gamma)(\lambda_I-\lambda_\gamma)} e^{-\lambda_\gamma t}$$

$$- \frac{\lambda_\gamma \lambda_g M_o}{(\lambda_g-\lambda_\gamma)(\lambda_I-\lambda_g)} e^{-\lambda_g t}$$

$$+ \frac{\lambda_g G_o}{(\lambda_I-\lambda_g)} e^{-\lambda_g t} \qquad \text{(II-A22)}$$

Setting t=0, solving for C, and substituting for C in this equation yields a total expression for I as a function of time:

$$I(t) = \frac{\lambda_\beta}{(\lambda_I-\lambda_T)} M_o \left[e^{-\lambda_T t} - e^{-\lambda_I t} \right]$$

$$+ \frac{\lambda_\gamma \lambda_g M_o}{(\lambda_g-\lambda_\gamma)(\lambda_I-\lambda_\gamma)} \left[e^{-\lambda_\gamma t} - e^{-\lambda_I t} \right]$$

$$- \frac{\lambda_\gamma \lambda_g M_o}{(\lambda_g-\lambda_\gamma)(\lambda_I-\lambda_g)} \left[e^{-\lambda_g t} - e^{-\lambda_I t} \right]$$

$$+ \frac{\lambda_g}{(\lambda_I-\lambda_g)} G_o \left[e^{-\lambda_g t} - e^{-\lambda_I t} \right]$$

$$+ I_o e^{-\lambda_I t} . \qquad \text{(II-A23)}$$

The activity of an unstable nuclide is given by

$$A^i = \lambda_i [i] \qquad \text{(II-A24)}$$

where [i] is the amount of the nuclide present. Assuming that the $^{131}Te^g$ activity is in transient equilibrium with the $^{131}Te^m$ I.T. activity at time zero results in the relationship,

$$A_o^\gamma / A_o^g = (\lambda_g - \lambda_\gamma)/\lambda_g \quad . \qquad \text{(II-A25)}$$

Writing eq. II-A23 in terms of activities and substituting for A_o^g using eq. II-A25 results in the following expression for ^{131}I activity as a function of time:

$$\begin{aligned} A^I(t) &= \lambda_I I(t) \\ &= \frac{\lambda_I}{(\lambda_I - \lambda_T)} A_o^\beta [e^{-\lambda_T t} - e^{-\lambda_I t}] \\ &\quad + \frac{\lambda_I \lambda_g}{(\lambda_g - \lambda_\gamma)(\lambda_I - \lambda_\gamma)} A_o^\gamma [e^{-\lambda_\gamma t} - e^{-\lambda_I t}] \\ &\quad + A_o^I e^{-\lambda_I t} \quad . \end{aligned} \qquad \text{(II-A26)}$$

The β and γ (I.T.) activities of $^{131}Te^m$ are related as

$$A^\gamma = A^\beta B_{IT} / (1 - B_{IT}) \qquad \text{(II-A27)}$$

in which B_{IT} is the I.T. branch value as determined in eq. II-A10. Upon substituting eq. II-A27 into eq. II-A26, there are only four variables to be determined: $A^I(t)$, A_o^I, A_o^β, and t.

The three activity values are determined in terms of spectrum peak areas and detector efficiencies. The following measured variables are defined:

$$P^t_{773} = \text{Peak area at 773+774-keV, at time t.}$$
$$P^t_{364} = \text{Peak area at 364+365-keV, at time t.}$$
$$E_{773} = \text{Detector efficiency at 773-keV.}$$
$$E_{364} = \text{Detector efficiency at 364-keV.}$$

(II-A28)

From the decay schemes of $^{131}Te^m$ (this work, Table I) and ^{131}I (74Mel), the activities of $^{131}Te^m$ and ^{131}I are

$$A^\beta(t) = 1.893\ P^t_{773}\ /[E_{773}(1-X)] \qquad \text{(II-A29)}$$

and

$$A^I(t) = [(P^t_{364}/E_{364}) - 0.031(P^t_{773}/E_{773})]/0.806\ . \qquad \text{(II-A30)}$$

In eq. II-A29, "X" is the fraction of the $^{131}Te^m$ β-decay which proceeds directly to the ground state of ^{131}I. Equation II-A30 contains a term dependent on P^t_{773} due to the unresolved 364.48-364.98-keV doublet observed in sources containing both $^{131}Te^m$ and ^{131}I.

Using eqs. II-A27, II-A29, and II-A30 to substitute into eq. II-A26 and solving for X results in the equation

$$X = 1 - \{ (1.893)\ 0.806\ P^o_{773}\ (E_{773})^{-1}\ \{F\} \times [(P^t_{364}/E_{364} - 0.031P^t_{773}/E_{773}) - (P^o_{364}/E_{364} - 0.031P^o_{773}/E_{773})\ e^{-\lambda_I t}] - 1 \} \qquad \text{(II-A31)}$$

in which {F} is a function of B_{IT} and is given as

$$\{F\} = \frac{\lambda_I}{(\lambda_I-\lambda_T)} \left(e^{-\lambda_T t} - e^{-\lambda_I t} \right)$$

$$+ \frac{B_{IT}\, \lambda_I\, \lambda_g}{(1-B_{IT})\ (\lambda_g-\lambda_\gamma)\ (\lambda_I-\lambda_\gamma)} \left(e^{-\lambda_\gamma t} - e^{-\lambda_I t}\right). \qquad \text{(II-A32)}$$

To calculate {F} the decay constants (λ) are as follows:

$$\lambda_I = 3.610 \times 10^{-3} \ \text{hr}^{-1}$$
$$\lambda_g = 1.664 \ \text{hr}^{-1}$$
$$\lambda_T = 2.310 \times 10^{-2} \ \text{hr}^{-1}$$
$$\lambda_\gamma = B_{IT}\, \lambda_T \ . \qquad \text{(II-A33)}$$

C. Iteration.

To accomplish the calculation of B_{IT} and X, I first assumed an initial value for X of

$$X = 0.06 \pm 0.02 \quad \text{(1st iteration)}. \qquad \text{(II-A34)}$$

This is the previously measured value (65De) with an assumed uncertainty. Using eq. II-A10 results in a value for B_{IT} of

$$B_{IT} = 0.224 \pm 0.014 \quad \text{(1st iteration)}. \qquad \text{(II-A35)}$$

In order to determine X using eq. II-A31, two 4000 second live-time counts were made on a $^{131}Te^{m}$ plus ^{131}I sample; the first just after chemical purification to remove iodine and

the second approximately two days later. The measured parameters in the notation of eqs. II-A31 and II-A32 were

$$\begin{aligned} P^{c}_{773} &= 640{,}128 \pm 1075 \text{ counts} \\ P^{o}_{364} &= 91{,}214 \pm 800 \text{ counts} \\ P^{t}_{773} &= 233{,}714 \pm 662 \text{ counts} \\ P^{t}_{773} &= 357{,}208 \pm 892 \text{ counts} \\ E_{773} &= 1.07 \pm 0.01 \text{ relative units} \\ E_{364} &= 2.28 \pm 0.02 \text{ relative units} \\ t &= 46.90 \text{ hours.} \end{aligned} \qquad \text{(II-A36)}$$

Using the values in eqs. II-A35 and II-A36 in eqs. II-A31 and II-A32 results in

$$X = 1 - \{S\}\{F\} \qquad \text{(II-A37)}$$

with

$$\begin{aligned} \{S\} &= 6.984 \pm 0.295 \\ \{F\} &= 0.1340 \end{aligned} \quad \text{(1st iteration)} \qquad \text{(II-A38)}$$

The value of {S} does not change with each iteration as it is not a function of B_{IT}. This gives a first iteration value for X of

$$X = 0.064 \pm 0.039 \quad \text{(1st iteration).} \qquad \text{(II-A39)}$$

The second iteration results in the values

$$\begin{aligned} B_{IT} &= 0.223 \pm 0.016 \\ X &= 0.068 \pm 0.038 \end{aligned} \quad \text{(2nd iteration).} \qquad \text{(II-A40)}$$

The third iteration results in the values

$$\begin{aligned} B_{IT} &= 0.222 \pm 0.016 \\ X &= 0.068 \pm 0.038 \end{aligned} \quad \text{(3rd iteration).} \quad \text{(II-A41)}$$

As the values are changing very slowly, the calculation is terminated with the third iteration. The absolute ground state β-branch is given by the expression

$$X_{ABS} = X\,(1-B_{IT}) \; . \qquad \text{(II-A42)}$$

Thus the final values for the percentage branches of $^{131}Te^{m}$ decay by I.T. and by β-decay to the ^{131}I ground state are:

I.T. branch = (22.2 ± 1.6) %

Ground state β-branch = (5.2 ± 3.0) % .

(II-A43)

APPENDIX III

CALCULATION OF THE g-FACTOR OF A ONE-PROTON-TWO-NEUTRON THREE QUASI-PARTICLE STATE

(This calculation is based on material in 63Sh, pages 52-55 and 519-522.)

The magnetic moment, μ_J, of a state, JM, is given as

$$\mu_J = \langle JM|\bar{\mu}|JM\rangle \qquad \text{(III-A1)}$$

where J is the total angular momentum of the state, M is the component of J along the direction of an external magnetic field, and $\bar{\mu}$ is the magnetic dipole moment operator given as

$$\bar{\mu} = \sum_i (g_\ell^{(i)} \ell_{i,z} + g_s^{(i)} s_{i,z}) \quad . \qquad \text{(III-A2)}$$

In the above equation the summation is over all nucleons, with g_ℓ and g_s being the individual nucleon orbital and spin g-factors, respectively, and with $\ell_{i,z}$ and $s_{i,z}$ being the single nucleon orbital and spin angular momentum components along the direction of the magnetic field, respectively. In the limit of strong pairing within the single-particle model, the above summation may be carried out over only the unpaired nucleons.

The nuclear g-factors are measured in units of nuclear magnetons which are given by

$$\text{One nuclear magneton} = eh/4\pi m_p c \qquad \text{(III-A3)}$$

where e is the positive unit of charge, h is Planck's constant, m_p is the proton mass, and c is the speed of light. In this unit the orbital g-factors of the proton and neutron are

$$g_\ell^{(p)} = 1$$
$$g_\ell^{(n)} = 0 \qquad \text{(III-A4)}$$

and the spin g-factors are

$$g_s^{(p)} = 5.5855$$
$$g_s^{(n)} = -3.8256 \quad . \qquad \text{(III-A5)}$$

The measured magnetic moment is defined to be the maximum component of μ along the direction of the magnetic field, ie. applying eq. III-A1 with J = M. The measured magnetic moment is related to the g-factor, g, of the state under consideration by

$$\mu_J = g\,J \quad . \qquad \text{(III-A5)}$$

Thus by calculating the magnetic moment, μ_J, and knowing the total angular momentum, J, one can calculate the g-factor of the state under consideration.

The three-quasi-particle states under consideration consist of one unpaired proton, π, and two unpaired neutrons, ν_1 and ν_2. Each of these nucleons has an individual magnetic moment operator ($\bar{\mu}_\pi$, $\bar{\mu}_{\nu 1}$, or $\bar{\mu}_{\nu 2}$) and magnetic moment (μ_π, $\mu_{\nu 1}$, or $\mu_{\nu 2}$). The total magnetic moment of the state, as given in eq. III-A1, is the result of a vector coupling of the three individual magnetic moments. To accomplish this, one

must work in terms of a "reduced magnetic moment."

The Wigner-Eckart theorem relates the magnetic moment to the reduced magnetic moment as

$$\mu_J = \langle JM|\tilde{\mu}|JM\rangle = (-1)^{J-M} \{CG\} (J||\tilde{\mu}||J) \qquad \text{(III-A6)}$$

where {CG} is a Clebsch-Gordon coefficient given as

$$\{CG\} = \begin{pmatrix} J & 1 & J \\ -M & 0 & M \end{pmatrix} = (-1)^{J-M} M \,/\, [J(2J+1)(J+1)]^{1/2}. \qquad \text{(III-A7)}$$

Since J = M, equation III-A6 becomes

$$\mu_J = \{WE\} (J||\tilde{\mu}||J) \qquad \text{(III-A8)}$$

in which the "Wigner-Eckart term," {WE}, is

$$\{WE\} = J \,/\, [J(2J+1)(J+1)]^{1/2} . \qquad \text{(III-A9)}$$

This relationship holds for the total state, JM, as well as for the individual nucleons; $J_\pi M_\pi$, $J_{\nu 1} M_{\nu 1}$, and $J_{\nu 2} M_{\nu 2}$. In the single nucleon cases, $J_{(i)}$ and $M_{(i)}$ are the single nucleon total angular momentum and its component along the magnetic field for the nucleon in its shell-model state.

When two nucleons, having total angular momentum values of J_1 and J_2, couple to give a total angular momentum, J, the reduced magnetic moment of the final state is given in terms of the single particle reduced magnetic moments as

$$(J_1J_2J||\bar{\mu}||J_1J_2J) = (J_1J_2J||\bar{\mu}_1+\bar{\mu}_2||J_1J_2J)$$
$$= |\mu_1|_{12} + |\mu_2|_{12} \qquad \text{(III-A10)}$$

where

$$|\mu_1|_{12} = (J_1J_2J||\bar{\mu}_1||J_1J_2J) \qquad \text{(III-A11a)}$$

$$|\mu_2|_{12} = (J_1J_2J||\bar{\mu}_2||J_1J_2J) \; . \qquad \text{(III-A11b)}$$

As the two nucleons in their shell-model states are non-identical systems, $|\mu_1|_{12}$ and $|\mu_2|_{12}$ are given by the following equations:

$$|\mu_1|_{12} = (-1)^{J_1+J_2+J+1}(2J+1) \times \{R_1\}\,(J_1||\bar{\mu}_1||J_1) \qquad \text{(III-A12a)}$$

$$|\mu_2|_{12} = (-1)^{J_1+J_2+J+1}(2J+1) \times \{R_2\}\,(J_2||\bar{\mu}_2||J_2) \; . \qquad \text{(III-A12b)}$$

The reduced magnetic moment terms on the right sides of eqs. III-A12a and III-A12b are related to the single particle magnetic moments as shown in eqs. III-A6 and III-A8. The terms, $\{R_1\}$ and $\{R_2\}$, are Racah coefficients and are given by the following two equations:

$$\{R_1\} = \begin{Bmatrix} J_1 & J & J_2 \\ J & J_1 & 1 \end{Bmatrix} \qquad \text{(III-A13a)}$$

$$= \frac{(-1)^{J_1+J_2+J+1}\,J_1(J_1+1)+J(J+1)-J_2(J_2+1)}{2\,[J_1(J_1+1)(2J_1+1)J(J+1)(2J+1)]^{1/2}}$$

and

$$\{R_2\} = \begin{Bmatrix} J_2 & J & J_1 \\ J & J_2 & 1 \end{Bmatrix} \qquad \text{(III-A13b)}$$

$$= \frac{(-1)^{J_1+J_2+J+1}\, J_2(J_2+1)+J(J+1)-J_1(J_1+1)}{2\,[J_2(J_2+1)(2J_2+1)J(J+1)(2J+1)]^{1/2}}$$

Thus for each coupling of a pair of non-identical systems to a total angular momentum, J, one can define coupling coefficients, $\{C_i\}$, such that the reduced magnetic moment of the resultant state is given as

$$(J_1J_2J||\bar{\mu}||J_1J_2J) = \{C_1\}(J_1||\bar{\mu}_1||J_1) + \{C_2\}(J_2||\bar{\mu}_2||J_2) \qquad \text{(III-A14)}$$

in which, for example, $\{C_1\}$, is given as

$$\{C_1\} = |(2J+1)\ \{R_1\}| \quad . \qquad \text{(III-A15)}$$

In the cases under consideration, the final state is presumed to result from the coupling of an odd parity two-neutron state in the ^{130}Te core and an even parity single-proton state. Thus, in this calculation of the total magnetic moment, the two neutrons are coupled and then treated as a separate total system. This two-neutron system is then coupled to the single proton.

The calculation begins by assuming a measurable single-particle magnetic moment for each of the unpaired nucleons (μ_π, $\mu_{\nu 1}$, and $\mu_{\nu 2}$). Equation III-A8 is used to calculate reduced magnetic moments for each particle. Then the two

neutrons are coupled to a total angular momentum, N, resulting in a reduced magnetic moment for the two neutron system of (Eqs. III-A10 to III-A14)

$$(J_{\nu 2}N||\bar{\mu}||J_{\nu 1}J_{\nu 2}N) = [\{C_{\nu 1}\}/\{WE_{\nu 1}\}]\ \mu_{\nu 1} + [\{C_{\nu 2}\}/\{WE_{\nu 2}\}]\ \mu_{\nu 2} \qquad \text{(III-A16)}$$

In like manner, the two neutron system is then coupled to the single proton resulting in a reduced magnetic moment for the total system of

$$(J_\pi[J_{\nu 1}J_{\nu 2}]N\ J||\bar{\mu}||J_\pi[J_{\nu 1}J_{\nu 2}]N\ J) = [\{C_\pi\}/\{WE_\pi\}]\ \mu_\pi + \{C_N\}\ [\{C_{\nu 1}\}/\{WE_{\nu 1}\}]\ \mu_{\nu 1} + \{C_N\}\ [\{C_{\nu 2}\}/\{WE_{\nu 2}\}]\ \mu_{\nu 2}\ . \qquad \text{(III-A17)}$$

In this notation, $\{C_N\}$ is given by

$$\{C_N\} = |(2J+1) \begin{Bmatrix} N & J & J_\pi \\ J & N & 1 \end{Bmatrix}| = |(2J+1)\ \{R_N\}|\ . \qquad \text{(III-A18)}$$

The reduced magnetic moment in eq. III-A17 is then transformed into a measurable magnetic moment by the use of eq. III-A8 resulting in the following formula for μ_J:

$$\mu_J = \{WE_J\}\{C_\pi\}\mu_\pi / \{WE_\pi\} + \{WE_J\}\{C_N\}\{C_{\nu 1}\}\mu_{\nu 1} / \{WE_{\nu 1}\} + \{WE_J\}\{C_N\}\{C_{\nu 2}\}\mu_{\nu 2} / \{WE_{\nu 2}\} \quad \text{(III-A19)}$$

Equation III-A5 is then used to calculate the g-factor of the total state.

In calculating μ_J using eq. III-A19, two different sets of values for the single-particle magnetic moments may be employed. The first of these consists of the Schmidt values (37Sh). These values are given by one of the two following equations:

$$\mu_{nucleon} = \ell g_\ell + g_s/2 \quad \text{for } J = \ell + 1/2$$
$$= \frac{J}{J+1}[(\ell+1)g_\ell - g_s/2] \quad \text{for } J = \ell - 1/2 \quad . \qquad \text{(III-A20)}$$

The first is applicable for states in which the orbital and spin angular momentum of the nucleon are parallel ($J=\ell+1/2$), and the second when they are antiparallel ($J=\ell-1/2$). The variables, ℓ and s, are as in eq. III-A2, and the values of g_ℓ and g_s are given by eqs. III-A4 and III-A5.

The second set of values consists of the "empirical" single-particle magnetic moments. The empirical magnetic moment may be viewed as the average of the measured magnetic moments of the single-particle states of interest in the nearby nuclides. In Table AIII-1 are listed 1.) the proton and neutron single-particle states of interest in ^{131}I,

Table AIII-1

Experimental, empirical, and theoretical (Schmidt limit) single nucleon magnetic moments for the shell model states of interest in ^{131}I.

Shell Model Orbital	$\mu_{Exp.}$ (n.m)	Nucleus	Ref.	$\mu_{Schmidt}/\mu_{Emp.}$
π $1g_{7/2}$	2.836	^{133}I	(60Al)	$1.717/2.65$
	2.738	^{131}I	(60Li)	
	2.617	^{129}I	(51Wa)	
	2.547	^{123}Sb	(69Fu)	
	2.51	$^{121}Sb^{m}$	(69Fu)	
	2.578	^{133}Cs	(69Fu)	
	2.729	^{135}Cs	(57St)	
	2.838	^{137}Cs	(57St)	
π $2d_{5/2}$	2.77	$^{131}I^{m}$	(67Ta)	$4.793/3.45$ (2.75)
	2.808	^{127}I	(69Fu)	
	3.46	^{115}Sb	(68Ja)	
	2.67	^{117}Sb	(68Ja)	
	3.45	^{119}Sb	(68Ja)	
	3.359	^{121}Sb	(69Fu)	
	3.537	^{131}Cs	(65Wo)	
	3.44	$^{133}Cs^{m}$	(68Ca)	

Table AIII-1 (cont'd)

Shell Model Orbital	$\mu_{Exp.}$ (n.m)	Nucleus	Ref.	$\mu_{Schmidt}/\mu_{Emp.}$
ν $2d_{3/2}$	0.66	^{127}Te	(72Si)	$1.148/0.67$
	0.67	^{129}Te	(72Si)	
	0.60	$^{125}Te^{m}$	(64Hu)	
	0.6908	^{131}Xe	(69Fu)	
	0.68	$^{119}Sn^{m}$	(69Fu)	
	0.70	^{121}Sn	(67Pr)	
ν $1h_{11/2}$	-1.00	$^{123}Te^{m}$	(72Va)	$-1.913/-1.05$
	-0.93	$^{125}Te^{m}$	(72Va)	
	-0.91	$^{127}Te^{m}$	(72Va)	
	-1.15	$^{129}Te^{m}$	(72Va)	
	-1.11	$^{111}Cd^{m}$	(68Lu)	
	-1.09	$^{113}Cd^{m}$	(64By)	
	-1.04	$^{115}Cd^{m}$	(67Ch)	
ν $3s_{1/2}$	-0.7359	^{123}Te	(53We)	$-1.914/-0.89$
	-0.8872	^{125}Te	(53We)	
	-0.879	^{113}Sn	(67Dy)	
	-0.918	^{115}Sn	(50Pr)	
	-1.000	^{117}Sn	(50Pr)	
	-1.046	^{119}Sn	(50Pr)	
	-0.7768	^{129}Xe	(68Br)	

2.) the measured magnetic moment values of these states in neighboring nuclides, 3.) the empirical magnetic moment value obtained for each state, and 4.) the Schmidt value for each state. The empirical magnetic moments deviate appreciably from the Schmidt values. This difference is primarily the result of polarization effects of closed shells (69Bo, pages 336-340), differences in the nuclear potential, and configuration mixing which results in the states in question not being purely single-particle in character. This latter configuration mixing effect may be observed in the measured magnetic moments of the $2d_{5/2}$ proton state. In the two iodine nuclei the magnetic moment was measured to be ≈2.8. This results in a g-factor of ≈1.1 (eq. III-A5). The empirical magnetic moment of 3.45 results in a g-factor of ≈1.4. Almar et al. (73Al) have proposed that the configuration of the 150 keV state in ^{131}I has an appreciable contribution (30-35 %) from the configuration $(1g_{7/2})^3$ 5/2. It has been noted by Stone et al. (68St1) that the g-factor of a three-quasi-particle state of the type $(j^3)_{J-1}$ is exactly that of a single nucleon in the J-state. The empirical magnetic moment of the $1g_{7/2}$ proton state is ≈2.65, resulting in a g-factor of ≈0.76. Thus the mixing of the $(1g_{7/2})^3$ 5/2 configuration with the $2d_{5/2}$ single-proton configuration is expected to reduce the empirical g-factor from ≈1.4, and the magnitude of the effect is nearly exactly accounted for by the postulated 30-35 % contribution of the three-proton cluster configuration to the state.

In the present three quasi-particle state g-factor calculation, the vector algebra has assumed that pure single-particle character shell-model states couple to form a pure three quasi-particle state. Thus, in the interest of consistency, it is deemed more appropriate to employ the Schmidt values in the calculation of the g-factor. This is also done because of the high energy of the state in question which makes it unlikely that the polarization and mixing are the same as included by employing empirical magnetic moments. The calculated magnetic moment can be quite sensitive to small changes in mixing and core excitation (74Ma2). The results obtained by employing Schmidt values for the single-particle magnetic moments are shown in the main text in Table IX . For the purpose of comparison, the calculated g-factors using empirical single-particle magnetic moments are shown in Table AIII-2.

Table AIII-2

Calculated g-factors for the possible one-proton-two-neutron configurations in ^{131}I which result in a spin and parity value of $15/2^-$. Empirical single particle magnetic moments were used in the calculation.

Configuration		Calculated g-factor
Proton	Neutrons	
$[1g_{7/2}$,	$(1h_{11/2}, 3s_{1/2})$ 5-] 15/2-	+0.26
$[1g_{7/2}$,	$(1h_{11/2}, 3s_{1/2})$ 6-] 15/2-	-0.01
$[1g_{7/2}$,	$(1h_{11/2}, 2d_{3/2})$ 4-] 15/2-	+0.13
$[1g_{7/2}$,	$(1h_{11/2}, 2d_{3/2})$ 5-] 15/2-	+0.16
$[1g_{7/2}$,	$(1h_{11/2}, 2d_{3/2})$ 6-] 15/2-	+0.14
$[1g_{7/2}$,	$(1h_{11/2}, 2d_{3/2})$ 7-] 15/2-	+0.10
$[2d_{5/2}$,	$(1h_{11/2}, 3s_{1/2})$ 5-] 15/2-	+0.42
$[2d_{5/2}$,	$(1h_{11/2}, 3s_{1/2})$ 6-] 15/2-	+0.08
$[2d_{5/2}$,	$(1h_{11/2}, 2d_{3/2})$ 5-] 15/2-	+0.33
$[2d_{5/2}$,	$(1h_{11/2}, 2d_{3/2})$ 6-] 15/2-	+0.24
$[2d_{5/2}$,	$(1h_{11/2}, 2d_{3/2})$ 7-] 15/2-	+0.13

APPENDIX IV

CALCULATION OF THE DIRECT β^+/EC BRANCH TO THE $7/2^+$ 25.5 keV STATE IN ^{105}Ag

The direct β^+/EC branch from $5/2^+$ ^{105}Cd to the $7/2^+$ 25.5 keV state in ^{105}Ag was determined by three different methods. In the first, a ^{105}Cd sample was produced in a short 14-MeV neutron irradiation and the ^{105}Cd γ-ray activity (representing decay to all levels in ^{105}Ag above the 25.5 keV state) was determined at the end of irradiation. The ^{105}Ag activity in the sample was determined ~31 days after irradiation by counting the sample in a known geometry. The direct β^+/EC branch to the 25.5 keV state was then determined from the equations of radioactive growth and decay. In the second method, the β^+/EC branch to the 25.5 keV state was determined from the positron annihilation (511.004-keV) peak relative intensity, correcting for other sources of 511-keV γ-rays in the spectrum (e.g. ^{106}Ag^g, ^{106}Ag^m, and β^+-feeding to other ^{105}Ag levels). In the third method, the ^{105}Ag^m activity in transient equilibrium with ^{105}Cd was observed to determine the total ^{105}Cd β^+/EC decay intensity. In all three methods, it was assumed that there is negligible direct β^+/EC decay from $5/2^+$ ^{105}Cd to the $1/2^-$ ground state or the $9/2^+$ 53.2 keV excited state in ^{105}Ag. The first method was expected to be the most precise as the second depends strongly on some poorly determined

branches in $^{106}Ag^{g}$ decay and the third depends strongly on the value for the $^{105}Ag^{m}$ EC-branch which has been determined to be (0.34 ± 0.07)% (72Kr).

A. ^{105}Ag Growth in a ^{105}Cd Sample.

A ^{105}Cd sample was produced in a ten minute 14-MeV neutron irradiation, and the decay of the 961.84-keV γ-ray was followed for a series of eight 13 minute counts in order to determine an activity at end of irradiation by extrapolation of the decay curve. The sample was then counted 45,019 minutes later to determine the 41-day ^{105}Ag activity present, arising principally from the decay of ^{105}Cd. If the following parameters are defined:

$$\left.\begin{aligned} A_1 &= {}^{105}\text{Cd activity},\\ A_2 &= {}^{105}\text{Ag activity},\\ \lambda_1 &= {}^{105}\text{Cd decay const.} = 1.249 \times 10^{-2}\ \text{min}^{-1},\\ \lambda_2 &= {}^{105}\text{Ag}^{g}\ \text{decay const.} = 1.174 \times 10^{-5}\ \text{min}^{-1},\\ t_0 &= \text{end of irradiation} = 0\ \text{minutes},\\ t_1 &= \text{time of late count} = 45{,}019\ \text{min},\\ t_b &= \text{length of irradiation} = 10\ \text{min}, \end{aligned}\right\} \quad \text{(IV-A1)}$$

then the activity of $^{105}Ag^{g}$ at the time of the late count, $A_2(t)$, is given by the following equation:

$$A_2(t) = \frac{\lambda_2}{\lambda_2 - \lambda_1} A_1(t_o)\ (e^{-\lambda_1 t} - e^{-\lambda_2 t}) + A_2(t_o)\ e^{-\lambda_2 t} . \quad \text{(IV-A2)}$$

Noting that $e^{-\lambda_1 t} \approx 0$ simplifies eq. IV-A2 to

$$A_2(t) = \frac{\lambda_2}{\lambda_2 - \lambda_1} A_1(t_o)\, e^{-\lambda_2 t} + A_2(t_o)\, e^{-\lambda_2 t} \quad . \qquad \text{(IV-A3)}$$

The activity, $A_2(t_o)$, is given by

$$A_2(t_o) = A_2(t_o)' + A_2(t_o)'' \quad , \qquad \text{(IV-A4)}$$

where $A_2(t_o)'$ is the $^{105}Ag^g$ activity at t_o arising from the decay of ^{105}Cd during irradiation and $A_2(t_o)''$ is the $^{105}Ag^g$ activity arising from direct production via the $^{106}Cd(n,np)$ nuclear reaction. Defining R_1 and R_2 to be the rates of direct production of ^{105}Cd and ^{105}Ag, respectively, results in the equations :

$$A_2(t_o)' = R_1 \left[1 - e^{-\lambda_2 t_b}\right] + \frac{\lambda_2 R_1}{\lambda_2 - \lambda_1} \left\{e^{-\lambda_1 t_b} - e^{-\lambda_2 t_b}\right\} \qquad \text{(IV-A5)}$$

and (since $t_b \ll t_{1/2}[^{105}Ag]$)

$$A_2(t_o)'' \cong R_2 \lambda_2 t_b \quad . \qquad \text{(IV-A6)}$$

The cross section for the (n,np) reaction has been observed to be $\sim 10^{-3}$ times the cross section for the (n,2n) reaction near A=100 (66Go). Thus it can be estimated that $R_2 \approx 10^{-3} R_1$.

Noting that

$$R_1 = A_1(t_o) \left[1 - e^{-\lambda_1 t_b} \right]^{-1} \qquad \text{(IV-A7)}$$

and that

$$e^{-\lambda_2 t_b} \approx 1 \qquad \text{(IV-A8)}$$

and substituting into eq. IV-A4 results in the following equation:

$$A_2(t_o) \approx \frac{\lambda_2}{\lambda_1 - \lambda_2} A_1(t_o) + 10^{-3} \lambda_2 t_b A_1(t_o) \left[1 - e^{-\lambda_1 t_b}\right]^{-1} . \qquad \text{(IV-A9)}$$

The second term is negligible when compared to the first, hence

$$A_2(t_o) \approx \frac{\lambda_2}{\lambda_1 - \lambda_2} A_1(t_o) . \qquad \text{(IV-A10)}$$

Substituting into eq. IV-A3 results in the equation for $A_2(t)$,

$$A_2(t) \approx \frac{2\lambda_1}{\lambda_1 - \lambda_2} A_1(t_o) e^{-\lambda_2 t} . \qquad \text{(IV-A11)}$$

The activity of $^{105}Ag^g$ at time = t was determined from the activity of the principal ^{105}Ag decay γ-ray (344.52-keV) by using the following formula:

$$A_2(t) = A_{344}(t) \quad [1 + \alpha_T] \; F^{-1} \quad , \qquad \text{(IV-A12)}$$

in which $A_{344}(t)$ is the measured 344-keV γ-ray activity, α_T is the total conversion coefficient for the 344-keV E2 transition (68Ha), and F is the fraction of $^{105}Ag^g$ decays leading to a 344-keV transition (74Be1). These values are

$$\begin{aligned} A_{344}(t) &= (5.883 \pm 0.060) \times 10^4 \text{ photons/min} \\ \alpha_T &= 0.019 \\ F &= 0.4167 \quad . \end{aligned} \qquad \text{(IV-A13)}$$

The ^{105}Cd activity at time, t=0, is related to the activity of the principal ^{105}Cd γ-ray (961.84-keV) and to the direct β^+/EC branch (B) to the $7/2^+$ 25.5 keV state by the equation

$$A_1(t_o) = A_{961}(t_o) \quad [I_G/I_{961}] \quad + \quad B \quad , \qquad \text{(IV-A14)}$$

in which I_G is the total transition relative intensity of all γ-transitions in ^{105}Ag feeding into the lower three states and I_{961} is the 961.84-keV γ-ray relative intensity. These are obtained from the data in Table X as

$$I_G = 10{,}330 \pm 60 \qquad \text{(IV-A15)}$$

and

$$I_{961} = 1000 \pm 7 \quad . \qquad \text{(IV-A16)}$$

The value for $A_{961}(t_o)$ was determined by extrapolating the decay curve of the 961.84-keV γ-ray peak to t=0. Table AIV-1 gives the 961.84-keV γ-ray activity in photons per minute for each of eight successive thirteen minute counts. The decay curve extrapolation resulted in

$$A_{961}(t_o) = (6.12 \pm 0.25) \times 10^6 \text{ photons/min} . \quad \text{(IV-A17)}$$

Substituting equations IV-A1 and IV-A12 through IV-A17 into equation IV-A11 and solving for B results in a value for the direct β^+/EC branch from ^{105}Cd to the $7/2^+$ 25.5 keV state of ^{105}Ag of

$$B = 0.514 \pm 0.040 . \quad \text{(IV-A18)}$$

TABLE AIV - 1

Activity of 961.84 - keV γ-ray in ^{105}Cd Sample Produced via a 10 minute ^{106}Cd $(n,2n)$ ^{105}Cd Irradiation.

961.84 - keV Activity (photons-min^{-1} x 10^{-6})		Time after Irradiation to Midpoint of Count
$A_{961}(t)$	σ	t (days)
4.941	0.150	0.01040
4.113	0.141	0.02280
3.254	0.116	0.03365
2.882	0.110	0.04445
2.172	0.083	0.05525
1.893	0.064	0.06610
1.420	0.054	0.07700
1.173	0.036	0.08795

B. Positron Intensity.

In the γ-ray singles spectra taken with the 50 cm^3 Ge(Li) detector, the 511-keV peak had a relative intensity value of 24,300 ± 900 (using the same relative base as in Table X). This intensity, however, included significant contributions from sources other than β^+ decay from ^{105}Cd to the $7/2^+$ 25.5 keV ^{105}Ag excited state.

The first such source considered was β^+ branches to other ^{105}Ag excited states from ^{105}Cd. An intensity balance was performed on all levels which could be fed in β^+ decay (i.e. levels with E < 1800 keV) to determine their direct β^+/EC feeding, and the β^+ contribution was calculated using the $\log(f_o^{\varepsilon} / f_o^{+})$ tables of Gove and Martin (71Go). The total contribution to the 511-keV peak from this source was determined to be 114 ± 20.

The second source of 511-keV γ-rays considered was $^{106}Ag^m$ decay. Using the relative intensity value for the $^{106}Ag^m$ 451-keV γ-ray from my spectra (29.3 ± 1.5) and the most recent $^{106}Ag^m$ decay study (73In), the contribution to the 511-keV peak intensity from the $^{106}Ag^m$ 511.85-keV γ-ray was calculated to be 91 ± 6.

In a similar manner, the 511.85-keV γ-ray intensity from $^{106}Ag^g$ decay was determined from my value for the relative intensity of the 622-keV $^{106}Ag^g$ γ-ray (13.8 ± 1.0) and the $^{106}Ag^g$ decay study of Rao and Fink (67Ra). This value was 880 ± 80.

The fourth source of 511-keV γ-rays was the positrons

arising from the β^+ decay of $^{106}Ag^g$. This was determined to be 6200 ± 1200 based on the 622-keV γ-ray intensity and the decay study of Rao and Fink (67Ra). The large uncertainty is due to the uncertainty in the absolute intensity (in γ-rays per $^{106}Ag^g$ decay) of the 622-keV transition (74Be2).

The total 511-keV intensity remaining after subtracting these four contributions is 17,000 ± 1500. Noting that each positron results in two 511-keV γ-rays and using the $\log(f_o^{\varepsilon}/f_o^{+})$ tables of Gove and Martin (71Go) results in a total β^+/EC decay to the $7/2^+$ state of 15,900 ± 1400 relative intensity units. Using the value of 10,330 ± 60 for all other ^{105}Cd β^+/EC decay (eq. IV-A15) results in

$$B = 0.61 \pm 0.06. \qquad \text{(IV-A19)}$$

This is in reasonable agreement with eq. IV-A18. It may be noted that this particular value (0.61) might be expected to be high as the net 511-keV intensity still included contributions from other extraneous sources, such as SE and DE event positrons, which were not considered.

C. $^{105}Ag^m$ Transient Equilibrium.

As indicated in Table X, several γ-rays arising from the EC decay of $^{105}AG^m$ were observed in spectra of the ^{105}Cd source. As these γ-rays were observed in spectra taken one to two hours after irradiation, it may be assumed that the 7.23-min $^{105}Ag^m$ activity was in transient equilibrium with the 55.5 min ^{105}Cd parent. The two activities, then, are related by the equation

$$A_{Cd} = A_{Ag}\{1 - t_{1/2}(Ag)/\, t_{1/2}(Cd)\}\ . \qquad \text{(IV-A20)}$$

The $^{105}Ag^{m}$ activity, A_{Ag}, may be determined from the relative intensity of the $^{105}Ag^{m}$ 319.23-keV γ-ray (189 ± 4) and the absolute intensity, in γ-rays per decay, of the 319.23-keV transition (0.0017 ± 0.0004) (72Kr, 74Bel). The resulting value is

$$A_{Ag} = 111{,}200 \pm 27{,}500 \text{ rel.intens. units.} \qquad \text{(IV-A21)}$$

substituting into IV-A20 gives

$$A_{Cd} = 96700 \pm 24{,}000 \text{ rel.intens. units.} \qquad \text{(IV-A22)}$$

The total γ-ray intensity feeding into the 7.23-min $7/2^{+}$ $^{105}Ag^{m}$ from ^{105}Cd decay is 7070 ± 40 (from Table X). The remaining intensity represents direct β^{+}/EC decay to the isomer. This results in a value for B (as in eqs. IV-A18 and IV-A19) of

$$B = 0.90 \pm 0.33. \qquad \text{(IV-A23)}$$

The large uncertainty is the result of the large uncertainty in the EC branch value for $^{105}Ag^{m}$ decay. It may be noted that a higher value for the EC branch would lower B and bring it into closer agreement with the values determined in Sections A and B.

37Sc T. Schmidt, Z. Physik 106, 358 (1937).

49Ha O. Haxel, H.H.D. Jensen, and S.E. Seuss, Phys. Rev. 75, 1766 (1949).

49Ma M.G. Mayer, Phys. Rev. 75, 1969 (1949).

50Gu J.R. Gum and M.L. Pool, Phys.Rev. 80, 315 (1950).

50Pr W.G. Proctor, Phys. Rev. 79, 35 (1950).

51Ve N.F. Verster, G.J. Nijgh, R. VanLieshout, and G.J. Bakker, Physica Acta 17, 637 (1951).

51Wa H. Walchi, R. Livingston, and G. Hebert, Phys. Rev. 82, 97 (1951).

52Bo A. Bohr, Mat. Fys. Medd. Dan. Vid. Selsk. 26, No. 14 (1952).

52Ro D. Rose, G. Hinman, and L.G. Lang, Phys. Rev. A86, 863 (1952).

53Bo A. Bohr and B.R. Mottelson, Matt. Fys. Medd. Dan. Vid. Selsk. 27, No. 16 (1953).

53Jo F.A. Johnson, Can. J. Phys. 31, 1136 (1953).

53We H.E. Weaver, Jr., Phys. Rev. 89, 923 (1953).

54Ch D.C. Choudhury, Matt, Fys. Medd. Dan. Vid. Selsk. 28, No. 4 (1954).

55Fo K.W. Ford and C. Levinson, Phys. Rev. 100, 1 (1955).

55He E. Hebb, Phys. Rev. 97, 987 (1955).

55Ma C.A. Mallman, A.H.W. Aten, Jr., D.R. Bess, and C.M. de McMillan, Phys. Rev. 99, 7 (1955).

57Ba J. Bardeen, L.N. Cooper, and J.R. Schrieffer, Phys. Rev. 108, 1175 (1957).

57La R.D. Lawson and J.L. Uretsky, Phys. Rev. 108, 1300 (1957).

57St H.H. Stroke, V. Jaccarino, D.S. Edmonds, Jr., and R. Weiss, Phys. Rev. 105, 590 (1957).

58Bo A. Bohr, B.R. Mottelson, and D. Pines, Phys. Rev. 110, 936 (1958).

59Ba A. Badescu, K.P. Mitrofanov, A.A. Sorokin, and V.S. Shpinel, Izv. Akad. Nauk SSSR Ser. Fiz. 23, 1434 (1959).

59Ba2 S.T. Balyaev, Kgl. Danske Vid. Selsk. Mat.-Fys. Medd. 31, No. 11 (1959).

60Al S.S. Alpert, E. Lipworth, and M.B. White, Bull. Am. Phys. Soc. 5, 273 (1960).

60Ki L.S. Kisslinger and R.A. Sorenson, Kgl. Danske Vid. Selsk. Mat.-Fys. Medd. 32, No. 9 (1960).

60Li E. Lipworth, H.L. Garvin, and T.M. Green, Phys. Rev. 119, 2022 (1960).

60Ta I. Talmi and I. Unna, Nucl. Phys. 19, 225 (1960).

61Ba A. Badescu, O.M. Kalinkina, K.P. Mitrofanov, A.A. Sorokin, N.V. Farafontov, and V.S. Shpinel, Sov. Phys. JETP 13, 65 (1961).

61Fe J.M. Fergusson and F.M. Tomnovec, Nucl. Phys. 26, 457 (1961).

61Ra L.A. Rayburn, Phys. Rev. 122, 168 (1961).

61Sh A. de-Shalit, Phys. Rev. 122, 1530 (1961).

62Pr M.A. Preston, Physics of the Nucleus, (Addison-Wesley, Reading, Mass., 1962).

63De S.H. Devare, P.N. Tandon, and H.G. Devare, Phys.Rev. 131, 1750 (1963).

63Ki L.S. Kisslinger and R.A. Sorenson, Revs. Mod. Phys. 35, 853 (1963).

63Sh A. de-Shalit and I. Talmi, Nuclear Shell Theory, (Academic Press, New York, 1963).

64By F.W. Byron, Jr., M.N. McDermott, R. Novik, B.W. Perry, and E.B. Saloman, Phys. Rev. 136, B1654 (1964).

64Hu J.J. Huntzicker, R.B. Franke, N.J. Stone, and D.A. Shirley, Bull. Am. Phys. Soc. 9, 741 (1964).

64La A.M. Lane, Nuclear Theory (W.A. Benjamin Inc., New York, 1964).

65De S.H. Devare, R.M. Singru, and H.G. Devare, Phys. Rev. 140, B536 (1965).

65Go M. Goldhaber and A.W. Sunyar, in Alpha-, Beta-, and Gamma-Ray Spectroscopy, edited by K. Siegbahn, (North-Holland, Amsterdam, 1965).

65Mo S.A. Moszkowski, in Alpha-, Beta-, and Gamma-Ray Spectroscopy, edited by K. Siegbahn, (North-Holland, Amsterdam, 1965).

65Wa W.B. Walters, C.E. Bemis, and G.E. Gordon, Phys. Rev. 140, B268 (1965).

65Wo R.D. Worley, V.J. Ehlers, W.A. Nierenberg, and H.A. Shugart, Phys. Rev. 140, B1483 (1956).

66Go M.D. Goldberg, S.F. Mughabghab, S.N. Purohit, B.A. Magurno, and V.M. May, BNL-325, Second Edition, Supplement No. 2, Brookhaven National Laboratories, 1966 (unpublished).

66Gr G. Graeffe, C.W. Tang, C.D. Coryell, and G.E. Gordon, Phys. Rev. 149, 884 (1966).

67Ah N. Ahmed, Nuovo Cim. 48, 2567 (1967).

67Al G. Alaga and G. Ialongo, Nucl. Phys. A97, 600 (1967).

67Ba M. Baranger, in Nuclear Structure and Nuclear Reactions, Proceedings of the International Summer School of Nuclear Physics, Varenna, Italy (Academic Press, New York, 1967) edited by M. Jean and R.A. Ricci.

67Be1 L.M. Beyer, G. Berzins, and W.H. Kelly, Nucl. Phys. A93, 456 (1967).

67Be2 L.M. Beyer, W.H. Kelly, Nucl. Phys. A104, 274 (1967).

67Ch R.L. Chaney, M.N. McDermott, and B.A. Myers, Bull. Am. Phys. Soc. 12, 891 (1967).

67Dy A. Dymanus, M.H. Prior, and H.A. Shugart, Bull. Am. Phys. Soc. 12, 1046 (1967).

67Go G.E. Gordon and C.D. Coryell, J. Chem. Ed. 44, 636 (1967).

67Gr1 A. Graue, E. Jastad, J.R. Lien, P. Torvund, and W.H. Moore, Nucl. Phys. A103, (1967).

67Gr2 G. Graeffe, E.J. Hoffman, and D.G. Sarantites, Phys. Rev. 158, 1183 (1967).

67Le G.M. Lederer, J.M. Hollander, and I. Perlman, Table of Isotopes, Sixth Edition, (John Wiley and Sons, New York, 1967).

67Ma R.D. Mattuck, A Guide to Feynman Diagrams in the Many Body Problem, (McGraw Hill, New York, 1967).

67Pr M.H. Prior, H.A. Shugart, and P.A. Vanden Bout, Bull. Am. Phys. Soc. 12, 904 (1967).

67Ra P. Venugopala Rao and R.W. Fink, Nucl. Phys. A103, 385 (1967).

67Ta P.N. Tandon and H.G. Devare, Nucl. Phys. A102, 203 (1967).

68Au R.L. Auble, J.B. Ball, and C.B. Fulmer, Phys. Rev. 169, 955 (1968).

68Bo M. Bormann, A. Behrend, I. Riehle, and O. Vogel, Nucl. Phys. A115, 309 (1968).

68Br D. Brinkman, Helv. Phys. Act. 41, 367 (1968).

68Ca L.E. Campbell and G.J. Perlow, Nucl. Phys. A109, 59 (1968).

68Ha R.S. Hager and E.C. Seltzer, Nucl. Data A4, 1 (1968).

68Ja A.D. Jackson, Jr., E.H. Rogers, Jr., and G.J. Carrett, PUC-937, 288 (1968).

68La N.S. Laulainen and M.N. McDermott, Bull. Am. Phys. Soc. 13, 357 (1968).

68Ru M.L. Rustgi, J.G. Lucas, and S.N. Mukherjee, Nucl.Phys. A117, 321 (1968).

68Stl N.J. Stone, R.B. Frankel, and D.A. Shirley, Phys. Rev. 172, 1243 (1968).

69Be G. Berzins, M.E. Bunker, and J.W. Starner, Nucl.Phys. A126, 273 (1969).

69Bl A.G. Blair, J.G. Beery, and E.R. Flynn, Phys. Rev. Letters 22, 470 (1969).

69Bo A. Bohr and B.R. Mottelson, Nuclear Structure: Vol. I Single-Particle Motion (W.A. Benjamin, New York, 1969).

69Ca D.C. Camp, in Proceedings of the International Conference on Radioactivity and Nuclear Spectroscopy Vol. I, 135 (1969).

69Co F.E. Coffman and J.H. Hamilton, Nucl. Phys. A127, 586 (1969).

69Di D.L. Ditmer and W.W. Daehnick, Phys. Rev. 187, 1553 (1969).

69Fu G.H. Fuller and V.W. Cohen, Nucl. Data Tables A5, 433 (1969).

69Ho P.K. Hopke, R.A. Naumann, E.H. Spejewski, and A.T. Strigachev, Phys. Rev. 187, 1704 (1969).

69Ok K. Okano, Y. Kawase, S. Uehara, T. Takeuchi, and T. Nayashi, Ann. Rept. Res. Reactor Inst. Kyoto Univ. 2, 83 (1969).

69Pe L.K. Peker, Proceedings of the Fourth Winter School for Nuclear Theory and High Energy Physics, Part 1, 167 (1969). Akad. Nauk SSSR, Leningrad.

69Ro R.L. Robinson, F.K. McGowan, P.H. Stelson, W.T. Milner, and R.O. Sayer, Nucl. Phys. A124, 553 (1969).

69Sc W.C. Schick, Jr. and W.L. Talbert, Jr., Nucl. Phys. A128, 353 (1969).

69St C.L. Starke, E.A. Phillips, and E.H. Spejewski, Nucl.Phys. A139, 33 (1969).

69Wa R.H. Wampler, J. of Research of the National Bureau of Standards, B. Mathematical Sciences 73B 59 (1969).

69Ya T. Yamazaki and G.T. Ewan, Nucl. Phys. A134, 81 (1969).

69Zo W.H. Zoller, Ph.D. Thesis, Massachusetts Institute of Technology, 1969 (unpublished).

70Ap1 K.E. Apt, W.B. Walters, and G.E. Gordon Nucl. Phys. A152, 344 (1970).

70Ap2 K.E. Apt, (unpublished), Los Alamos Scientific Laboratory, private communication (1970).

70Ba P.A. Baedecker, A. Pakkanen, and W.B. Walters, Nucl.Phys. A158, 607 (1970).

70Br G. Bruge, J.C. Faivre, H. Faraggi, and A. Bussiere, Nucl. Phys. A146, 597 (1970).

70Ei J. Eidens, E. Roeckl, and P. Armbruster, Nucl. Phys. A141, 289 (1970).

70Fl E.R. Flynn, J.G. Beery, and A.G. Blair, Nucl. Phys. A154, 225 (1970).

70Gr R.C. Greenwood, R.G. Helmer, and R.J. Gehrke, Nucl. Instrum. Methods 77, 141 (1970).

70Ka H. Kawakami and K. Hisatake, Nucl. Phys. A149, 523 (1970).

70Ma E.S. Macias and W.B. Walters, Nucl. Phys. A160 274 (1970).

70Pi J.A. Pinston and F. Schussler, Nucl. Phys. A144, 42 (1970).

70Ta H.W. Taylor, A.H. Kukoc, and B. Singh, Nucl. Phys. A141, 641 (1970).

70UM University of Maryland, UNIVAC 1108 Exec 8 Math-Pack User's Guide, User Reference 70-03 (Computer Science Center, Univ. of Md. - June, 1970).

70UN UNIVAC 1108 Multi-Processor System, Processor and Storage, UP4053 Revision 1, Sperry Rand Corp., 1970.

71Apl K.E. Apt, Ph.D. Thesis, Massachusetts Institute of Technology, 1971 (unpublished).

71Ap2 K.E. Apt and W.B. Walters, Phys. Rev. Letters 26, 1189 (1971).

71Be F.E. Bertrand, Nucl. Data Sheets B6, 1 (1971).

71Ci R.J. Ciecka and G.R. Ryan, A Guide to Assembly Language Programming for the UNIVAC 1108, Computer Note CN-9 (Computer Science Center, Univ. of Md.- Sept., 1971).

71De M.K. Dewanjee, I.L. Preiss, O.B. Okon, and H. Bakhru, Bull. Am. Phys. Soc. 16, 80 (1971).

71Do T.A. Doron and M. Blann, Nucl. Phys. A171, 273 (1971).

71Go N.B. Gove and M.J. Martin, Nucl. Data Tables A10, 205, (1971).

71Gu R. Gunnink and J.B. Niday, UCRL - 51061 Vol. I, Vol. II, Vol. III, Vol. IV (1971 and 1972).

71He R.G. Helmer, R.C. Greenwood, and R.J. Gehrke, Nucl. Instrum. Methods 96, 173 (1971).

71Ka Y. Kawase, K. Okano, S. Uehara, and T. Hayashi, Nucl. Phys. A163, 534 (1971).

71Ku A. Kuriyama, T. Marumori, and K. Matsuyanagi, Progr. Theoret. Phys. 45, 784 (1971).

71Mal E.S. Macias and W.B. Walters, Nucl. Phys. A161, 471 (1971).

71Mu F. Munnich, A. Kjelberg, and D.J. Hnatowich, Nucl.Phys. A178, 97 (1971).

71Ra S. Raman and H.J. Kim, Nucl. Data Sheets B6, 39 (1971).

71Re B.K. Reid, A Guide to Programming with RALPH, Computer Note CN-3 (Computer Science Center, Univ. of Md., July, 1971).

71Se R. Seltz and N.M. Hintz, COO-1265-116, 97 (1971).

71Wa A.H. Wapstra and N.B. Gove, Nucl. Data Tables A9, 267 (1971).

72Au1 R.L. Auble, Nucl, Data Sheets B8, 77 (1972).

72Au2 R.L. Auble, Nucl. Data Sheets B7, 465 (1972).

72Be F.E. Bertrand, Nucl. Data Sheets B7, 419 (1972).

72Be2 F.E. Bertrand and D.J. Horen, Nucl. Data Sheets B7, 1 (1972).

72Bo R. Booth and H.H. Barschall, Nucl. Instrum. Methods 99, 1 (1972).

72Go G.E. Gordon, V.E. Viola, Jr., and W.B. Walters, MNC-4028-0004, 40 (Progress report - 1972).

72Ho D.J. Horen, Nucl. Data Sheets B8, 123 (1972).

72Ke1 A. Kerek, Nucl, Phys. A185, 497 (1972).

72Ke2 A. Kerek, P. Carle, and J. McDonald, Nucl. Phys. A198, 466 (1972).

72Kr K. Krien, E.H. Spejewski, R.A. Naumann, and H. Hübel, Phys. Rev. C6, 1847 (1972).

72Ku A. Kuriyama, T. Marumori, and K. Matsuyanagi, Progr. Theoret. Phys. 47, 498 (1972).

72Ku2 A. Kuhfield and N.M. Hintz, COO-1265-126, 77, 1972 (unpublished).

72Pr I.L. Preiss, COO-3464-10, 1972 (unpublished).

72Si R.E. Silverans, R. Coussement, E. Schoeters, and L. Vanneste, in Proceedings of the International Conference on Nuclear Moments and Nuclear Structure, Osaka, 1972 (J. Phys. Soc. Japan 34 supplement, 421 (1973)).

72Si2 N.C. Singhal, Noah R. Johnson, E. Eichler, and J.H. Hamilton, Phys. Rev. C5, 948 (1972).

72Ti G. Tirsell and L. Multauf, (unpublished), Lawrence Livermore Laboratory, private communication (1972).

72Va L. Vanneste, R. Coussement, G. Dumont, H. Pattyn, E. Schoeters, and R.E. Silverans, in Proceedings of the International Conference on Nuclear Moments and Nuclear Structure, Osaka, 1972 (J. Phys. Soc. Japan 34, supplement, 423 (1973)).

72Wa W.B. Walters and R.A. Meyer, Bull. Am. Phys. Soc. 17, 907 (1972).

73Al R. Almar, O. Civitarese, and F. Krmpotić, Phys. Rev. C8, 1518 (1973).

73Au1 R.L. Auble, Nucl. Data Sheets 9, 157 (1973).

73Au2 R.L. Auble, Nucl. Data Sheets 9, 125 (1973).

73Au3 R.L. Auble, F.E. Bertrand, Y.A. Ellis, and D.J. Horen, Phys. Rev. C8, 2308 (1973).

73Ba H.H. Barschall and E. Goldberg, IEEE Trans. Nucl. Sci. NS20, 472 (1973).

73Be F.E. Bertrand, Nucl. Data Sheets 10, 91 (1973).

73In H. Inoue, J. Phys. Soc. Japan 35, 957 (1973).

73Pa V. Paar, Nucl. Phys. A211, 29 (1973).

73Re B.W. Renwick, B. Byrne, D.A. Eastham, P.D. Forsyth, and D.G.E. Martin, Nucl. Phys. A208, 574 (1973).

73Si K. Sibbald, (unpublished) computer Science Center, Univ. of Maryland, private communication (1973).

73To R.R. Todd, W.H. Kelly, F.M. Bernthal, and W.C. McHarris, Nucl. Data Sheets 10, 47 (1973).

73UM University of Maryland, UNIVAC 1108 Reference Manual, CN-13, ed. by A.E. Pottala, (Computer Science Center, Univ. of Md. - March, 1973).

73UN1 UNIVAC 1100 Series, Exec 8 Programmer Reference Manual, UP-4144 Revision 3, Sperry Rand Corp. (1973).

73UN2 UNIVAC 1100 Series, Uniservo VIIIC Magnetic Tape Subsystem,UP-4123, Sperry Rand Corp. (1973).

73Va G. Vanden Berghe, (unpublished). Seminaire voor Wiskundige Natuurkunde, Gent, Belgium. Private communication (1973).

73Vi V.E. Viola, Jr., G.E. Gordon, and W.B. Walters, MNC-4028-0012, 95 (Progress report - 1973).

74An R.E. Anderson, (unpublished) Univ. of Colorado, private communication (1974).

74Ap K.E. Apt and W.B. Walters, Phys. Rev. C9, 310 (1974).

74Be1 F.E. Bertrand, Nucl. Data Sheets 11, 449 (1974).

74Be2 F.E. Bertrand, Nucl, Data Sheets 13, 397 (1974).

74Bu V.R. Burmistrov and V.A. Didorenko, Izv. Akad. Nauk SSSR. Ser. Fiz. 38, 791 (1974). Translation: Bull. of the Acad. of Sci. USSR, Physical Series 38, 113 (1974).

74Ci O. Civitarese and F. Krmpotic, Nucl. Phys. A229, 133 (1974).

74De J. DeRaedt, M. Rots, and H. Van de Voorde, Phys. Rev. C9, 2391 (1974).

74Fu I. Fujiwara, N. Imanishi, and T. Nishi, J. Inogr. Nucl. Chem. 36, 1921 (1974).

74Hi H.R. Hiddleston and C.P. Browne, Nucl. Data Sheets 13, 133 (1974).

74Ke A. Kerek, P. Carle, and S. Borg, Nucl. Phys. A224, 367 (1974).

74Ko D.C. Kocher, Nucl. Data Sheets 13, 337 (1974).

74Ku1 A. Kuriyama, T. Marumori, and K. Matsuyanagi, Progr. Theoret. Phys. 51m 779 (1974).

74Ku2 A. Kuriyama, T. Marumori, K. Matsuyanagi, and R. Okamoto, Institute for Nuclear Studies, Tokyo,INS-220, 1974 (unpublished).

74Ku3 A. Kuriyama, T. Marumori, K. Matsuyanagi, R. Okamoto, and T. Suzuki, 1974 (to be published).

74Ku4 A. Kuriyama, T. Marumori, K. Matsuyanagi, and R. Okamoto, Institute for Nuclear Studies, Tokyo, INS-217, 1974 (unpublsihed).

74Ma1 L.G. Mann. R.A. Meyer, and W.B. Walters, (unpublished) Lawrence Livermore Laboratory, private communications (1974).

74Ma2 G.J. Mathews,(unpublished) Univ. of Maryland, private communication (1974).

74Ma3 T. Marumori, Invited paper, Topical Conference on Problems of Vibrational Nuclei, Zagreb, Yugoslavia, Sept., 1974 (unpublished).

74Me1 R.A. Meyer, F. Momyer, and W.B. Walters, Z. Physik 268, 387 (1974).

74Me2 R.A. Meyer, UCRL-76027, 1974 (unpublished).

74Me3 L.R. Medsker, Nucl. Data Sheets 12, 431 (1974).

74Pa T. Paradellis and C.A. Kalfas, Z. Physik 271, 79 (1974).

74UN UNIVAC 1100 Series, Assembler, UP-4040 Revision 4, Sperry Rand Corp., 1974.

74Va G. Vanden Berghe, Z. Physik 266, 139 (1974).

75An1 R.E. Anderson and J.J. Kraushaar, Nucl. Phys. A241, 189 (1975).

75An2 R.E. Anderson, R.L. Bunting, J.D. Burch, S.R. Chinn, J.J. Kraushaar, R.J. Peterson, D.E. Prull, B.W. Ridley, and R.A. Ristinen Nucl. Phys. A242, 75 (1975).

75Ku A. Kuhfield and N.M. Hintz, to be published (1975).

75La1 J. Landrum, R.A. Meyer, S.V. Jackson, and W.B. Walters, Bull. Am. Phys. Soc. 20, 688 (1975).

75La2 J.T. Larsen, (unpublished) Lawrence Livermore Laboratory, private communication (1975).

75Ma M. Matoba, M. Hyakutake, K. Yagi, and Y. Aoki, Nucl. Phys. A237, 260 (1975).

75Me R.A. Meyer and E.S. Macias, (unpublished),Lawrence Livermore Laboratory, private communication (1975).